Mitochondrial retrograde signalling in the nervous system

Hunt, Rachel Joanna

Awarding institution:
King's College London

Mitochondrial retrograde signalling in the nervous system

Thesis submitted to King's College London for the degree of Doctor of Philosophy in Molecular Biology

Rachel J. Hunt

Wolfson Centre for Age-Related Diseases
The Institute of Psychiatry, Psychology & Neuroscience
King's College London
2014-18

Declaration

I hereby declare that all the work presented in this thesis is a result of my own research, and has not been accepted for any other degree. Contributions from others have been clearly acknowledged throughout.

Rachel Hunt

September 2018

Acknowledgements

Firstly, I express my immense gratitude to my supervisor, Dr. Joe Bateman, for all his patient guidance, help, support and tolerance; it has made an enormous difference to my work.

Many thanks go also to the fabulous members of the Bateman lab, who made the place so friendly. Olivia Duncan, Ariana Gatt, Katja Maierbrugger and Elin Vinsland, for puzzles, laughs, dining extravaganzas and general support. To Olivia and Ariana in particular for their help with dissections and imaging. More recently, thanks to new lab members Prane, Lucy, Ramya and Simo for being equally humorous and helpful, and my new office mates Earl and Jianne for being so welcoming and willing to chat. I thank King's College London students Jordan Briscoe and Rhian Ford for assistance with climbing assays and optimising aspects of other experiments, and gap-year volunteer Rachel Finlay for preparing gels, solutions, flipping flies and generally giggling.

The Wolfson CARD is a lovely place to work, and I also thank the wider Wolfson community, in particular John Chesson for his assistance in the lab and frequent, enjoyable chats on sport, politics and humanity. I thank John G, Brenda, Carl and Fiona for ensuring that everything in the building and the lab ran smoothly, and that nothing was a problem so long as you owned up. And, amongst many others, I thank Leanne, Supanida, Lizzie, Emily B, Keshi, and Elisa for being supportive and friendly fellow students. I am grateful for the approachability of my second supervisor, Prof. Clive Ballard, despite his exile to Devon.

I am also indebted to Drs Alison Snape, Stuart Knight and Steve Jones, for inspiring my interest in molecular biology in the first place, and for their subsequent guidance as I attempted to teach it.

Lastly and most importantly, I express my utmost gratitude to my parents, Claire and Richard, for being a constant support, and always striving to ensure that I would have as many opportunities as they could provide. I thank my siblings, Rob and Laura, for their sarcasm and gentle ridicule.

Abstract

Mitochondrial retrograde signalling communicates the functional status of mitochondria to the cell by regulating nuclear gene transcription. Mitochondrial dysfunction is strongly associated with several neurodegenerative diseases, but little is known about mitochondrial retrograde signalling in the nervous system. Mitochondria and the endoplasmic reticulum (ER) share physical and functional links, but the impact of mitochondrial dysfunction on ER biology has been underexplored. In this thesis, I harnessed the array of genetic and functional tools available in the fruit fly, *Drosophila melanogaster*, to investigate mitochondrial retrograde signalling via the ER in the nervous system.

I employed overexpression of mitochondrial transcription factor A (TFAM) as a model of mitochondrial dysfunction. The mitochondrial network was fragmented in the cell bodies of motor neurons overexpressing TFAM, and the morphology of the ER was also changed. There was an increase in the number of candidate ER-mitochondrial contact sites. Mitochondrial Ca^{2+} levels were substantially increased by TFAM overexpression, as were the levels of cytosolic Ca^{2+} in stimulated neurons.

Mitochondrial dysfunction activated the ER stress signalling pathway, the unfolded protein response (UPR), in *Drosophila* motor neurons. Genetic manipulation of the UPR revealed that multiple components modify the function of *Drosophila* motor neurons with mitochondrial dysfunction. In particular, knock-down of the UPR transcription factors ATF4, XBP1 and ATF6 suppressed the neuronal functional impairments caused by mitochondrial dysfunction.

Characterisation of the transcriptional response to mitochondrial dysfunction suggested that ATF4 is a key regulator of retrograde signalling in the *Drosophila* nervous system; 58% of genes that were significantly regulated by TFAM overexpression, were similarly regulated by overexpression of ATF4. Knock-down of ATF4 in conjunction with TFAM overexpression reversed the transcriptional changes caused by TFAM overexpression for 30% of genes. Therefore, I have established that the ER UPR is a mitochondrial retrograde signalling pathway in *Drosophila* neurons, and importantly, that targeting the UPR can alleviate the effects of mitochondrial dysfunction in neurons.

Contents

List of Figures

List of Tables

List of abbreviations

4-PBA	4-phenyl butyric acid
5’ UTR	5’ untranslated region
ALS	Amyotrophic lateral sclerosis
ATF4	Activating transcription factor 4
β-gal	β-galactosidase
BDNF	Brain-derived neurotrophic factor
BSA	Bovine serum albumin
bZIP	Basic leucine zipper domain
Ca^{2+}	Calcium ion(s)
cDNA	Complementary DNA
CHOP	CCAAT-enhancer-binding protein (C/EBP) homologous protein
CL	Cardiolipin
CNS	Central nervous system
DNA	Deoxyribonucleic acid
DTT	Dithiothreitol
eIF2α	Eukaryotic translation initiation factor 2 subunit 1
EMRE	Essential MCU regulator, mitochondrial
ER	Endoplasmic reticulum
ERAD	ER-associated degradation
ERMES	ER-mitochondria encounter structure
ETC	Electron transport chain
FCCP	Carbonyl cyanide-4-(trifluoromethoxy)phenylhydrazone
FPKM	Fragments per kilobase of transcript per million reads
g	Gravity
GCN2	General control noderepressible 2
GFP	Green fluorescent protein
GRP78	Glucose-regulated protein 78
GRP94	Glucose-regulated protein 94
HIF-1α	Hypoxia-inducible factor 1α
HRI	Heme regulated inhibitor
IMM	Inner mitochondrial membrane
IRE1	Inositol-requiring enzyme 1
ISR	Integrated stress response
LHON	Leber’s hereditary optic neuropathy
m^6A	N^6-methyladenosine
MAM	Mitochondria-associated membrane
MCU	Mitochondrial calcium uniporter
Mcu	Mitochondrial calcium uniporter – pore-forming subunit
MEFs	Mouse embryonic fibroblasts
MELAS	Mitochondrial encephalopathy, lactic acidosis and stroke-like episodes
MERRF	Myoclonic epilepsy with red-ragged fibers
MPP^+	1-methyl-4-phenylpyridinium
MPTP	1-methyl-4-phenyl-1,2,5,6-tetrahydropyridine

N2a	Neuro-2a
NMJ	Neuromuscular junction
nSyb	Neuronal synaptobrevin
o/e	overexpression
OMM	Outer mitochondrial membrane
OXPHOS	Oxidative phosphorylation
PBS	Phosphate buffered saline
PC	Phosphatidylcholine
PE	Phosphatidylethanolamine
P-eIF2α	Phosphorylated eukaryotic translation initiation factor 2 subunit 1
PERK	Protein kinase RNA-like endoplasmic reticulum kinase
PINK1	PTEN-induced kinase 1
PKR	Protein kinase RNA-activated
PP1	Protein phosphatase 1
PS	Phosphatidylserine
PTPIP51	Protein tyrosine phosphatase interacting protein 51
RIDD	Regulated IRE1-dependent decay
RNA	Ribonucleic Acid
RNAi	RNA interference
RNA-Seq	RNA sequencing
ROS	Reactive oxygen species
RPM	Revolutions per minute
RyR	Ryanodine receptor
S.D.	Standard deviation
S1P	Site-1 protease
S2P	Site-2 protease
SEM	Standard error of the mean
SERCA	Sarco/endoplasmic reticulum Ca^{2+} ATPase
SOD	Superoxide dismutase
TFAM	Mitochondrial transcription factor A
TFB2M	Mitochondrial transcription factor B2
TIM	Translocase of the inner membrane
TOI	Transgene of interest
TOM	Translocase of the outer membrane
uORF	Upstream open reading frame
UPR	Unfolded protein response
VAPB	Vesicle-associated membrane protein-associated protein B/C
VDRC	Vienna *Drosophila* Resource Center
VNC	Ventral nerve cord

1. Introduction

1.1 Mitochondria

Mitochondria are bimembraneous subcellular organelles that produce the majority of cellular ATP, and also play key roles in calcium (Ca^{2+}) homeostasis, lipid synthesis and intracellular signalling pathways.

1.1.1 Origins and discovery

Mitochondria or their vestiges are found in all eukaryotes (Hampl, Silberman et al. 2008), and are thought to be derived from an α-proteobacteria (Yang, Oyaizu et al. 1985) that was endocytosed by a host cell at least 1.45 billion years ago (Javaux, Knoll et al. 2001) in a symbiotic act. The identity of the host cell is debated and intimately entwined with attempts to understand the domains of life (reviewed in (Williams and Embley 2014)), but is thought to be an archaebacteria (Kelly, Wickstead et al. 2011, Williams, Foster et al. 2012). Mitochondria are social entities that make physical and functional contacts with many other subcellular organelles, including the endoplasmic reticulum (Vance 1990), lysosomes (Wong, Ysselstein et al. 2018), and peroxisomes (Mattiazzi Ušaj, Brložnik et al. 2015). An alternative to the standard theory of endosymbiotic evolution proposes that extrusions of the archaebacterial membrane progressively surrounded a city of α-proteobacteria until finally closing around them (Fig. 1.1) (Baum and Baum 2014). This 'inside-out' sequence of events would explain the creation of the extensive endomembrane system and inter-organellar contacts within the eukaryotic cell that are not explained by the simple mechanism of endocytosis.

Mitochondria were first discovered as intracellular granules by 19th century microscopists, but remained without designation until 1890 when histologist Richard Altmann noted their ubiquity and, with immense foresight, proposed that they were 'elementary organisms' with metabolic and genetic roles, colonising a host cell (reviewed in (Ernster and Schatz 1981)). Intensive work over the intervening years has established mitochondria as multifaceted organelles at the crossroads of metabolism and signalling.

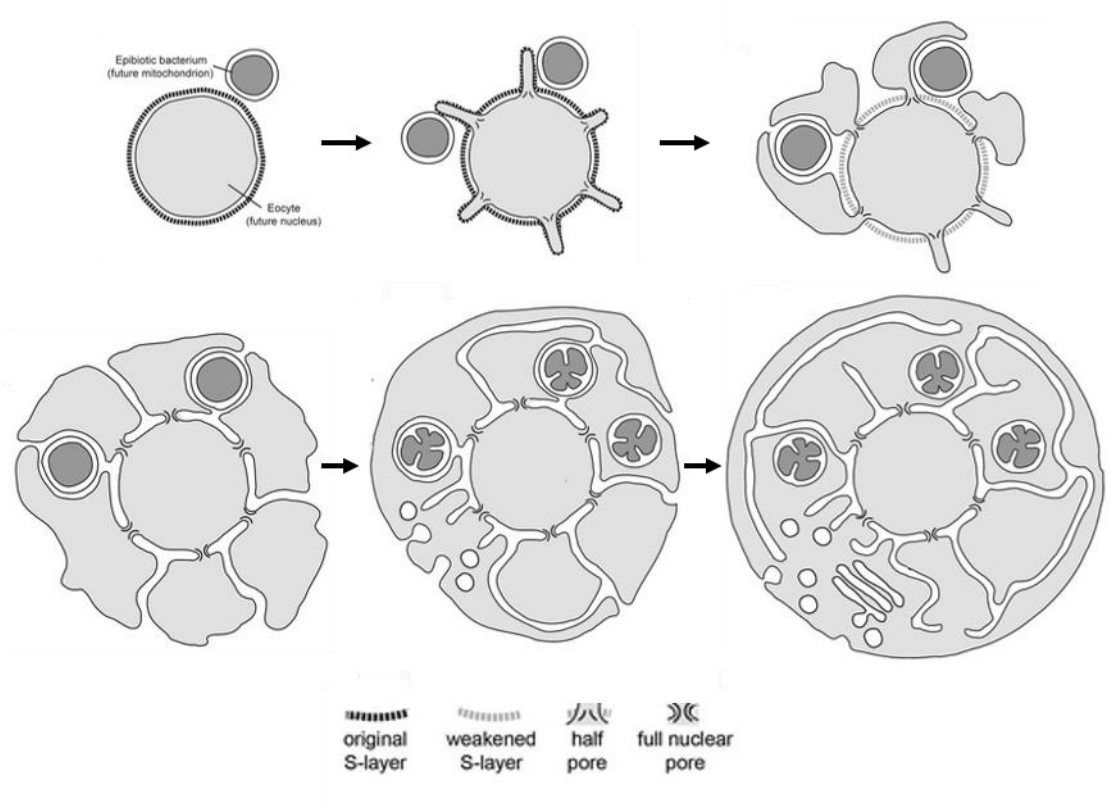

Figure 1.1 Schematic of the 'inside-out' theory of eukaryotic cell origin. Adapted from (Baum and Baum 2014).

1.1.2 Energy production pathways in mitochondria

Mitochondria have two membranes. The outer mitochondrial membrane (OMM) separates the organelle from the cytosol, whilst the inner mitochondrial membrane (IMM) divides the mitochondria into two major compartments; the matrix and the intermembrane space. The IMM is configured in a series of folds, termed cristae (Palade 1953).

Three major metabolic pathways are situated within the mitochondria generating the bulk of cellular energy; fatty acid oxidation supplies acetyl-CoA for the Krebs (Citric acid cycle), and both pathways generate reduced co-factors (NADH and $FADH_2$) for the production of ATP via oxidative phosphorylation. The oxidation of fatty acids and the Krebs cycle occur in the mitochondrial matrix (with the exception of succinate oxidation, see below), whilst the enzyme complexes mediating oxidative phosphorylation are found in the IMM.

1.1.2.1 Fatty acid oxidation and the Krebs cycle (Citric acid cycle)

Activated fatty acids are transported into mitochondria via the carnitine shuttle. Once inside the matrix, a series of enzymatic reactions add a ketone group to the β carbon and the fatty acid chain is cleaved between the α and β carbons, producing two-carbon units in the form of acetyl-CoA (discovery milestones reviewed in (Ghisla 2004)).

Elucidation of the molecular mechanisms by which aerobic respiration produces CO_2 represents one of the scientific achievements of the 20th century. In a series of papers in 1937-8 (Krebs 1937, Krebs and Johnson 1937, Krebs, Salvin et al. 1938), Hans Krebs and collaborators outlined eight reactions (Fig. 1.2), beginning and ending with citrate, that oxidise the two-carbon acetyl-CoA, generating CO_2, NADH, and GTP.

In the first three steps of the reaction, citrate is oxidised to succinyl-CoA with the release of two CO_2 molecules. Succinyl-CoA is hydrolysed to succinate, which is then oxidised by Complex II (succinate dehydrogenase) of the ETC (see 1.1.2.2), reducing FAD to $FADH_2$ and forming fumarate. The following two steps create oxaloacetate, which in the last step condenses with acetyl-CoA to reform citrate.

In 1949, Kennedy and Lehninger demonstrated that the enzymes of the Krebs cycle reside within the mitochondria (Kennedy and Lehninger 1949).

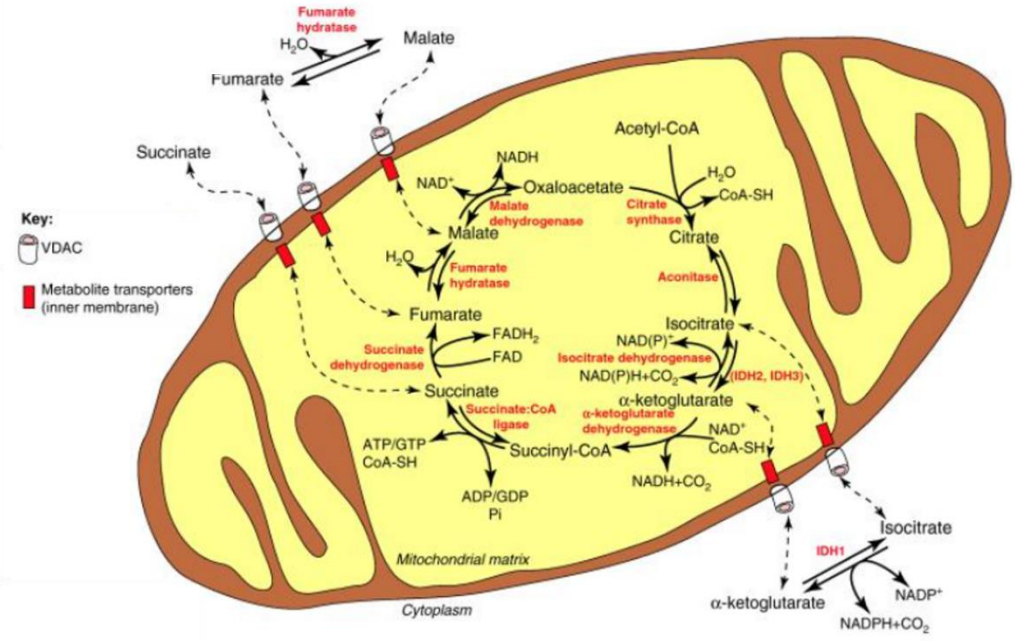

Figure 1.2 Reactions of the Krebs cycle occurring within the mitochondrial matrix. Adapted from (Raimundo, Baysal et al. 2011).

1.1.2.2 Oxidative phosphorylation (OXPHOS)

Mitochondria generate the majority of cellular ATP via a process termed oxidative phosphorylation (OXPHOS). Four protein complexes embedded within the IMM oxidise the NADH and $FADH_2$ produced by the Krebs cycle, glycolysis (in the cytosol) and fatty acid oxidation, and convey the electrons to acceptors of progressively increased reduction potential in a series of steps known as the electron transport chain (ETC) (Fig. 1.3). In the final step, two electrons are donated to oxygen (1/2 O_2), reducing it to H_2O. The free energy released by the ETC is used to pump protons from the matrix into the intermembrane space, creating a chemiosmotic H^+ gradient across the IMM. This gradient is used to drive the synthesis of ATP from ADP by a fifth protein complex.

The concept that proton pumping could be coupled to phosphorylation was first mooted in 1950 (Davies and Ogston 1950), but not followed up until Peter Mitchell proposed his chemiosmotic hypothesis in 1961 (Mitchell 1961). Much subsequent theoretical and experimental work, particularly from the laboratories of Paul Boyer and Efraim Racker, led to the mainstream acceptance of the chemiosmotic hypothesis by the mid-1970s (reviewed in (Ernster and Schatz 1981)).

Complex I (NADH:ubiquinone oxidoreductase) of the ETC is a multi-subunit L-shaped protein complex which accepts electrons from the reduced NADH (+ H^+) generated by the Krebs cycle and glycolysis, and donates them to the mobile electron carrier ubiquinone (Q). NADH binds the peripheral (matrix) arm of the Complex I, where it is oxidised by the prosthetic flavin mononucleotide (FMN). Single electrons are subsequently transferred from $FMNH_2$ through a series of iron-sulfur clusters, eventually reducing ubiquinone to ubiquinol (QH_2) via its semiquinone state ($Q^{\cdot-}$). The membrane arm of Complex I translocates four protons across the IMM. Structural analyses of Complex I indicate that proton pumping occurs via four Na^+/H^+ antiporter homologues, that are activated by conformational changes caused by the reduction of ubiquinone and the stabilisation of the semiquinone state (reviewed in (Wirth, Brandt et al. 2016)).

QH_2 shuttles through the membrane to Complex III (ubiquinol-cytochrome c oxidoreductase) where is reoxidised via the Q cycle with the concomitant transfer of four protons into the intermembrane space and reduction of cytochrome c. Complex III has single binding sites for QH_2 (site Q_o) and Q (site Q_i). Binding of QH_2 to Q_o is via hydrogen bonds to an Rieske iron-sulfur cluster and cytochrome b1 located within Complex III. Electron transfer from QH_2 bound at Q_o bifurcates; one electron is carried

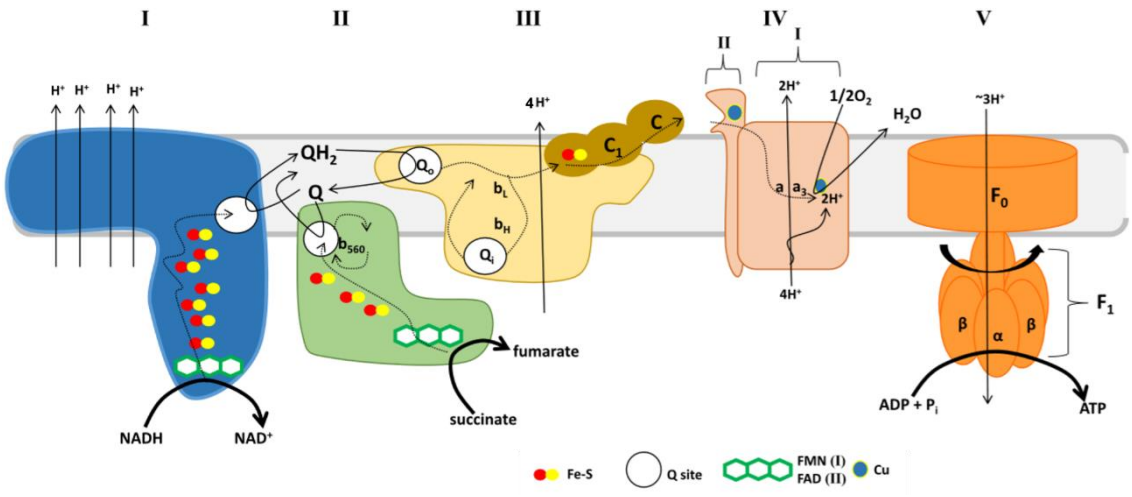

Figure 1.3 The electron transport chain and ATP synthase. Adapted from (Mailloux 2015).

to cytochrome c via the Rieske iron-sulfur cluster, whilst the other passes to cytochrome b1, and thence onto Q bound at Q_i, creating semiquinone, $Q^{\cdot-}$. The newly oxidised Q, leaves Q_o, whilst the protons involved in the hydrogen bonding of QH_2 at Q_o are released into the intermembrane space. A second turn of the Q cycle oxidises another molecule of QH_2 at Q_o and reduces the $Q^{\cdot-}$ at Q_i to QH_2, with the simultaneous uptake of two protons from the matrix. QH_2 then leaves Q_i and is free to reenter the Q cycle at Q_o. The Q cycle was first proposed by Peter Mitchell (Mitchell 1976). Experimental evidence in support of the mechanism is reviewed in (Slater 1983).

Cytochrome c is mobile in the membrane, and is oxidised by Complex IV (cytochrome c oxidase). The energy released is used to pump four more electrons (per two molecules of NADH oxidised at Complex I) across the IMM. Electrons from cytochrome c molecules are transferred across Complex IV via a cytochrome a-copper centre, and transferred to O_2 with the simultaneous uptake of four protons from the matrix to form $2H_2O$ ((Iwata, Ostermeier et al. 1995, Tsukihara, Aoyama et al. 1995) and reviewed in (Yoshikawa, Muramoto et al. 2011)).

Electrons can also enter the ETC via Complex II. In this reaction, succinate is oxidised by the Complex II FAD cofactor, and the electrons pass through a series of iron-sulfur clusters before reducing ubiquinone (which can then be re-oxidised by Complex III) (Yankovskaya, Horsefield et al. 2003). The difference in reduction potential between Complex II and ubiquinone is small, and therefore insufficient free energy is generated by the oxidation of succinate to pump protons into the intermembrane space.

The combined affect of Complexes I-IV is therefore to generate a electrochemical proton gradient across the IMM, the membrane potential component of which is ~140 mV in healthy mammalian mitochondria (Gerencser, Chinopoulos et al. 2012). Dissipation of the proton gradient 'across' Complex V, drives the synthesis of ATP from ADP.

Complex V (ATP synthase) is a composed of two subunits; the F_O subunit is situated within the IMM, and the F_1 subunit protrudes into the matrix. The 'flow' of protons back across the IMM drives rotation of the F_O subunit within the IMM which creates the conformational changes necessary in the F_1 subunit for the synthesis of ATP. The first crystal structure of ATP synthase was determined in the lab of John Walker (Abrahams, Leslie et al. 1994).

ATP exits the mitochondria via the ADP/ATP transporter, which catalyses the export of one ATP molecule, coupled to the import of one ADP molecule (Pebay-Peyroula, Dahout-Gonzalez et al. 2003).

1.1.2.2.1 Generation of reactive oxygen species (ROS)

Early in the biochemical characterisation of mitochondria it was discovered that the organelle could produce the reactive oxygen species (ROS) hydrogen peroxide (H_2O_2) (Hinkle, Butow et al. 1967). Subsequent investigation established that complexes of the ETC can produce the ROS superoxide ($O_2^{\cdot -}$) by transferring an electron to O_2 (Loschen, Azzi et al. 1974). $O_2^{\cdot -}$ is rapidly converted to H_2O_2 by an intra-mitochondrial superoxide dismutase (SOD) (Weisiger and Fridovich 1973), which therefore acts as an $O_2^{\cdot -}$ sink, favouring the production of further $O_2^{\cdot -}$ from O_2. Abnormal ROS production can lead to oxidative stress-induced tissue damage, and is associated with disease, including a wide range of neurodegenerative conditions (reviewed in (Manoharan, Guillemin et al. 2016)).

Complex I produces the majority of mitochondrial $O_2^{\cdot -}$, via two mechanisms. When the matrix NADH/NAD^+ ratio is high - driving electron transfer to the FMN co-factor in Complex I - but the production of ATP is low, electrons 'back up' onto FMN, from where they can be transferred to O_2, creating $O_2^{\cdot -}$. When ATP production is low, but the electrochemical gradient (proton motive force) high, electrons are forced backwards along the ETC and transferred from Q to Complex I. The site of electron transfer from Complex I to O_2 has not been definitively established, but is likely to be either or both FMN or the Q binding site within the IMM. The rate of $O_2^{\cdot -}$ production is determined by

the matrix concentration of O_2 and the proportion of reduced electron carriers available for reaction with O_2 (reviewed in (Murphy 2009)).

Both Complex II (Quinlan, Orr et al. 2012) and Complex III (Cadenas, Boveris et al. 1977) can also produce ROS.

1.1.3 Mitochondria structure and function

With the exception of erythrocytes, all mammlian cells contain mitochondria. The area and density of mitochondria in eukaryotic cells varies immensely, and is not always correlated with energy demand (Veltri, Espiritu et al. 1990).

1.1.3.1 Composition and permeability of mitochondrial membranes

The IMM and OMM present different barriers to the transfer of ions and proteins from the cytosol. The OMM is permeable to charged and neutral species ≤ ~5 kDa (Parsons, Williams et al. 1966) via the abundant voltage-dependent anion channel (VDAC) (also known as porin) (Colombini 1979, Zalman, Nikaido et al. 1980). The IMM is permeable only to uncharged molecules ≤ ~100-150 Da (Klingenberg and Pfaff 1966), and the passage of ions across the IMM requires the activity of specific channels. Proteins translated in the cytosol are canonically targeted to the mitochondrial compartments by N-terminal (matrix) and internal (IMM, OMM and intermembrane space) amino acid sequences, and are transported across the IMM and OMM by separately regulated complexes known as the translocase of the outer membrane (TOM) and translocase of the inner membrane (TIM) (reviewed in (Wiedemann and Pfanner 2017)). The activity of TIM requires the mitochondrial membrane potential (Gasser, Daum et al. 1982).

In common with other eukaryotic membranes, the bilayer-forming lipid phosphatidylcholine (PC) is a substantial element of both mitochondrial membranes, constituting ~41-49% of the total lipid content (Vance 2015). In line with α-proteobacterial origins, phosphatidylethanolamine (PE) is enriched in the mitochondria, whilst cardiolipin (CL) is unique to the organelle (Marinetti, Erbland et al. 1958, Getz, Bartley et al. 1968, Tian, Feng et al. 2012). Both lipids have small headgroups that give them a wedge shape, thought to assist the shaping of mitochondrial cristae (reviewed in (Rampelt, Zerbes et al. 2017)). In yeast, PE and CL are synthetic lethal – the

organism cannot survive without both (Gohil, Thompson et al. 2005). They are enriched in the IMM where they interact with multiple proteins and have important roles in ETC activity. CL is essential for the proper function and stability of Complex III (Yu and Yu 1980), Complex IV (Robinson, Zborowski et al. 1990) and Complex V (Smith Eble, Coleman et al. 1990), in addition to stabilising supercomplex assemblies of the ETC proteins (Pfeiffer, Gohil et al. 2003). The headgroup of CL can buffer protons and has been proposed to function as a 'proton trap' for OXPHOS; maintaining the pH of the intermembrane space within a tolerable window, whilst supplying protons to, or absorbing them from, the ETC complexes and Complex V (Haines and Dencher 2002). PE is required for full activity of Complexes I and IV (Tasseva, Bai et al. 2013), and has disputed roles in supercomplex formation (Bottinger, Horvath et al. 2012, Tasseva, Bai et al. 2013). Both lipids have extensive and specific regulatory roles in mitochondrial protein import that go beyond maintaining mitochondrial membrane potential via the ETC (reviewed in (Bottinger, Ellenrieder et al. 2016)).

1.1.3.2 Mitochondrial DNA (mtDNA)

Mitochondria contain a double-stranded circular genome (mtDNA) (Nass and Nass 1963, Nass 1966, Van Bruggen, Borst et al. 1966) enclosed by the IMM, and composed of light (C-rich) and heavy (G-rich) strands. In humans, mtDNA is approximately 16.5 kb, and encodes 13 polypeptide subunits of the OXPHOS complexes, 2 rRNAs and 22 tRNAs (Anderson, Bankier et al. 1981). *Drosophila* mtDNA encodes the same array of genes, and is approximately 19.5 kb in size (Lewis, Farr et al. 1995). mtDNA is transcribed polycistronically (Aloni and Attardi 1971, Ojala, Montoya et al. 1981) by a mitochondrial-specific RNA polymerase, POLRMT (Greenleaf, Kelly et al. 1986, Tiranti, Savoia et al. 1997). mtDNA replication is performed by a DNA polymerase and accessory factors specific to the mitochondria (reviewed in (Holt and Reyes 2012)). Transcription of mtDNA occurs from two promoters, the light strand promoter (LSP) and the heavy strand promoter (HSP) (Montoya, Christianson et al. 1982). The presence of just two transcription factors, mitochondrial transcription factor A (TFAM) and mitochondrial transcription factor B2 (TFB2M) is sufficient for POLRMT initiation (Litonin, Sologub et al. 2010, Ramachandran, Basu et al. 2017). TFAM and TFBM2 bind to LSP and HSP, separate the mtDNA strands by inducing bends and recruit POLRMT

(Ramachandran, Basu et al. 2017). The transcribed mtDNA is translated by mitochondria-specific ribosomes (O'Brien 1971).

TFAM is a ~25 kDa protein with DNA-binding high mobility group (HMG) domains (Fig. 1.4 A) (Fisher and Clayton 1988, Fisher, Lisowsky et al. 1992, Parisi, Xu et al. 1993). mtDNA is packaged into protein-nucleic acid complexes termed nucleoids (Nass 1969). A role for mammalian TFAM in mtDNA packaging was initially inferred by its colocalisation and co-purification with nucleoids (Garrido, Griparic et al. 2003, Istiaq Alam, Kanki et al. 2003) and ability to bend DNA (Fisher, Lisowsky et al. 1992). Subsequently, it has been demonstrated that TFAM is the only protein required for compaction of mammalian mtDNA into nucleoids (Kaufman, Durisic et al. 2007, Kukat, Davies et al. 2015), however the mechanism and mtDNA content of the nucleoids are disputed. In agreement with previous studies (Iborra, Kimura et al. 2004, Legros, Malka et al. 2004), Kaufman et al. reported multiple mtDNA molecules in a single nucleoid, and proposed that mtDNA was condensed via the creation of loops that were progressively filled in by other TFAM molecules (Fig. 1.4 B) (Kaufman, Durisic et al. 2007). By contrast, Kukat et al. described single mtDNA copies per nucleoid, and a mechanism whereby TFAM bends the mtDNA, bringing regions of the circle into close apposition and facilitating cross-strand binding (Fig. 1.4 C) (Kukat, Davies et al. 2015).

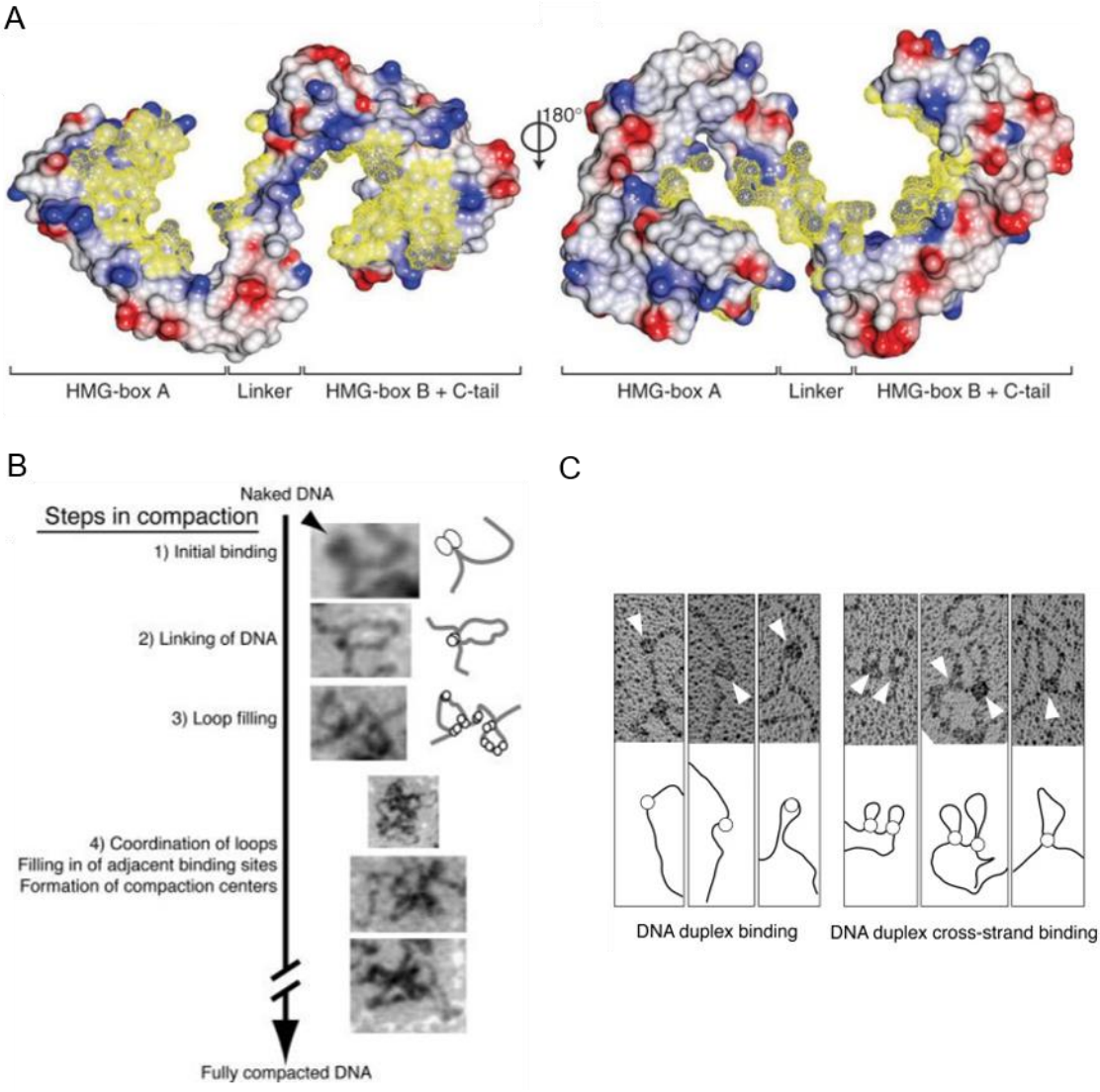

Figure 1.4 Structure of TFAM and models of mtDNA condensation by TFAM. (A) Electrostatic surface potential plots of TFAM inferred from 2.5 Å crystal structure. Yellow = mtDNA binding surfaces. Blue = positive potential, red = negative potential. From (Ngo, Kaiser et al. 2011) (B) Loop filling model of TFAM condensation of mtDNA by (Kaufman, Durisic et al. 2007). (C) Cross-strand binding model of TFAM condensation of mtDNA by (Kukat, Davies et al. 2015).

1.1.3.3 Mitochondrial Ca^{2+} handling

Mitochondria are intracellular stores of Ca^{2+} (Deluca and Engstrom 1961). The uptake of Ca^{2+} into mitochondria is an energetically favourable process, driven by the large negative electrochemical potential across the IMM of healthy mitchondria (Gunter and Gunter 1994, Kirichok, Krapivinsky et al. 2004). Ca^{2+} influx proceeds across the OMM through VDAC, and then via facilitated diffusion across the IMM, predominantly carried and regulated by the mitochondrial calcium uniporter (MCU) complex (Fig. 1.5) (De Stefani, Raffaello et al. 2011). Transport of Ca^{2+} into the mitochondria is therefore not directly coupled to the import or export of any another ion. In mammals, the MCU complex comprises oligomers of the pore-forming Mcu (Baughman, Perocchi et al. 2011) and six regulatory subunits, including the essential MCU regulator, mitochondrial (EMRE) (Sancak, Markhard et al. 2013). The MCU complex, including a homologue of EMRE, is conserved in *Drosophila*, but it is not known whether the other regulatory subunits are conserved (Choi, Quan et al. 2017). In mammals, an isoform of the ryanodine receptor (RyR) has been discovered in the IMM of cardiomyocytes and striatal neurons, and makes a minor contribution to mitochondrial Ca^{2+} influx (Jakob, Beutner et al. 2014). *Drosophila* possess a single RyR isoform (Takeshima, Nishi et al. 1994, Sullivan, Scott et al. 2000), and it is not known whether any fraction of the protein localises to the IMM.

Efflux of Ca^{2+} from the mitochondria is mediated by Na^{+}-dependent (Crompton, Kunzi et al. 1977) and Na^{+}-independent mechanisms (Crompton, Moser et al. 1978). The Na^{+}/Ca^{2+} exchanger NCLX mediates the Na^{+}-dependent mechanism (Palty, Silverman et al. 2010), whilst the *Drosophila* protein LETM1 has been identified as a mitochondrial H^{+}/Ca^{2+} antiporter (Jiang, Zhao et al. 2009). Approximately 33kJ of energy is required to export one mole of Ca^{2+} from the matrix to the intermembrane space (Gunter and Pfeiffer 1990).

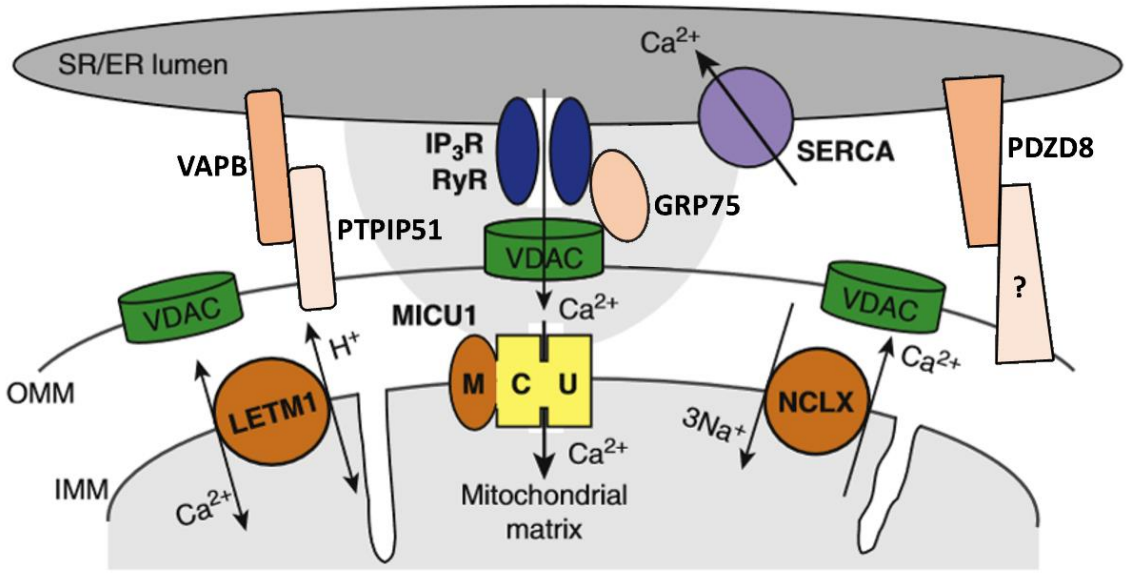

Figure 1.5 Mitochondrial Ca^{2+} handling. Adapted from (Hajnóczky and Csordás 2010). For ER Ca^{2+} handling, see Section 1.3.4. For ER-mitochondrial Ca^{2+} transfer, including information on ER-mitochondrial tethers known to regulate Ca^{2+} transfer, see Section 1.4.2.

1.1.3.4 Mitochondrial dynamics

Mitochondria exist as a dynamic network in the cell, undergoing frequent remodelling via fission and fusion. The biogenesis of mitochondria occurs via the augmentation and reconfiguration of existing mitochondrial networks, and requires the co-ordinated synthesis of nuclear-encoded and mtDNA-encoded proteins. The transcriptional co-activator peroxisome proliferator activated receptor γ co-activator 1α (PGC-1α) is considered the master regulator of the nuclear genes for mitochondrial biogenesis (Puigserver, Wu et al. 1998). Interaction of (PGC-1α) with the nuclear respiratory factor 1 and 2 (NRF1 and NRF2) transcription factors can control the transcription of OXPHOS genes (Wu, Puigserver et al. 1999). NRF1/2 can also regulate the transcription of TFAM (Virbasius and Scarpulla 1994).

Mitochondrial fusion is regulated by distinct but co-regulated mechanisms of IMM and OMM fusion. Fusion of the OMM requires the proton (but not electrical) gradient across the IMM and the minimal hydrolysis of GTP, while conversely, fusion of the IMM requires a high input of GTP and the IMM membrane potential (Meeusen, McCaffery et al. 2004). The GTPases mitofusin and OPA1 (Cipolat, Martins de Brito et

al. 2004) mediate the fusion of the OMM and IMM respectively. Mitofusin operates via homotypic interactions that require the presence of the protein on both fusing mitochondria (Koshiba, Detmer et al. 2004).

Mitochondrial fission occurs via recruitment of dynamin-related protein 1 (Drp1) to the OMM by a complex of Fis1 and Mdv (Karren, Coonrod et al. 2005) and its subsequent constriction of the mitochondria, and scission of the membranes.

The components of damaged mitochondria are recycled in a process known as mitophagy. In mammals, the best characterised regulators of mitophagy are the Parkinson's Disease (PD) associated genes *pink1* and *parkin*. PINK1 is imported into healthy mitochondria and degraded. When the mitochondrial membrane potential is reduced by dysfunctional OXPHOS, translocation of PINK1 fails, and it remains in the OMM where it phosphorylates and thereby activates the E3 ubiquitin ligase Parkin, which then marks the mitochondria for degradation (Kim, Park et al. 2008, Narendra, Tanaka et al. 2008, Sha, Chin et al. 2010).

1.1.4 Mitochondrial dysfunction and disease

Given the critical role of the organelle in the metabolic and signalling life of the cell, it is unsurprising that mitochondrial dysfunction is associated with a panoply of diseases. Tissue-specific energy demands and heteroplasmy ensure that these diseases display a wide range of clinical symptoms and variable penetrance. Diseases can be caused by mutations/deletions in both mtDNA-encoded genes and nuclear-encoded proteins related to mitochondrial function.

Early onset mitochondrial diseases are predominantly severe, and often caused by autosomal recessive mutations in nuclear genes. The estimated prevalence of childhood onset mitochondrial disease is 6.2/100,000 births (Skladal, Halliday et al. 2003). The high energy demand of the nervous system means that mitochondrial dysfunction frequently causes neurological syndromes, such as Leigh syndrome, associated with mutations in the OXPHOS complexes and their assembly factors (reviewed in (Lake, Bird et al. 2015)), and Alpers-Huttenlocher syndrome, caused by mutations in the (nuclear-encoded) mtDNA polymerase (reviewed in (Saneto, Cohen et al. 2013)). Patients with these diseases can also present pathologies in other tissue with high energy demand, including

cardiac and skeletal muscle. Mitochondrial diseases diagnosed in adulthood are estimated to affect ~1/4,300 adults, and are predominantly caused by mtDNA mutations (~87% of cases) (Gorman, Schaefer et al. 2015). There are recognised mitochondrial syndromes caused by mtDNA mutations, such as Leber's hereditary optic neuropathy (LHON), myoclonic epilepsy with red-ragged fibers (MERRF) and mitochondrial encephalopathy, lactic acidosis and stroke-like episodes (MELAS), but many patients do not display the well-defined symptoms of these syndromes (reviewed in (Lightowlers, Taylor et al. 2015)).

Mitochondrial dysfunction is also convincingly linked to the pathogenesis of neurodegenerative disease. Parkinson's Disease (PD) is classically defined by the specific loss of dopaminergic neurons from the substantia nigra pars compacta, manifesting symptoms of bradykinesia, resting tremor and rigidity due to the location of the SNc within the motor circuits of the basal ganglia. The association between PD and mitochondrial dysfunction first came to light in a study of recreational drug users who had developed PD-like symptoms. It was established that they had injected 1-methyl-4-phenyl-1,2,5,6-tetrahydropyridine (MPTP) (Langston, Ballard et al. 1983), whose metabolite, MPP^+, was characterised as an inhibitor of Complex I (Nicklas, Vyas et al. 1985). Subsequently, post-mortems of PD patients revealed deficient Complex I activity (Schapira, Cooper et al. 1989). Genes mutated in juvenile onset PD include the mitochondrial quality control proteins *PINK1* (Valente, Abou-Sleiman et al. 2004) and *parkin* (Kitada, Asakawa et al. 1998), *LRRK2* (Zimprich, Biskup et al. 2004), which is known to associate with the OMM, and the ROS-sensitive chaperone *DJ-1* (Bonifati, Rizzu et al. 2003). Reduced activity of the ETC complexes has been found in Alzheimer's disease cases (Maurer, Zierz et al. 2000), as well as downregulation of the mRNA encoding the ETC subunits (Manczak, Park et al. 2004). The mitochondrial cascade hypothesis of Alzheimer's disease proposes that baseline mitochondrial function and the rate of decline – affected by e.g. exposure to environmental factors – ultimately determine the onset of synapse loss, neurodegeneration and the formation of plaques and tangles (Swerdlow, Burns et al. 2014).

1.1.5 Mitochondrial retrograde signalling

The nuclear genome encodes the vast majority (~1,200) of mitochondrial proteins (Calvo, Clauser et al. 2016), as well as the signalling and transcription factors that control mitochondrial biogenesis and dynamics. These species constitute an anterograde signal from the nucleus to the mitochondria. Mitochondrial retrograde signals communicate the health and integrity of mitochondria to the cell, and in particular, the nucleus where gene transcription is altered in response to these retrograde signals. Given the strong association of mitochondrial dysfunction with disease, understanding these retrograde signals presents a valuable opportunity to gain insight into the pathogenesis of diseases associated with mitochondrial dysfunction.

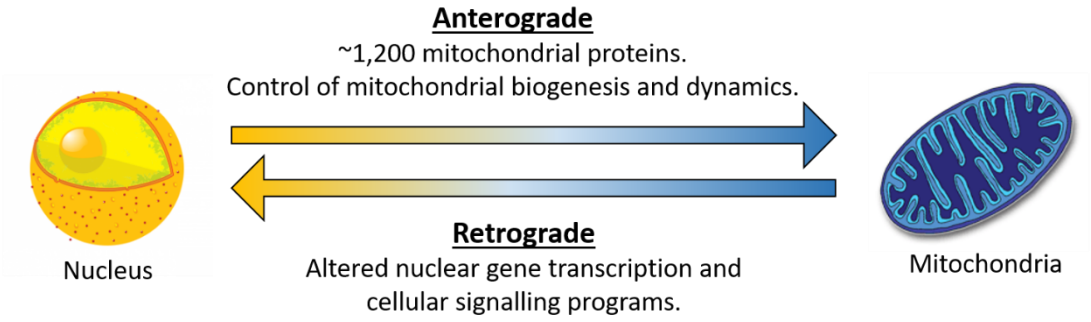

Figure 1.6 Schematic of anterograde and retrograde signalling.

1.1.5.1 Mitochondrial retrograde signalling in yeast [adapted excerpt from (Hunt and Bateman 2018)]

The phenomenon of retrograde signalling was identified in a landmark paper from the Butow laboratory in 1987. Subtractive hybridisation of cDNAs from yeast strains harbouring mtDNA lesions uncovered variations in the abundance of nuclear-encoded mRNAs, both compared to controls and between the disparate dysfunction models (Parikh, Morgan et al. 1987). Subsequent studies have focused upon rho^0 cells - an extreme form of mitochondrial dysfunction whereby mtDNA is entirely absent. In addition to ETC deficiency, the Krebs cycle is not operational in rho^0 cells due to the compromised function of succinate dehydrogenase. The classical marker of retrograde signalling in yeast is upregulation of the peroxisomal isoform of citrate synthase (*CIT2*) (Liao, Small et al. 1991). CIT2 operates within the glyoxylate cycle, supplying citrate that

can be oxidised to α-ketoglutarate by the first three enzymes of the Krebs cycle. α-ketoglutarate can subsequently be transaminated to glutamate, supplying the cells with nitrogen. In addition, the glyoxylate cycle permits the net synthesis of glucose from the β-oxidation of fatty acids; isocitrate is cleaved to form succinate and glyoxylate, the latter of which can undergo condensation with acetyl-CoA to form malate, and then ultimately glucose via gluconeogenesis. The β-oxidation (Chelstowska and Butow 1995, Epstein, Waddle et al. 2001), glycolytic, and mitochondrial biogenesis pathways are also upregulated by retrograde signalling in rho^0 cells (Traven, Wong et al. 2001), alongside a substantial proliferation of peroxisomes (Epstein, Waddle et al. 2001).

Transcriptional control of this metabolic adaptation can be exerted by a heterodimer of two bHLH/ZIP proteins, Rtg1 and Rtg3 (Fig. 1.6), in concert with the histone acetyltransferase complex, SAGA-like (SLIK) (Liao and Butow 1993, Chelstowska and Butow 1995, Pray-Grant, Schieltz et al. 2002). Localisation of Rtg1/Rtg3 is regulated by the putative phosphatase Rtg2 (Sekito, Thornton et al. 2000). Rtg2 is also a core component of SLIK (Pray-Grant, Schieltz et al. 2002), and therefore has a chromatin remodelling role in addition to promoting the partial dephosphorylation of Rtg3 and its consequent translocation to the nucleus in tandem with Rtg1. A wealth of positive and negative regulators act on the pathway; whilst bound to the mutually redundant 14-3-3 proteins Bmh1/2, the phosphoprotein Mks1 inhibits the nuclear translocation of Rtg1/3. When Mks1 binding switches reversibly to Rtg2, retrograde signalling is activated (Liu, Sekito et al. 2003). The evolutionarily conserved TOR pathway is a negative regulator of yeast retrograde signalling, integrating nutrient sensing with the response to mitochondrial dysfunction. TOR modulates the Rtg pathway both upstream and downstream of Rtg2, likely via the TORC1/2 component Lst8 (Chen and Kaiser 2003).

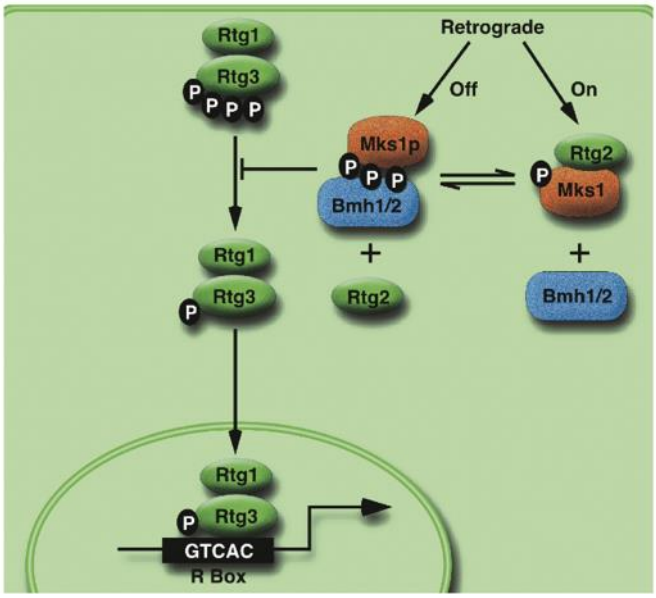

Figure 1.7 The canonical yeast Rtg1-3 retrograde signalling pathway in yeast. From (Butow and Avadhani 2004)

Experimental adjustment of mitochondrial membrane potential, in both rho^0 and rho^+ cells, controlled the expression of CIT2, the nuclear translocation of Rtg1/3, and the retrograde response-associated increase in replicative lifespan, indicating that this parameter may be the proximal signal of mitochondrial dysfunction. A ROS scavenger did not prevent the transduction of defective membrane potential to Rtg2, and therefore the signalling intermediaries between mitochondrial dysfunction and the Rtg pathway remain unknown (Miceli, Jiang et al. 2011). The fate of succinate formed in the glyoxylate cycle has not been determined – it cannot be efficiently oxidised to fumarate by succinate dehydrogenase – and the metabolite may yet be found to have a signalling role.

Many of the nuclear gene changes in response to mitochondrial dysfunction are not Rtg-dependent (Epstein, Waddle et al. 2001), and a more recently discovered pathway places mitochondrial ROS upstream of epigenetic changes that downregulate subtelomeric transcription (Schroeder, Raimundo et al. 2013). Phosphorylation of the histone demethylase Rph1 by Rad53 and Tel1 – kinases previously associated only with nuclear DNA damage – reduced its binding to subtelomeric chromosomal regions. Consistent with this observation, HSK36me3 marks increased in the same locations, as did the binding of the silencing protein Sir3.

Other recent work in yeast has uncovered mechanisms that promote cytosolic proteostasis in response to impaired import of mitochondrial proteins (Wang and Chen 2015, Wrobel, Topf et al. 2015). Whilst changes in nuclear gene expression were detected when translocation into the intermembrane space was diminished (Wrobel, Topf et al. 2015), studies have largely focused on alterations in the proteome. Upregulation of proteasome activity and the abundance of its assembly factors, was hypothesized to ameliorate the burden of mistargeted mitochondrial proteins in the cytosol in a direct model of impaired import (Wrobel, Topf et al. 2015). Proteosomal activity, alongside modifications to translation rates and specificity, was also regulated in response to mutations in the adenine nucleotide translocase, the inner membrane protease *YME1* and the F_1-ATPase (Wang and Chen 2015).

1.1.5.2 Calcium

Mitochondrial dysfunction is strongly associated with the initiation and metastasis of cancerous tumours. As a result, much retrograde signalling research in mammals has been performed in cancer models. The yeast Rtg1-3 genes are not conserved in higher eukaryotes, and mammalian cells do not possess an alternative 'signature' retrograde signalling pathway. Instead, the identified cellular responses to mitochondrial dysfunction have been strongly cell-type-specific, myriad and sometimes contradictory.

Pulmonary carcinoma (Amuthan, Biswas et al. 2001, Amuthan, Biswas et al. 2002, Guha, Srinivasan et al. 2007), breast carcinoma (Yu, Shi et al. 2009), prostate cancer (Moro, Arbini et al. 2009) and colorectal cancer (Guo, Zheng et al. 2011) cell lines all became increasingly proliferative, invasive, and/or resistant to apoptosis, following a reduction in mtDNA copy number. However, in rho^0 osteosarcoma cells, proliferation was reduced (Arnould, Vankoningsloo et al. 2002). Cytosolic Ca^{2+} levels regulate many signalling pathways, and elevated Ca^{2+} was detected in both the pulmonary carcinoma and osteosarcoma cells. The differing pathways activated by raised Ca^{2+} may hold the key to the phenotypic outcomes; in the rho^0 osteosarcoma cells the calcium/calmodulin-dependent kinase IV (CaMKIV) stimulated the CREB transcription factor, whilst in the pulmonary carcinoma cells, the phosphatase calcineurin and Ca^{2+}-dependent MAP kinases were activated. Even when the same Ca^{2+}-dependent factors are activated, the downstream pathways frequently differ. In a skeletal muscle model, retrograde signalling

via calcineurin was found to cause proliferation via upregulation of the insulin-like growth factor-1 receptor, independently of growth factors. Events downstream of calcineurin included the activation and nuclear-localisation of the classical stress-response transcription factors NFAT, CREB, C/EBPδ and NFκB, the latter via a novel dephosphorylation of inhibitor IκBβ by calcineurin. These transcription factors functioned collaboratively and required phosphorylated RNA-binding protein heterogeneous ribonucleoprotein hnRNPA2 as a transcriptional co-activator for the upregulation of target genes, the full complement of which is currently unknown (Guha, Srinivasan et al. 2007, Guha, Pan et al. 2009, Guha, Tang et al. 2010).

1.1.5.3 ROS

One of the earliest demonstrations of retrograde signalling in mammalian cells was the finding that ROS-based signals from the mitochondria were required for the transcriptional response to hypoxia mediated by HIF-1α in hepatoma cells. The increase in ROS production in response to hypoxia was abolished in rho^0 cells, and upregulation of hypoxia-responsive transcripts also failed to occur (Chandel, Maltepe et al. 1998). Subsequently, ROS have been shown to regulate the activity of NF-κB in colorectal carcinoma cells (Formentini, Sanchez-Arago et al. 2012), and the relative mitochondrial/nuclear localisation of the ubiquinone biosynthesis factor demethoxyubiquinone monooxygenase (CLK-1/COQ7) in a manner akin to ATFS-1 in the mtUPR (see below). In *C. elegans*, nuclear localised CLK-1 functions to reduce ROS, but counterintuitively, also to downregulate transcription of mtUPR chaperones (Monaghan, Barnes et al. 2015).

1.1.5.4 The mitochondrial unfolded protein response (mtUPR) [adapted excerpt from (Hunt and Bateman 2018)]

The mitochondrial unfolded protein response (mtUPR) is a collection of retrograde signalling pathways that are activated by unfolded or aggregated proteins in the mitochondria. These pathways serve to restore proteostasis within the organelle, and mitigate reduced mitochondrial ATP production. Whilst early mammalian mtUPR research established the use of a mitochondrially-targeted aggregation-prone truncated ornithine transcarbamylase (OTC-Δ) model (Zhao, Wang et al. 2002), subsequent

research in generalised mitochondrial stress models has not always strictly confirmed an unfolded protein burden within the mitochondria, and the results must be considered with this caveat. Transcriptional upregulation of the nuclear-encoded mitochondrial chaperones of the Hsp60, Hsp70 and Hsp10 families is conserved across *C. elegans*, *Drosophila* and mammalian mtUPR models, and bolsters mitochondrial protein folding capacity (Martinus, Garth et al. 1996, Zhao, Wang et al. 2002, Haynes, Petrova et al. 2007, Nargund, Pellegrino et al. 2012, Owusu-Ansah, Song et al. 2013, Baqri, Pietron et al. 2014, Wu, Williams et al. 2014, Munch and Harper 2016). Components of the mitochondrial import machinery, in particular the stress-sensitive *tim-17*/*Tim17A*, can also be regulated by the mtUPR, but results are not consistent across experimental paradigms, with both up- and down-regulation witnessed (Aldridge, Horibe et al. 2007, Nargund, Pellegrino et al. 2012, Rainbolt, Atanassova et al. 2013). In some models, clearance of unfolded matrix proteins is enhanced by upregulation of the Lon and ClpP/ClpX proteases, and this degradation may also have a signalling role (see below) (Zhao, Wang et al. 2002, Owusu-Ansah, Song et al. 2013, Baqri, Pietron et al. 2014, Wu, Williams et al. 2014, Fiorese, Schulz et al. 2016). In a direct unfolded protein model in HeLa cells, downregulation of the RNase P component MRPP3 impaired processing of mt-tRNA precursors, and consequently contributed to an observed reduction in translation of mtDNA-encoded proteins (Munch and Harper 2016). Microarray analysis in *C. elegans* has also indicated that the mtUPR invokes ROS scavenging, increased iron-sulfur cluster assembly, and metabolic reprogramming that includes the upregulation of glycolytic and regulatory enzymes (Nargund, Pellegrino et al. 2012). There are also branches of the mtUPR, such as the enhancement of AMPK-mediated autophagy seen in a *Drosophila* OTC-Δ model (Pimenta de Castro, Costa et al. 2012), that do not signal via the nucleus.

The most comprehensive investigation of mtUPR pathways has been undertaken in *C. elegans*. In that organism, transcriptional induction of *hsp-60* can be regulated by the transcription factors DVE-1 (Haynes, Petrova et al. 2007) and ATFS-1 (Nargund, Pellegrino et al. 2012), and the ubiquitin-like protein UBL-5 (Haynes, Petrova et al. 2007). A small fraction of DVE-1 is found complexed with UBL-5 under conditions of mitochondrial stress, but the requirement for this physical interaction in activating the mtUPR has not been established (Haynes, Petrova et al. 2007). Knock-down of the ClpP protease attenuated upregulation of hsp-60 and ubl-5, and nuclear accumulation of DVE-1 (Haynes, Petrova et al. 2007) and ATFS-1 (Haynes, Yang et al. 2010), placing ClpP at

the head of all known *C. elegans* mtUPR pathways. ClpP-mediated hydrolysis of matrix proteins is increased under conditions of mitochondrial stress and the resultant peptides are exported into the intermembrane space by the ABC transporter HAF-1 (Haynes, Yang et al. 2010), from where they diffuse through the semi-porous outer membrane into the cytosol. Both inhibition of the proteolytic activity of ClpP, and a *haf-1* deletion mutant, decreased the induction of *ubl-5*, indicating a yet-to-be elucidated role for the effluxed peptides in the signal transduction of at least one mtUPR pathway. HAF-1 was also required for the nuclear accumulation of ATFS-1 in some mitochondrial stress conditions (Nargund, Pellegrino et al. 2012), but is not required for the nuclear translocation of DVE-1 (Haynes, Yang et al. 2010).

ATFS-1 activity is controlled by organelle partitioning: it has both a nuclear localisation sequence (NLS) within its C-terminal leucine zipper domain and an N-terminal mitochondrial targeting sequence (MTS) (Fig. 1.7). Under normal physiological conditions, ATFS-1 is imported into the mitochondrial matrix and degraded by the Lon protease. When the mitochondrial import machinery is compromised and/or HAF-1 is activated by upstream mtUPR components, mitochondrial import of ATFS-1 is impaired, and instead the protein accumulates in the nucleus and upregulates its target genes (Nargund, Pellegrino et al. 2012). An ATFS-1 orthologue has been identified in *Litopenaeus vannamei* (King Prawn) (Chen, Yue et al. 2016), but the protein does not have known homologues in the common model organisms.

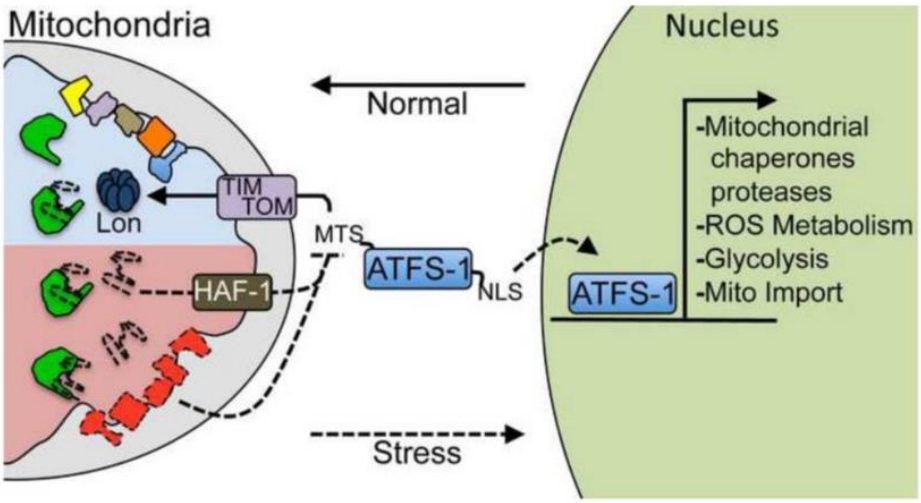

Figure 1.8 ATFS-1 signalling in the C.elegans mtUPR. From (Haynes, Fiorese et al. 2013)

The mammalian mtUPR presents a more complex picture. The pathways activated have proven to be myriad, acutely dependent on cell and stress type, and in many experimental paradigms the mtUPR appears cross-regulated with the integrated stress response (ISR) [see Section 1.5.2, The PERK pathway]. Activating Transciption Factor 5 (ATF5) was recently proposed to signal the mammalian mtUPR in a manner analogous to ATFS-1. A weak N-terminal MTS was identified in ATF5, in addition to its known NLS in the bZip domain. Expression of ATF5 is activated at the level of translation by phosphorylation of the initiation factor eIF2α, and hence at least in part by the ISR. When eIF2α phosphorylation was induced by the proteasome inhibitor Bortezomib, endogenous ATF5 became detectable in HeLa cells, and was enriched in the mitochondrial fraction. In the absence of experimental confirmation, nuclear translocation of ATF5 in response to mitochondrial stress was inferred from the transcriptional dependence of mtUPR targets on the protein; upregulation of *HSP60*, *mtHSP70* and the protease *LONP1* was abolished by knockdown of ATF5 in paraquat and OTC-Δ HEK293T cell models. Induction of *LONP1* was also ATF5-dependent in HEK293T cells treated with the mitochondrial toxins piericidin, antimycin and oligomycin (Fiorese, Schulz et al. 2016).

However, more latterly, a multi-omics study of four diverse mammalian mitochondrial stress models identified ATF4 and the ISR as key co-ordinators of the stress response in HeLa cells, and failed to detect upregulation of the proposed mtUPR targets or ATF5. In addition, neither paraquat treatment of HeLa cells, nor transfection of OTC-Δ, recapitulated the ATF5 results seen by Fiorese and colleagues in the HEK293T line (Quiros, Prado et al. 2017). Further, whilst a direct unfolded protein model in HeLa cells again described an ATF4-mediated response, involvement of the ISR was excluded, and instead a role for ATF3 was suggested (Munch and Harper 2016). Pioneering work from the Hoogenrad lab that established the OTC-Δ model had previously implicated the bZIP transcription factor CHOP in the mtUPR in COS-7 cells (Zhao, Wang et al. 2002) and subsequently involvement of the c-Jun/JNK pathway (Horibe and Hoogenraad 2007), as later seen in *Drosophila*, and murine intestinal epithelial cells (Rath, Berger et al. 2012). In the latter study, the authors proposed a mtUPR pathway that placed ClpP-mediated proteolysis upstream of phosphorylation of c-Jun and eIF2α by the ISR kinase PKR. A mtUPR pathway that utilises estrogen receptor activity and is unique to protein stress within the intermembrane space has also been outlined in MCF-7 adenocarcinoma cells (Papa and Germain 2011). In HepG2 liver cells, knockdown of ABCB10, the putative human homologue of *C. elegans* HAF-1, reduced expression of the mtUPR

chaperones and the *LONP1* protease, but did not affect the efflux of peptides from the mitochondria, suggesting a conserved role for ABCB10 in some, but not all, of the mtUPR pathways (Yano 2017). Involvement of the mammalian homologues of UBL5 and DVE-1 in the mtUPR has not been explored (Haynes, Petrova et al. 2007).

1.1.5.5 Mitochondrial retrograde signalling in the nervous system

Despite the strong association between mitochondrial dysfunction and neurodegenerative disease, comparatively little retrograde signalling research is conducted in the nervous system.

With regards to the mtUPR, it has been established in *C. elegans* that the ATFS-1 pathway is active in neurons. Additionally, under certain types of mitochondrial stress, the nervous system has cell non-autonomous control over mtUPR activation in distal tissues of the worm, adapting the biology of these tissues to the stress conditions. This non-autonomous control is dependent on the presence of functional ATFS-1 and DVE-1 - but not UBL-5 or HAF-1 - in the nervous system, and could be induced by neural overexpression of an N-terminally truncated form of ATFS-1 lacking an MTS (Shao, Niu et al. 2016).

In mammals, mitochondrial metabolic activity appears pivotal for the development of neuronal phenotypes. Pharmacological inhibition of the ETC in human-induced pluripotent stem cells (Fang, Qing et al. 2016), and genetic ETC manipulation in murine adult neural stem cells (Beckervordersandforth, Ebert et al. 2017) results in diminished neuronal differentiation, however the underlying mechanisms and contribution, if any, of mitochondria-to-nucleus signalling remain to be determined.

Gene expression profiling of the mammalian response to neuronal mitochondrial dysfunction has highlighted how the sophisticated biomolecular composition of the organelle, and its role as an integrator of multifarious signalling pathways, renders the mitochondrion a chaotic system; very similar perturbations in mitochondrial function can result in widely differing cellular responses. Transcription of nuclear-encoded OXPHOS genes was found to be unchanged in differentiated human neuronal precursors treated with Complex I inhibitor MPP^+ (Krug, Gutbier et al. 2014), but broadly downregulated in murine primary cortical neurons exposed to an alternative Complex I inhibitor,

rotenone (Yap, Chen et al. 2013). Similarly contradictory results arose for the import of extracellular cysteine. Upregulation of the cystine transporter SLC7A11 was considered an important facilitator in the synthesis of the antioxidant glutathione (Krug, Gutbier et al. 2014), whilst downregulation of the Slc1a1 cysteine transporter was identified as an obstacle to this synthesis, despite the upregulation of other genes involved in glutathione production (Yap, Chen et al. 2013). Two *in vivo* PD models of Complex I inhibition in the substantia nigra contain little overlap in the transcriptional changes they report. In rotenone-treated rats, the defining transcriptional response was an antagonistic up- and down-regulation of cell death pathway components (Meurers, Zhu et al. 2009), whilst MPTP-treated mice predominantly displayed changes in the regulation of synaptic and cell cycle-related genes (Miller, Callahan et al. 2004). However, encouragingly, two *in vitro* PD models utilising the Complex I and V inhibitor 6-OHDA report some common transcriptional changes (Holtz and O'Malley 2003, Ryu, Angelastro et al. 2005), and in one of the studies, the antagonistic upregulation of pro- and anti-apoptotic genes and increased expression of cell cycle-related genes, reported in the rat rotenone model (Ryu, Angelastro et al. 2005). In both 6-OHDA models, genes from the endoplasmic reticulum unfolded protein response pathways (ER UPR) (see Section 1.5) were upregulated. In common with other transcriptional analyses of neuronal mitochondrial dysfunction (Moisoi, Klupsch et al. 2008, Mazzio and Soliman 2012, Yap, Chen et al. 2013, Krug, Gutbier et al. 2014), expression of the ER UPR transcription factor ATF4 was upregulated in one 6-OHDA model (Ryu, Angelastro et al. 2005).

The functional consequences of mitochondrial retrograde signalling appear detrimental. A mtDNA mutation that causes hereditary deafness in humans, was shown to cause the apoptotic loss of murine spiral ganglion neurons via ROS-dependent activation of the transcription factor E2F1 (Raimundo, Song et al. 2012). Mutation of the molecular chaperone TRAP1 protects *Drosophila* against ROS-induced death via the transcription factor FOXO, implying that activity of wild-type TRAP1 is a damaging response to mitochondrial dysfunction (Kim, Yang et al. 2016).

1.2 *Drosophila* as a model organism

The fruit fly *Drosophila melanogaster* gained worldwide scientific recognition as a model genetic organism in the 'fly room' of Thomas Hunt Morgan at Columbia University in the early 1900s. *Drosophila* breed rapidly (~10 days from embryo to adult at 25 °C) and require little space to house, and therefore allow the conduct of large scale investigations spanning multiple generations. Morgan and his students used both naturally occurring and induced mutations to demonstrate that genes are inherited as distinct units on chromosomes, and could be mapped by their recombination frequency ((Morgan, Sturtevant et al. 1915) and reviewed in (Benson 2001)). Subsequent work over the intervening century has built an extensive *Drosophila* genetic toolkit for investigations of fundamental biological processes and disease mechanisms.

As early as 1918 the first balancer chromosome was introduced by Herman Muller, who used females with the dominant eye mutation *Bar* on an X chromosome with inversions to examine the rate of lethality caused by irradiation of males flies (Muller 1918). Balancers are homozygous lethal chromosomes created by mutagenisation and characterised by multiple inversions. Balancers chromosomes are sufficiently corrupted to prevent homologous recombination with a wild-type chromosome partner when they are present in heterozygotes. Dominant markers identify the presence of the balancer, and therefore allow heterozygous mutations or other genetic manipulation on the partner chromosome to be tracked and identified through generations (by the absence of the marker) (reviewed in (Kaufman 2017)).

Despite gaining fame with Thomas Hunt Morgan, *Drosophila* had actually made their laboratory debut a few years previously, in the lab of William Castle at Harvard University, where they were employed in behavioural analyses (reviewed in (Greenspan 2008)). The first *Drosophila* paper from the Castle lab detailed the reactions of the fly to gravity, light and mechanical stimulation (Carpenter 1905), and the findings underpin many of the today's functional assays, including the climbing assay. Behavioural analysis in *Drosophila* accelerated in the 1960s, driven by the work of Seymour Benzer who, amongst many discoveries, identified genes controlling circadian rhythm (Konopka and Benzer 1971), learning (Dudai, Jan et al. 1976) and lifespan (Lin, Seroude et al. 1998), and there are now many established protocols for the assessment of *Drosophila* function.

In late 1970s and early 1980s, Christiane Nüsslein-Volhard and Eric Wieschaus again utilised *Drosophila*'s tractability to pioneer the large-scale forward genetic screen,

looking for genes contributing to the patterning of the larva (Nüsslein-Volhard and Wieschaus 1980). They screened over 10,000 *Drosophila* lines produced by mutagenisation with ethyl methane sulfonate, and discovered 61 loci contributing to patterning on Chromosome II alone (Nüsslein-Volhard, Wieschaus et al. 1984).

A drawback to forward genetic screens is the subsequent need to map the identified mutations to the gene in which they reside. A first step towards large scale reverse genetic screens, in which the gene under manipulation is known, was taken by Brand and Perrimon in 1993, when they optimised the upstream activation sequence (UAS) for use in *Drosophila* with the yeast transcriptional activator, Gal4. The spatiotemporal expression of *Gal4* is controlled by the location of its insertion into the genome, for example, *Gal4* inserted into the synaptobrevin locus (*nSyb-Gal4*) is expressed in all post-mitotic neurons. Flies carrying the *Gal4* insert are crossed to flies with the *UAS* sequence upstream of a transgene of interest, and their progeny express the transgene in a time and tissue-specific manner (Brand and Perrimon 1993).

Subsequently, the discovery of RNA interference (RNAi) (Fire, Xu et al. 1998) and completion of the *Drosophila* genome sequence – which revealed that between 62-75% of human disease genes have homologues in the fly, dependent on scoring stringency (Adams, Celniker et al. 2000, Fortini, Skupski et al. 2000, Bier 2005) – paved the rest of the way towards reverse genetic screens in *Drosophila*. The first *Drosophila UAS*-RNAi library, the 'GD' library, covering 88% of predicted protein-coding genes in the genome was announced in 2007 (Dietzl, Chen et al. 2007), and was used to conduct the first ever tissue-specific reverse genetic screen – in any organism – which identified 23 new regulators of the Notch pathway in the development of thoracic sensory bristles (Mummery-Widmer, Yamazaki et al. 2009). There are now four large *Drosophila UAS*-RNAi libraries available worldwide (reviewed in (Heigwer, Port et al. 2018)), as well as *UAS*-open reading frame (ORF) lines for the overexpression of genes of interest (Bischof, Bjorklund et al. 2013). Drosophilists studying mitochondria are also aided by MitoDrome, the complete catalogue of all the *Drosophila* mitochondrial genes that are encoded by the nuclear genome (Sardiello, Licciulli et al. 2003).

In recent years, *Drosophila* have been successfully exploited to model human disease, either by manipulating the homologous *Drosophila* gene, or ectopically expressing the human disease gene. For example, the first mutant animal models of the PD-associated gene *parkin* were established in flies, and demonstrated that mutation of *parkin* led to mitochondrial defects (Greene, Whitworth et al. 2003, Pesah, Pham et al.

2004). Subsequently, the first *in vivo* models of *PINK1* mutation were also fly models, displaying similar mitochondrial dysfunction to that of the *parkin* mutants. In these *PINK1* models it was first shown that overexpression of wild-type *parkin* could compensate for loss of *PINK1*, and that the two genes operated within the same pathway (Clark, Dodson et al. 2006, Park, Lee et al. 2006, Yang, Gehrke et al. 2006). Both mutation of *parkin*, and downregulation of the catalytic subunit of mtDNA polymerase lead to dopaminergic neuron loss in *Drosophila* (Whitworth, Theodore et al. 2005, Humphrey, Parsons et al. 2012). Genetic and pharmacological manipulations of glutathione S-transferase (Whitworth, Theodore et al. 2005) and the cap-dependent translation inhibitor 4E-BP (Tain, Mortiboys et al. 2009) in *Drosophila parkin* mutants have been shown to suppress this neuron loss, and therefore represent therapeutic targets for neurodegenerative disease identified via the *Drosophila* model system.

1.2.1 *Drosophila* models of neuronal mitochondrial dysfunction and retrograde signalling

The *Drosophila* model system has been used to examine mitochondrial retrograde signalling in a variety of contexts. The mtUPR has not been methodically determined in *Drosophila*, but hsp60 and the fly homologue of mtHsp70 were both upregulated by overexpression or mutation of the mitochondrial chaperone *TRAP1* (Baqri, Pietron et al. 2014), knockdown of the ETC Complex I component ND-75 (Owusu-Ansah, Song et al. 2013), ubiquitous overexpression of OTC-Δ, and in *PINK1* and *parkin* mutant flies (Pimenta de Castro, Costa et al. 2012). In addition to induction of the canonical chaperones, nuclear translocation of Dve and upregulation of ClpP (Baqri, Pietron et al. 2014) and ClpX (Owusu-Ansah, Song et al. 2013) were also detected in some models. In the *Drosophila* ND-75 RNAi model, it was discovered that the raised levels of hsp60, mthsp70 and ClpX could be abrogated by overexpression of the antioxidant enzymes catalase and glutathione peroxidase I. Additionally, overexpression of the D-Jun and Relish transcription factors of the JNK and NF-κB redox signalling pathways induced chaperone and protease expression in wild-type flies (Owusu-Ansah, Song et al. 2013), lending weight to the idea that ROS production and signalling may be downstream of unfolded protein stress in some branches of the mtUPR.

Whilst much research has focused on the molecular changes invoked by mitochondrial unfolded protein stress, little attention has been paid to the functional consequences of mtUPR activation. In wild-type *Drosophila*, overexpression of Hsp60 isoforms extended lifespan and improved the locomotor function of aged flies. Knockdown of Hsp60C or ClpX reduced the mitohormetic effect of ND-75 RNAi on fly lifespan and mobility, and also similarly impaired wild-type controls (Owusu-Ansah, Song et al. 2013).

Drosophila possess a complex nervous system that is topologically similar to the mammalian one; two brain lobes and a spinal cord equivalent (the ventral nerve cord (VNC)) are composed of a neuronal cortex containing cell bodies that project into, and form circuits via, a neuropil (Fig. 1.9) (Power 1943). Functionally, signal propagation in *Drosophila* neurons is via Na^+/K^+ action potentials (Tanouye, Ferrus et al. 1981), and the identity and release mechanisms of neurotransmitters are also closely aligned with the mammalian system (reviewed in (Martin and Krantz 2014)). Synaptic plasticity occurs in both larvae (Budnik, Zhong et al. 1990) and the adult fly (Devaud, Acebes et al. 2001).

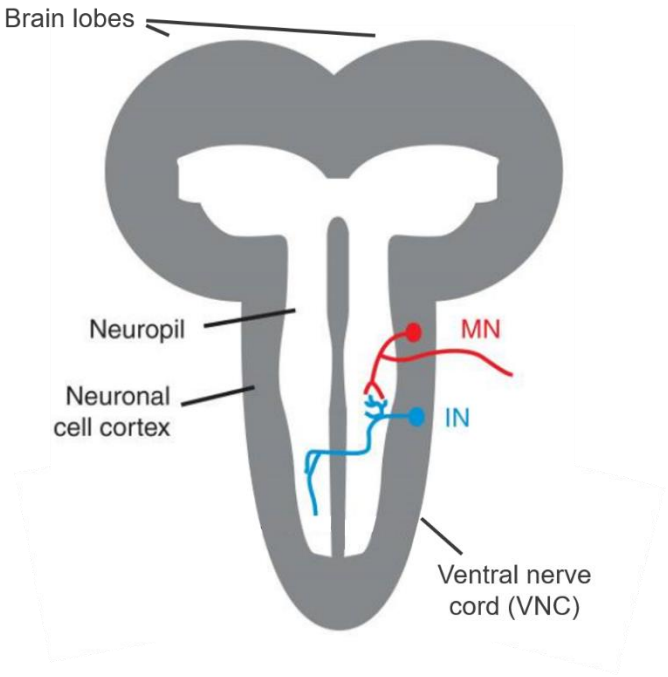

Figure 1.9. Schematic of the Drosophila central nervous system. MN = motor neuron. IN = interneuron. Adapted from (Freeman 2015).

The immense variety of retrograde signals that can occur in response to mitochondrial dysfunction are highly cell-type and context specific. Mitochondrial retrograde signalling in the nervous system remains underinvestigated, despite the potential to shed light on the numerous neurodegenerative diseases associated with mitochondrial dysfunction; the number of studies conducted is modest, and many have been purely molecular investigations of gene expression changes using *in vitro* models of acute toxic insult. By using *in vivo Drosophila* models of neuronal mitochondrial dysfunction, the extensive genetic tools and behavioural assays at the disposal of fly researchers, can be harnessed to tie the functional consequences of retrograde signalling to the molecular changes.

Analysis of retrograde signals in *Drosophila PINK1* and *parkin* mutants uncovered the upregulation of genes co-ordinating one-carbon metabolism and nucleotide salvage pathways (Tufi, Gandhi et al. 2014, Celardo, Lehmann et al. 2017). Further enhancement of these pathways by genetic manipulation or food supplements, was able to suppress the neurodegenerative phenotypes, once again demonstrating that therapeutic targets can be identified by work in the *Drosophila* model system.

Whilst the *PINK1* and *parkin* mutants are extremely relevant direct models of disease genes, the mutations are systemic. The *Gal4-UAS* system has enabled the specific targeting of genetic manipulations causing mitochondrial dysfunction to subsets of neurons. Overexpression of the mitochondrial transcription factor and mtDNA packaging protein TFAM in *Drosophila* neurons has been found to inhibit the expression of mitochondrially-encoded genes. When targeted to motor neurons, TFAM overexpression significantly reduced the number and volume of mitochondria in the distal axon and synapse of third instar larvae, and prevented normal active zone development, but did not lead to cell loss (Cagin, Duncan et al. 2015). TFAM overexpression has been used in *Drosophila* sensory neurons alongside overexpression of the mitochondrial structural protein prel as a mitochondrial dysfunction model to examine dendritic arborisation (Tsuyama, Tsubouchi et al. 2017). Both TFAM overexpression and prel overexpression caused dendritic arbor loss in sensory neurons. The retrograde signal was determined to travel via phosphorylation of the translation initiation factor eIF2α, and arborisation could be rescued by promoting the dephosphorylation of eIF2α.

Importantly, TFAM overexpression in motor neurons produces flies with locomotor and wing inflation deficits, thus allowing functional assays of candidate modifiers of neuronal mitochondrial retrograde signalling (Cagin, Duncan et al. 2015).

Climbing and wing inflation ability is reduced to about 50% of wild-type in the TFAM overexpression model, meaning that both suppression and exacerbation of the phenotype can be detected in the assays. Knock-down of the fly homologue of HIF-1α, and components of the Ras-ERK-ETS pathway, in *Drosophila* motor neurons suppressed the locomotor impairments caused by overexpression of TFAM (Cagin, Duncan et al. 2015, Duncan, Granat et al. 2018), identifying both pathways as therapeutic targets to be followed up in mammalian systems.

1.3 The endoplasmic reticulum (ER)

Mitochondria are physically and functionally connected to the endoplasmic reticulum (ER). The (ER) is a membrane system within the cytoplasm of eukaryotes. The ER was discovered in the first successful electron micrographs of cells (Porter, Claude et al. 1945). The net-like structure was not initially detected in the ectoplasm (near the plasma membrane) and was therefore named the endoplasmic reticulum (Porter and Kallman 1952). We know today that the ER is both continuous with the outer nuclear envelope (Watson 1955) and in contact with the plasma membrane (Pichler, Gaigg et al. 2001). In neurons, the ER extends from the cell bodies down the length of the axon into the synaptic boutons (Broadwell and Cataldo 1983, Broadwell and Cataldo 1984). The lipid composition of the ER membranes varies temporally and spatially according to the demand for synthesis, the trafficking of lipids to other organelles, and secretion into the extracellular space. In yeast, over half the ER membrane lipid content is phosphatidylcholine (PC), with phosphatidylinositol (24%) and phosphatidylethanolamine (10%) also constituting significant fractions (Tuller, Nemec et al. 1999). Functionally and morphologically (Palade 1955), the ER is divided into 'rough' and 'smooth' compartments, although the distinction is not always absolute.

1.3.1 The rough ER

The rough ER is classically composed of membrane sheets decorated with synthesising ribosomes, and is the site of folding and modification of proteins to be secreted or embedded in cellular membranes (Redman 1969). ER targeting signals are located at the N-termini of proteins and vary considerably, but all contain a central stretch of ≥8 hydrophobic residues (reviewed in (Martoglio and Dobberstein 1998)). The translated signal sequences of the nascent polypeptides bind to signal recognition particles (SRPs) in the cytosol and the ribosome-SRP complex is recruited to the ER by SRP receptors in the ER membrane. The SRP is then switched for a subunit of the Sec61 translocon and the protein is transferred through, or into, the ER membrane as it is synthesised (reviewed in (Walter, Gilmore et al. 1984) and (Nyathi, Wilkinson et al. 2013)). Once in the ER lumen, under normal conditions proteins are folded with the assistance of molecular chaperones and post-translationally modified by glycosylation. A 14-sugar precursor oligosaccharide is transferred to target asparagines co-translationally, and the group is

subsequently trimmed and/or added to with other sugar residues (reviewed in (Aebi 2013)). ER-resident proteins are retained within the ER by a four-amino acid KDEL motif (Munro and Pelham 1986, Pelham 1989), whilst proteins destined for secretion or other subcellular compartments are trafficked to the Golgi. Proteins that are not folded or processed correctly can be retrotranslocated back into the cytosol for degradation in a pathway termed ER-associated degradation (ERAD) (reviewed in (Meusser, Hirsch et al. 2005)).

1.3.2 The smooth ER

The smooth ER lacks ribosomes and is canonically composed of membrane tubules. It is the site of lipid and steroid synthesis, detoxification of xenobiotics and the products of metabolism, Ca^{2+} buffering and the final stages of the protein production. New subdomains of the ER continue to be identified, including ER exit sites (ERES) which mark the transition of ER tubules to vesicles which transit to the Golgi, cortical ER, the site of ER-plasma membrane contacts, and the ER quality control compartment (ERQC) where improperly processed proteins are held for ERAD (reviewed in (Lynes and Simmen 2011)).

1.3.3 Creation and maintenance of ER morphology

The cylindrical shape of ER tubules is maintained by the reticulon and REEP families (Voeltz, Prinz et al. 2006), along with ADP-ribosylation factor-like 6 interacting protein 1 (Arl6IP1) (Fig. 1.10) (Yamamoto, Yoshida et al. 2014). These factors are composed of two partial-membrane-width α-helices (Reticulon-homology domains (RHDs)) and reside in the outer leaflet of the ER membrane where they act as wedges that induce positive curvature.

The diameter of ER sheets and tubules are similar, at around 60-100 nm, thought to be due to the same families of proteins creating both the cylindrical tubules and the curves at the edges of the sheets. The intra-luminal distance within the sheets is maintained by the phosphoprotein Climp-63, which acts as a spacing bridge between the membranes (Shibata, Shemesh et al. 2010). The flat surface of the sheets is maintained by the coiled coil domain proteins Kinectin and p180 (Shibata, Shemesh et al. 2010).

Climp-63, Kinectin and p180 are not conserved in *Drosophila* (Goldstein and Gunawardena 2000, Shibata, Shemesh et al. 2010), and the diameter of ER tubules and sheets is reduced to around 30 nm in flies (Shibata, Shemesh et al. 2010), theoretically because of the absence of the Climp-63 spacer.

ER morphology is dynamic, and reconfigurations are an energy-dependent process. The mammalian, yeast and plant GTPases, Atlastin and Sey1p and RHD3 respectively, possess RHDs (Hu, Shibata et al. 2009, Chen, Stefano et al. 2011, Anwar, Klemm et al. 2012). They mediate membrane fusion via the dimerisation of their GTPase domains. Subsequent hydrolysis of GTP causes conformational changes in the proteins that pull the ER membranes together and force fusion (Bian, Klemm et al. 2011, Byrnes and Sondermann 2011, Byrnes, Singh et al. 2013, Yan, Sun et al. 2015). The *Drosophila* homologue of Atlastin has displayed fusion capabilities *in vitro* (Orso, Pendin et al. 2009). The genesis of new tubules appears to be dependent on distortions created by microtubules sliding (reviewed in (Westrate, Lee et al. 2015)).

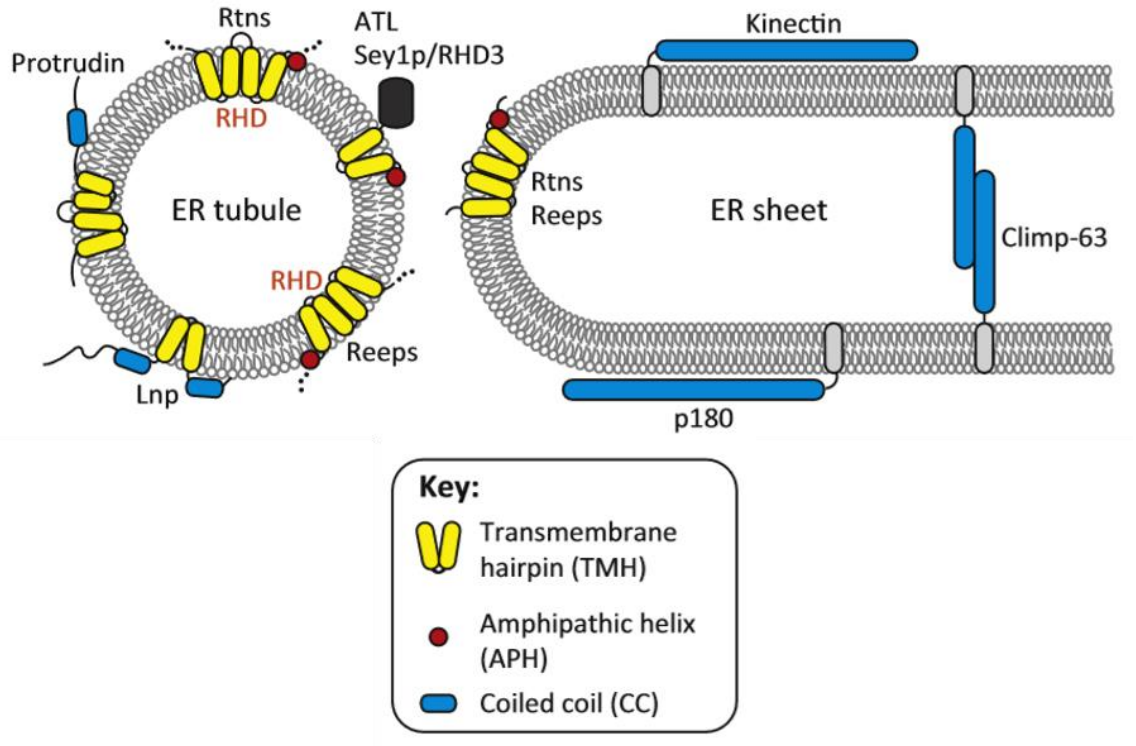

Figure 1.10 Proteins shaping the ER. From (Zhang and Hu 2016)

1.3.4 ER Ca^{2+}

The ER is the major intracellular Ca^{2+} store. ER Ca^{2+} uptake from the cytosol is mediated by the Sarco/endoplasmic reticulum Ca^{2+} ATPase (SERCA). Depletion of Ca^{2+} from the ER lumen results in the activation of store-operated Ca^{2+} entry (SOCE) by physical interaction of the ER membrane-resident Ca^{2+} sensor STIM with the plasma membrane Ca^{2+} channel Orai (Fig. 1.11) (Liou, Kim et al. 2005, Roos, DiGregorio et al. 2005, Feske, Gwack et al. 2006, Vig, Peinelt et al. 2006, Zhang, Yeromin et al. 2006). SOCE elevates the cytosolic Ca^{2+} concentration, which is used to replenish the ER stores via the SERCA pump. Ca^{2+} is released from the ER in response to activation of inositol triphosphate (IP_3) or ryanodine (RyR) receptors. In neurons, the RyR mediates calcium-induced calcium release - is activated by raised cytosolic Ca^{2+}. The IP_3 receptor is activated by IP_3 created by the cleavage of phosphatidylinositol 4,5-bisphosphate (PIP_2) in the plasma membrane by activated phospholipase C (reviewed in (Putney and Tomita 2012, Carreras-Sureda, Pihán et al. 2018)).

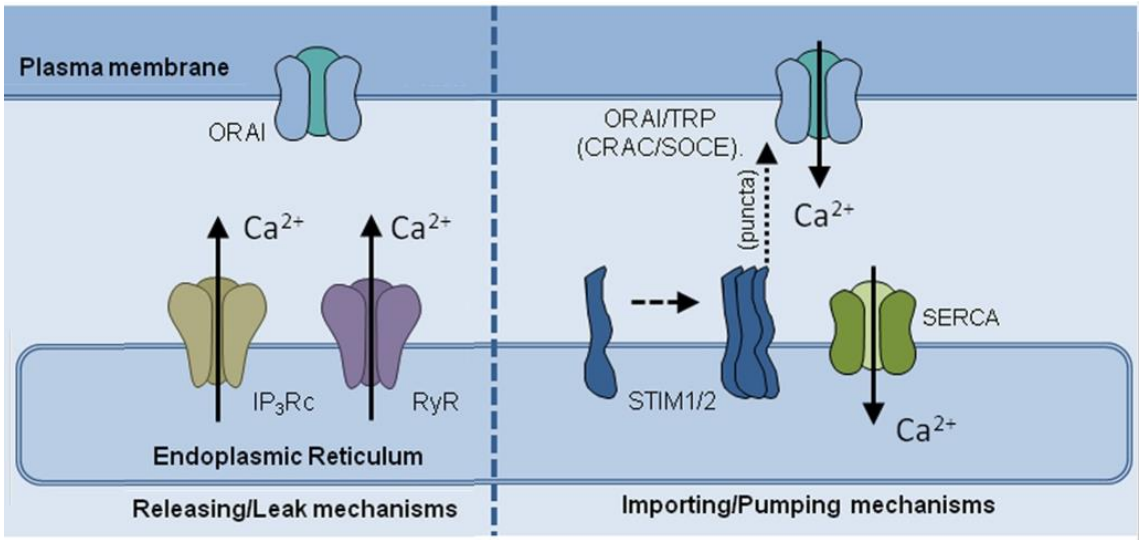

Figure 1.11 Major ER Ca^{2+} uptake and release mechanisms. Adapted from (Carreras-Sureda, Pihán et al. 2018).

1.4 ER-mitochondrial contacts

The physical and functional links between the ER and mitochondria are the subject of much recent research. Protrusions from the ER can mark the site of mitochondrial fission and play an active role in constriction of the mitochondrial membrane (Friedman, Lackner et al. 2011). Separately, the two organelles are tethered together at regions of the ER called mitochondria-associated membranes (MAMs), which can occur in both the rough and smooth ER (Csordás, Renken et al. 2006). The close apposition of the ER and mitochondria was first noted in 1960 (Robertson 1960), but it was another thirty years before biochemical evidence of their physical association was obtained, when a membrane fraction sedimenting immediately above the mitochondrial band from rat liver homogenate was found to contain the enzymes required for phospholipid synthesis (Vance 1990). MAMs facilitate the shared functions of the ER and mitochondria, including the transfer of Ca^{2+}, lipid synthesis and the regulation of autophagy (Gomez-Suaga, Paillusson et al. 2017). Abnormal ER-mitochondrial contacts are a feature of many diseases, including Alzheimer's, PD and amyotrophic lateral sclerosis (reviewed in (Paillusson, Stoica et al. 2016)), metabolic diseases such as diabetes (reviewed in (López-Crisosto, Bravo-Sagua et al. 2015)) and lysosomal storage diseases (reviewed in (Annunziata, Sano et al. 2018)).

1.4.1 ER-mitochondrial tethering proteins

In yeast, the maintenance of mitochondrial morphology protein 1 (Mmm1) and three members of the mitochondrial distribution and morphology protein (Mdm) family form a well-characterised tethering complex termed the ER-mitochondria encounter structure (ERMES) (Kornmann, Currie et al. 2009). The components of ERMES are not conserved in higher eukaryotes, and the identity of the mammalian ER-mitochondrial tethers is controversial. Binding between mitofusin2 in the ER and mitofusin 1/2 in the OMM has been proposed to constitute part of the mammalian connection between the ER and mitochondrial (de Brito and Scorrano 2009). However, the effect of mitofusin ablation on ER-mitochondria contacts is the subject of impassioned debate, with studies finding that a lack of mitofusin reduces ER-mitochondria contacts (Naon, Zaninello et al. 2016, Naon, Zaninello et al. 2017), whilst others fiercely defend their observation that mitofusin is a negative regulator of MAM formation, and that mitofusin knockout increases

ER-mitochondrial contacts (Cosson, Marchetti et al. 2012, Filadi, Greotti et al. 2015, Wang, Garcin et al. 2015, Leal, Schreiner et al. 2016, Filadi, Greotti et al. 2017). Regardless of how this debate is resolved, the inter-organelle distance at MAMs varies considerably (Csordás, Renken et al. 2006) and, accordingly, over 20 different proteins have been proposed to have roles in the physical linkage of mitochondria to the ER (Fig. 1.9) (reviewed in (Csordás, Weaver et al. 2018)). The identity of ER-mitochondrial tethering machinery – with the possible exception of mitofusin - remains unknown in flies.

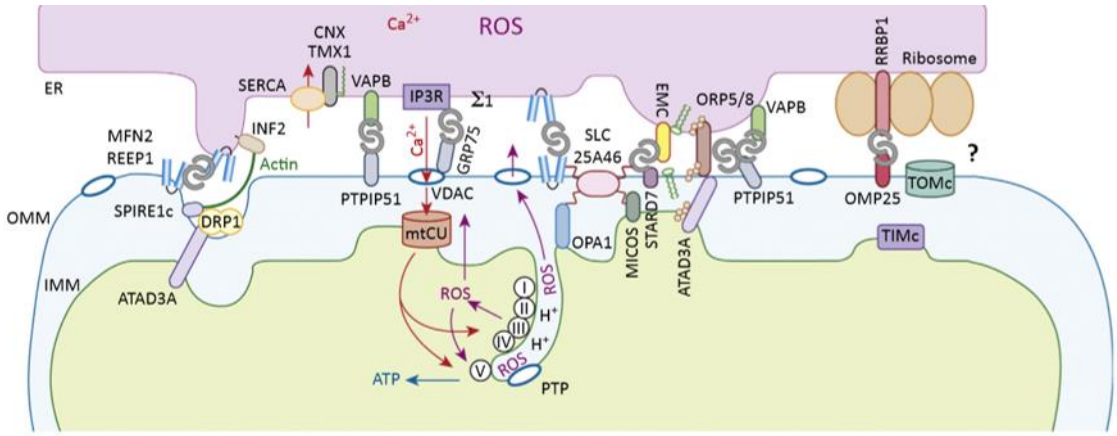

*Figure 1.12 ER-mitochondrial contact proteins.*From (Csordás, Weaver et al. 2018).

1.4.2 ER-mitochondrial Ca^{2+} transfer

Ca^{2+} transfer between the ER and mitochondria is mediated by the close appostion of VDAC and the IP_3 receptor, linked by the chaperone GRP75 (Szabadkai, Bianchi et al. 2006, De Stefani, Bononi et al. 2012). Locally high concentrations of Ca^{2+} in these 'microdomains' overcome the low Ca^{2+} affinity of the MCU in the IMM, and facilitate efficient import of Ca^{2+} into the matrix (Rizzuto, Brini et al. 1993, Rizzuto, Pinton et al. 1998). The VDAC-to-IP_3 receptor linkage is not required for the maintenance of ER-mitochondrial contacts (Csordás, Renken et al. 2006), and the efficacy of Ca^{2+} transfer is also regulated in the dendrites of mouse cortical neurons by the SMP-domain protein PDZD8 (Hirabayashi, Kwon et al. 2017), and in HEK293 cells by the presence of tethering complexes comprised of the transmembrane ER protein vesicle-associated membrane protein-associated protein B/C (VAPB) and the OMM resident protein tyrosine phosphatase interacting protein 51 (PTPIP51) (De Vos, Mórotz et al. 2012). *Drosophila* do not possess a homologue of PTPIP51.

1.4.3 ER-mitochondrial lipid synthesis

ER-mitochondria contacts are also the site of lipid exchange for the co-operative synthesis of phosphatidylethanolamine (PE), cardiolipin (CL) and phosphatidylcholine (PC). PE is synthesised in the IMM by the decarboxylation of phosphatidylserine (PS) (Borkenhagen, Kennedy et al. 1961, Dennis and Kennedy 1972, Percy, Moore et al. 1983), and PE generated elsewhere in the cell is not substantially trafficked to mitochondria (Burgermeister, Birner-Grunberger et al. 2004). PS is synthesised in the ER, and transferred to the mitochondria via MAMs. Some PE is returned to the ER where it can be methylated to create PC (reviewed in (Flis and Daum 2013)). Phosphatidic acid, the precursor to CL is also synthesised within the ER, transported to the mitochondria via MAMs and then converted to CL in a series of enzymatic reactions (Chang, Heacock et al. 1998, Chang, Heacock et al. 1998, Osman, Haag et al. 2010).

In yeast, a number of candidates for the ER-to-mitochondria transfer of phospholipids have been identified, including ERMES (AhYoung, Jiang et al. 2015), interaction of a second complex, the endoplasmic reticulum membrane protein complex (EMC), with the mitochondrial TOM protein, Tom5 (Lahiri, Chao et al. 2014), and binding of the intermembrane space proteins Ups1 (Connerth, Tatsuta et al. 2012, Watanabe, Tamura et al. 2015) and Ups2 (Miyata, Watanabe et al. 2016) with Mdm35. The exact molecular mechanism(s) by which the transfer occurs is unknown. In mammals, the OMM protein SLC25A46 interacts with homologues of the EMC, and mutation of SLC25A46 can alter the phospholipid composition of mitochondria (Janer, Prudent et al. 2016), but little else is known about the machinery of ER-mitochondria lipid transfer.

1.5 The ER unfolded protein response (UPR)

The ER unfolded protein response (UPR) is the collective term for three pathways that are activated by a loss of proteostasis in the ER and function to ameliorate the protein stress. Each branch of the ER UPR begins with a ER transmembrane protein, and ends with a transcription factor (Fig. 1.13).

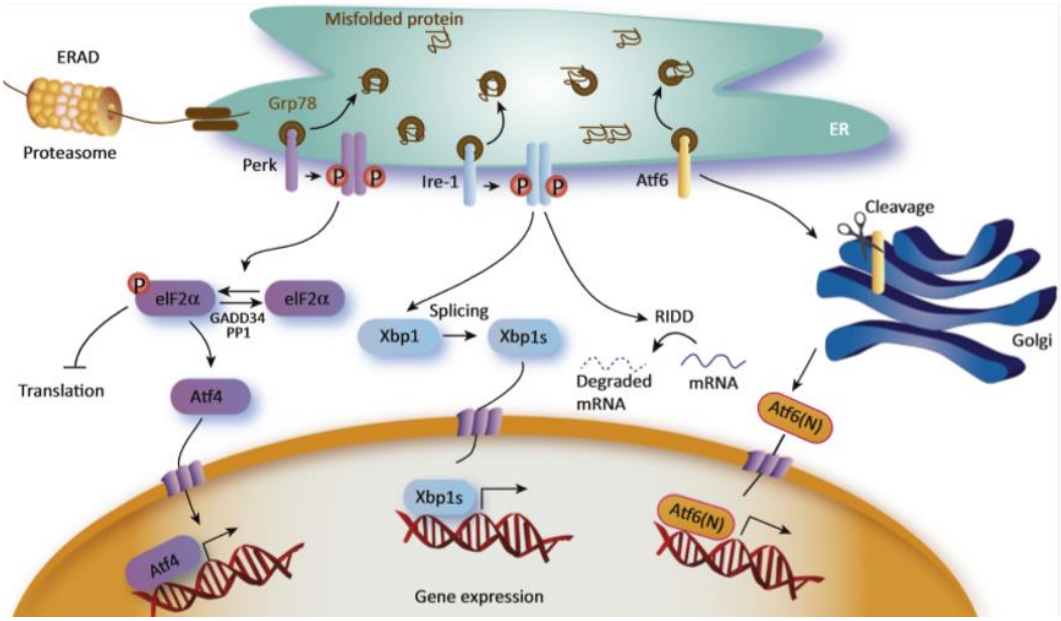

Figure 1.13 Overview of the ER UPR. From (Godin, Creppe et al. 2016).

1.5.1 The IRE1 pathway

Inositol-requiring enzyme 1 (IRE1) is the most conserved of the ER UPR transmembrane proteins, and is found in all eukaryotes (Mori 2009). IRE1 exists as a monomer in the membrane of the unstressed ER, but oligomerises in response to ER stress, permitting autophosphorylation of its cytoplasmic domain (Zhou, Liu et al. 2006, Korennykh, Egea et al. 2009, Ali, Bagratuni et al. 2011). Once phosphorylated, IRE1 gains ribonuclease activity (Ali, Bagratuni et al. 2011) and catalyses the specific splicing of the basic leucine zipper domain (bZIP) transcription factor XBP1 (Sidrauski and Walter 1997, Gonzalez, Sidrauski et al. 1999). In the absence of IRE1 activation, XBP1 mRNA is processed by

the canonical spliceosome, leading to the production of an inactive, truncated form of the protein. In response to ER stress, the phosphorylated IRE1 dimer removes an additional 26-nucleotide intron from XBP1 mRNA, creating a messenger that encodes a full-length active transcription factor. XBP1 translocates to the nucleus where it upregulates transcription of genes that serve to alleviate the unfolded burden within the ER (Cox and Walter 1996, Yoshida, Matsui et al. 2001).

IRE1 ribonuclease activity can also catalyse the bulk degradation of ER-targeted mRNAs encoding secreted and plasma membrane proteins, in a process termed regulated IRE1-dependent decay (RIDD). RIDD is quickly activated in response to ER stress, and functions to reduce the protein folding demand on the ER before the transcriptional alterations mediated by XBP1 take effect (Hollien and Weissman 2006). RIDD requires ER stress in addition to activated IRE1, indicating that other stress-responsive factors regulate the process (Hollien, Lin et al. 2009). Recently, inhibition of the ER transmembrane Protein kinase RNA-like endoplasmic reticulum kinase (PERK) was shown to block the degradation of a subset of RIDD-targeted transcripts (Moore and Hollien 2015) indicating that mRNA degradation is regulated by at least two branches of the ER UPR.

1.5.2 The PERK pathway

PERK is at the head of the second ER UPR branch. Like IRE1, PERK also undergoes oligomerisation and transautophosphorylation in response to ER stress (Harding, Zhang et al. 1999, Zhou, Liu et al. 2006, Su, Wang et al. 2008) and upon this activation, PERK gains kinase activity and phosphorylates Ser51 of the translation initiation factor eIF2α (Harding, Zhang et al. 1999, Harding, Zhang et al. 2000). P-eIF2α inhibits the exchange of GDP for GTP on eIF2β (Rowlands, Panniers et al. 1988), thus decreasing the availability of the ternary complexes eIF2-GTP-$tRNA_iMet$ and therefore reducing ribosome initation. Phosphorylation of eIF2α therefore suppresses global cap-dependent translation, reducing the load on the cell's protein folding machinery.

In mammals, eIF2α is the substrate of four kinases that are stimulated by separate cellular insults, and its phosphorylation marks the point of convergence of what is termed the integrated stress response (ISR). In addition to PERK, eIF2α can be phosphorylated by the heme regulated inhibitor (HRI) when the availability of heme is reduced (Levin,

Ranu et al. 1976, Ranu and London 1976, Farrell, Balkow et al. 1977), General control nonderepressible 2 (GCN2) in response to amino acid starvation (Chen, Throop et al. 1991, Dever, Feng et al. 1992, Sood, Porter et al. 2000), and Protein kinase RNA-activated (PKR) in response to viral infection (Galabru and Hovanessian 1985). Only PERK and GCN2 are conserved in *Drosophila* (Malzer, Szajewska-Skuta et al. 2013).

GADD34 functions as a negative feedback loop within the PERK branch of the ER UPR by targeting protein phosphatase 1 (PP1) to eIF2α, resulting in its dephosphorylation (Novoa, Zeng et al. 2001). In mammals, GADD34 is translationally regulated by 5'UTR uORFs (Lee, Cevallos et al. 2009), and transcriptionally upregulated by the ATF4 (see below) target CHOP (Marciniak, Yun et al. 2004). *Drosophila* do not possess a homologue of CHOP, but fly GADD34 is also regulated by 5'UTR uORFs that lead to its direct upregulation in response to phosphorylation of eIF2α (Malzer, Szajewska-Skuta et al. 2013).

1.5.2.1 Activating transcription factor 4 (ATF4)

Whilst eIF2α phosphorylation inhibits cap-dependent translation, it upregulates the translation of a specific subset of proteins that contain upstream open reading frames (uORFs) in their 5'UTRs. One such protein is activating transcription factor 4 (ATF4). In unstressed conditions, the ribosome initiates at the first uORF in the ATF4 5'UTR, and after translating the short peptide sequence, scans to the second uORF where translation reinitiates. The second uORF overlaps the ATF4 start codon, thus preventing the translation of ATF4. When the supply of ternary complexes is reduced by phosphorylation of eIF2α, the ribosome is unable to reinitiate at the second uORF and instead scans further to the ATF4 start codon where it begins translation (Vattem and Wek 2004).

ATF4 is a bZIP transcription factor of the ATF/CREB family, and was previously known as CREB2 (Hai, Liu et al. 1989, Karpinski, Morle et al. 1992). ATF4 can form heterodimers with the AP-1 and C/EBP transcription factor family members, and transcriptional regulation by ATF4 is context dependent, with both activation and repression reported (reviewed in (Hai and Hartman 2001)). ATF4 interacts with a number of proteins which regulate its stability and transcriptional targets. In particular, P300/CBP-associated factor is a ATF4 co-activator required for the full induction of

CCAAT-enhancer-binding protein (C/EBP) homologous protein (CHOP) in response to amino acid starvation in mammalian cell cultures (Chérasse, Maurin et al. 2007), and ATF4 complexes with Nrf2 to upregulate the anti-oxidant heme-oxygenase-1 in response to the ROS-inducer cadmium (He, Gong et al. 2001). ATF4 has a half-life of approximately 30 minutes in HeLa cells, with its degradation mediated by association with the E3 ubiquitin ligase component βTrCP, followed by proteasomal digestion (Lassot, Ségéral et al. 2001).

In *Drosophila*, ATF4 is also known as cryptocephal, as the heads of mutants fail to fully emerge from the thorax. *Drosophila* ATF4 plays a key role in the regulation of molting (ecdysis), by upregulation of ecdysis triggering hormone (ETH) in response to activation of the ecdysone receptor isoform B2 (Hewes, Schaefer et al. 2000, Gauthier and Hewes 2006, Gauthier, VanHaaften et al. 2012). The translational regulation of ATF4 by uORFs is conserved in *Drosophila* (Kang, Ryoo et al. 2015).

1.5.3 The ATF6 pathway

Another bZip transcription factor, ATF6, resides in the ER membrane and constitutes the entirety of the third branch of the ER UPR (Yoshida, Haze et al. 1998). In response to ER unfolded protein stress, vesicles containing ATF6 bud from the ER membrane and are trafficked to the Golgi, where the Site-1 (S1P) and -2 proteases (S2P) hydrolyse ATF6 within the luminal and membrane segments respectively. The cleaved cytoplasmic portion translocates to the nucleus where it activates ER UPR target genes (Haze, Yoshida et al. 1999, Ye, Rawson et al. 2000, Chen, Shen et al. 2002). A single isoform of ATF6 is conserved in *Drosophila*, and has been demonstrated to activate mTor in response to ER stress in S2R+ cells, in a manner dependent on S1P and S2P (Allen and Seo 2018).

1.5.4 Activation and regulation of the ER UPR pathways

In the 1970s and 80s, expression of two heat shock protein-related genes, glucose-regulated protein 78 (GRP78) and 94 (GRP94), was found to be increased by stresses related to the endoplasmic reticulum, including manipulation of calcium homeostasis, inhibition of glycosylation and the deliberate expression of mutated, unfoldable proteins ((Kozutsumi, Segal et al. 1988) and reviewed in (Lee 1987)). GRP78 was confirmed as a

molecular chaperone (Munro and Pelham 1986), also known as BiP, and binds the luminal face of IRE1, PERK (Bertolotti, Zhang et al. 2000) and ATF6 (Shen, Chen et al. 2002) monomers in unstressed cells. How IRE1, PERK and ATF6 are activated by unfolded protein stress remains to be fully elucidated, however it seems that separation of BiP from the three proteins plays a role in their activation. Deletion of the BiP-interacting regions of PERK and ATF6 led to the constitutive activation of PERK (Ma, Vattem et al. 2002), and translocation of ATF6 to the Golgi (Shen, Chen et al. 2002), suggesting that dissociation of BiP – probably to assist in the processing of unfolded proteins - directly activates those pathways. The dimersiation of IRE1 is promoted by loss of BiP (Bertolotti, Zhang et al. 2000, Kimata, Ishiwata-Kimata et al. 2007), but the subsequent binding of unfolded proteins is also thought necessary for IRE1 activation (Kimata, Ishiwata-Kimata et al. 2007), and BiP is considered a negative regulator of IRE1 that prevents excessive activation, rather than a direct activator (Pincus, Chevalier et al. 2010).

Whilst the IRE1, PERK and ATF6 branches of the ER UPR constitute separate pathways that are capable of simultaneous activation, it is also clear that cross-regulation of the branches can occur. PERK and ATF4 activation are required for both the transcriptional induction and ER-to-Golgi trafficking of ATF6 in mouse liver and MEFs treated with the ER stressor tunicamycin (Teske, Wek et al. 2011). ATF4 also upregulates transcription of IRE1 in mouse liver in response to tunicamycin treatment (Tsuru, Imai et al. 2016), whilst transcription of XBP1 is induced by ATF6 (Yoshida, Matsui et al. 2001).

1.5.5 The ER UPR in disease

The ER UPR is implicated in an extremely wide range of human diseases. Both PERK and IRE1 activation have been shown to drive the migration of T cells into skin lesions caused by the autoimmune disease vitiligo (Li, Zhu et al. 2017). Treatment with the chemical lipid chaperone 4-phenyl butyric acid (4-PBA) reduced ER stress and suppressed cell death in a macrophage model of atherosclerosis (Erbay, Babaev et al. 2009). Similarly, IRE1 activity was increased in macrophages extracted from the synovial fluid of rheumatoid arthritis patients, and blocking IRE1 ribonuclease activity via the small molecule inhibitor 4μ8C reduced joint inflammtion in a mouse model of the disease (Qiu, Zheng et al. 2013). Phosphorylation of eIF2α and induction of XBP1 splicing associated with apoptosis in pancreatic β-cells, were prevented by treatment with the

unsaturated fatty acid oleate in a model of palmitate-induced diabetes (Sommerweiss, Gorski et al. 2013).

In the nervous system, the ER UPR is associated with ischaemia, neurodegeneration and neuropsychiatric disorders. Blood cells from patients with bipolar disorder displayed attenuated activation of the ER UPR in response to thapsigargin or tunicamycin treatment (So, Warsh et al. 2007). Reducing eIF2α dephosphorylation via the phosphatase inhibitor salubrinal protected rat hippocampal neurons from excitotoxicity produced by administration of the glutamate receptor agonist kainate (Sokka, Putkonen et al. 2007). Manipulation of the ER UPR to alleviate the symptoms of neurodegenerative disease has also been achieved. Boosting the level of eIF2α phosphorylation by salubrinal treatment was also neuroprotective in a PD mouse model generated by overexpression of mutant α-synuclein (Colla, Coune et al. 2012). Another inhibitor of eIF2α dephosphorylation, Sephin1, alleviated the motor symptoms of mice in models of Charcot-Marie-Tooth 1B disease and amyotrophic lateral sclerosis (ALS), whilst also reducing the aggregation of SOD1 (Das, Krzyzosiak et al. 2015). Ablation of XBP1 in the same mouse model of ALS upregulated autophagy and increased the removal of the mutant SOD1, leading to increased life span (Hetz, Thielen et al. 2009). XBP1 knockout also increased survival in developing mice with the 6-OHDA model of PD, but was detrimental in older mice, causing neuron loss even without 6-OHDA treatment (Valdés, Mercado et al. 2014).

1.5.6 Impact of ER stress on mitochondria

Dysfunction of the ER can have dramatic consequences for mitochondria. A rare study of the early adaptations to ER stress caused by the glycosylation inhibitor tunicamycin, found increased ER-mitochondrial contacts and the enhanced transfer of Ca^{2+} to the mitochondria from the ER, which at this stage was associated with enhanced respiratory function (Bravo, Vicencio et al. 2011). Many investigations of apoptosis induced by ER stress that has not been adequately rectified by activation of the UPR, have reported the fragmentation of mitochondria, frequently attributed to Ca^{2+} overload and dissipation of the mitochondrial membrane potential (Frank, Gaume et al. 2001, Breckenridge, Stojanovic et al. 2003, Hom, Gewandter et al. 2007).

Given the close association of the ER with mitochondria, it is unsurprising that many studies have examined the effect of ER stress on mitochondrial morphology and function. Strikingly, however, the reverse is not true. Whilst investigations have established that the ER UPR can been activated by mitochondrial dysfunction (see 4.1), and ER-mitochondrial contacts are altered in disease models (see 6.1.4), none has examined the effect of impaired mitochondrial function on ER morphology.

1.6 Premise of this thesis

Mitochondrial dysfunction is associated with a wide range of neurodegenerative diseases, however few therapies exist, and comparatively little research has focused upon mitochondrial signalling in the nervous system. The *Drosophila* model system has been used to show that defective neuronal mitochondria can alter nuclear gene transcription and cellular signalling programs via mitochondrial retrograde signalling. Crucially, this signalling can be manipulated to improve neuronal function. There are close physical and functional links between mitochondria and the endoplasmic reticulum (ER), and ER stress has been shown to alter mitochondrial form and function. The impact of mitochondrial dysfunction on ER biology has been less explored, but given their physical links and shared functions, it is likely that perturbed ER biology has a critical role in the communication of mitochondrial dysfunction in the nervous system.

In this thesis, I hypothesise that mitochondrial dysfunction will alter aspects of ER biology and activate retrograde stress signalling in the form of the ER UPR. I further hypothesise that these retrograde signals will have functional consequences for the affected neurons, and that their characterisation and manipulation will identify novel therapeutic targets for neurodegenerative disease. I use the *Drosophila* model system in order that the functional consequences of manipulation of ER UPR genes can be assessed alongside characterisation of the molecular changes they may mediate.

I will address my hypotheses via the following aims:

1. Characterise the impact of neuronal mitochondrial dysfunction on ER biology, in particular, ER morphology, ER-mitochondrial contacts and Ca^{2+} handling.

2. Determine whether the ER UPR is activated by mitochondrial dysfunction in neurons, and whether this activation has functional consequences.

3. Determine the nature of ER UPR retrograde signalling (if any) to the nucleus in neurons with mitochondrial dysfunction by characterising transcriptional changes regulated by an ER UPR transcription factor.

2. Materials and Methods

2.1 Materials

2.1.1 Kits

Absolutely RNA Microprep kit (Agilent Technologies, Stratagene)

QIAquick Nucleotide Removal Kit (Qiagen)

QIAquick Gel Extraction Kit (Qiagen)

DNAse I Amplification Grade kit (Sigma-Aldrich)

First Strand cDNA Synthesis Kit (Fermentas)

2.1.2 Antibodies

Primary antibodies:

P-eIF2α (1:500, rabbit Anti-Phospho-eIF2α (Ser51), Cell Signaling Technology 9721), ATF4 (1:250, rat, produced in this study, see Section 2.2.5), β-Gal (1:1,000, mouse Anti-β-Galactosidase, Promega Z378A), Puromycin (1:500, mouse Anti-Puromycin, clone 12D10, Millipore MABE343)

Secondary antibodies:

All 1:1,000. Goat anti-rabbit Alexa Fluor 546 (Invitrogen A11035), Cy5 AffiniPure donkey anti-rat (JIR 712-175-153), goat anti-mouse Alexa Fluor 633 (Invitrogen, A21052), goat anti-mouse Alexa Fluor 680 (Invitrogen A21058).

Conjugated antibodies:

HRP-Cy3 (1:1,000, Cy3 AffiniPure Goat Anti-Horseradish Peroxidase, Stratech 123-165-021-JIR), HRP-Alexa Fluor 647 (1:1,000, Alexa Fluor 647 AffiniPure Goat Anti-Horseradish Peroxidase, Strateach 123-605-021-JIR)

2.1.3 Fly stocks

Spacial and temporal control of transgene expression in *Drosophila* utilised the *Gal4-UAS* system (Brand and Perrimon 1993). The yeast transcriptional activator *Gal4* is inserted into the control locus of a relevant gene, which then regulates the tissue- and time-specific expression of the Gal4 protein. The upstream activation sequence (*UAS*) has been optimised for Gal4 binding, and is cloned upstream of a transgene of interest. Flies carrying a *Gal4* insert (the driver line) are crossed to flies carrying the *UAS*-transgene insert, producing offspring which express the transgene in a tissue- and time-specific manner (Fig. 2.1). For example, in the *OK371-Gal4* driver line, *Gal4* is inserted into the locus of the vesicular glutamate transporter and thus Gal4 is expressed in all glutamatergic neurons (Mahr and Aberle 2006).

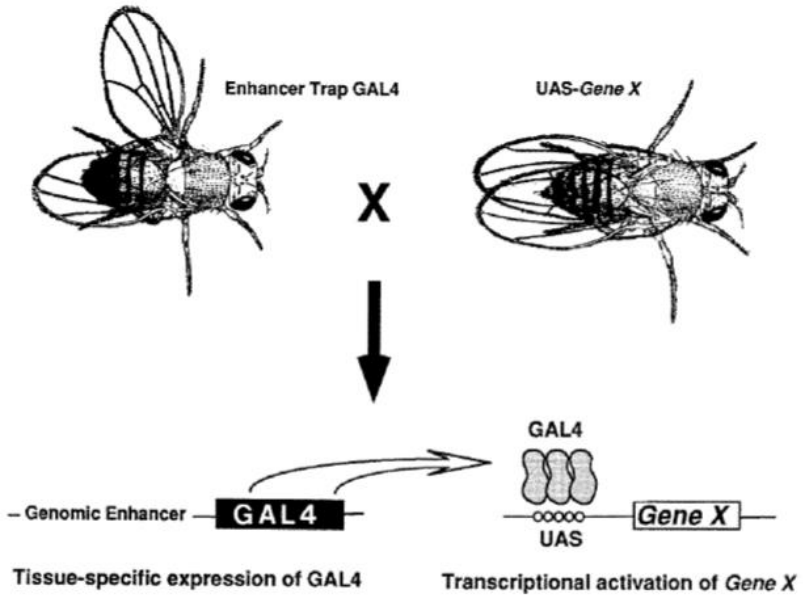

Figure 2.1 Overview of the Gal4-UAS system. From (Brand and Perrimon 1993).

Stock	Source & stock number	Construct ID
Background strain		
w^{1118}	Bloomington 6326	
Gal4 driver lines		
w^{*};*D42-Gal4*	Bloomington 8816	
w^{*};*Da-Gal4*	Bloomington 55851	
w^{1118};*OK371-Gal4*	Bloomington 26160	
nSyb-Gal4	Sousa-Nunes Lab, King's College London	
Balancer stocks		
w; *Sco*/*Cyo*; *MKRS*/*TM6B*	Alic Lab, University College London	
w; *Sco*/*Cyo*	Bateman Lab, King's College London	
UAS-TFAM3M; *Mef2*/*TM6B*	*Mef2* from Bloomington 27390	
Mitochondrial dysfunction models		
w^{1118};*UAS-TFAM3M*	(Cagin, Duncan et al. 2015)	
y^{1},*sc*,*v^{1};*UAS-ND75 dsRNA*	Bloomington 33910	HMS00853
ER morphology reporters		
w^{1118}; *OK371-Gal4,UAS-BiP-sfGFP-HDEL*	*UAS-BiP-sfGFP-HDEL (III) attP2* from Bloomington 64749	
w^{1118}; *OK371-Gal4,UAS-tdTomato-Sec61β*	*UAS-tdTomato-Sec61β (III) attP2* from Bloomington 64747	
w^{*}; *OK371-Gal4,UAS-lyso-RFP-KDEL*	*UAS-lyso-RFP-KDEL (III)* from Bloomington 30909	
OK371-Gal4,Rtnl1::YFP	*Rtnl1::YFP (II)* from (Lowe, Rees et al. 2014)	
Mitochondrial reporter		
w^{1118}; *OK371-Gal4,UAS-mitoGFP*	*UAS-mitoGFP* (II) from Bloomington 8442	

Ca^{2+} imaging		
w^{1118};OK371-Gal4, UAS-GCAMP6m	*UAS-GCAMP6m (II) attP40* from Bloomington 42748	
w^{1118};OK371-Gal4, UAS-CaMPARI	*w*;UAS-CaMPARI (II) attP40* from Bloomington 58761	
w^{1118};OK371-Gal4; UAS-4mtGCAMP3	*UAS-4mtGCAMP3 (III)* from (Drago and Davis 2016)	
w^{*};UAS-dTrpA1 (III) attP2	Bloomington 26264	
y^{1},v^{1};UAS-Stim dsRNA	Bloomington 27263	JF02567
ER UPR		
w^{1118}; UAS-PERK dsRNA	VDRC 16427	GD5584
y^{1},sc,v^{1};UAS-PERK dsRNA*	Bloomington 35162	GL00030
y^{1},v^{1};UAS-PERK dsRNA	Bloomington 42499	HMJ02063
w^{1118};UAS-PERK (III)	(Malzer, Daly et al. 2010)	
y^{1},v^{1};UAS-eIF2α dsRNA/TM3, Sb^{1}	Bloomington 44449	GLC01598
UAS-eIF2α (III) AttP 86Fb	FlyORF F001282	P002239
y^{1},sc,v^{1};UAS-GADD34 dsRNA*	Bloomington 33011	HMS00811
UAS-GADD34 dsRNA	VDRC 107545	KK104106
UAS-GADD34-HA (III) AttP 86Fb	FlyORF F003018	P006001
y^{1},v^{1};UAS-ATF4 dsRNA	Bloomington 25985	JF02007
w^{1118};UAS-ATF4 dsRNA	VDRC 2935	GD1407
UAS-ATF4-HA (III) AttP 86Fb	FlyORF F000106	P000084
y^{1},sc,v^{1};UAS-IRE1 dsRNA*	Bloomington 35253	GL00141
y^{1},sc,v^{1};UAS-IRE1 dsRNA*	Bloomington 62156	HMC05163
UAS-IRE1 (III)	(Coelho, Cairrão et al. 2013)	
y^{1},v^{1};UAS-XBP1 dsRNA	Bloomington 25990	JF02012
y^{1},sc,v^{1};UAS-XBP1 dsRNA*	Boomington 36755	HMS03015
w^{*};UAS-XBP1-EGFP (II)	Bloomington 60730	
y^{1},v^{1};UAS-ATF6 dsRNA	Bloomington 26211	JF02109
UAS-ATF6-HA (III) AttP 86Fb	FlyORF F000476	P000494

Integrated stress response		
y^1,sc,v^1;UAS-GCN2 dsRNA*	Bloomington 35355	GL00267
UAS-GCN2 dsRNA	VDRC 103976	KK103566
***Lacz* reporters**		
w^{1118};OK371-Gal4,UAS-nlacz	*UAS-nlacz* from Bloomington 3955	
w^{1118};OK371-Gal4,Thor-lacz	*y^1,w*;Thor-lacz* from Bloomington 9558	
Membrane marker		
w^{1118};OK371-Gal4,UAS-CD8-GFP	*UAS-CD8-GFP* from Tear lab, King's College London	

Table 1. Fly stocks used in this thesis.

2.2 Methods

2.2.1 Fly maintenance and breeding

Flies were maintained in incubators with a 12 hour light/dark cycle. General fly stocks were maintained at 18 °C, and working stocks at 25 °C. Virgin females were collected in the morning and evening. With the exception of experimental crosses, all fly work (maintenance of stocks, collection of flies for assays, storage of virgins etc) utilised R1 food (see below). Experimental crosses were set up on R2 (see below) supplemented with dried active yeast (Allinson), and unless otherwise stated, were incubated at 25 °C for the duration of the experiment.

Fly food recipe 1 (R1) was made as follows: 6.4 g Agar (Fisher), 64 g glucose (Sigma), 16 g ground yellow corn and 40 g Brewer's yeast (MP Biomed Europe) were mixed and cooked in 1 L (total volume) distilled water in a Systec MediaPrep steriliser. After cooling to below 60 °C, the preservative propionic acid (3 mL, Fisher), and antimicrobial agents methyl 4-hydroxybenzoate (1.8 g, Sigma) and ethanol (16 mL, Sigma) were added, and the mixture stirred for a further 10 minutes. The molten food was then dispensed into vials and bottles (Regina Industries Ltd), left to solidify, and stored

at 4 °C. Recipe 2 (R2) was identical in preparation, except for the addition of 80 g Brewer's yeast in place of the 40 g contained within the less rich R1.

2.2.1.1 Generation of fly stocks

To generate stocks where the transgene of interest (*TOI*), e.g. a dsRNA hairpin against an ER UPR factor, was on the third chromosome (i.e. not the same chromosome as *UAS-TFAM3M*), male flies with the *TOI* were crossed to virgins from the multiple balancer stock *w*; *Sco*/*Cyo*; *MKRS*/*TM6B*. Male progeny of the genotype +/*Cyo*; *TOI*/*MKRS* were collected, and crossed to <u>*UAS-TFAM3M*</u>; *Mef2*/*TM6B* virgins. Virgin and male progeny from that cross were collected to form the stock *UAS-TFAM3M*/(*Cyo*); *TOI*/(*TM6B*).

Homologous recombination in the female germline was harnessed to create stocks where the transgene of interest (*TOI*) resided on the same chromosome as *UAS-TFAM3M* (chromosome II). *UAS-TFAM3M* virgins were crossed to males with the *TOI*. *UAS-TFAM3M*/*TOI* virgins were collected from the progeny, and crossed to the double balancer stock *Sco*/*Cyo*. The progeny from this cross were examined for the presence of recombination. Flies heterozygous for the *UAS-TFAM3M* insert have orange eyes, and where the *TOI* also carried an eye colour marker, successful recombination could be judged by a darker combined eye colour. All recombinations were confirmed by PCR. Before genotyping by PCR, single males from the last cross, balanced over *Cyo*, were crossed to *Sco*/*Cyo* virgins. Males and virgins were collected from the progeny of this cross to create the final stock, and if the genotyping PCR was positive, the stock was kept.

To genotype each line, a single male fly was homogenised with a pestle in 50 µL of squishing buffer (25 mM NaCl (Fisher), 10 mM Tris-HCl (Fisher) pH 8, 1 mM EDTA (Fisher) pH 8). The homogenate was pulsed down in a microfuge, 1 µL of 10 mg/mL Proteinase K (Thermo Fisher) was added and the tube incubated at 37 °C for one hour. The Proteinase K was then inactivated by transferring the tube to 95 °C for 3 minutes. After centrifugation at 13,000 RPM for 5 minutes, 2 µL of the supernatant was used as the DNA template in PCR reactions.

For all genotyping, except the location of KK line hairpin RNA insertion sites (see below), the following PCR mix was used: 4 µL 5X Green GoTaq reaction buffer, 2 µL 8 mM dNTPs, 0.1 µL GoTaq G2 DNA polymerase (all from Promega), 1 µL 10 mM forward primer, 1 µL 10 mM reverse primer, 2 µL DNA template (from squished fly),

9.9 µL ddH_2O. See Table 2 for primers. The following program was then run on the PTC-200 Gradient Thermal Cycler PCR machine (MJ Research): 95 °C for 3 minutes, then 35 cycles of 95 °C for 30 seconds, 55 °C for 30 seconds and 72 °C for 90 seconds, followed by a final extension of 72 °C for 10 minutes.

The KK library of RNAi lines was designed to provide integration of the RNA hairpins at a single site, 40D on chromosome 2L. However, during construction of the library, RNA hairpins were instead aberrantly inserted at the 30B locus (also on chromosome 2L) in all lines, and additionally at the 40D locus in some lines. Therefore, a subset of KK lines possess duplicated RNA hairpins. This was discovered in 2016 (Vissers, Manning et al. 2016), and multiplex primers made available to test for the presence of these hairpins at 30B and 40D. Therefore KK line genotyping also included PCR to determine the presence or absence of the hairpins at 30B and 40D. The reaction mix was as follows: 4 µL 5X Green GoTaq reaction buffer, 2 µL 8 mM dNTPs, 0.1 µL GoTaq G2 DNA polymerase, 1 µL 10 mM C_Genomic_F primer OR 1 µL 10 mM NC_Genomic_F primer, 1 µL 10 mM pKC26_R primer, 1 µL pKC43_R primer, 2 µL DNA template (from squished fly), 8.9 µL ddH_2O. The PCR program was: 95 °C for 3 minutes, then 35 cycles of 95 °C for 30 seconds, 51 °C for 30 seconds and 72 °C for 90 seconds, followed by a final extension of 72 °C for 10 minutes.

Stock/primer name	Primer	Sequence
UAS-TFAM3M	Fwd	5’-GAGTCGCGCAAGGAGATG-3’
UAS-TFAM3M	Rvs	5’-GGATCGATAAGATTTCCGTGA-3’
Transgenic RNAi Project (TRiP) lines (from Bloomington):		
pVALIUM20	Fwd	5’-ACCAGCAACCAAGTAAATCAAC-3’
pVALIUM20	Rvs	5’-TAATCGTGTGTGATGCCTACC-3’
GD and KK lines (from VDRC):		
SV2	Universal Rvs	5’-CACAGAAGTAAGG TTCCTTCACAAAGATCC-3’
UAS-PERK dsRNA 16427	Fwd	5'-AGGATGATACCGACGACGACTAT-3'
UAS-GADD34 dsRNA 107545	Fwd	5'-GCGTTGTTATTCCGGTCACT-3'
UAS-ATF4 dsRNA 2935	Fwd	5'-AGGCGTCTTCATCTTTAGACAGC-3'
UAS-GCN2 dsRNA 103976	Fwd	5'-TGGCGAAGTGATGATTTATGAAT-3'
For KK line RNA hairpin insertion site(s):		
C_Genomic_F	Fwd	5'-GCCCACTGTCAGCTCTCAAC-3'
NC_Genomic_F	Fwd	5'-GCTGGCGAACTGTCAATCAC-3'
pKC26_R primer	Rvs	5’-TGTAAAACGACGGCCAGT-3’
pKC43_R primer	Rvs	5’-TCGCTCGTTGCAGAATAGTCC-3’

Table 2. Primers used for the genotyping of fly stocks.

2.2.2 Dissections and immunofluorescence

All dissections for imaging experiments were performed on larvae at wandering late third instar stage.

2.2.2.1 CNS dissections for immunofluorescence

The relevant fly crosses were left to egg-lay at 25°C for 3 days. The adults were then removed and the embryos incubated at 29°C (to enhance Gal4 activity) until dissection at third instar larval stage. For fixed imaging of the central nervous system (CNS), larvae were removed from their vial, cleaned in ice-cold PBS (Oxoid, Thermo Scientific), and then transferred to a drop of PBS on a Sylgard plate. The larvae were bisected with forceps (Agar Scientific), and the mouth end retained in the PBS. The cuticle was then inverted by coaxing the open end of the larvae over forceps holding the mouth parts. After the viscera was removed, the inverted cuticle with attached CNS was transferred to a 0.5 mL Eppendorf and fixed for 25 minutes in 4% formaldehyde (Thermo Scientific)/PBS. After three 10-minute washes with 0.1% Triton X-100 (Sigma)/PBS (PBS-T), the samples were blocked for one hour in 5% normal goat serum (NGS) (Yorlab)/PBS-T. The relevant primary antibodies were applied in 5% NGS/PBS-T, and left rocking overnight at 4°C. Following three further 10-minute PBS-T washes, the samples were incubated with secondary antibody/PBS-T at room temperature for one hour, and then washed x2 with PBS-T and x1 with PBS (10 minutes per wash). The samples were then transferred in PBS onto SuperFrost Plus microscope slides (ThermoScientific), where the cuticle was removed and the CNS mounted dorsal side up in Vectashield (Vector Laboratories) under 22 x 22 mm size 0 coverslips (Academy). The slides were stored at 4 °C in the dark.

2.2.2.2 NMJ dissections for immunofluorescence

For fixed imaging of the neuromuscular junction (NMJ), larvae were cleaned, stunned and placed in PBS on a Sylgard plate, as for the CNS. The head and tail ends of the larvae were then immobilised by micro-pin (Entomoravia) with the larvae dorsal side up, and the larvae cut open longitudinally with iridectomy scissors (Fine Science Tools). After the viscera was removed, two cuts perpendicular to the original central cut were made at each end to open up the larval cuticle into a rectangular fillet. The four corners of the

cuticle were pinned, and the PBS removed and replaced with 4% formaldehyde/PBS, in which the sample was fixed for 15 minutes. After fixation, the samples were transferred to 0.5 mL Eppendorfs in PBS-T, and the washes and primary/secondary antibody incubation proceeded as described for the CNS. Conjugated HRP antibodies were treated as secondary antibodies, and applied for one hour at room temperature (alongside any secondary antibodies relevant to the experiment). For mounting, samples were transferred cuticle side down to SuperFrost Plus microscope slides in PBS, the head and tail removed by iridectomy scissors, and the PBS replaced by Vectashield mounting medium. After 22 x 22 mm size 0 coverslips were applied, the slides were stored at 4 °C in the dark.

2.2.3 Microscopy and quantifications

All fixed and live images were taken on a Zeiss LSM 710 confocal microscope with ZEN software (Version 6, 2010). Settings were resolution = 1024 x 1024 pixels, averaging = 2, and speed = 9, unless otherwise stated. Samples were aligned using a 10x objective (numerical aperture (NA) = 0.30), and then images were taken using a 40x oil immersion objective (NA = 1.30). z-stacks were taken with inter-section intervals of 1 µm and 0.5 µm for the CNS and NMJ respectively. All image quantification was via the image processing software ImageJ (National Institutes of Health, USA).

For calcium imaging, see Section 2.2.4.

2.2.3.1 Quantification of mitochondrial morphology

A single section through the centre of the motor neuron cell bodies was selected from each z-stack. The images were then thresholded in ImageJ, and binary masks created. Regions of interest containing seven cell bodies were selected via the freehand tool, and then the number of mitochondria, and the area and perimeter of each mitochondria, was obtained via Analyze > Analyze particles. The minimum size cut-off was 0.01 μm^2 (particles below this size were not counted).

2.2.3.2. Quantification of ER morphology

Quantification of ER morphology was adapted from the method in (Yalçın, Zhao et al. 2017). ER morphology in neuronal cell bodies was quantified in the dorsal medial motor neuron clusters. After maximum intensity z-projections across 3 consecutive sections through the centre of the cells were obtained, the cells in each projection were numbered, and then three were selected by random number generator. Three lines per selected cell were drawn orthogonally from the nuclear to plasma membrane according to one of four pre-defined patterns - also selected by random number generator - giving a total of nine quantified lines per sample. The fluorescence intensity profile along each line was obtained via Analyze > Plot profile, and these values were transferred to an Excel spreadsheet. The variance and mean intensity of the fluorescent signal were computed across rolling windows of 5 pixels (~346 nm) for BiP-sfGFP-HDEL and lyso-RFP-KDEL, and 7 pixels (~363 nm) for tdTomato-Sec61β, and combined into the quotient 'Variance/mean intensity' to provide a readout of local fluctuations in fluorescence normalised to the local intensity of the signal. To compute the overall 'Variance/mean intensity' per sample, the mean of 'Variance/mean intensity' values per window (i.e. per 5 or 7 pixels) was calculated for each line, and then the mean of these nine values was obtained to give the final figure. To obtain the 'Variance/mean intensity' positional values, the 'Variance/mean intensity' for each successive window, from the nuclear membrane outwards, was averaged across all the lines drawn (giving n = 9 x no. of samples), and was plotted for all windows with $n \geq 20$. (i.e. the mean 'Variance/mean intensity' of the first window across all n lines, followed by the mean 'Variance/mean intensity' of the second window across all n lines, and so on until fewer than 20 lines were long enough to have the *i*th window). ER morphology at the neuromuscular junction was quantified in type 1b NMJs, on muscle 4, abdominal segment 2, of third instar larvae. 'Variance/mean intensity' was calculated along a segmented line that followed the contours of the axon from a terminal bouton to the junction of the axon with the segmental nerve. One line was drawn per sample. Overall 'Variance/mean intensity' and positional 'Variance/mean intensity' were calculated as described for cell bodies.

2.2.3.3. Quantification of ER-mitochondrial contacts

For quantifications of ER-mitochondrial contacts in the cell bodies of dorsal medial motor neurons, single sections across the centre of the cells were selected from the acquired z-stacks. Nine lines per sample were drawn orthogonally from the nuclear to plasma membranes, using the same random selection procedure described for ER morphology quantification (2.2.3.1), and the fluorescence intensity profile was obtained for each line and transferred to an Excel spreadsheet. To accommodate the wide range of fluorescence intensities displayed by the tdTomato-Sec61β and lyso-RFP-KDEL reporters, local thresholding was applied to determine the boundaries of the ER along the lines. Firstly, the profiles were smoothed to reduce noise by two rounds of averaging across 5 pixel windows. After this smoothing, pixels that represented peaks in the signal were identified as those for which the immediately adjacent pixels either side had lower fluorescence intensities. Troughs were similarly identified as pixels whose two immediate neighbours both had higher fluorescence intensities. Pixels along the smoothed fluorescence intensity profiles were considered to fall within the ER if they had an intensity value greater than the average of their nearest peak and trough. The same thresholding was applied to the mitoGFP signal, with the addition of a minimum cut-off because the signal was cleaner. The distance (in pixels) between the boundaries of the two organelles was then calculated. At ER-mitochondrial contact sites, the distance between the two organelles is 10-25 nm (Csordás, Renken et al. 2006). 106.27 µm x 106.27 µm images of tdTomato-Sec61β and mitoGFP were taken in 2048 x 2048 pixel frames (so 1 pixel represents ~52 nm), and therefore 0 pixel gaps between the ER and mitochondrial boundaries were considered to represent candidate ER-mitochondrial contact sites (i.e. the thresholded boundary of each organelle was located in the same pixel). For quantification of ER-mitochondria contacts at the neuromuscular junction, fluorescent intensity profile plots from the terminal boutons to the junction of the axon with the segmental nerve were obtained as described for ER morphology. These profile plots were then processed as described above for ER-mitochondria contacts in cell bodies.

2.2.3.4. Quantification of all other fluorescent images

For experiments with either a nuclear (*UAS-nlacz*) or membrane marker (*UAS-CD8-GFP*), maximum intensity projections of z-stacks through the dorsal side of the VNC were obtained. 50 points in the nuclear or cytoplasmic region of interest were then selected in the marker channel (e.g. CD8-GFP) without reference to the channel of interest (e.g. P-eIF2α). The average fluorescence intensity of those 50 points was then obtained in the channel of interest.

For experiments without nuclear or membrane markers, see Calcium imaging and quantifications (Section 2.2.4)

2.2.4 Calcium imaging and quantifications

2.2.4.1 Basal (unstimulated) calcium levels

2.2.4.1.1 Cytosolic and mitochondrial GCaMP imaging

Live imaging was performed for all experiments with the genetically encoded Ca^{2+} sensors, GCaMPs. Larvae were dissected in Schneider's medium (Sigma) to allow the high glutamate concentration to reduce muscle twitching. Pinned flat-preparations were created as described for NMJ dissections in 2.2.2.2, but instead of fixing, the tail and mouth structures were removed, the CNS retained and the sample then transferred to a SuperFrost Plus microscope slide by forceps, taking care to preserve the integrity of the axonal bundles and neuromuscular junction contacts. A coverslip was applied with 15 µL of Schneider's underneath to hydrate the sample. z-stacks were taken on the LSM710 confocal using the 488 nm laser, with 0.5 µm and 1 µm inter-slice intervals for the NMJ and VNC respectively. Maximum intensity projections were created for quantification of both the cytosolic and mitochondrial GCaMPs. 50 points were selected in fluorescent regions, and the average of those points computed to give the mean fluorescence for each sample.

2.2.4.1.2 Calcium modulated photoactivatable ratiometric integrator (CaMPARI) imaging

Individual wandering third instar larvae were selected from a vial, washed in room temperature PBS, and then allowed to orient themselves in normal crawling posture dorsal side up on a 22 x 22 mm size 0 coverslip. A drop of PBS was applied to a SuperFrost Plus microscope slide, and the coverslip was then inverted onto the slide, placing the larvae ventral side up in PBS. The ventral head region was then exposed to 30 seconds of UV epifluorescence, with the larvae tracked down the ocular to ensure that the CNS remained within the field of the laser for the duration of the UV exposure. Each larva was then immediately bisected, inverted and fixed in 4% formaldehyde/PBS for 25 minutes (as described for CNS dissections in 2.2.2.1). After 3 x 10 minute washes in PBS-T, and 1 x 10 minute wash in PBS, the CNS was mounted on a microscope slide in Vectashield, also as described in 2.2.2.1. The samples were imaged on the LSM 710 confocal with the default (green) and photoconverted (red) isoforms excited using 488 nm and 543 nm lasers respectively. For quantification, 50 points were selected in the cell bodies in the green channel of a maximum intensity projection of the dorsal half of the VNC. The average of those 50 points was then measured in both the green and red channels to give the red:green fluorescence ratio.

2.2.4.2 Stimulated calcium level imaging

After the removal of adults from the experimental cross, embryos were retained at 25 °C (i.e. not transferred to 29 °C) to avoid overactivation of TrpA1 channel. Wandering third instar larvae were bisected and the cuticle inverted (as described in 2.2.2.1) in hemolymph-like 3.1 (HL3.1) media (70 mM NaCl, 5 mM KCl (Fisher), 1.5 mM $CaCl_2$ (Sigma), 4 mM $MgCl_2$ (Sigma), 10 mM $NaHCO_3$ (Life Technologies), 5 mM Trehalose (Fisher), 115 mM sucrose (Sigma) and 5 mM HEPES (Alfa Aesar), from (Feng, Ueda et al. 2004)). The CNS was dissected from the inverted cuticle, and retained on the microscope slide in residual HL3.1. A 1 mm thick, 10 mm external diameter, rubber o-ring was placed around the CNS to serve as a mould for the agarose that was used to immobilise the sample during imaging. The o-ring was flooded with molten 1% low-melt agarose (2-hydroxyethyl agarose (Sigma), in HL3.1 media) ejected from a P1000 pipette with sufficient force to carry the CNS to the surface of the agarose. The slide was then placed in the fridge for ~5 minutes to allow the agarose to set, after which the o-ring was

carefully removed and a 22 x 22mm size 0 coverslip placed directly onto the agarose. Activation of the TrpA1 channel was achieved via a peltier (Hebei TEC1-12706) secured flush underneath the microscope slide during imaging. The peltier was connected to the Thurlby Thandar PL154 powerpack (RS Components) and calibrated to ramp to a temperature of 25 °C using an infrared thermometer (GM320, L-FENG-UK) pointed at the surface of the peltier whilst the voltage was adjusted. Time series were taken at 2 Hz on the LSM710 confocal microscope using the 20x objective (NA = 0.50). The duration of peltier on/off intervals were timed using a standard laboratory timer. Times series were quantified by plotting the profile of 50 points (selected within the region of interest e.g. the cell bodies) across each frame.

2.2.5 ATF4 antibody creation

A 180 bp region common to all isoforms of *Drosophila ATF4*, but upstream of the conserved DNA binding domain, was cloned into the pGEX4T-2 (Amersham) vector to create a 60 amino acid region of ATF4 tagged with full-length glutathione-s-transferase (GST).

Cloning procedure: the 180 bp insert was amplified by PCR from the *Drosophila* wild-type Oregon-R genome using primers

ATATTGGATCCGAATGTCTTTTGGACCAAAAGGC (Fwd – BamHI site)

AGCGACTCGAGAGCCATCATTGAGCTGGTAAT (Rvs – XhoI site)

and the high fieldity Q5 polymerase (NEB) according to the manufacturer's protocol. The PCR program was: 98 °C for 30 seconds, then 35 cycles of 55 °C for 30 seconds, 72 °C for 1 minute, 98 °C for 10 seconds, followed by a final extension of 72 °C for 5 minutes. The insert was purified using the Qiagen QIAquick Nucleotide Removal Kit and both insert and plasmid were double digested with BamHI and XhoI in the buffers recommended by the supplier (NEB). The digested fragments were purified with Qiagen QIAquick Gel Extraction Kit before being combined in a 1:3 vector:insert molar ratio with T4 DNA ligase (HC) (Thermo Fisher Scientific). After 6 days at 4 °C, 1 µL of the ligation mixture was used to transform One Shot TOP10 chemically competent *E. coli* (Thermo Fisher Scientific), which were then plated onto ampicillin-agar plates. After overnight incubation at 37 °C, colonies were miniprepped using the alkaline lysis method,

and tested for the presence of cloned plasmid by restriction enzyme digest. Positive preps were Sanger sequenced (Souce BioScience) to confirm correct cloning.

Fusion protein (antigen) expression and purification: The pGEX-4T-2-ATF4 plasmid was transformed into competent BL21 (DE3) cells (NEB) for protein expression. A 3 mL positive culture of BL21 (DE3)-pGEX-4T-2-ATF4 in LB broth (Fisher) was then grown at 37 °C and induced by 0.1 mM (final concentration) IPTG (Sigma). After two hours the cells were pelleted, lysed and run on an SDS-PAGE gel (see 2.2.6) and stained with Coomassie (Pierce, Thermo Fisher Scientific) to confirm the solubility of the ATF4-GST fusion. For larger scale production of the antigen, a 3mL starter culture in 2xTY media (1.6 g Bacto-Tryptone (Becton, Dickinson & Co.), 1 g yeast extract (Oxoid, Thermo Scientific) 0.5 g NaCl in 100 mL ddH_2O, pH 7) was grown all day in a shaking incubator at 37 °C, and then 400 µL was used to innoculate a 20 mL 2xTY overnight culture. The following day, 10 mL of the overnight culture was used to innoculate a 500 mL final culture of BL21 (DE3)-pGEX-4T-2-ATF4 in 2xTY. Protein expression was induced by 0.1 mM IPTG when the culture reached an OD600 of 0.8. The culture was left shaking at 37 °C for a further 5 hours after induction, and then decanted into 10 x 50 mL Falcon tubes and pelleted at 4,000 g for 15 minutes. The pellets were combined and resuspended in 30 mL ice-cold lysis buffer (50 mM Tris, 50 mM NaCl, pH 7.5) and then sonicated on ice. The sonicated solutions were re-pelleted at 12,000 RPM, 4 °C, for 10 minutes, the supernatant removed and saved, and the pellet resuspended in 20 mL lysis buffer. The 20 mL solution was re-sonicated, then re-pelleted (12,000 RPM, 4 °C for 10 minutes) and the supernatant combined with the 30 mL saved from the first sonication to give 50 mL of supernatant containing cellular proteins. 0.75 mL (bed volume) of glutathione sepharose beads (4B, GE Healthcare), pre-washed x4 in ice-cold lysis buffer, were added to this supernatant and it was left rocking at 4 °C for three hours. The beads were then pelleted (2,000 RPM, 4 °C, for 2 minutes), the unbound proteins removed, and the beads washed three times with 50 mL lysis buffer (resuspended in lysis buffer, then re-pelleted at 2,000 RPM, 4 °C, for 2 minutes). The ATF4-GST fusion was eluted in 3 x 1 mL elution buffer (PBS + 10 mM glutathione (Sigma)) by adding 1 mL of buffer, rocking at 4 °C for 10 minutes and then pelleting at 2,000 RPM, 4 °C for 2 minutes. 10 µL of eluate was run on an SDS-PAGE gel alongside bovine serum albumin (BSA) standards, and the estimated concentration of ATF4-GST was 700 µg/mL.

Antibody production from the antigen: 2.5 mL of purified ATF4-GST was sent on ice to Envigo RMS UK Ltd, who immunised Sprague Dawley rats with the antigen alongside Freund's Complete Adjuvant, performed three booster injections of the antigen with Freund's Incomplete Adjuvant and then harvested the antisera, which was shipped to us at -20 °C. On arrival, 0.01% (final concentration) sodium azide was added, and the antibody stored at -20 °C.

2.2.6 Translation assay and western blot analysis

For each genotype, the CNS were dissected from 30 third instar larvae by bisection and inversion of the cuticle (as described in 2.2.2.1). Dissection was performed in room temperature Schneider's medium, and the 30 CNS placed in a 1.5 mL Eppendorf containing 500 µL room temperature Schneider's. The Schneider's was then removed from the Eppendorf by a gel-loading pipette tip (VWR) - further narrowed by compression with forceps, to avoid removing the CNS alongside the media – and replaced with 24 µL of ice-cold solubilisation buffer (300 mM NaCl, 15 mM $MgCl_2$, 15 mM Tris-HCl pH 7.5, 1% Triton-X100, 2 mM DTT (Fisher Scientific), 100 µM puromycin (Sigma)) + 1.2 µL of 20 U/mL RiboLock RNAse inhibitor (Thermo Fisher Scientific). The samples were pipetted up and down 50 times with a P200 pipette to homogenise, and then left at 4 °C for 10 minutes to allow puromycin incorporation into nascent polypeptides. To quench the reactions and prepare the samples for sodium dodecyl sulfate-polyacrylamide gel electrophoresis (SDS-PAGE), 6 µL of 5x SDS loading buffer (30% glycerol (Sigma), 4.5% SDS (VWR), 250 mM Tris pH 6.8, trace of bromophenol blue (Fisher)) was added and the samples incubated at 95 °C for 10 minutes, before storage at -20 °C.

The incorporation of puromycin was assessed by western blot (the samples were run on an SDS-PAGE gel, transferred to a nitrocellulose membrane, and probed with an antibody to puromycin) as follows:

Creation of the SDS-PAGE gel: The 13% running gel was made by mixing 3.2 mL 40% acrylamide (Fisher), 2.5 mL 1.5 M Tris pH 8.8, 0.15 mL 10% SDS and 4.15 mL ddH_2O in a 15 mL Falcon. The polymerising agents 20 µL tetramethylethylenediamine (TEMED) (Sigma) and 70 µL 10% ammonium persulfate/ddH_2O (APS) (Sigma) were then added and the gel poured between glass plates (Bio-Rad) set at 1 mm distance. A

layer of isopropanol was applied to level the top surface of the gel. After 30 minutes, the isopropanol was removed, the top of the gel rinsed with ddH_2O and the inter-plate gap dried with filter paper. An 8% stacking gel was made by mixing 1 mL acrylamide, 1.25 mL 0.5 M Tris pH 6.8, 0.05 mL 10% SDS and 2.7 mL ddH_2O, then adding 7 µL TEMED and 45 µL APS. The stacking gel was poured on top of the polymerised running gel, and a 10-well comb added to create the wells for protein loading.

Electrophoresis: After the stacking gel was left to polymerise for 30 minutes, the comb was removed and the gel plates secured within the running module of a Bio-Rad electrophoresis cell, opposite a buffer dam. Running buffer (0.025 M Tris, 0.19 M glycine, 0.1 % SDS, pH 8.3) was added to the indicated level on the tank. Prior to loading, the samples were thawed, briefly microfuged, and the supernatant transferred to a new Eppendorf. 0.5 µL 1 M DTT was added and the samples re-incubated at 95 °C for 2 minutes. After cooling, 25 µL of each sample was loaded into the gel and run at 70 V for 30 minutes through the stacking gel, and then 100 V for two hours.

Transfer: Separated proteins were transferred to a 0.2 µm nitrocellulose membrane (GE Healthcare) via the Xcell SureLock transfer chamber at 25 V for 2 hours. Transfer buffer was 0.025 M Tris, 0.19 M glycine, 0.1 % SDS, 20% methanol, pH 8.3.

Antibody and imaging: After the blot was blocked in 10% dried milk (Marvel)/Tris-buffered saline (TBS), the primary anti-puromycin antibody was added 1:500 in 5% dried milk in Tween 20(Sigma)/TBS (TBS-T) and incubated overnight at 4 °C. The following morning the blot was washed four times in TBS-T (10 minutes per wash) and then incubated with secondary antibody (Alexa Fluor 680) in 5% milk/TBS-T for one hour. After washes x2 with TBS-T and x2 with TBS, the blot was scanned on the Odyssey Imager (LI-COR).

2.2.7 Assays of neuronal function

2.2.7.1 Climbing assay

Male flies of appropriate genotype were selected under CO_2 anaesthesia, within 24 hours of eclosion. Assays were undertaken 24-48 hours later to allow the flies to recover from

the anaesthetic, 1-3 hours after morning illumination. Individual flies were aspirated from a vial into a 10 mL serological pipette (Falcon). Flies were relocated to the base of the pipette by tapping against the bench. The height obtained in three, continuous, 10 second climbs was measured for each fly, and the mean computed to give the data point for that insect (Fig. 2.2 A). Wandering (i.e. non-vertical) or discontinuous climbs were excluded. Climbing assays assessing the impact of XBP1 knock-down (line 25990) and XBP1-EGFP overexpression were performed by Rhian Ford and Jordan Briscoe respectively.

2.2.7.2 Wing inflation assay

All flies that eclosed from each cross were collected under CO_2 anaesthesia, and stored at 25°C for ≥24 hours to ensure that an uninflated wing phenotype was not due to young age. The number of flies in each category - inflated, semi-inflated and uninflated (Fig. 2.2 B) - were then counted. Chi-squared tests were performed on the raw data (i.e. not the percentages) to determine significance.

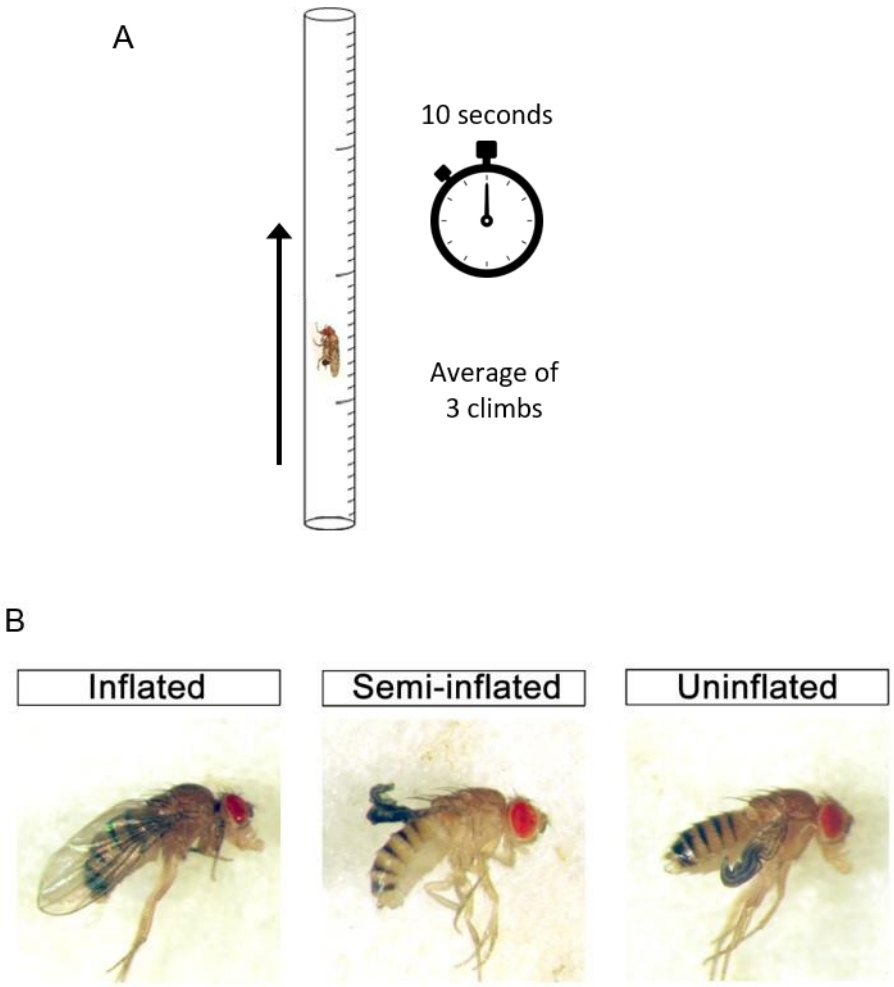

Figure 2.2 Assays of neuronal function. (A) Schematic of the climbing assay. (B) Adult *Drosophila* with inflated, semi-inflated and uninflated wings. Photos courtesy of Olivia Duncan.

2.2.8 RNA sequencing

2.2.8.1 qRT-PCR

Before RNA sequencing was undertaken, qRT-PCR was performed to confirm that expression of dsRNA against ATF4 by RNAi line 25985 caused a knock-down of ATF4 mRNA. The follow intron-spanning primers were used for *ATF4* and the housekeeping gene *Rpl4*:

ATF4 forward:	5'- ATTCACTGCTGCCGCAAAA-3'
ATF4 reverse:	5'-GTTCAACGTTGCCTTTTGGT-3'
Rpl4 forward:	5'-TCCACCTTGAAGAAGGGCTA-3'
Rpl4 reverse:	5'-TTGCGGATCTCCTCAGACTT-3'

RNAi line 25985 was driven ubiquitously by the Daughterless-Gal4 (*Da-Gal4*) driver. Control larvae were the progeny of *Da-Gal4* crossed to w^{1118}. After egg-laying for three days at 25 °C, the embryos were incubated at 29 °C until wandering third instar larval stage, when the larvae were homogenised for RNA extraction.

Three larvae per replicate were homogenised with a pestle in 100 µL TRIzol (Life Technologies). The homogenate was left at room temperature for five minutes before the addition of 20 µL chloroform, followed by shaking for 15 seconds, and then another three minutes incubation at room temperature. After microcentrifuging at 12,000 g, 4 °C for 15 minutes, the upper phase was decanted into a new Eppendorf. 50 µL of isopropanol was added (to the new tube) and the mixture vortexed for 10 seconds. After incubation at room temperature for 10 minutes, the samples were spun at 12,000 g, 4 °C for 10 minutes and the supernatant discarded. The RNA pellet was washed by the addition of 200 µL 70% ethanol, spun at 12,000 g, 4 °C for five minutes, and the ethanol removed. The RNA was then resuspended in 34 µL RNAse-free water, the concentration of each replicate measured using the NanoDrop Spectrophotometer (Thermo Scientific), and each replicate diluted to 150 ng/µL.

DNAse I treatment was performed with the DNAse I Amplification Grade kit from Sigma-Aldrich. For each sample, 2 µL of reaction buffer and 2 µL of RNAse-free DNAse I were added to 16 µL of RNA, and the mixture incubated at room temperature

for 15 minutes before 2 µL of Stop solution was added and the samples then incubated at 70 °C for 10 minutes.

cDNA was synthesised from 10 µL RNA via the Fermentas First Strand cDNA Synthesis kit. DNAse I-treated RNA was incubated in a PCR tube at 70 °C for five minutes with 1 µL 0.2 mg/mL random hexamer primers, then chilled on ice momentarily and briefly pulsed in the microfuge. 4 µL of 5X M-MuLV buffer, 1 µL 20 U/mL RiboLock RNAse inhibitor (Thermo Fisher Scientific), 2 µL 10 mM dNTPs and 2 µL (20 U/µL) M-MuLV reverse transcriptase were then added, and place in the PTC-200 Gradient Thermal Cycler PCR machine for the following program: 25 °C for 10 minutes, 37 °C for one hour, 70 °C for 10 minutes.

The cDNA was tested for genomic DNA contamination by 'normal' PCR with the primers to be used for qRT-PCR (above). The reaction mixture was as follows: 5 µL 2X PCRBio Ultramix (PCR Biosystems), 0.5 µL 10 µM forward primer, 0.5 µL 10 µM reverse primer, 2µL cDNA, 2 µL ddH_2O. The PCR program: 95 °C for 10 minutes, then 35 cycles of 95 °C for 10 seconds, 60 °C for 15 seconds, 72 °C for 20 seconds. All samples were free of genomic DNA.

qRT-PCR was then performed on 30 ng/µL cDNA using the Roche Lightcycler 480 Instrument II. Eight replicates of each condition (control and ATF4 knock-down) were run in triplicate. The mix per reaction was: 5 µL qPCRBIO Sygreen Mix Lo-ROX (PCRBiosystems), 0.4 µL forward primer, 0.4 µL reverse primer, 4.2 µL cDNA. The qPCR program was: 95°C for 10 minutes, then 45 cycles of 95 °C for 10 seconds, 60 °C for 15 seconds and 72 °C for 20 seconds, and then a ramp to 95 °C to obtain the melt curves. cDNA standards from 120 ng/µL to 1 ng/µL were made by serial dilution and run under the same protocol to assess the efficiencies of the *ATF4* and control (*Rpl4*) primers, which were comparable. Relative gene expression was calculated by the $2^{-\Delta\Delta Ct}$ method: the mean Ct value for *Rpl* was subtracted from the mean Ct value for *ATF4* for each sample, giving ΔCt. The smallest of the ΔCt values was then subtracted from the other ΔCt values, giving ΔΔCt. Both the *ATF4* and *Rpl4* primers had efficiencies of ~100%, so it could be assumed that a ΔCt equal to 1 implied a two-fold decrease in expression level, and therefore relative gene expression for each sample could be expressed as $2^{-\Delta\Delta Ct}$.

2.2.8.2 RNA sequencing

Fly crosses were carried out as described in 2.2.1, and incubated at 25 °C for the duration. For each replicate, 20 CNS were dissected from third instar larvae in cold PBS, and placed into 100 µL of lysis buffer + β-mercaptoethanol from the Absolutely RNA Microprep kit (Agilent Technologies) after excess PBS had been removed from the forceps by touching against a paper towel. The lysis buffer was kept on ice for the duration of the dissections, and each larval CNS was transferred individually to the lysis buffer immediately after dissection. Each genotype was prepared in quadruplicate. RNA was extracted from the CNS tissue using the Absolutely RNA Microprep kit according to the manufacturer's protocol, and RNA quality was confirmed using the RNA Pico Chip (Agilent Technologies) by Dr David Chambers. The samples were sent to the NGS Laboratory at Glasgow Polyomics, where they prepared polyA cDNA libraries using the TruSeq Stranded mRNA kit (Illumina), and oversaw 75 bp single-end sequencing at a depth of 25 million reads on the Illumina NextSeq 500. The raw unaligned reads were received in fastq format, and mapped to the *Drosophila melanogaster* genome by Bateman Lab postdoc Dr Ramya Ranganathan, using TopHat software (Trapnell, Roberts et al. 2012). Alignment quality was high, with ≥ 92% overall read alignment for all samples. I then analysed the BAM files containing the aligned reads via the remainder of the Tuxedo protocol (Trapnell, Roberts et al. 2012) (Fig. 2.2). Cufflinks software was first used to assemble the transcriptomes – to assign the mapped reads to specific transcripts – and these assemblies were then passed to the Cuffdiff program to analyse differential gene expression. Cufflinks and Cuffdiff were both accessed via the web-based user interface software Galaxy (usegalaxy.org). Volcano plots and heatmaps were created in R Studio via the cummeRbund package.

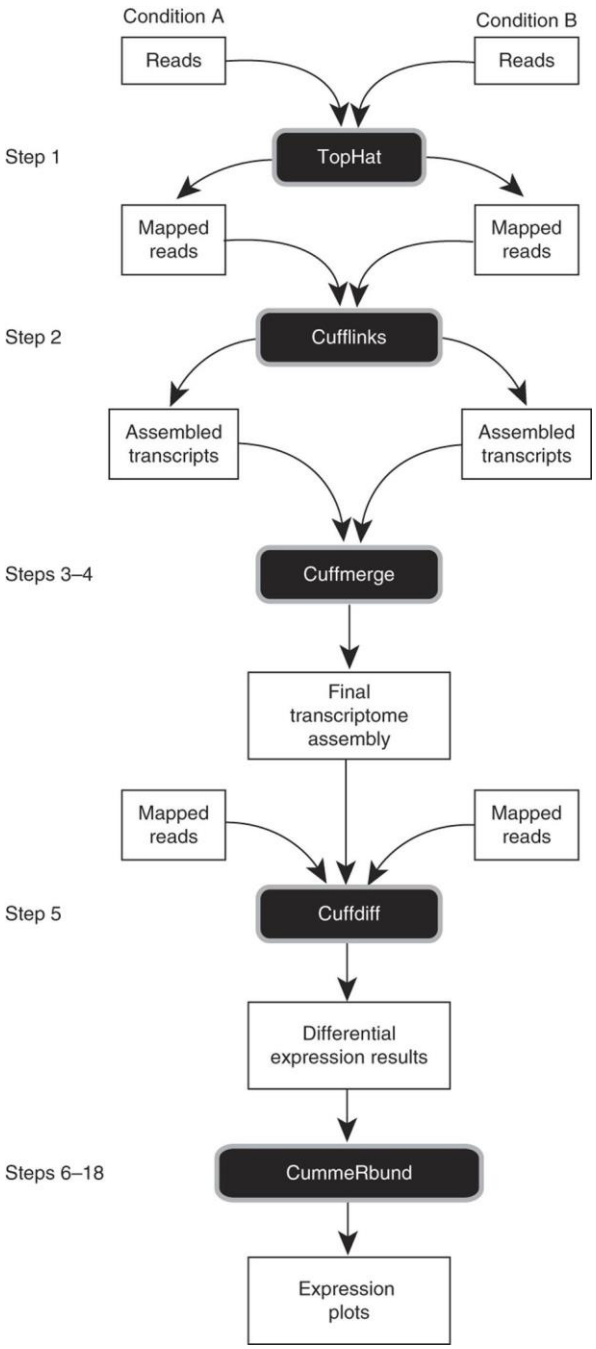

Figure 2.3 Overview of the Tuxedo protocol for RNA-Seq analysis. From (Trapnell, Roberts et al. 2012). Cuffmerge, which integrates replicate samples to produce one final merged assembly, is an optional step that was considered unnecessary in the analysis of my samples due to the high quality annotation of the *Drosophila melanogaster* genome, and the likelihood therefore that it would serve only to introduce or amplify assembly errors.

Cufflinks was run within Galaxy with the following parameters:

Maximum intron = 300,000 bp. Fragments that appear to align either side of a putative intron ≥300,000 bp are ignored.
Minimum isoform fraction = 0.1. Transcripts that appear to account for < 10% of the expression of a particular gene are ignored.
Pre-mRNA fraction = 0.15. Intra-intronic transcripts that appear to account for < 15% of the expression of a particular gene are ignored.
Use reference annotation = Yes. The August 2014 assembly of the *Drosophila melanogaster* genome (dm6) accessed from University of California Santa Cruz (UCSC) (https://genome-euro.ucsc.edu/) was used to guide transcript assembly.
Perform bias correction = Yes. Corrections are made for positional biases introduced by library preparation i.e. the over-representation of fragments at certain locations within a transcript (Roberts, Trapnell et al. 2011).
Use multi-read correct = Yes. Initial estimates of transcript abundance are made before reads that could be mapped to multiple locations in the genome are assigned fractional locations. For example, if multi-read correct is not enabled, and a read could map to four positions within the genome, each position would be assigned 0.25 of a read. With multi-read correct enabled, read fractions (e.g. 0.15, 0.2, 0.3 & 0.35) are assigned to each location based on transcript abundance estimates, corrections for fragment length and fragment bias.
Apply length correction = Cufflinks effective length correction. Fragments per kilobase of transcript per million reads (FPKM) values for short transcripts are adjusted upwards in accordance with the overall size distribution of library fragments, to account for the fact that short transcripts will produce very few fragments above the minimum read length.

Cuffdiff was run within Galaxy with the following parameters:

Library normalization method = geometric. Geometric means of fragment counts for each replicate/library are calculated. FPKMs and fragment counts are then scaled via the median of the geometric mean for each replicate/library.
Dispersion estimation method = pooled. Provides an estimate for dispersion by modelling how far the variance in the samples extends beyond that expected for a Poisson

distribution (where variance = mean). Pooled method averages the models for each replicate into one model for all conditions within the experiment.
False discovery rate = 0.05.
Minimum alignment count = 10. Significance tests to determine differential gene expression were conducted on all locuses with at least 10 alignments.
Use multi-read correct = Yes. See parameters for Cufflinks.
Perform bias correction = Yes. See parameters for Cufflinks.
Apply length correction = Cufflinks effective length correction. See parameters for Cufflinks.

The following thresholds were applied to the data output from Cuffdiff: A gene was considered to be meaningfully expressed if the average FPKM across the four replicates was ≥ 1 for at least one condition. A gene was considered to be significantly up- or downregulated if the fold-change was $\geq \pm 1.5$ (and the adjusted p value < 0.05).

Gene ontology clustering was performed using the Database for Annotation, Visualization and Integrated Discovery (DAVID), accessed at https://david.ncifcrf.gov, with guidance from (Huang da, Sherman et al. 2009). The significantly regulated genes in each condition (Control vs. TFAM overexpression, Control vs. ATF4 overexpression and TFAM overexpression vs. TFAM overexpression, ATF4 RNAi) were entered into DAVID in 'Official gene symbol' format (i.e. gene name), and the functional annotation clustering feature used with default settings.

2.2.9 Statistical methods

For RNA-Seq statistical methods see 2.2.8.

All other statistical tests were performed in GraphPad Prism (Version 5.02, 2008, GraphPad Software Inc.). GraphPad Prism was also used to create all graphs, with the exception of the RNA-Seq heatmaps and volcano plots which were created in R Studio via the cummeRbund package.

Pairwise comparisons were analysed via unpaired two-tailed t-test, with Welch's correction applied if the variances of the samples was significantly different. Data requiring multiple comparisons (continuous data with three or more conditions) were

analysed by parametric one-way ANOVA with Tukey's post-hoc test. Chi-squared tests were used to analyse categorical data. p values < 0.05 were considered significant ($*p < 0.05$, $**p < 0.01$, $***p < 0.001$).

3. Investigating the impact of mitochondrial dysfunction on ER biology in *Drosophila* neurons

3.1 Introduction

Mitochondrial retrograde signals communicate the functional status of the mitochondria to the nucleus. Mitochondrial dysfunction is strongly implicated in oncogenesis and metastasis, and therefore most retrograde signalling research has been performed in profilerating cell models. Given that mitochondrial dysfunction is also a hallmark of many neurodegenerative diseases, understanding mitochondrial retrograde signalling in neurons represents an important opportunity to identify novel therapeutic targets.

Mitochondria are not spatial or functional islands, they interact physically and functionally with many other organelles. In particular, significant areas of the ER are closely apposed to mitochondria, in regions termed mitochondria-associated membranes (MAMs). An array of protein tethering complexes secure the organelles together at sites within MAMs, and facilitate the performance of collective biological roles, including autophagy, lipid synthesis and Ca^{2+} handling (see main Introduction).

It has been extensively demonstrated that both lethal (apoptosis-inducing) and sub-lethal ER stressors cause changes to mitochondrial morphology and bioenergetics (for review see (Vannuvel, Renard et al. 2013)), but investigation of the reverse situation - mitochondrial dysfunction producing alterations to ER biology - has been neglected. I have hypothesised that neuronal mitochondrial dysfunction will alter aspects of ER biology, and that these changes will activate ER stress signalling that will communicate with the nucleus as a mitochondrial retrograde signal. In this chapter, I test the first part of my hypothesis, namely that neuronal mitochondrial dysfunction will cause changes to ER biology. I will use fluorescent reporters to examine mitochondrial morphology, ER morphology, ER-mitochondrial contacts and Ca^{2+} handling in a *Drosophila* model of neuronal mitochondrial dysfunction.

3.1.1 Aims

In this chapter, I test the hypothesis that mitochondrial dysfunction in *Drosophila* motor neurons alters aspects of ER biology by:

1) Investigating whether mitochondrial morphology is altered in neurons with mitochondrial dysfunction.
2) Investigating whether ER morphology is altered in neurons with mitochondrial dysfunction.
3) Assessing whether ER-mitochondrial contacts are altered in neurons with mitochondrial dysfunction.
4) Investigating cytosolic and mitochondrial Ca^{2+} levels in neurons with mitochondrial dysfunction.

3.2 Results

3.2.1 Increased mitochondrial fragmentation in neurons with mitochondrial dysfunction.

Mitochondria are physically and functionally coupled to the endoplasmic reticulum and I have therefore hypothesised that mitochondrial dysfunction will produce changes in ER biology. Given the physical apposition of the two organelles, it is likely that any alterations to mitochondrial morphology caused by mitochondrial dysfunction would impact upon ER morphology and/or ER-mitochondria contacts. I therefore began my investigation of ER biology in *Drosophila* neurons with mitochondrial dysfunction by assessing mitochondrial morphology.

Overexpression of mitochondrial transcription factor A (TFAM) in *Drosophila* neurons causes mitochondrial dysfunction by suppressing mtDNA gene expression (Cagin, Duncan et al. 2015, Duncan, Granat et al. 2018). I chose to examine ER and mitochondrial biology in neurons whose function can be readily assayed (see next chapter), and therefore employed the *D42-Gal4* driver, which is expressed in all motor neurons and some body wall sensory neurons (Sanyal 2009). Overexpression of TFAM alongside a mitochondrially-targeted GFP (mitoGFP) (Pilling, Horiuchi et al. 2006) by *D42-Gal4* revealed a striking change to mitochondrial macromorphology in the motor neuron cell bodies of wandering late third instar larvae (Fig. 3.1 A-B). Morphological parameters were quantified specifically in the dorsal medial motor neuron clusters in the ventral nerve cord (VNC). There was a non-significant enlargement of the total area of the mitochondrial network in the TFAM overexpression condition (Fig. 3.1 C). The number of mitochondria was increased by TFAM overexpression ($p < 0.05$, Fig. 3.1 D), and the median size of each mitochondrion significantly decreased ($p < 0.001$, Fig. 3.1 E). The circularity of the mitochondria was unchanged between the control and mitochondrial dysfunction conditions (Fig. 3.1 F). The interconnectivity parameter (mean area/mean perimeter) (Dagda, Cherra et al. 2009) was significantly reduced by TFAM overexpression ($p < 0.001$, Fig. 3.1 G), in line with the increased mitochondrial fragmentation strongly indicated by the number and size of the mitochondria.

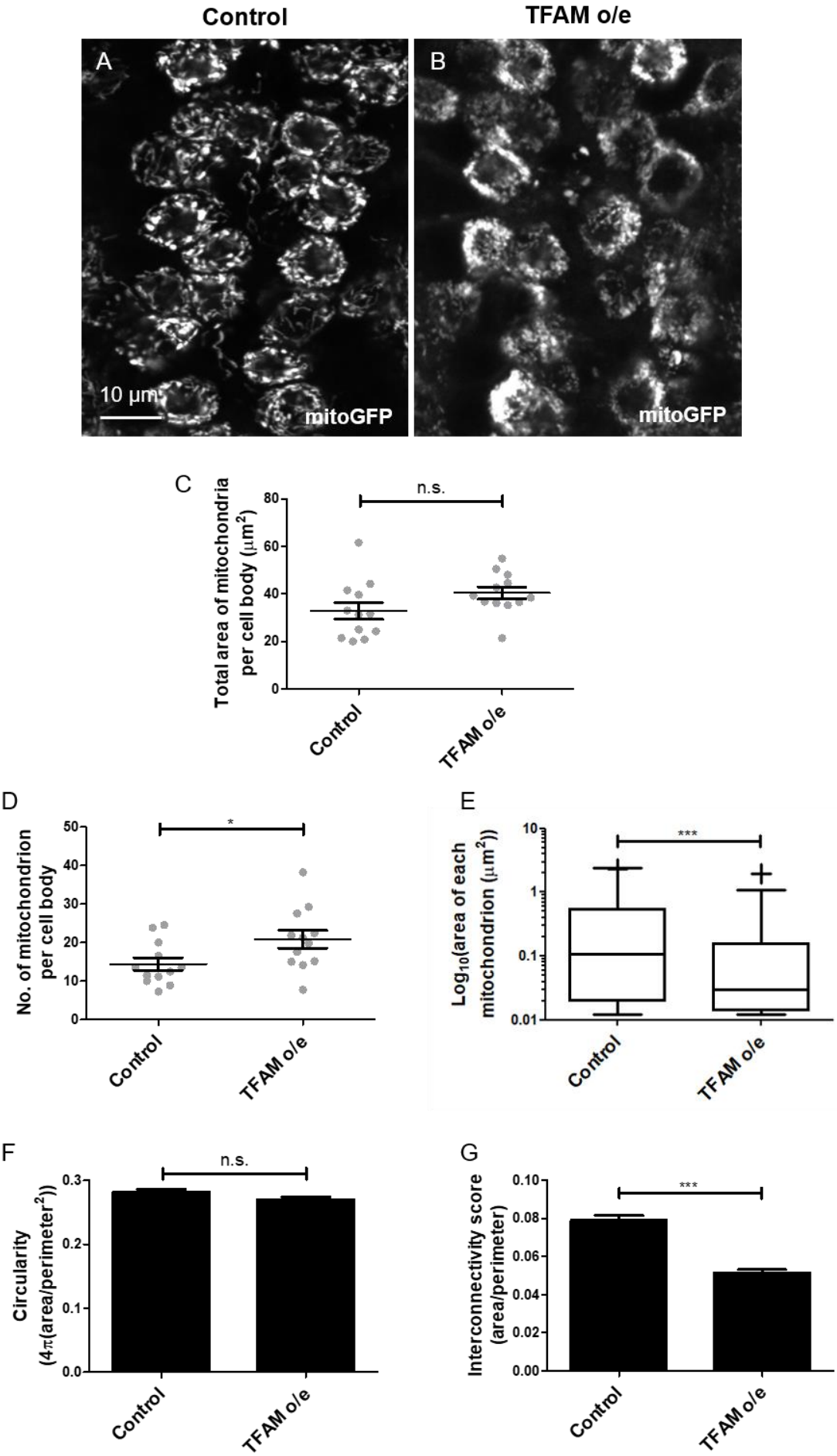
Control
TFAM o/e
A
B
10 µm
mitoGFP
mitoGFP
C
n.s.
Total area of mitochondria per cell body (µm²)
80
60
40
20
0
Control
TFAM o/e
D
*
No. of mitochondrion per cell body
50
40
30
20
10
0
Control
TFAM o/e
E
***
Log10(area of each mitochondrion (µm²))
10
1
0.1
0.01
Control
TFAM o/e
F
n.s.
Circularity (4π(area/perimeter²))
0.3
0.2
0.1
0.0
Control
TFAM o/e
G
***
Interconnectivity score (area/perimeter)
0.10
0.08
0.06
0.04
0.02
0.00
Control
TFAM o/e

Figure 3.1 Increased mitochondrial fragmentation in the cell bodies of Drosophila motor neurons with mitochondrial dysfunction. (A, B) mitoGFP fluorescence in control (A) or TFAM overexpressing (B) dorsal medial motor neurons. (C) Total area of mitochondria per cell body (μm^2), n = 12. (D) Number of mitochondrion per cell body, n = 12. (E) Area of each mitochondrion (μm^2) on $\log_{10}$ scale. Box = interquartile range, whiskers = 10^{th}-90^{th} percentiles, + = mean, n = 1,213 (control) and 1,751 (TFAM o/e). (F) Circularity ($4\pi(area/perimeter^2)$) of each mitochondrion, n = 1,213 (control) and 1,751 (TFAM o/e). (G) Interconnectivity (area/perimeter) of each mitochondrion, n = 1,213 (control) and 1,751 (TFAM o/e). (C, D, F, G) Means compared by two-tailed unpaired t-test. Bars = mean ± SEM. (E) Medians compared by two-tailed Mann-Whitney test. *$p < 0.05$, ***$p < 0.001$, n.s. = not significant.

3.2.2 Cell body ER morphology is altered by mitochondrial dysfunction in neurons.

Having established that mitochondrial dysfunction in *Drosophila* neurons causes alterations to mitochondrial morphology, I next investigated whether ER morphology was also changed under conditions of mitochondrial dysfunction. I employed the TFAM overexpression model, and three fluorescent *UAS* reporter constructs that mark the ER. Two of the reporters were targeted to, and retained within, the ER by specific signal sequences; a superfolder GFP with the ER targeting sequence from chaperone BiP and the HDEL retention motif from calreticulin (BiP-sfGFP-HDEL) (Summerville, Faust et al. 2016), and RFP fused to hen's egg lysozyme and the retention motif KDEL (lyso-RFP-KDEL) (Chowdhary, Tomer et al. 2017). The third reporter was an ER membrane marker comprised of the translocase subunit Sec61β fused to the fluorophore tdTomato (tdTomato-Sec61β) (Summerville, Faust et al. 2016).

The constructs were driven in motor neurons by *D42-Gal4*, and ER morphology quantified in the cell bodies. Local variance in fluorescence normalised to the local mean fluorescence (variance/mean intensity) was computed along straight lines drawn orthogonally from the nuclear envelope to the plasma membrane, as per (Yalçın, Zhao et al. 2017). Overexpression of TFAM alongside the BiP-sfGFP-HDEL reporter resulted in a significant decrease in variance/mean intensity compared to control cells ($p < 0.05$, Fig. 3.2 A-C), suggesting that ER structure is less reticular in the mitochondrial dysfunction condition. This decrease was particularly marked in the perinuclear region ($p < 0.001$, Fig. 3.2 J), but persisted as a trend across most of the cytoplasm to the plasma membrane. Raw fluorescence intensity was also significantly decreased in the nuclear membrane and perinuclear region in the TFAM overexpression condition ($p < 0.001$, Fig. 3.2 K). These results were recapitulated when TFAM was overexpressed with tdTomato-Sec61β; there was a significant decrease in variance/mean intensity ($p < 0.05$, Fig. 3.2 D-F) that was most evident in the perinuclear region ($p < 0.001$ Fig. 3.2 L) and accompanied by a decrease in raw fluorescence intensity in the same region ($p < 0.001$, Fig. 3.2 M). By contrast, variance/mean intensity as reported by lyso-RFP-KDEL was unchanged across the cell body by TFAM overexpression (Fig. 3.2 G-I, N) and the reduction in raw RFP fluorescence intensity was almost uniform (Fig. 3.2 O).

Taken together, these results indicate that there are changes in ER morphology in the cell bodies of *Drosophila* motor neurons with mitochondrial dysfunction that may correspond to specific domains of the ER.

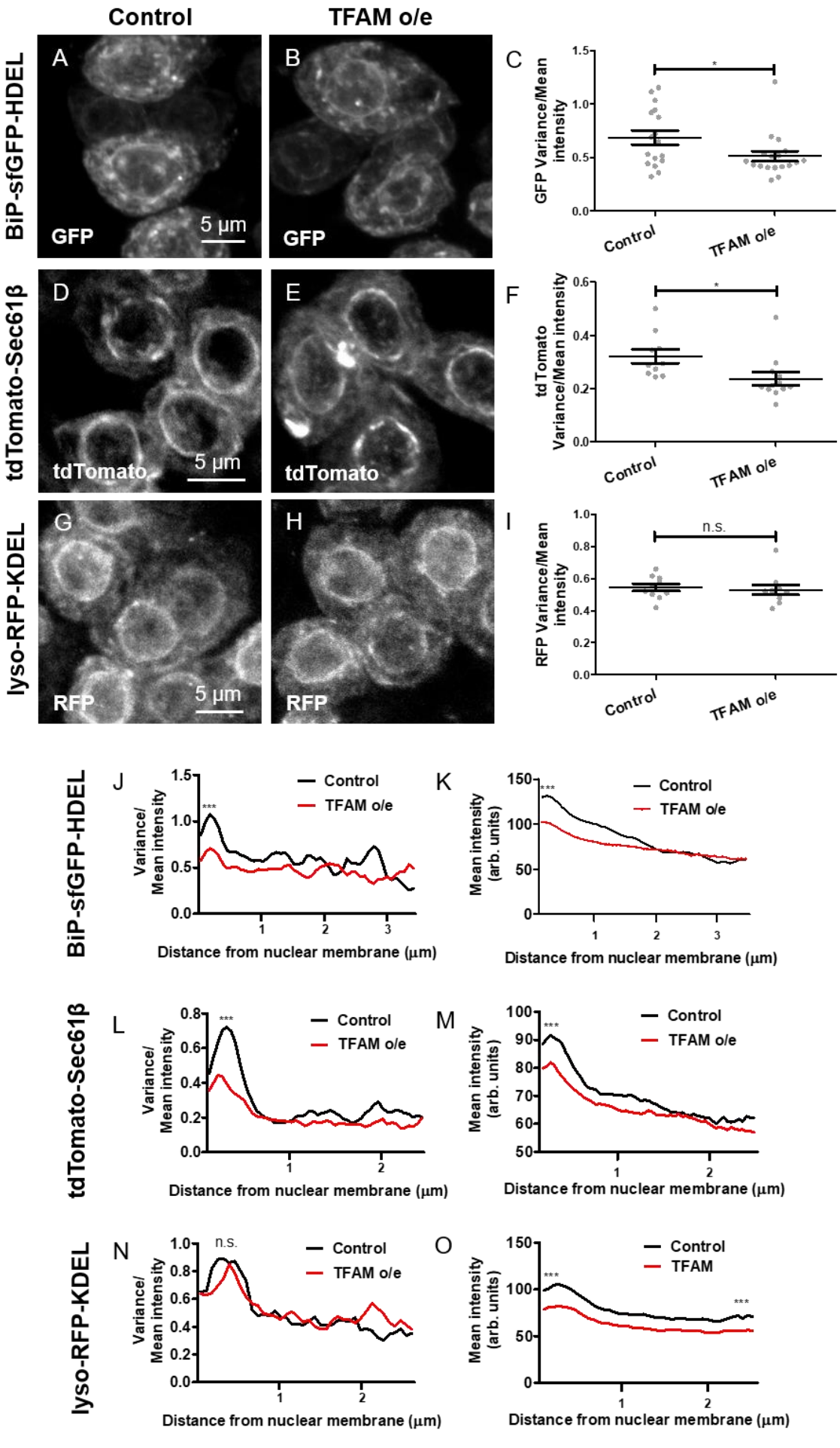
Control
TFAM o/e
BiP-sfGFP-HDEL
tdTomato-Sec61β
lyso-RFP-KDEL
A
B
C
D
E
F
G
H
I
GFP
tdTomato
RFP
5 μm
GFP Variance/Mean intensity
tdTomato Variance/Mean intensity
RFP Variance/Mean intensity
n.s.
J
K
L
M
N
O
Variance/ Mean intensity
Mean intensity (arb. units)
Distance from nuclear membrane (μm)
Control
TFAM o/e
TFAM

Figure 3.2 Changes to ER morphology in Drosophila motor neuron cell bodies with mitochondrial dysfunction (A, B) BiP-sfGFP-HDEL fluorescence in control (A) or TFAM overexpressing (B) dorsal medial motor neurons. (D, E) tdTomato-Sec61β fluorescence in control (D) or TFAM overexpressing (E) dorsal medial motor neurons. (G, H) lyso-RFP-KDEL fluorescence in control (G) or TFAM overexpressing (H) dorsal medial motor neurons. (C, F, I) Variance in fluorescence intensity/mean fluorescence intensity (Variance/Mean intensity) was calculated across rolling windows of 5 pixels (BiP-sfGFP-HDEL, lyso-RFP-KDEL) or 7 pixels (tdTomato-Sec61β), along lines drawn orthogonally from the nuclear to plasma membranes. (C, F, I) Variance/Mean intensity plotted as mean per sample. (J, L, N) Variance/Mean intensity plotted positionally from the nuclear membrane outwards as mean per pixel, for all pixels with n ≥20. (K, M, O) Raw fluorescence intensity computed across the same rolling pixel windows, and plotted positionally for all pixels with n ≥20. Significance in J-N was determined by two-tailed unpaired t-test performed on the first 10 values (from the nuclear membrane outwards) in each condition. Significance in O was determined by two-tailed unpaired t-test performed on the first 10, and (separately) the last 10, values (from the nuclear membrane outwards) in each condition. Means in C, F & I were also compared by two-tailed unpaired t-test. BiP-sfGFP-HDEL: n = 17 larvae (=153 lines from nuclear to plasma membrane) for control, 18 (=162 lines) for TFAM o/e. tdTomato-Sec61β: n = 10 larvae (= 90 lines) for control, 12 (= 108 lines) for TFAM o/e. lyso-RFP-KDEL: n = 10 larvae (= 90 lines) for control and TFAM o/e. Bars = mean ± SEM. *$p < 0.05$, ***$p < 0.001$, n.s. = not significant.

Having identified morphological changes in the ER of motor neuron cell bodies caused by mitochondrial dysfunction, I examined ER shape at the neuromuscular junction (NMJ). The *OK371-Gal4* P-element is inserted in the enhancer of the vesicular glutamate transporter, and therefore drives *UAS* transgenes in *Drosophila* motor neurons (Mahr and Aberle 2006). The tdTomato-Sec61β reporter was driven by this stronger motor neuron driver to provide robust expression at the distal end of the axon. *Drosophila* larval NMJs are highly stereotyped, and therefore the same synapse can be reliably located in each sample. Variance/mean intensity of tdTomato fluorescence was quantified in the type 1b NMJ on muscle four, abdominal segment 2, along a line that followed the contours of the synapse into the terminal. Overexpression of TFAM did not alter either the overall variance/mean intensity of tdTomato fluorescence in the NMJs (Fig. 3.3 A-C), or the spatial pattern of variance/mean intensity, which fluctuated around a constant level along the length of the synapse (Fig. 3.3 G). Raw fluorescence intensity gradually decreased towards the synaptic terminal in both the control and TFAM overexpression conditions (Fig. 3.3 H).

To verify the results of the tdTomato-Sec61β overexpression construct, I employed a reporter which utilises the endogenous transcriptional control of the ER shaping protein Reticulon-like-1 (Rtnl1). An artificial exon encoding YFP was inserted into an intron of *Rtnl1* to create the fluorescent fusion Rtnl1::YFP (Lowe, Rees et al. 2014), and this has been shown to mark the ER in motor neuron terminals (O'Sullivan, Jahn et al. 2012). Replicating the results seen with the tdTomato-Sec61β reporter, overexpression of TFAM did not change either the overall variance/mean intensity of YFP fluorescence in the NMJs (Fig. 3.3 D-F), or the spatial patterning of the parameter, which again oscillated about a fixed level along the length of the axon (Fig. 3.3 I). Raw YFP fluorescence intensity also reproduced the results of the tdTomato-Sec61β fusion, showing progressive attenuation towards the synaptic boutons in both the control and TFAM overexpression conditions (Fig. 3.3 J). These results indicate that there are not gross changes in the morphology of the ER in the NMJs of *Drosophila* motor neurons with mitochondrial dysfunction.

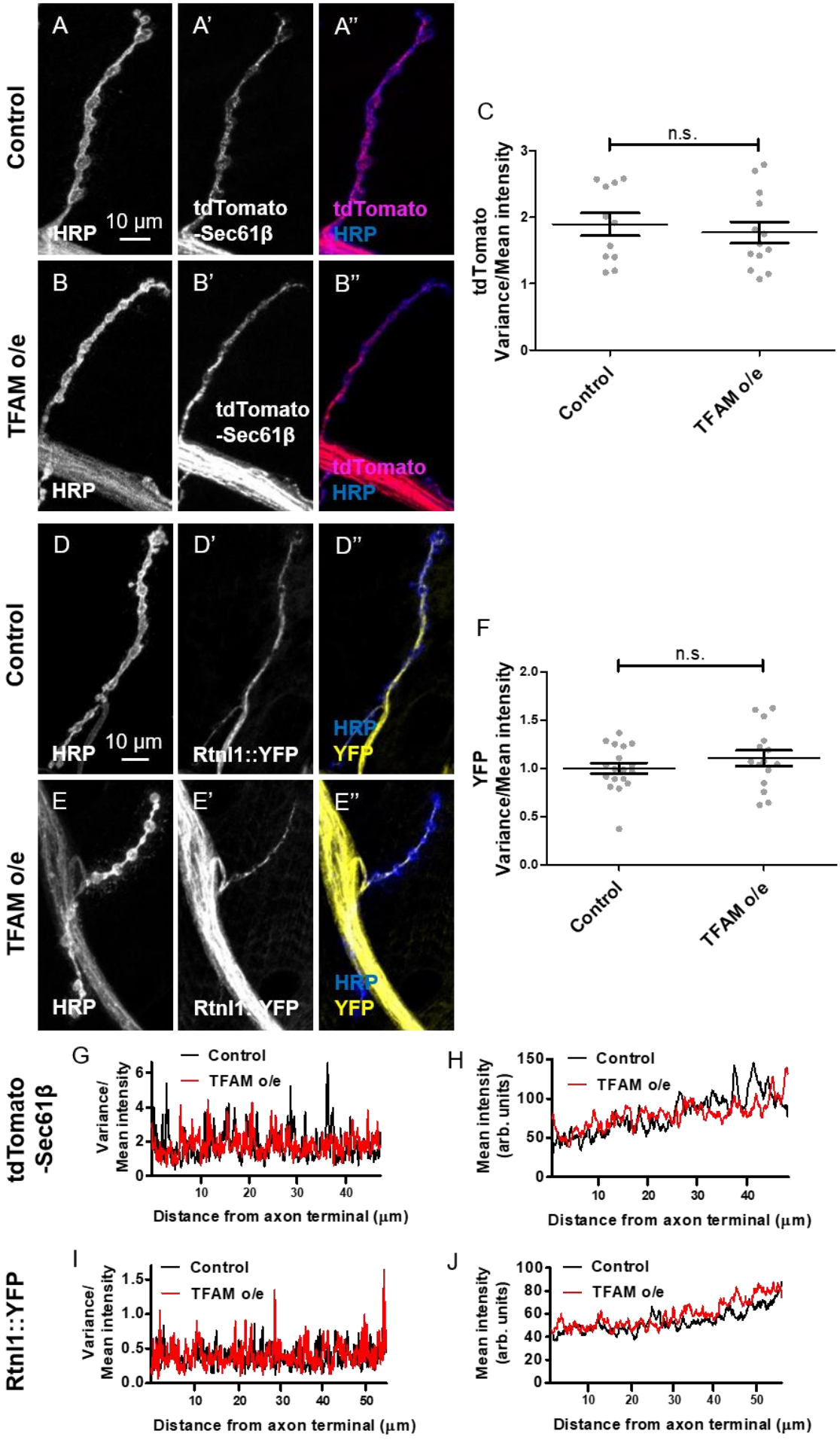
A
A'
A"
Control
HRP
10 μm
tdTomato
-Sec61β
tdTomato
HRP
B
B'
B"
TFAM o/e
HRP
tdTomato
-Sec61β
tdTomato
HRP
C
n.s.
tdTomato
Variance/Mean intensity
Control
TFAM o/e
D
D'
D"
Control
HRP
10 μm
Rtnl1::YFP
HRP
YFP
F
n.s.
YFP
Variance/Mean intensity
Control
TFAM o/e
E
E'
E"
TFAM o/e
HRP
HRP
YFP
tdTomato
-Sec61β
G
Control
TFAM o/e
Variance/
Mean intensity
Distance from axon terminal (μm)
H
Control
TFAM o/e
Mean intensity
(arb. units)
Distance from axon terminal (μm)
Rtnl1::YFP
I
Control
TFAM o/e
Variance/
Mean intensity
Distance from axon terminal (μm)
J
Control
TFAM o/e
Mean intensity
(arb. units)
Distance from axon terminal (μm)

Figure 3.3 Unchanged ER morphology at the Drosophila neuromuscular junction in neurons with mitochondrial dysfunction. (A-B'') tdTomato-Sec61β and HRP fluorescence in control (A-A'') or TFAM overexpressing (B-B'') NMJs. (D-E'') Rtnl1::YFP and HRP fluorescence in control (D-D'') or TFAM overexpressing (E-E'') NMJs. (A, B, D, E) HRP. (A', B', D', E') Rtn1::YFP fluorescence. (A'', B'', D'', E'') Merged images. Variance in fluorescence intensity/mean fluorescence intensity (Variance/Mean intensity) was calculated across rolling windows of 7 pixels (tdTomato-Sec61β) and 4 pixels (Rtnl1::YFP), along segmented lines drawn outward from the axon terminal. (C, F) Variance/Mean intensity plotted as mean per sample. (G, I) Variance/mean intensity plotted positionally from the axon terminal outwards as mean per pixel, for all pixels with n ≥5. (H, J) Raw fluorescence intensity computed across the same rolling pixel windows, and plotted positionally for all pixels with n ≥5. Means in C & F were compared by two-tailed unpaired t-test. tdTomato-Sec61β: n = 11 NMJs for control, 13 for TFAM o/e. Rtnl1::YFP: n = 18 NMJs for control, 15 for TFAM o/e. Bars = mean ± SEM. n.s.= not significant.

3.2.3 Mitochondrial dysfunction alters ER-mitochondrial contacts in neurons.

ER-mitochondria contacts enable the two organelles to share the performance of key biological functions. Having identified changes to mitochondrial and ER morphology that occur in *Drosophila* motor neurons under conditions of mitochondrial dysfunction, I hypothesised that ER-mitochondrial contacts may also be altered - either as a direct result of the morphological changes of the organelles, or another aspect of mitochondrial dysfunction.

To investigate ER-mitochondria contacts, I employed the tdTomato-Sec61β and lyso-RFP-KDEL reporters to label the ER, and mitoGFP to label the mitochondria. The constructs were driven by *D42-Gal4*, and ER-mitochondria distances were quantified in the motor neuron cell bodies of third instar larvae. To accommodate the wide range of fluorescence intensities displayed by the tdTomato-Sec61β and lyso-RFP-KDEL reporters, local thresholding was applied to determine the boundaries of the ER along lines drawn from the nuclear membrane to the plasma membrane (see Materials and Methods). After a similar thresholding was applied to the mitoGFP signal, the distance between the boundaries of the two organelles was computed. At ER-mitochondrial contact sites, the distance between the two organelles is 10-25 nm (Csordás, Renken et al. 2006). Images of the ER and mitochondrial reporters driven by *D42-Gal4* were taken at a scale of 1 pixel = 52 nm, and therefore 0 pixel gaps between the ER and mitochondrial boundaries were considered to represent candidate ER-mitochondrial contact sites (i.e. the thresholded boundary of each organelle was located in the same pixel). Using this method, I found a significant increase in the number of candidate ER-mitochondria contacts in the TFAM overexpression condition when the ER was marked by either tdTomato-Sec61β ($p < 0.001$, Fig. 3.4 A-B’’’, E) or lyso-RFP-KDEL ($p < 0.01$, Fig. 3.4 C-D’’’, E). Consistent with my finding that the perinuclear ER, as reported by tdTomato-Sec61β, appears less reticular in the TFAM overexpression condition - and therefore hypothetically presents fewer surfaces for ER-mitochondrial contacts - the mean distance of the candidate ER-mitochondrial contact sites from the nuclear membrane was significantly increased by TFAM overexpression when the ER was demarcated by tdTomato-Sec61β ($p < 0.001$, Fig. 3.4 F). Conversely, when the ER was marked by lyso-RFP-KDEL, the distribution of the candidate ER-mitochondria contacts was unchanged between control and TFAM overexpression conditions, in line with the absence of ER morphological changes reported by lyso-RFP-KDEL (Fig. 3.4 F). These

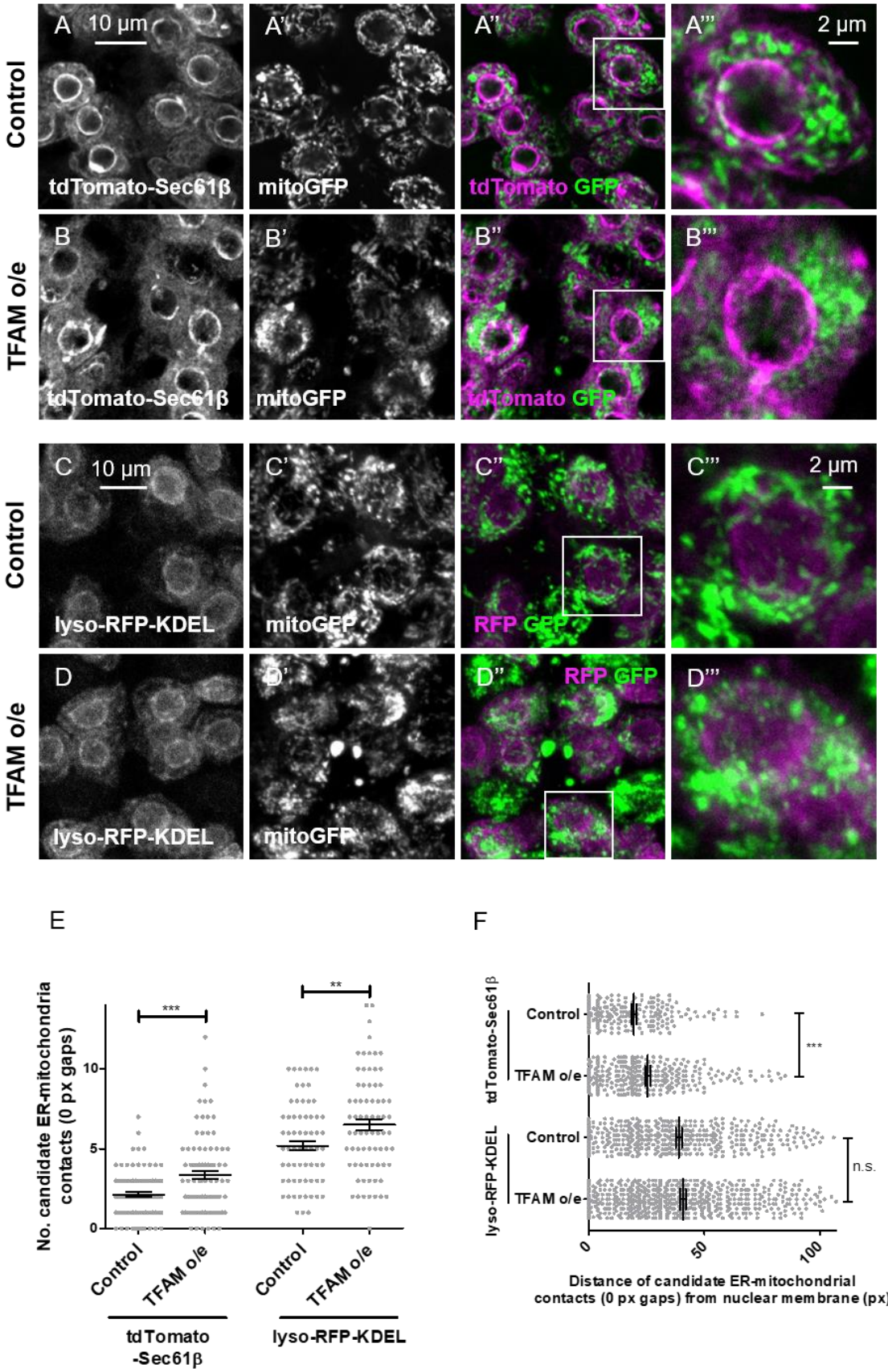
Control
TFAM o/e
A
10 µm
A'
A''
A'''
2 µm
tdTomato-Sec61β
mitoGFP
tdTomato GFP
B
B'
B''
B'''
C
C'
C''
C'''
lyso-RFP-KDEL
RFP GFP
D
D'
D''
D'''
E
No. candidate ER-mitochondria contacts (0 px gaps)
***
**
Control
TFAM o/e
tdTomato -Sec61β
lyso-RFP-KDEL
F
tdTomato-Sec61β
lyso-RFP-KDEL
n.s.
Distance of candidate ER-mitochondrial contacts (0 px gaps) from nuclear membrane (px)

Figure 3.4 Changes to ER-mitochondria contacts in the cell bodies of Drosophila neurons with mitochondrial dysfunction. (A-B’’’) tdTomato-Sec61β and mitoGFP fluorescence in control (A-A’’’) or TFAM overexpressing (B-B’’’) dorsal medial motor neurons. (C-C’’’) lyso-RFP-KDEL and mitoGFP fluorescence in control (C-C’’’) or TFAM overexpressing (D-D’’’) dorsal medial motor neurons. (A, B) tdTomato-Sec61β fluorescence. (A’, B’) mitoGFP fluorescence. (A’’, B’’) Merged images. (A’’’, B’’’) Magnification of regions demarcated by white box in (A’’ & B’’). (C, D) lyso-RFP-KDEL fluorescence. (C’, D’) mitoGFP fluorescence. (C’’, D’’) Merged images. (C’’’, D’’’) Magnification of regions demarcated by white box in (C’’ & D’’). ER and mitoGFP signals were locally thresholded to determine the boundaries of the organelles along lines drawn orthogonally from the nuclear to plasma membranes (see Materials & Methods), and ER-mitochondrial distances then computed. (E) Number of candidate ER-mitochondrial contacts identified (0 pixel gaps between the organelle boundaries). (F) Distance of the candidate ER-mitochondrial contacts from the nuclear membrane in pixels. Means in E & F compared by two-tailed unpaired t-test. tdTomato-Sec61β: n = 10 larvae (= 90 lines) for both conditions. lyso-RFP-KDEL: n = 10 larvae (= 90 lines) for control and 9 (= 81 lines) for TFAM overexpression. Bars = mean ± SEM. **p < 0.01, ***p < 0.001. n.s. = not significant.

results strongly suggest both an increase in the number of ER-mitochondrial contacts in the cell bodies of *Drosophila* motor neurons with mitochondrial dysfunction, and some relocation of these contacts in line with possible changes in the perinuclear morphology of the ER.

Whilst I have observed alterations to ER morphology (Fig. 3.2) and ER-mitochondria contacts (Fig. 3.4) in the cell bodies of *Drosophila* motor neurons with mitochondrial dysfunction, I did not detect anomalies in ER morphology at the NMJ (Fig. 3.3). TFAM overexpression is known to result in a dramatic loss of mitochondria from the synapse of motor neurons (Cagin, Duncan et al. 2015), and therefore the number and/or location of ER-mitochondrial contacts at the NMJ might be altered even in the absence of changes to ER morphology. To examine this proposal, I quantified ER-mitochondrial (tdTomato-Sec61β-mitoGFP) distances along a segmented line drawn from a terminal bouton outwards to the junction of the single motor axon with the peripheral nerve. There was a significant reduction in the number (normalised to the length of axon sampled) of candidate ER-mitochondria contacts in the TFAM overexpression condition ($p < 0.001$, Fig. 3.5 C), and the location of the candidate ER-mitochondria contacts was shifted significantly towards the nerve terminal ($p < 0.05$, Fig 3.5 D). These data indicate that changes in ER-mitochondrial contacts occur in both the cell bodies and NMJs of *Drosophila* motor neurons with mitochondrial dysfunction.

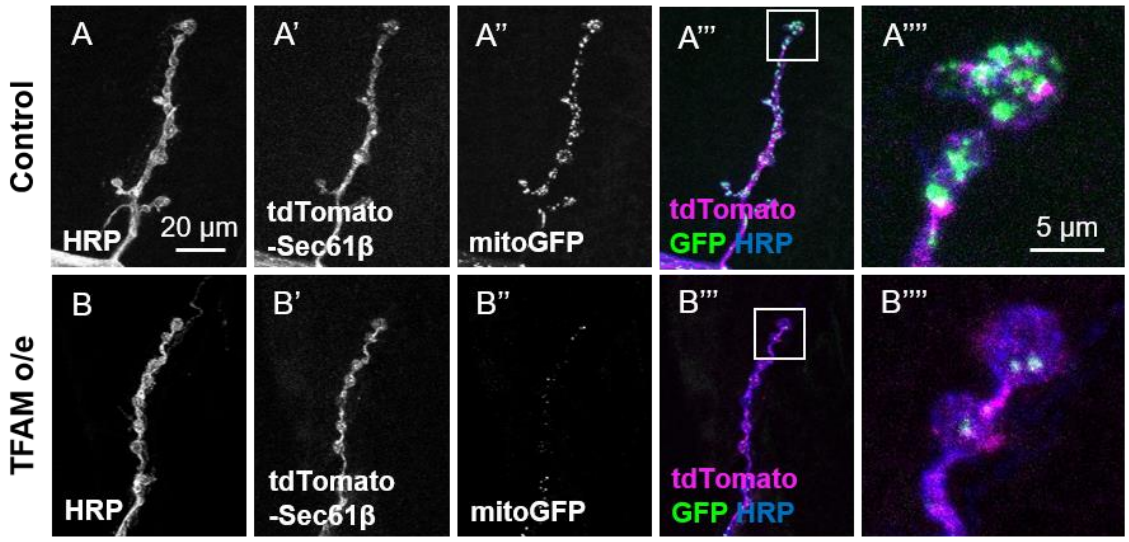
Control
TFAM o/e
A
A'
A''
A'''
A''''
HRP
20 μm
tdTomato
-Sec61β
mitoGFP
tdTomato
GFP HRP
5 μm
B
B'
B''
B'''
B''''
HRP
tdTomato
-Sec61β
mitoGFP
tdTomato
GFP HRP

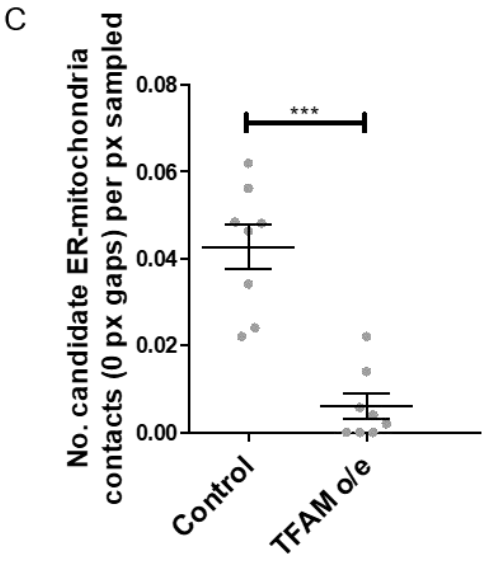
C
No. candidate ER-mitochondria contacts (0 px gaps) per px sampled
0.08
0.06
0.04
0.02
0.00
***
Control
TFAM o/e

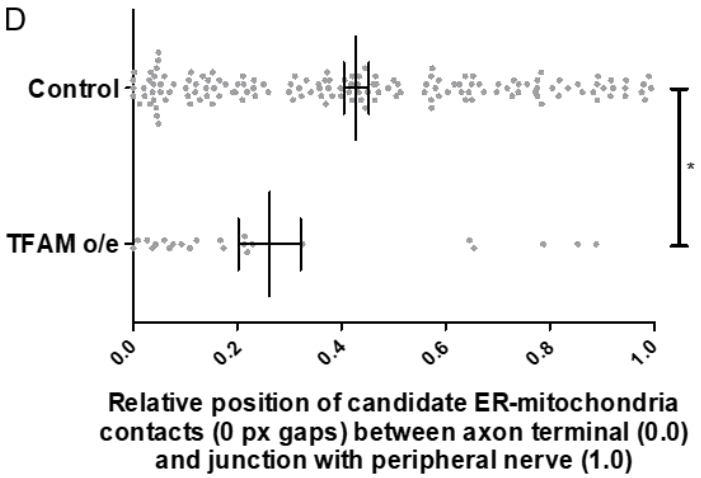
D
Control
TFAM o/e
*
0.0
0.2
0.4
0.6
0.8
1.0
Relative position of candidate ER-mitochondria contacts (0 px gaps) between axon terminal (0.0) and junction with peripheral nerve (1.0)

Figure 3.5 Changes to ER-mitochondria contacts at the neuromuscular junction of Drosophila neurons with mitochondrial dysfunction. (A-B’’’’) tdTomato-Sec61β, mitoGFP and HRP fluorescence in control (A-A’’’’) or TFAM overexpressing (B-B’’’’) neuromuscular junctions. (A,B) HRP. (A’,B’) tdTomato-Sec61β fluorescence (A’’,B’’) mitoGFP fluorescence. (A’’’,B’’’) Merged images. (A’’’’,B’’’’) Magnification of regions demarcated by white box in (A’’’ & B’’’). ER and mitoGFP signals were locally thresholded to determine the boundaries of the organelles along lines drawn outwards from the axon terminal (see Materials & Methods), and ER-mitochondrial distances then computed. (C) Number of candidate ER-mitochondrial contacts identified (0 pixel gaps between the organelle boundaries). (D) Relative distance of the candidate ER-mitochondrial contacts from the axon terminal. Means in C & D compared by two-tailed unpaired t-test, n = 8 NMJs for both conditions. Bars = mean ± SEM. * $p < 0.05$, ***$p < 0.001$.

3.2.4 Mitochondrial Ca^{2+} levels are increased in neurons by mitochondrial dysfunction.

ER-mitochondria contacts are important regulators of intracellular calcium homeostasis and signalling. Having established that both the number and spatial distribution of ER-mitochondria contacts are altered by mitochondrial dysfunction in *Drosophila* motor neurons, I hypothesised that Ca^{2+} handling would also be affected by mitochondrial dysfunction.

To measure the basal levels of cytosolic Ca^{2+}, I used the genetically encoded calcium indicator GCaMP6m under *UAS* control (Chen, Wardill et al. 2013). GCaMPs are chimeric proteins that undergo a structural rearrangement that activates GFP fluorescence upon the binding of Ca^{2+} to their calmodulin domain (Nakai, Ohkura et al. 2001). I expressed GCaMP6m in motor neurons via the *OK371-Gal4* driver. Quantification of live images revealed that TFAM overexpression did not alter the levels of cytosolic Ca^{2+} in either the cell bodies (Fig. 3.6 A-C) or NMJs (Fig. 3.6 H-J) of unstimulated motor neurons. A second reporter construct, CaMPARI, exhibits irreversible green-to-red photoconversion in the presence of both Ca^{2+} and UV light (Fosque, Sun et al. 2015). Replicating the results seen with GCaMP6m, TFAM overexpression driven alongside CaMPARI by *OK371-Gal4* did not significantly alter the red:green fluorescence ratio in the cytosol of motor neuron cell bodies of larvae exposed to UV light (Fig. 3.6 D-G). By contrast, knock down of the store-operated Ca^{2+} entry facilitator, Stim (Liou, Kim et al. 2005, Roos, DiGregorio et al. 2005), resulted in significantly increased red:green fluorescence ratios ($p < 0.001$, Fig.3.6 D-G), indicating increased basal Ca^{2+} levels in this condition, and confirming that the dynamic range of the CaMPARI sensor is suitable for detecting changes in Ca^{2+} abundance in *Drosophila* neurons.

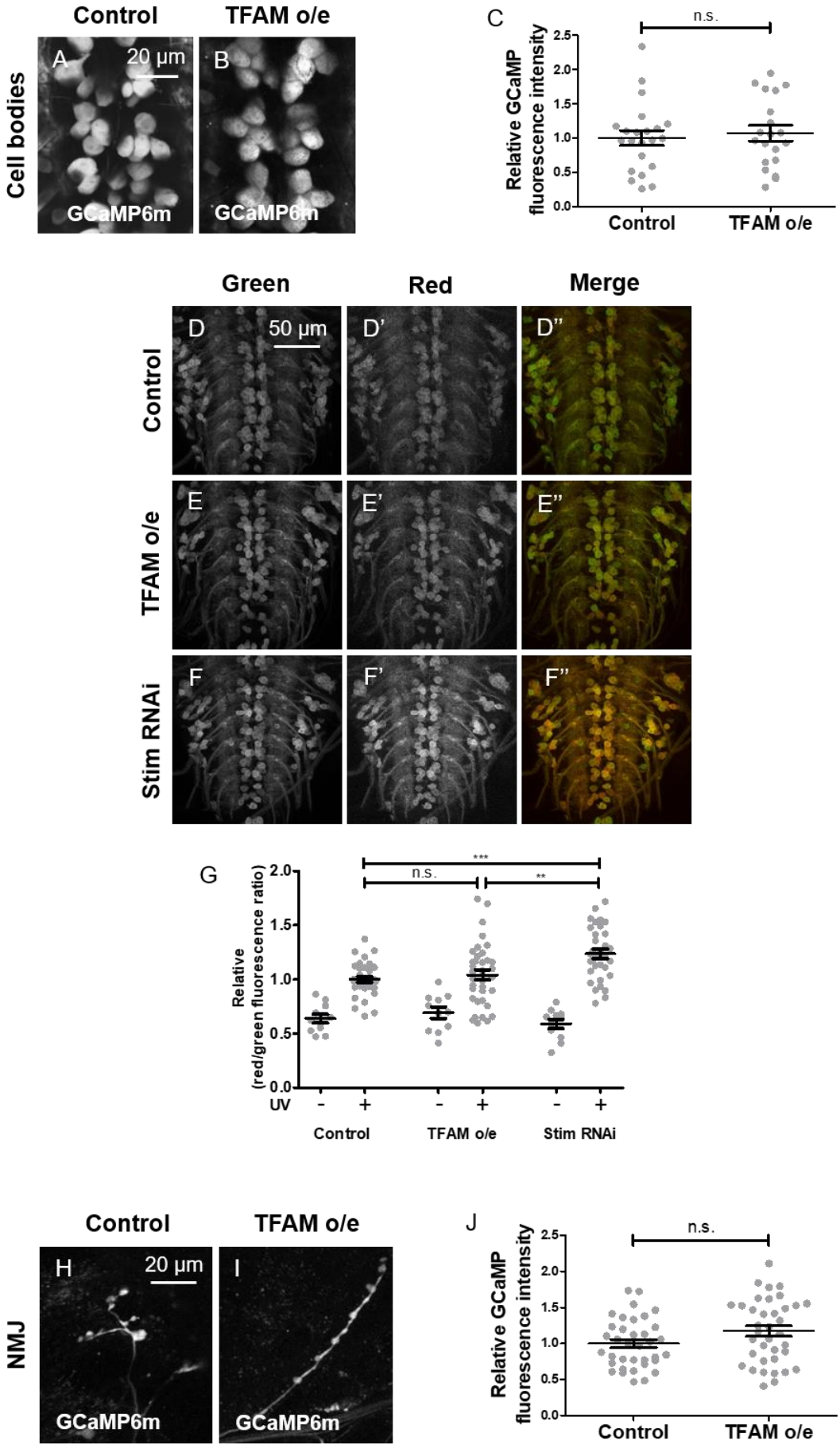
Control
TFAM o/e
Cell bodies
A
20 µm
B
GCaMP6m
GCaMP6m
C
n.s.
Relative GCaMP fluorescence intensity
2.5
2.0
1.5
1.0
0.5
0.0
Control
TFAM o/e
Green
Red
Merge
Control
D
50 µm
D'
D''
TFAM o/e
E
E'
E''
Stim RNAi
F
F'
F''
G
***
n.s.
**
Relative (red/green fluorescence ratio)
2.0
1.5
1.0
0.5
0.0
UV
-
+
-
+
-
+
Control
TFAM o/e
Stim RNAi
Control
TFAM o/e
NMJ
H
20 µm
I
GCaMP6m
GCaMP6m
J
n.s.
Relative GCaMP fluorescence intensity
2.5
2.0
1.5
1.0
0.5
0.0
Control
TFAM o/e

Figure 3.6 Basal Ca^{2+} levels are unchanged in the cell bodies and NMJ of Drosophila motor neurons with mitochondrial dysfunction. GCaMP6m fluorescence in control (A) or TFAM overexpressing (B) dorsal medial motor neurons. (C) Quantification of GCaMP6m fluorescence in cell bodies, n = 22 larvae for control, 20 for TFAM o/e. (D-F'') CaMPARI fluorescence in dorsal medial motor neurons of control (D-D''), TFAM overexpressing (E-E'') or Stim knock-down (F-F'') larvae. (D, E, F) Green (default) channel. (D', E', F') Red (photoconverted) channel. (D'', E'', F'') Merged images. (G) Quantification of CaMPARI red/green fluorescence ratio in cell bodies, n = 34 larvae for control, 11 for control no UV, 37 for TFAM o/e, 11 for TFAM o/e no UV, 33 for Stim RNAi and 11 for Stim RNAi no UV. (H, I) GCaMP6 fluorescence in control (H) or TFAM overexpressing (I) NMJs. (J) Quantification of GCaMP6m fluorescence in NMJs, n = 36 NMJs for control, 37 for TFAM o/e. Means in C & J compared by two-tailed unpaired t-test. Means in G compared by one-way parametric ANOVA with Tukey's post-hoc test. Bars = mean ± SEM. **p < 0.01, ***p < 0.001, n.s. = not significant.

Given the critical roles that mitochondria and the ER play in Ca^{2+} handling, and the alterations to ER morphology and ER-mitochondrial contacts caused by mitochondrial dysfunction, it was unexpected that cytosolic Ca^{2+} levels were unchanged by TFAM overexpression. To assess whether the anticipated Ca^{2+} defect was present within mitochondria, a mitochondrially-targeted GCaMP3 (mitoGCaMP) (Drago and Davis 2016) was driven in motor neurons by *OK371-Gal4*. Overexpression of TFAM resulted in a striking increase in Ca^{2+} levels within the mitochondria of motor neuron cell bodies ($p < 0.001$, Fig. 3.7).

Mitochondria are integral regulators of wide-ranging, dynamic cellular processes via Ca^{2+} signalling. The increase in mitochondrial Ca^{2+} levels caused by TFAM overexpression therefore suggested that defects in cytosolic Ca^{2+} handling may only be apparent in stimulated neurons. Activation of *Drosophila* motor neurons by targeted expression of the heat-activated Transient Receptor Potential ion channel, dTrpA1 (Hamada, Rosenzweig et al. 2008), revealed that TFAM overexpression causes a marked increase in cytosolic Ca^{2+} levels in the cell bodies of repeatedly stimulated neurons (Fig. 3.8). There was no significant difference in GCaMP6m fluorescence between control and TFAM overexpression neurons after the first stimulation, but significant differences in GCaMP6m fluorescence upon second and third stimulations ($p < 0.05$ for differences in peak fluorescence, Fig. 3.8 A-C). This outcome was also seen in the axons - for which there was also a significant difference in GCaMP6m fluorescence minima ($p < 0.01$ for first trough, $p < 0.05$ for second trough, Fig. 3.8 D) – and neuropil (Fig. 3.8 E) of the samples. These results indicate that neuronal mitochondrial dysfunction causes alterations to cytosolic Ca^{2+} handling in addition to defects within the organelle itself.

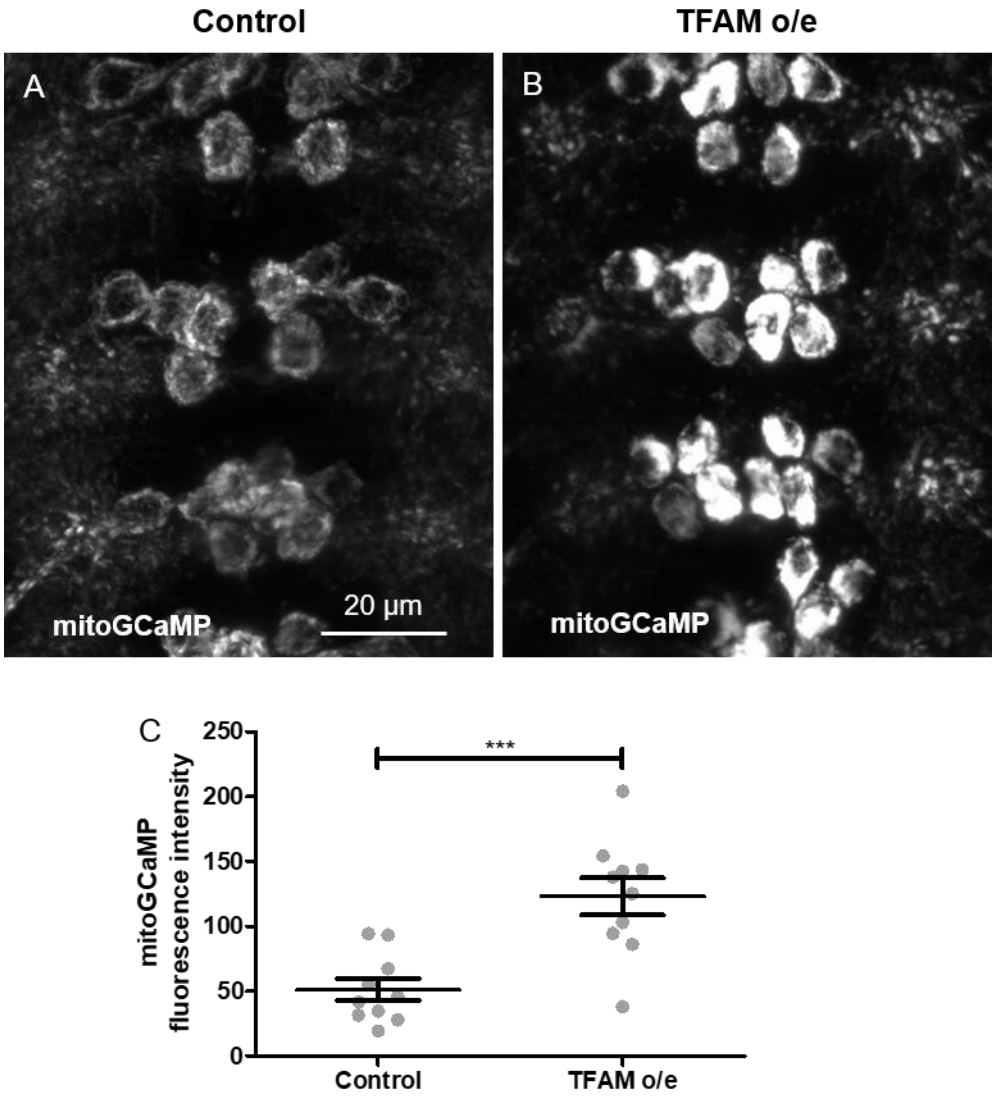

Figure 3.7 Basal mitochondrial Ca^{2+} levels are significantly higher in the cell bodies of Drosophila motor neurons with mitochondrial dysfunction. mitoGCaMP fluorescence in control (A) and TFAM overexpressing (B) dorsal medial motor neurons. (C) Quantification of mitoGCaMP fluorescence. Means compared by two-tailed unpaired t-test. n = 10 larvae for both conditions. Bars = mean ± SEM. ***p < 0.001.

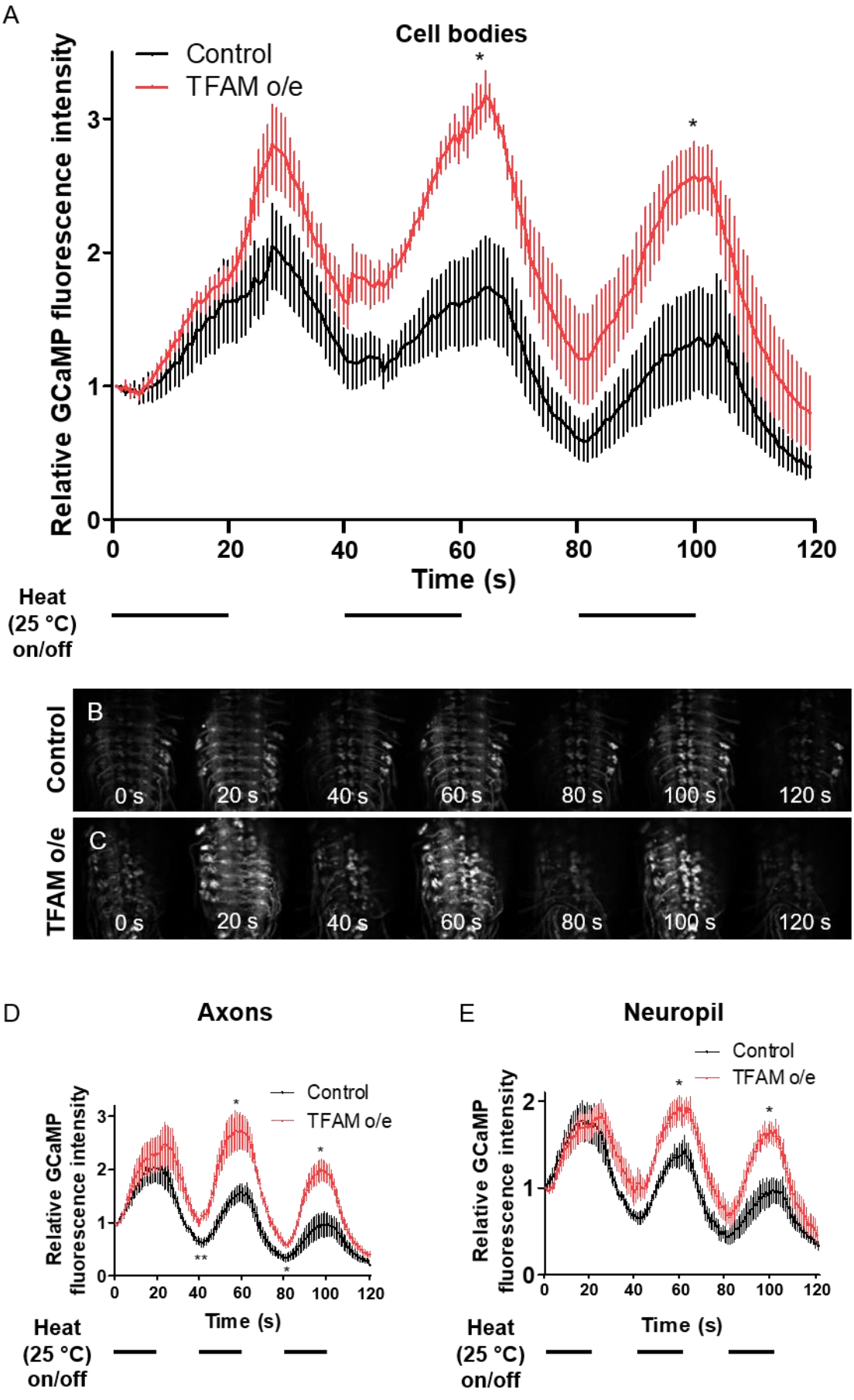
A
Cell bodies
Control
TFAM o/e
Relative GCaMP fluorescence intensity
Time (s)
Heat (25 °C) on/off
B
Control
0 s
20 s
40 s
60 s
80 s
100 s
120 s
C
TFAM o/e
D
Axons
E
Neuropil

Figure 3.8 Changes to dynamic cytosolic Ca^{2+} levels in Drosophila motor neurons with mitochondrial dysfunction. (A) Mean of traces for GCaMP6m fluorescence in dorsal medial motor neuron cell bodies as TrpA1 channels were activated by 20 second (s) on/off pulses of 25 °C heat, as indicated by the horizontal black lines below the graph (line = heat on, space = heat off). Control = black trace, TFAM overexpression = red trace. (B, C) Sample images of control (B) and TFAM overexpressing (C) samples showing change in GCaMP6m fluorescence over the three heat pulses (images are aligned to the graph in (A) and the black lines denoting heat on/off). (D, E) Mean traces for GCaMP6m levels in the axons (D) and neuropil (E). Lines and error bars in graphs are mean ± SEM. In the cell bodies and axons, for first heat on/off cycle (0-40 seconds), n = 6 larvae for both conditions, for the second cycle onwards (41-120 seconds), n = 5 for both conditions. In the neuropil, for first heat on/off cycle (0-40 seconds), n = 6 larvae for control and 7 for TFAM o/e, for the second cycle onwards (41-120 seconds), n = 5 for control and 6 for TFAM o/e. (A, D, E) Significant differences in fluorescent peaks and troughs were assessed by two-tailed unpaired t-test performed on the mean of the ten frames spanning the relevant peak or trough for each sample. *$p < 0.05$, **$p < 0.01$. Individual GCaMP6m fluorescent traces from which the mean ± SEM plots in A, D & E were calculated, can be found in the Appendix 8.1.

3.3 Summary

Mitochondria are physically and functionally linked to the ER. I have therefore hypothesised that mitochondrial dysfunction causes changes to ER biology, that these changes activate ER stress signalling, and that this signalling communicates with the nucleus as a mitochondrial retrograde signal. In this chapter, I aimed to determine whether mitochondrial dysfunction does indeed alter aspects of ER biology in *Drosophila* motor neurons. I used a series of fluorescent reporters to examine the relationships between mitochondrial dysfunction and ER morphology, ER-mitochondrial contacts and Ca^{2+} handling.

Overexpression of TFAM caused fragmentation of the mitochondrial network in the cell bodies of *Drosophila* neurons. I assessed ER morphology in the cell bodies of *Drosophila* motor neurons using the fluorescent ER membrane marker tdTomato-Sec61β, and two fluorescent reporters that are targeted to, and retained within, the ER; BiP-sfGFP-HDEL and lyso-RFP-KDEL. For all three reporters, quantification of local variance in fluorescence intensity normalised to local mean fluorescence intensity, revealed a reduction in normalised variance in the mitochondrial dysfunction condition, suggesting that the ER had become less reticular. The decrease in normalised variance was particularly prominent in the perinuclear region, and was accompanied by a reduction in fluorescence intensity in the same area.

ER morphology at the NMJ was assessed via the tdTomato-Sec61β construct and an exon trap fusion Rtnl1::YFP, and did not recapitulate the changes seen in the motor neuron cell bodies. There was no difference in either the overall variance/mean intensity, or the spatial patterning of the parameter.

There is extensive physical juxtaposition of mitochondrial and the ER, and this permits the organelles to jointly execute key biological functions. It has been shown that TFAM overexpression dramatically alters the morphology of the mitochondrial network in *Drosophila* motor neuron cell bodies. Having identified putative changes to ER morphology in those same cells, I hypothesised that ER-mitochondrial contacts may also be altered in the TFAM overexpression model of mitochondrial dysfunction.

I examined ER-mitochondrial contacts in motor neuron cell bodies via a mitochondrially-targeted GFP and the tdTomato-Sec61β and lyso-RFP-KDEL reporters. There was a significant increase in the number of candidate ER-mitochondrial contacts (0 pixel gaps between the ER and mitochondrial boundaries). Consistent with the perinuclear changes to ER morphology indicated by the tdTomato-Sec61β reporter, the mean distance of the candidate ER-mitochondrial contacts from the nuclear membrane was significantly further in the mitochondrial dysfunction condition when the ER was demarcated by tdTomato-Sec61β.

I did not identify morphological differences in the ER at the NMJ of motor neurons with mitochondrial dysfunction. However, in addition to modifying the macromorphology of mitochondria in motor neuron cell bodies, TFAM overexpression also results in a substantial loss of mitochondria at the synapse. Consistent with this, the number of ER-mitochondrial distances and candidate ER-mitochondria contacts at the NMJ was significantly reduced in the mitochondrial dysfunction condition. The location of the candidate ER-mitochondrial contact sites was shifted significantly towards the synaptic terminal by TFAM overexpression.

Ca^{2+} handling is a key shared function of the mitochondria and ER. Having identified changes to ER-mitochondrial contact sites, I investigated levels of Ca^{2+} in the cytosol and mitochondria of unstimulated motor neurons. Basal Ca^{2+} was unchanged in the cytosol of motor neurons with mitochondrial dysfunction, as measured by two independent reporters. By contrast, levels of Ca^{2+} in the mitochondria and the cytosol of stimulated neurons were strikingly raised in the mitochondrial dysfunction condition.

Overall, these data demonstrate clear affects of mitochondrial dysfunction on ER biology in *Drosophila* neurons.

4. Investigating ER stress signalling in *Drosophila* neurons with mitochondrial dysfunction.

4.1 Introduction

In Chapter 3, I identified changes in ER morphology, ER-mitochondria contacts, and calcium handling that occur in *Drosophila* neurons with mitochondrial dysfunction. These changes suggest substantial alterations to ER biology, and I therefore hypothesise that ER stress signalling will be activated by mitochondrial dysfunction in *Drosophila* neurons, and that this signalling will modify the function of affected neurons.

Stress signalling from the ER occurs via the conserved ER unfolded protein response (UPR) (Fig. 4.1), that I describe more thoroughly in the main Introduction, but will also outline here. The ER UPR comprises three individual, but cross-regulated pathways that each culminate in the activation of a transcription factor. At the head of each pathway is an ER-resident transmembrane protein; the kinases PERK and IRE1 form homo-oligomers in response to unfolded protein stress in the ER, and subsequently undergo activation by trans-autophosphorylation of their cytoplasmic domains. A loss of ER proteostasis causes the transcription factor ATF6 to traffic from the ER to the Golgi complex where it is cleaved, and a cytosolic portion translocates to the nucleus to activate transcription of ER UPR genes. Whilst ATF6 itself forms one complete branch of the ER UPR, PERK and IRE1 have other downstream effectors. PERK phosphorylates the translation initiation factor eIF2α, leading to a broad reduction in translation, but the specific induction of a subset of proteins with novel 5'UTRs, including the ER UPR transcription factor ATF4, and phosphatase scaffold GADD34. In mammals, transcription of GADD34 is also upregulated by the ATF4 target CHOP, and GADD34 opposes PERK by targeting the PP1 phosphatase to eIF2α, thus forming a negative feedback loop within the ER UPR. Activated IRE1 acquires ribonuclease activity and, in addition to the targeted degradation of a subset of messenger RNAs, specifically catalyses the splicing of mRNA encoding the transcription factor XBP1 to create an active form of the protein.

There is evidence from *in vitro* and non-neuronal *in vivo* experiments that mitochondrial dysfunction can activate the ER UPR. Dissipation of mitochondrial membrane potential by the protonophore carbonyl cyanide *m*-chlorophenyl hydrazine

(CCCP) resulted in ER stress in HEK293T and SH-SY5Y cells and activated ATF4 (Bouman, Schlierf et al. 2011). The complex I inhibitor rotenone also triggered transcriptional regulation by ATF4 in SH-SY5Y cells (Wu, Luo et al. 2014), the ATP synthase inhibitor oligomycin was found to cause ER stress in a human liver cell line (Lim, Lee et al. 2009), and ER stress signalling activated by the antiretroviral Efavirenz was suppressed in human hepatoma cells lacking mtDNA (Apostolova, Gomez-Sucerquia et al. 2013). Disease pathogenesis driven by mitochondrial dysfunction also triggered ER stress pathways in a rat model of acute pancreatitis (Biczo, Vegh et al. 2018). To test for activation of the ER UPR in *Drosophila* neurons with mitochondrial dysfunction, I will employ a second model in addition to TFAM overexpression. Ubiquitous knock-down of the homologue of the Complex I subunit NDUFS1, the highly conserved ND-75 (Fearnley and Walker 1992, Weidner, Geier et al. 1993) in adult fly heads causes a reduction in NADH oxidase-ferrireductase activity and reduced expression of other complex I subunits (Hegde, Vogel et al. 2014). If my conjecture that the ER UPR is activated by mitochondrial dysfunction in *Drosophila* neurons is correct, I will examine the consequences of this activation by assessing neuronal function via climbing and wing inflation assays, and the rate of global translation.

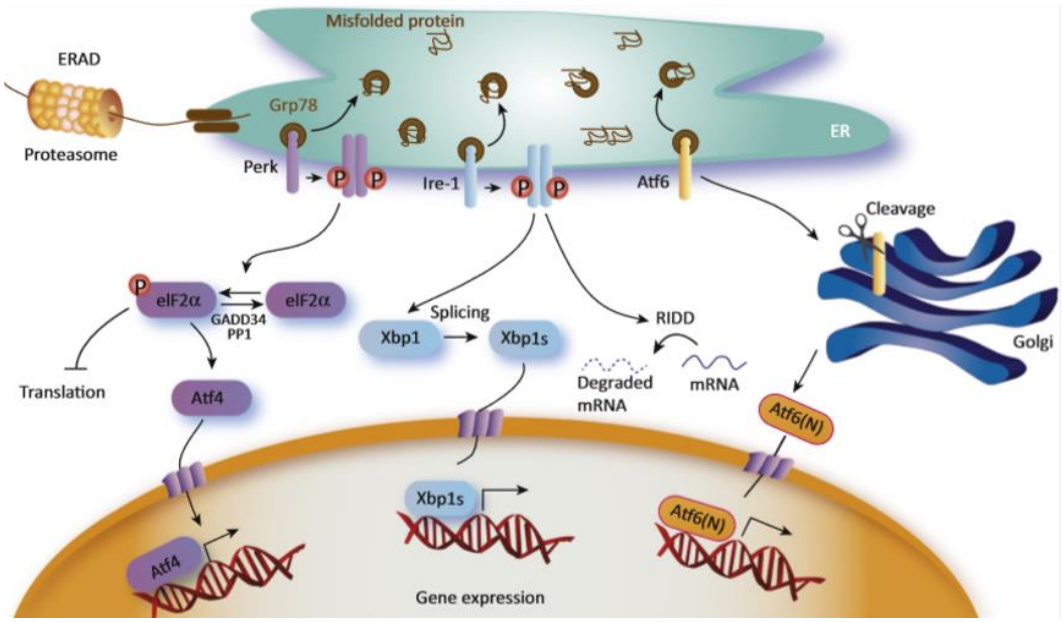

Figure 4.1 Overview of the ER UPR. From (Godin, Creppe et al. 2016).

4.1.1 Aims

In this chapter, I test the hypothesis that mitochondrial dysfunction in *Drosophila* neurons activates ER stress signalling, and that this signalling has functional consequences for the affected neurons by:

1) Determining whether components of the ER UPR are activated in models of mitochondrial dysfunction, and if there is a consequent reduction in global translation.
2) Assessing the impact of genetic manipulation of ER UPR components in two assays of neuronal function.

4.2 Results

4.2.1 The PERK and IRE1 branches of the ER UPR are activated in models of mitochondrial dysfunction.

In Chapter 3, I described changes to ER biology that occur in *Drosophila* neurons with mitochondrial dysfunction. Given these changes, I have hypothesised that neuronal mitochondrial dysfunction will activate ER stress signalling in the form of the ER UPR, and that this signalling will have functional consequences for the affected neurons. To test this proposal, I first examined the activation of components of the PERK and IRE1 branches of the ER UPR in models of *Drosophila* neuronal mitochondrial dysfunction.

The kinase PERK is resident in the ER membrane. Classically, an overload of unfolded proteins within the lumen of the ER causes the oligomerisation and autophosphorylation of PERK. Once activated in this manner, the cytosolic domain of PERK directly phosphorylates the translation initiation factor eIF2α (Fig. 4.1). I used immunofluorescence staining in wandering third instar larvae to examine the extent of eIF2α phosphorylation in our models of mitochondrial dysfunction. Overexpression of TFAM and a membrane-targeted GFP were driven in motor neurons by *OK371-Gal4*. TFAM overexpression caused a significant increase in the level of phosphorylated eIF2α (P-eIF2α) in the cytosol of affected cells ($p < 0.001$, Fig. 4.2 A-C). This result was recapitulated by knock-down of the complex I subunit ND-75 in motor neurons ($p < 0.01$, Fig. 4.2 D-F). In mammals, eIF2 α is at the convergence of four pathways which comprise the integrated stress response, and can therefore be phosphorylated by three other kinases in addition to PERK. Only one of these additional kinases, GCN2, is conserved in *Drosophila*. The relative contribution of PERK and GCN2 to eIF2α phosphorylation under conditions of mitochondrial dysfunction will be addressed in the next chapter.

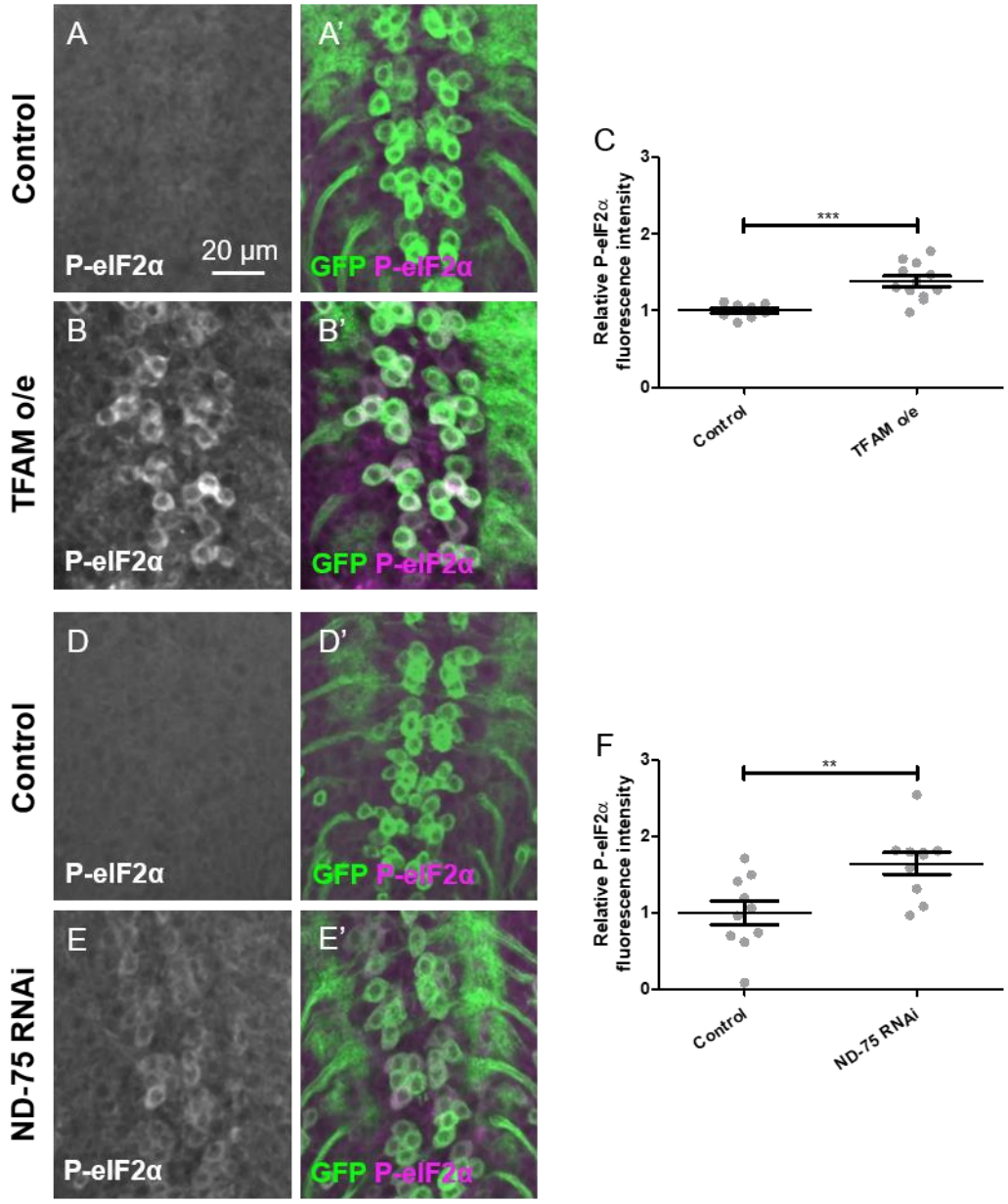

Figure 4.2 Levels of phosphorylated eIF2α are increased in Drosophila neurons with mitochondrial dysfunction. (A-B') Immunofluorescence staining with P-eIF2α antibody in control (A-A') or TFAM overexpressing (B-B') dorsal medial motor neurons. (D-E') Immunofluorescence staining with P-eIF2α antibody in control (D-D') or ND-75 knock-down (E-E') dorsal medial motor neurons.(A, B, D, E) P-eIF2α fluorescence. (A', B', D' E') Merged images of P-eIF2α (magenta) and membrane-targeted GFP (green). P-eIF2α staining quantified in C (TFAM overexpression, n = 8 larvae for control, 12 for TFAM o/e) and F (ND-75 RNAi, n = 10 larvae for control and ND-75 RNAi). Bars = mean ± SEM. Means compared by two-tailed unpaired t-test, **p < 0.01, ***p < 0.001.

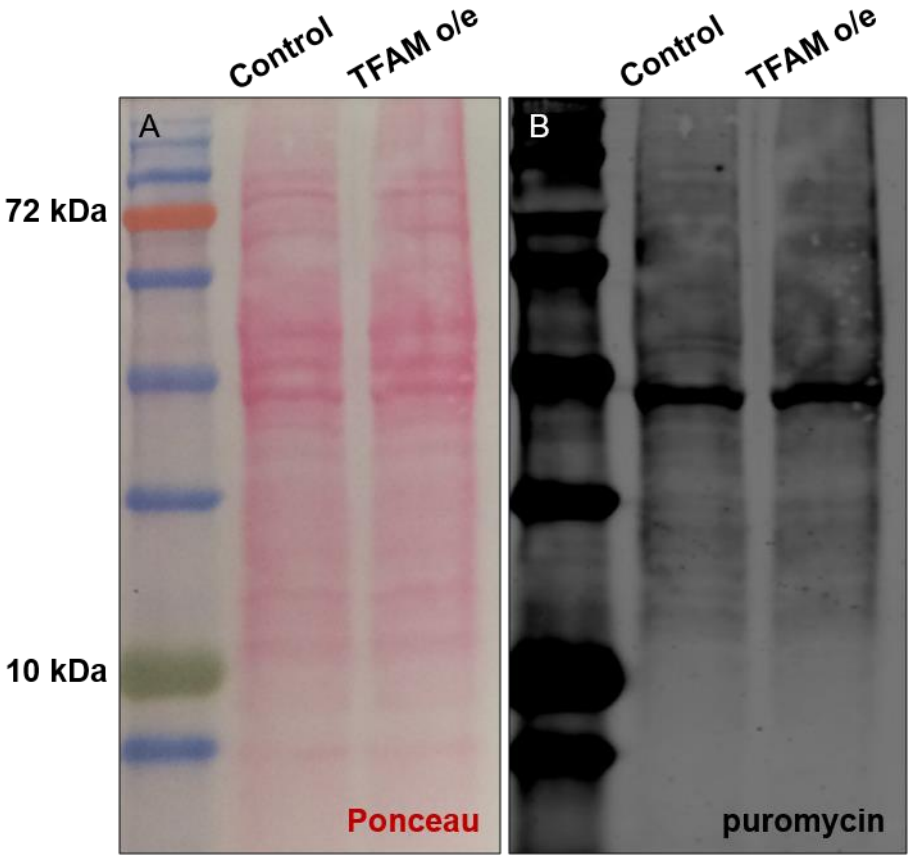

Figure 4.3 Preliminary indication that pan-neuronal overexpression of TFAM does not affect the rate of translation in the Drosophila CNS. Western blot of CNS homogenate from control or TFAM overexpressing wandering late third instar larvae. (A) Ponceau staining. (B) Immunostaining for puromycin.

Phosphorylation of eIF2α is typically observed to cause a reduction in cap-dependent translation (Fig. 4.1). Having observed increased levels of P-eIF2α in the TFAM overexpression and ND-75 knock-down models, I conjectured that translation may be globally reduced in *Drosophila* neurons with mitochondrial dysfunction as a protective bioenergetic measure. To test this proposal, I used the peptide chain terminator puromycin (Nathans 1964) to examine the rate of translation. Immunostaining for puromycin reports on the rate of incorporation of the toxin into nascent polypeptides. No difference was detected in the levels of puromycin incorporation in CNS homogenate between control larvae and those with pan-neuronal TFAM overexpression driven by *nSyb-Gal4* (Fig 4.3). Whilst there is obviously a glial contribution in the homogenate that could be confounding the result, these preliminary data indicate that TFAM overexpression does not cause a profound reduction in the rate of translation in *Drosophila* neurons.

Canonically, whilst phosphorylation of eIF2α usually reduces the rate of global translation, it translationally upregulates the ER UPR transcription factor ATF4 by inducing the ribosome to skip initiation at a series of decoy uORFs in the ATF4 5' UTR (see main Introduction). Therefore, I next examined ATF4 protein levels in *Drosophila* neurons with mitochondrial dysfunction by creating a polyclonal antibody directed at a 60 amino acid region common to all known isoforms of *Drosophila* ATF4, but outside of the widely-conserved DNA binding domain. Immunostaining of CNS tissue from larvae overexpressing ATF4 isoform B in motor neurons via the *OK371-Gal4* driver confirmed the specificity of the antibody; fluorescence was not detectable above background in the nuclei of motor neuron clusters in control VNCs, but was clearly visible in the ATF4-overexpressing larvae ($p = 0.0286$, Fig. 4.4).

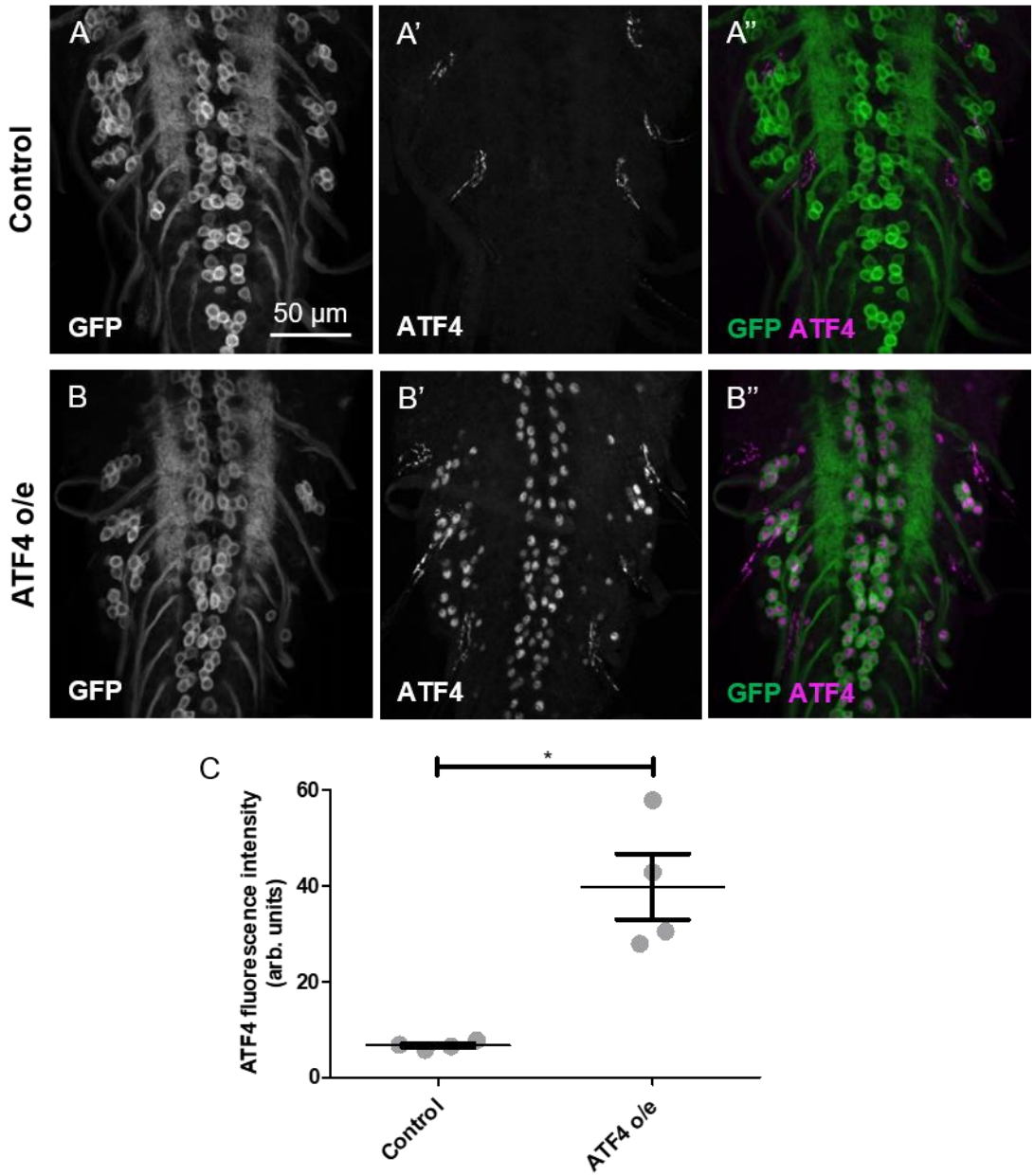

Figure 4.4 Validation of Drosophila ATF4 antibody. Immunofluorescence staining with ATF4 antibody, created as described in Materials and Methods 2.2.5, in control (A'-A'') or ATF4 overexpressing (B-B'') dorsal medial motor neurons. (A, B) Membrane-targeted GFP (*UAS-CD8-GFP;* green in A'', B''). (A', B') ATF4 antibody (magenta in A'', B''). (A'', B'') Merged images. (C) Quantification of ATF4 staining, n = 4 larvae for both control and ATF4 overexpression conditions. Bars = mean ± SEM. Medians compared by two-tailed Mann-Whitney test, *p = 0.0286.

The validated antibody was then used to test whether ATF4 is upregulated in our models of mitochondrial dysfunction. Strong ATF4 staining was seen in the nuclei of motor neurons of flies overexpressing TFAM ($p < 0.001$, Fig. 4.5 A-C) or ND-75 RNAi ($p < 0.001$, Fig. 4.5 D-F) via *OK371-Gal4*, indicating that ATF4 is indeed upregulated by mitochondrial dysfunction in *Drosophila* motor neurons. Once again, membrane-targeted GFP was used to mark the cells in which the genetic manipulation had taken place.

Having established that proteins that can form components of the PERK branch of the ER UPR are activated by neuronal mitochondrial dysfunction in *Drosophila*, I next examined the IRE1 pathway. Like PERK, IRE1 is a transmembrane ER protein which oligomerises and autophosphorylates in response to unfolded protein stress in the ER. Unlike PERK, IRE1 acquires ribonuclease activity upon autophosphorylation, and splices mRNA of the transcription factor XBP1 to produce an active form of the protein (Fig. 4.1). To assess activation of XBP1 in our models of mitochondrial dysfunction, I used a *UAS* reporter construct that has EGFP subcloned downstream of the IRE1 splice site in XBP1 (Ryoo, Domingos et al. 2007). The EGFP encoded by the reporter is in frame only when XBP1 is spliced to its active form (Fig. 4.6 A). XBP1-EGFP and nuclear-targeted β-galactosidase (β-gal) were driven in motor neurons by *OK371-Gal4*. In control larvae, EGFP fluorescence was largely undetectable (Fig. 4.6 B', E'). However, when TFAM was overexpressed alongside the reporters, EGFP was clearly visible and colocalised with β-Gal, demonstrating that the XBP1-EGFP fusion protein had been targeted to the nucleus as expected for an active transcription factor (Fig. 4.6 C-C''). The increase in EGFP was significant compared to control larvae ($p < 0.001$, Fig. 4.6 D). Knock-down of the complex I subunit ND-75 in motor neurons resulted in even stronger EGFP expression compared to controls ($p < 0.001$, Fig. 4.6 F-F'', G). Taken together, these results indicate that the splicing of XBP1 to active form occurs in the motor neurons of *Drosophila* with mitochondrial dysfunction.

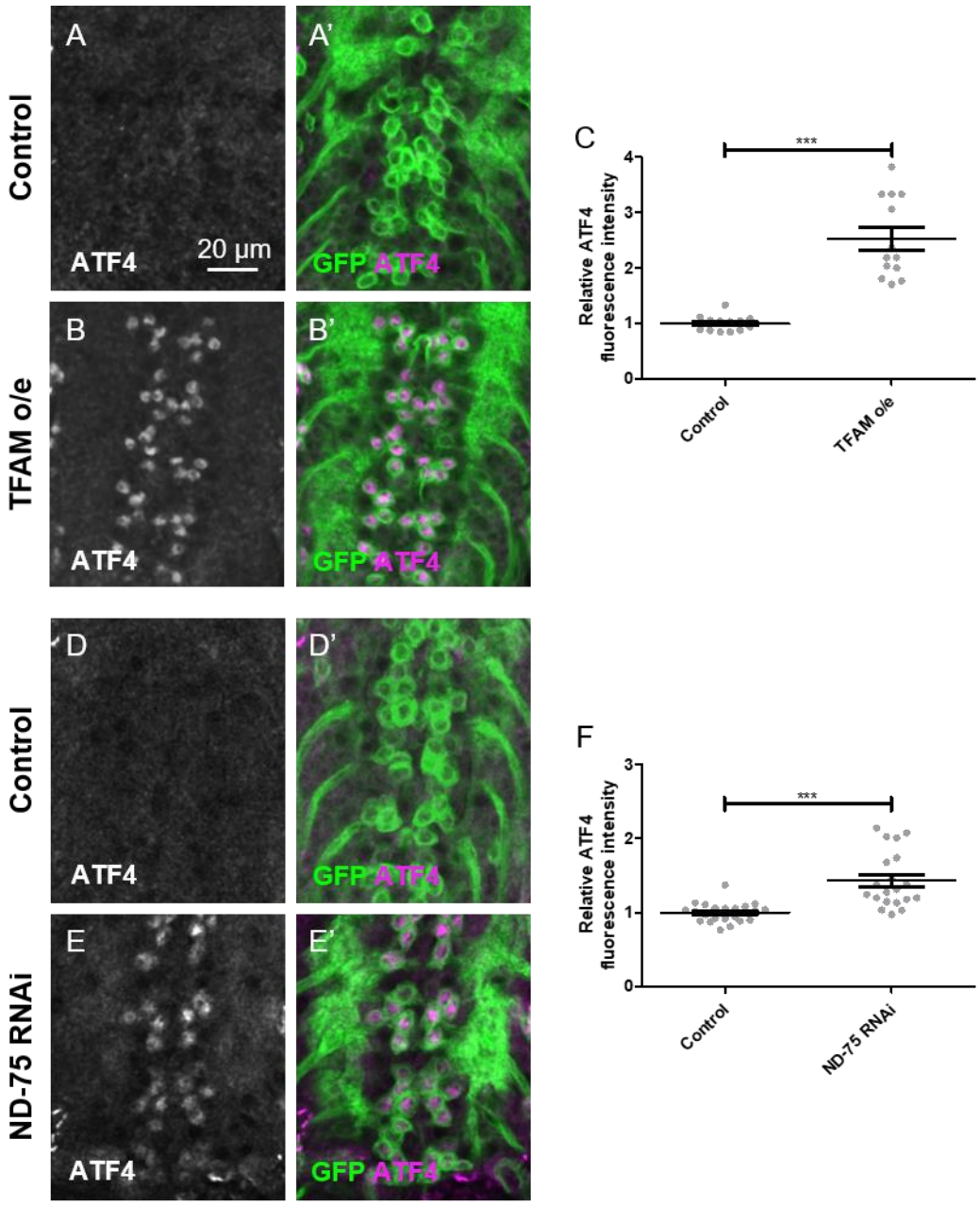

Figure 4.5 Levels of ATF4 are increased in Drosophila neurons with mitochondrial dysfunction (A-B') Immunofluorescence staining with ATF4 antibody in control (A-A') or TFAM overexpressing (B-B') dorsal medial motor neurons. (D-E') Immunofluorescence staining with P-eIF2α antibody in control (D-D') or ND-75 knock-down (E-E') dorsal medial motor neurons. (A, B, D, E) ATF4 fluorescence. (A', B', D' E') Merged images of ATF4 (magenta) and membrane-targeted GFP (green). ATF4 staining quantified in C (TFAM overexpression, n = 13 larvae for control and TFAM o/e) and F (ND-75 RNAi, n = 23 larvae for control and 20 for ND-75 RNAi). Bars = mean ± SEM. Means compared by two-tailed unpaired t-test, ***$p < 0.001$.

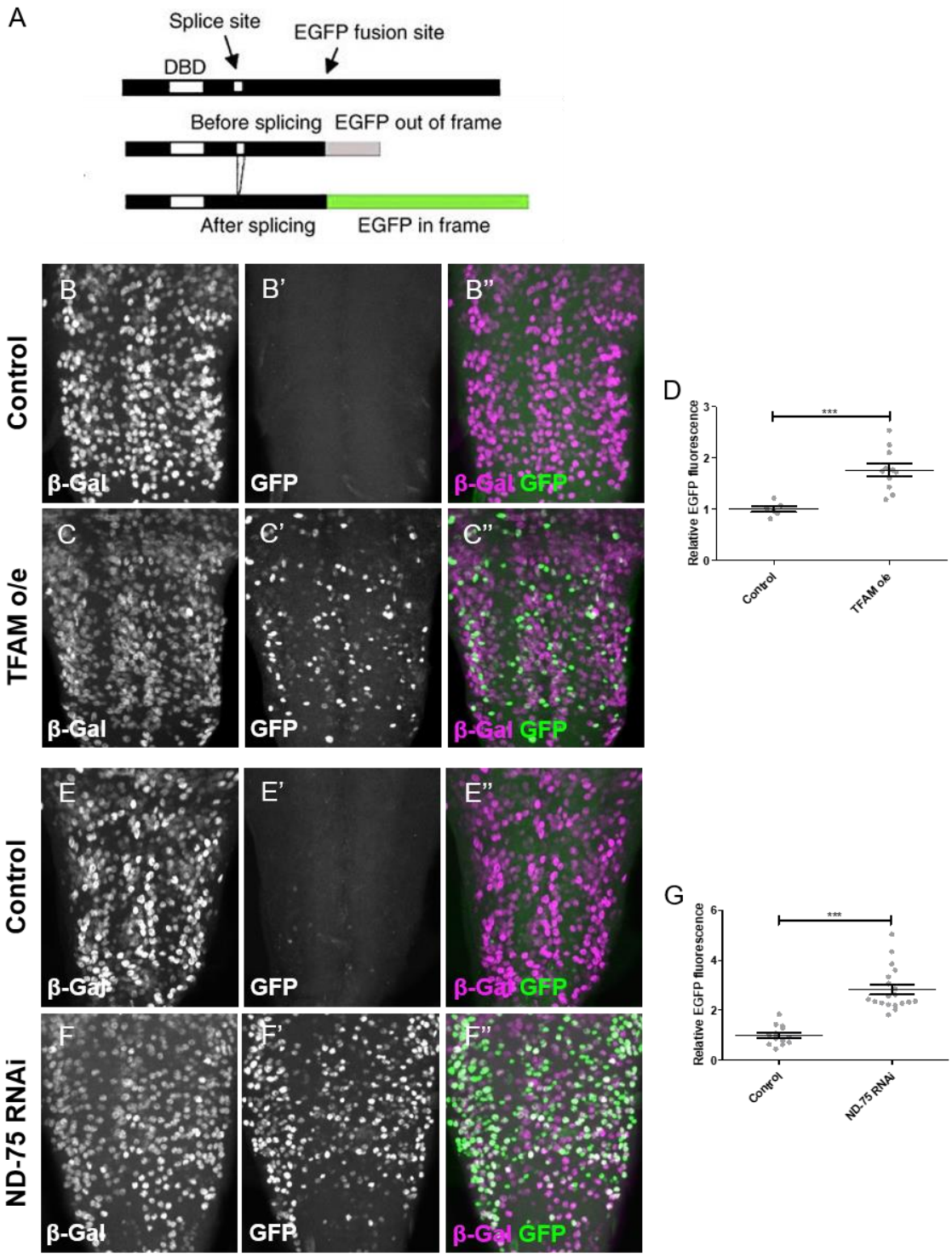

Figure 4.6 Splicing of XBP1 mRNA to produce an active form of the protein is increased in Drosophila neurons with mitochondrial dysfunction. (A) EGFP is in frame only when XBP1 mRNA is spliced to encode an active form of the protein, from (Ryoo, Domingos et al. 2007). (B-C'') XBP1-EGFP fluorescence and nuclear-targeted β-Gal in control (B-B'') or TFAM overexpressing (C-C'') motor neurons. (E-F'') XBP1-EGFP fluorescence and nuclear-targeted β-Gal in control (E-E'') or ND-75 knock-down (F-F'') motor neurons. (B, C, E, F) Immunofluorescence staining with β-Gal antibody. (B', C', E', F') XBP1-EGFP fluorescence. (B'', C'', E'', F'') Merged images. (D) Quantification of EGFP fluorescence in control and TFAM overexpressing motor neurons (n = 6 larvae for control, 11 for TFAM o/e). (G) Quantification of EGFP fluorescence in control and ND-75 knock-down motor neurons (n = 13 larvae for control and 19 for ND-75 RNAi). Bars = mean ± SEM. Means compared by two-tailed unpaired t-test, ***$p < 0.001$.

4.2.2 Genetic manipulation of ER UPR components in *Drosophila* motor neurons with mitochondrial dysfunction affects neuronal function.

I have demonstrated that components of the stress signalling ER UPR are activated in *Drosophila* models of neuronal dysfunction. To test the second part of my hypothesis - that this signalling will have functional consequences for the affected neurons - I performed two functional assays on all elements of the canonical ER UPR.

Adult *Drosophila* display negative geotaxis; when forcibly relocated to a base point they reflexively climb back upwards against gravity (Carpenter 1905). This behaviour enables us to use the climbing assay - a schematic of which is shown in Materials and Methods Fig. 2.2 A - to assess the motor system of the fly. Overexpression of TFAM in motor neurons by the *D42-Gal4* driver reduces the distance climbed by adult flies to about 50% of the control value ($p < 0.001$, Fig. 4.7 A), confirming that mitochondrial dysfunction can cause functional deficits in *Drosophila* neurons. Knock-down of ND-75 in motor neurons is pupal lethal and so was not used for ER UPR genetic interaction assays. Knock-down of PERK in conjunction with TFAM overexpression caused a significant exacerbation of the climbing phenotype ($p < 0.01$, Fig 4.7 A) when the knock-down was mediated by RNAi line 16427. PERK knock-down by a second RNAi line, 35162, resulted in a non-significant exacerbation of the climbing impairment induced by TFAM overexpression and a third RNAi line, 42499, was pupal lethal when combined with TFAM overexpression (both Appendix 8.2.1). Knock-down of PERK alone by the three RNAi lines did not cause any reduction in climbing ability compared to control flies (Fig.4.7 A and Appendix Fig. 8.2.1). Overexpression of PERK by *D42-Gal4* was lethal both alone, and in combination with TFAM overexpression at both 25 °C and 20 °C.

A second functional assay examines the status of the adult wing. Flies eclose from their pupal casing with folded wings (Materials and Methods Fig. 2.2 B). Secretion of the neurohormone buriscon from a population of crustacean cardioactive peptide (CCAP)-expressing neurons in the abdominal ganglion of the VNC controls the inflation that results in the flat wing of the mature adult (Luan, Lemon et al. 2006). Genetic manipulation of the amyotrophic lateral sclerosis-associated protein TDP-43 by both the *CCAP-Gal4* and *D42-Gal4* drivers (independently) results in adult flies with uninflated

wings (Vanden Broeck, Naval-Sánchez et al. 2013), likely due to the expression pattern of *D42-Gal4* overlapping that of CCAP/bursicon in the abdominal ganglion. Overexpression of TFAM via the *D42-Gal4* driver also results in approximately 50% of mature adult flies with uninflated wings (Fig. 4.7 B). Having determined that PERK knock-down exacerbates the climbing phenotype of TFAM-overexpressing flies, I examined the effect that knock-down of the protein has on wing inflation. In line with the climbing assay results, both of the PERK RNAi lines that were non-lethal when combined with TFAM overexpression caused a significant increase in the number of flies with uninflated wings in the mitochondrial dysfunction condition ($p < 0.001$ for both, Fig. 4.7 B & Appendix 8.2.1).

Subsequent examination of each of the remaining ER UPR elements via climbing and wing inflation assays suggested diverse functional implications for each of the components, with the unifying theme that knock-down of the transcription factors at the end of each UPR branch appears functionally beneficial. These results are described below and summarised in Table 3.

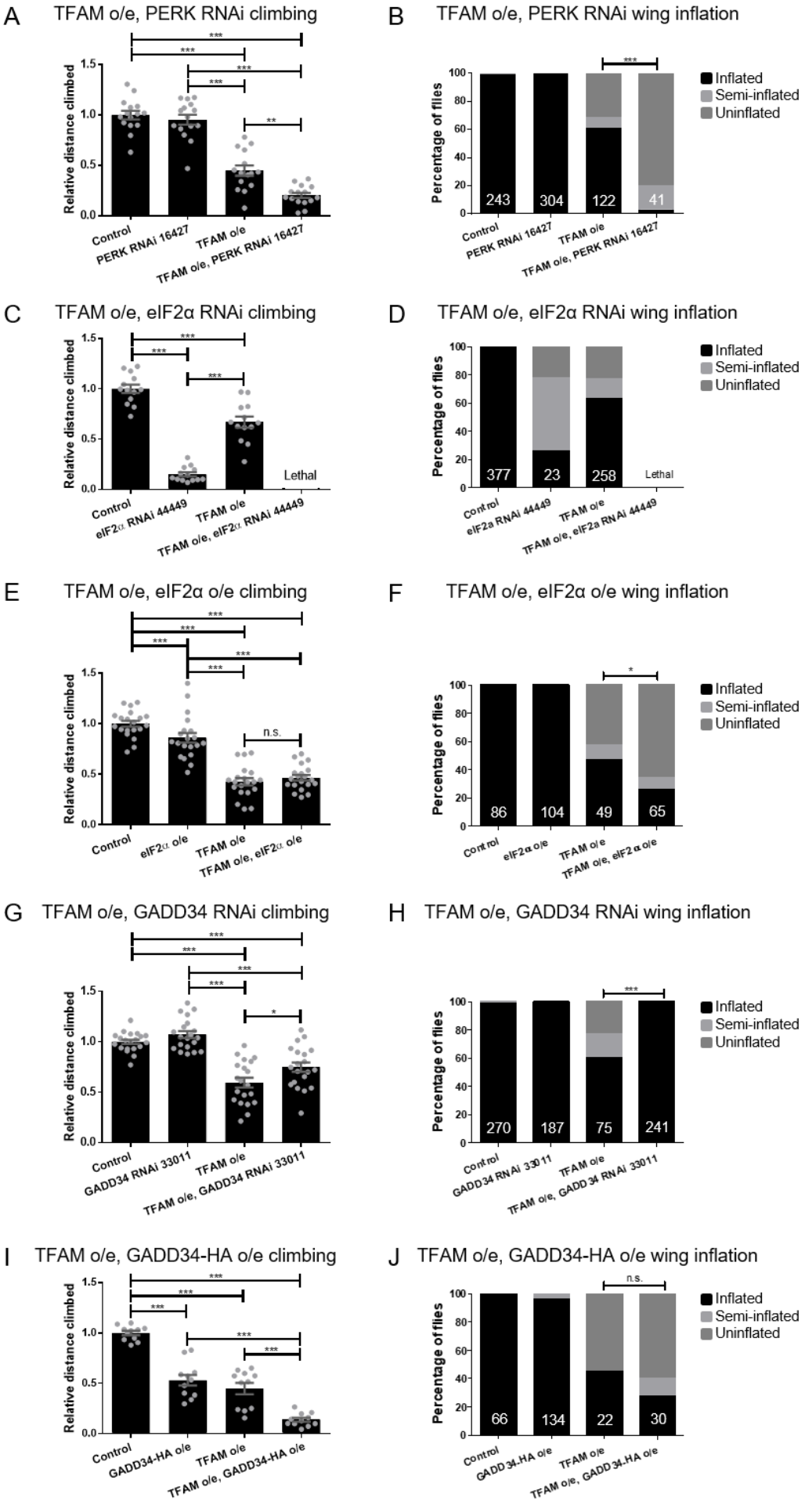
A
TFAM o/e, PERK RNAi climbing
Relative distance climbed
Control
PERK RNAi 16427
TFAM o/e
TFAM o/e, PERK RNAi 16427
B
TFAM o/e, PERK RNAi wing inflation
Percentage of flies
Inflated
Semi-inflated
Uninflated
243
304
122
41
C
TFAM o/e, eIF2α RNAi climbing
Lethal
eIF2α RNAi 44449
TFAM o/e, eIF2α RNAi 44449
D
TFAM o/e, eIF2α RNAi wing inflation
377
23
258
eIF2a RNAi 44449
TFAM o/e, eIF2a RNAi 44449
E
TFAM o/e, eIF2α o/e climbing
n.s.
eIF2α o/e
TFAM o/e, eIF2α o/e
F
TFAM o/e, eIF2α o/e wing inflation
86
104
49
65
G
TFAM o/e, GADD34 RNAi climbing
GADD34 RNAi 33011
TFAM o/e, GADD34 RNAi 33011
H
TFAM o/e, GADD34 RNAi wing inflation
270
187
75
241
I
TFAM o/e, GADD34-HA o/e climbing
GADD34-HA o/e
TFAM o/e, GADD34-HA o/e
J
TFAM o/e, GADD34-HA o/e wing inflation
66
134
22
30

Figure 4.7 Functional consequences of genetic manipulation of components of the PERK ER UPR pathway (PERK, eIF2α and GADD34) in Drosophila motor neurons with TFAM overexpression. (A, B) Climbing (A) and wing inflation (B) assays with PERK knock-down (line 16427). (C, D) Climbing (C) and wing inflation (D) assays with eIF2α knock-down (line 44449), flies incubated at 20 °C for the duration of the assay (25 ° C for all other climbing and wing inflation assays). (E, F) Climbing (E) and wing inflation (F) assays with eIF2α overexpression. (G, H) Climbing (G) and wing inflation (H) assays with GADD34 knock-down (line 33011). (I, J) Climbing (I) and wing inflation (J) assays with GADD34 overexpression. TFAM overexpression and all ER UPR RNAi and overexpression lines were driven by *D42-Gal4*. Wing inflation assay: number of flies per genotype displayed at the base of each column. Climbing assays: n = 15 for all genotypes in A, n = 13 for all genotypes in C, n = 20 for E & G, and n = 11 for I. Bars = mean ± SEM. Means were compared by one-way parametric ANOVA with Tukey's post-hoc test. Wing inflation: significance was tested by Chi-squared test on the raw data. n.s. = not significant, * $p < 0.5$, ** $p < 0.01$, *** $p < 0.001$.

Knock-down of eIF2α caused a substantial reduction in viability, even at 20 °C, and highly significant climbing and wing inflation impairments compared to control flies ($p < 0.001$, Fig. 4.7 C & D). When combined with TFAM overexpression, knock-down of eIF2α was pupal lethal. Overexpression of eIF2α alone also reduced climbing ability compared to control flies, and when combined with TFAM overexpression increased the number of flies with uninflated wings ($p < 0.05$, Fig. 4.7 F) compared to the TFAM overexpression condition, but did not significantly affect the TFAM-overexpression climbing phenotype (Fig. 4.7 E).

GADD34 recruits a phosphatase that functions in a negative feedback loop within the UPR to oppose the action of PERK, by dephosphorylating eIF2α (Fig. 4.1). Two GADD34 RNAi lines generated inconsistent outcomes; line 33011 suppressed the TFAM-overexpression functional deficits ($p < 0.05$ (climbing), $p < 0.001$ (wing), Fig 4.7 G & H), whilst line 107545 did not alter the climbing ability of TFAM-overexpressing flies (Appendix 8.2.1), but did cause a significant increase in the number of flies with uninflated wings ($p < 0.001$, Appendix Fig 8.2.1). Overexpression of GADD34 exacerbated the climbing deficiencies of the mitochondrial dysfunction flies ($p < 0.001$, Fig 4.7 I), but did not significantly alter the number of flies with uninflated wings (Fig. 4.7 J).

Knock-down of ATF4 by RNAi line 25985 slightly reduced climbing ability compared to control flies ($p < 0.001$), but produced a significant suppression of both the TFAM-overexpression climbing and wing inflation phenotypes ($p < 0.001$ for both, Fig. 4.8 A & B). Knockdown of ATF4 by another RNAi line, 2935, resulted in impaired climbing versus control flies ($p < 0.05$), but had no significant effect when combined with TFAM overexpression in either the climbing or wing inflation assays (Fig. 4.8 C & D). Overexpression of ATF4 also resulted in a climbing deficit compared to control flies ($p < 0.01$, Fig. 4.8 E), and, in this case, also exacerbated the TFAM-overexpression climbing and wing phenotypes ($p < 0.01$ and $p < 0.001$ respectively, Fig. 4.8 E & F).

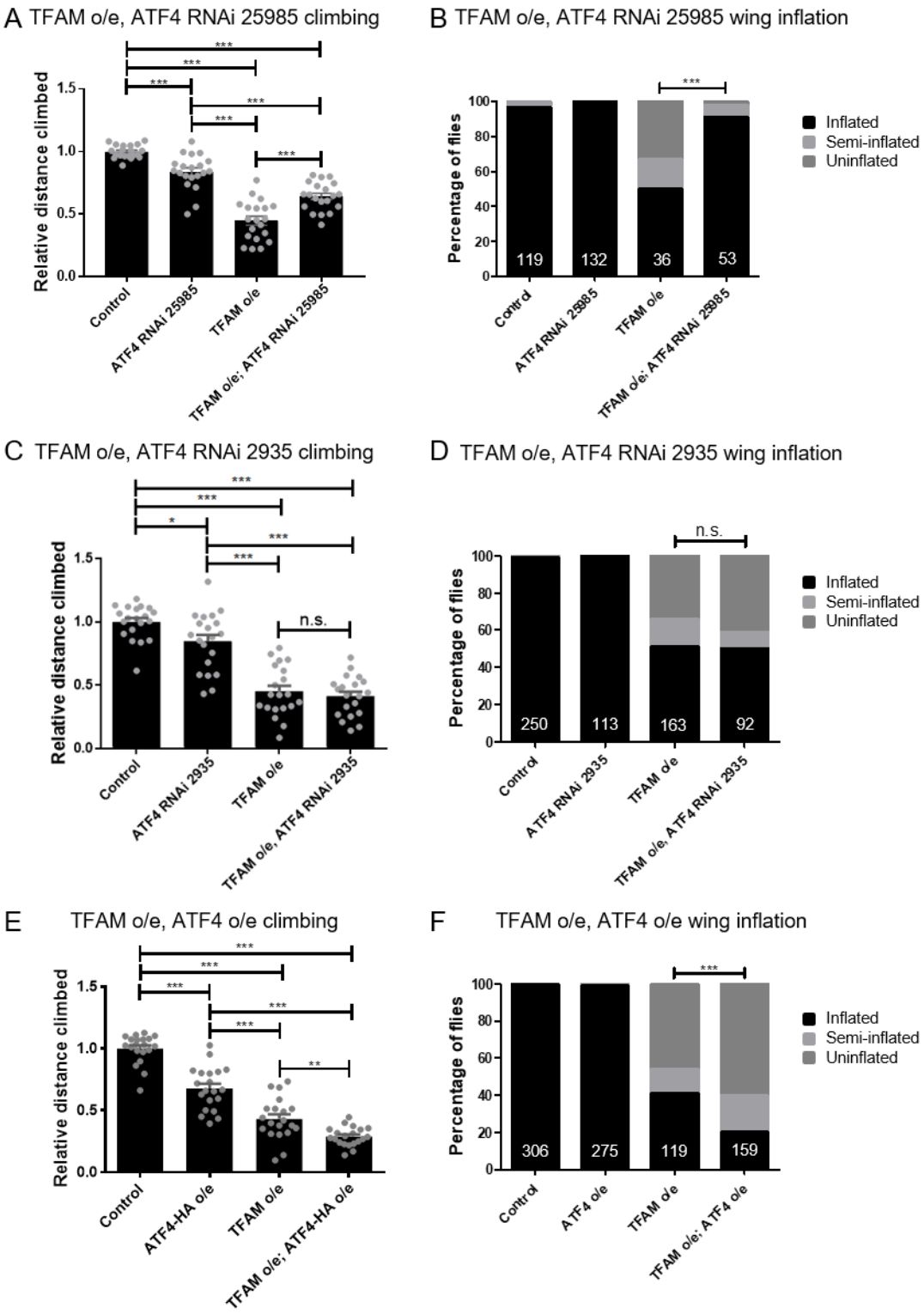

Figure 4.8 Functional consequences of genetic manipulation of ATF4 in Drosophila motor neurons with TFAM overexpression. (A, B) Climbing (A) and wing inflation (B) assays with ATF4 knock-down (line 25985). (C, D) Climbing (C) and wing inflation (D) assays with ATF4 knock-down (line 2935). (E, F) Climbing (E) and wing inflation (F) assays with ATF4 overexpression. TFAM overexpression and all ATF4 RNAi and overexpression lines were driven by *D42-Gal4*. Wing inflation assay: number of flies per genotype displayed at the base of each column. Climbing assays: n = 20 for all genotypes. Bars = mean ± SEM. Means were compared by one-way parametric ANOVA with Tukey's post-hoc test. Wing inflation: significance was tested by Chi-squared test on the raw data. n.s. = not significant, * $p < 0.5$, ** $p < 0.01$, *** $p < 0.001$.

Knock-down of IRE1 at the head of the second ER UPR pathway produced inconsistent results. One RNAi line (35253) significantly suppressed both the climbing and wing inflation deficits of TFAM-overexpressing flies ($p < 0.001$, Fig. 4.9 A & B), whilst another line, (62156) precipitated an increase in these impairments ($p < 0.5$ for climbing, $p < 0.001$ for wing inflation, Appendix 8.2.2). Flies heterozygous for the (homozygous lethal) loss-of-function mutant $IRE1^{f02170}$ displayed a small, but non-significant, improvement in climbing ability, and a significantly improved wing inflation ability ($p < 0.001$ Appendix 8.2.2). Overexpression of IRE1 did not alter the climbing ability of flies with neuronal mitochondrial dysfunction, but did significantly reduce the number of flies with uninflated wings ($p < 0.01$, Fig. 4.9 D).

Knock-down of XBP1 by two RNAi lines consistently suppressed the climbing and wing inflation impairments of TFAM-overexpressing flies ($p < 0.05$ for line 36755 climbing, $p < 0.001$ for all other comparisons, Fig. 4.9 E & F and Appendix 8.2.2). Overexpression of the C-terminally truncated XBP1-EGFP fusion that was used to test activation of XBP1 caused a non-significant exacerbation of the TFAM-overexpression climbing phenotype (Fig. 4.9 G) and a significant increase in the number of flies with uninflated wings ($p < 0.001$, Fig. 4.9 H).

The transcription factor ATF6 comprises the third branch of the mammalian ER UPR (Fig. 4.1). Knock-down of ATF6 suppressed the climbing and wing inflation phenotypes of TFAM-overexpressing flies ($p < 0.001$ for both, Fig. 4.10 A & B). Overexpression of ATF6 did not significantly impact the climbing or wing inflation deficits of TFAM-overexpressing flies (Fig. 4.10 C & D).

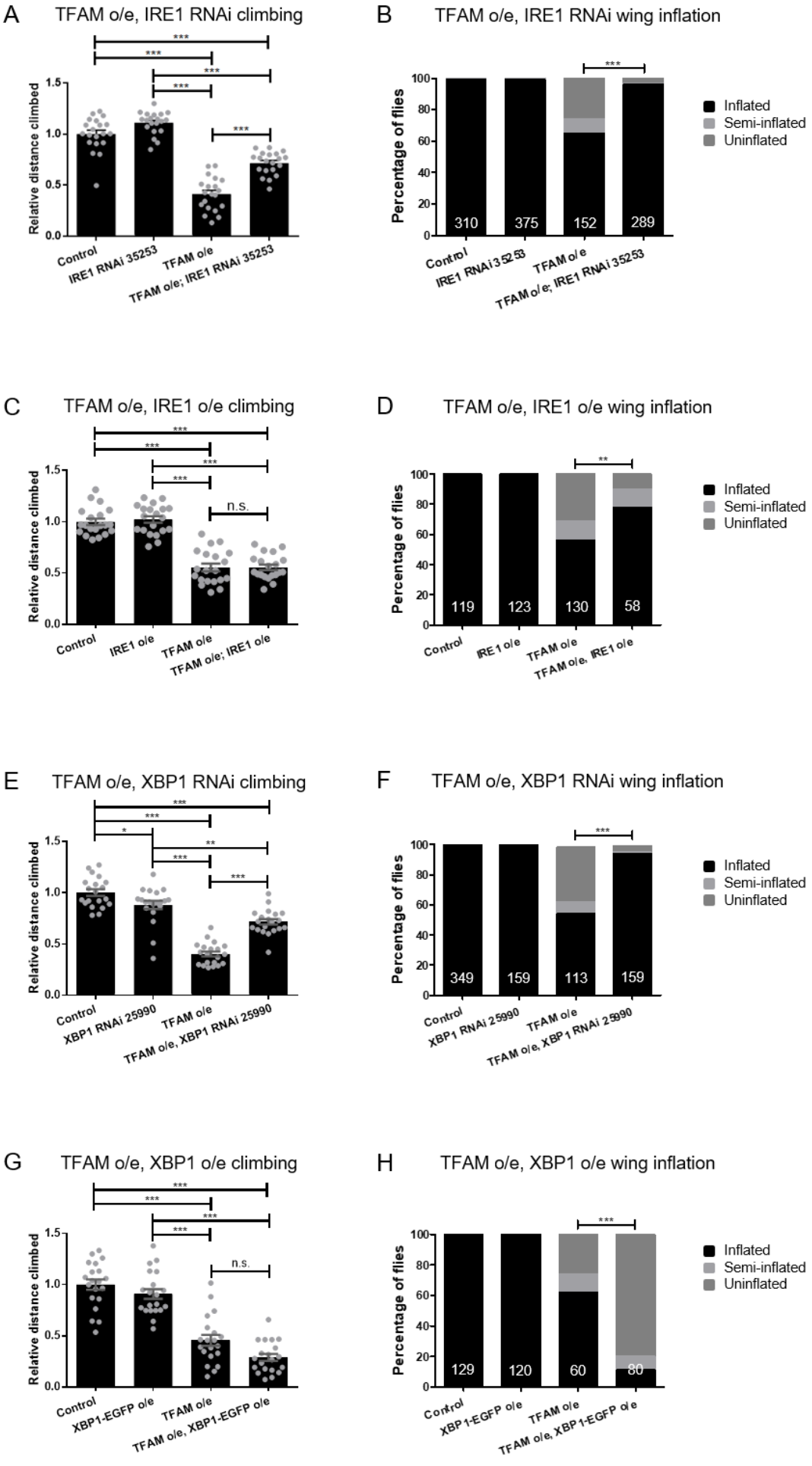
A
TFAM o/e, IRE1 RNAi climbing
Relative distance climbed
Control
IRE1 RNAi 35253
TFAM o/e
TFAM o/e; IRE1 RNAi 35253
B
TFAM o/e, IRE1 RNAi wing inflation
Percentage of flies
310
375
152
289
Inflated
Semi-inflated
Uninflated
C
TFAM o/e, IRE1 o/e climbing
n.s.
IRE1 o/e
TFAM o/e; IRE1 o/e
D
TFAM o/e, IRE1 o/e wing inflation
119
123
130
58
E
TFAM o/e, XBP1 RNAi climbing
XBP1 RNAi 25990
TFAM o/e, XBP1 RNAi 25990
F
TFAM o/e, XBP1 RNAi wing inflation
349
159
113
159
G
TFAM o/e, XBP1 o/e climbing
XBP1-EGFP o/e
TFAM o/e, XBP1-EGFP o/e
H
TFAM o/e, XBP1 o/e wing inflation
129
120
60
80

Figure 4.9 Functional consequences of genetic manipulation of the IRE1 ER UPR pathway in Drosophila motor neurons with TFAM overexpression. (A, B) Climbing (A) and wing inflation (B) assays with IRE1 knock-down (line 35253). (C, D) Climbing (C) and wing inflation (D) assays with IRE1 overexpression. (E, F) Climbing (E) and wing inflation (F) assays with XBP1 knock-down (line 25990). Performed by Rhian Ford. (G, H) Climbing (G) and wing inflation (H) assays with XBP1-EGFP overexpression. Performed by Jordan Briscoe. TFAM overexpression and all ER UPR RNAi and overexpression lines were driven by *D42-Gal4*. Wing inflation assay: number of flies per genotype displayed at the base of each column. Climbing assays: n = 20 for all genotypes. Bars = mean ± SEM. Means were compared by one-way parametric ANOVA with Tukey's post-hoc test. Wing inflation: significance was tested by Chi-squared test on the raw data. n.s. = not significant, *$p < 0.05$, **$p < 0.01$, ***$p < 0.001$.

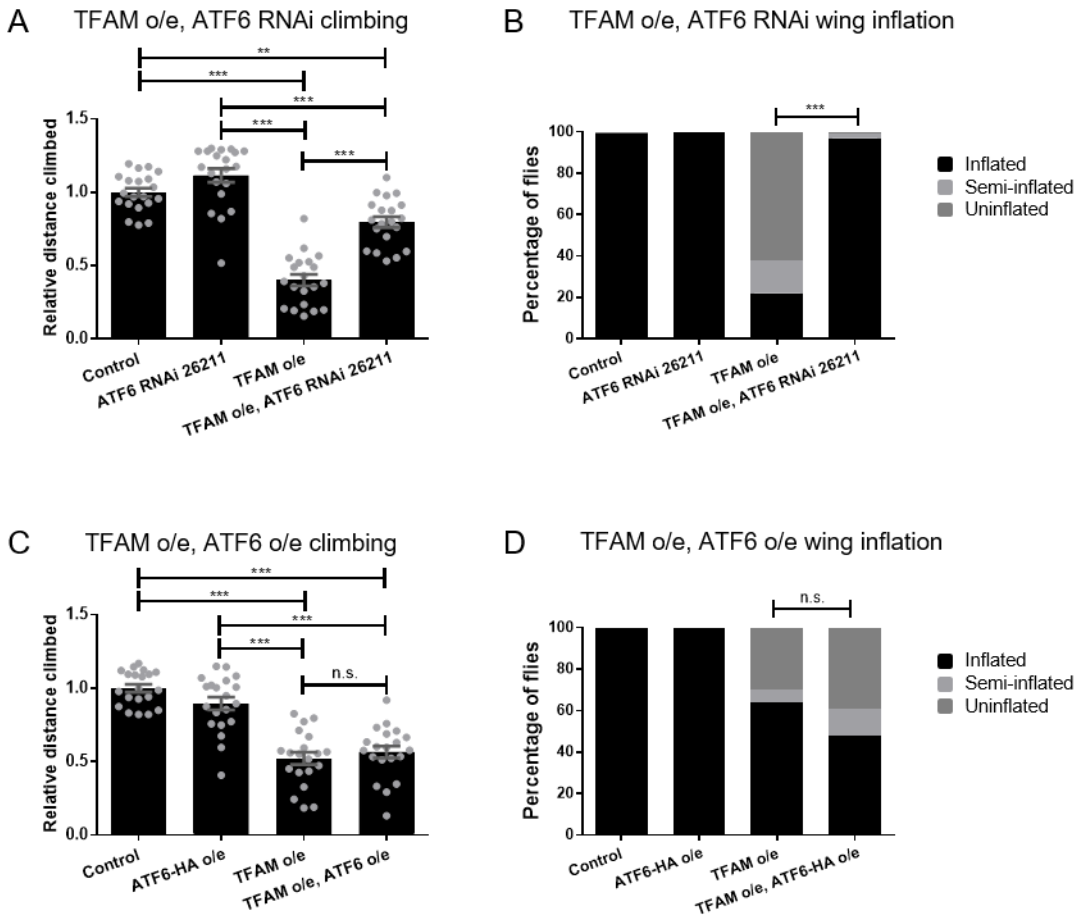

Figure 4.10 Functional consequences of genetic manipulation of ATF6 in Drosophila motor neurons with TFAM overexpression. (A, B) Climbing (A) and wing inflation (B) assays with ATF6 knock-down (line 26211). (C, D) Climbing (C) and wing inflation (D) assays with ATF6 overexpression. TFAM overexpression and ATF6 RNAi and overexpression lines were driven by *D42-Gal4*. Wing inflation assay: number of flies per genotype displayed at the base of each column. Climbing assays: n = 20 for all genotypes. Bars = mean ± SEM. Means were compared by one-way parametric ANOVA with Tukey's post-hoc test. Wing inflation: significance was tested by Chi-squared test on the raw data. n.s. = not significant, **p < 0.01, ***p < 0.001.

			Climbing		Wing inflation	
ER UPR Gene	Manipulation	Stock number	vs. control	vs. TFAM o/e	vs. control	vs. TFAM o/e
PERK	RNAi	V 16427		↓		↓
		BM 35162				↓
		BM 42499		Lethal		Lethal
	O/e	Δ	Lethal	Lethal	Lethal	Lethal
eIF2α	RNAi	BM 44449	↓	Lethal	↓	Lethal
	O/e	F 001282	↓			↓
ATF4	RNAi	BM 25985	↓	↑		↑
		V 2935	↓			
	O/e	F 000106	↓	↓		↓
GADD34	RNAi	BM 33011		↑		↑
		V 107545				↓
	O/e	F 003018	↓	↓		
IRE1	RNAi	BM 35253	↓	↑		↑
		BM 62156		↓		↓
	O/e	ψ				↑
	Mutant [f02170]	BM18520				↑
XBP1	RNAi	BM 25990	↓	↑		↑
		BM 36755	↓	↑		↑
	O/e	BM 60730				↓
ATF6	RNAi	BM 26211		↑		↑
	O/e	F 000476				

Table 3. Summary of climbing and wing inflation phenotypes produced by genetic manipulation of ER UPR components in Drosophila motor neurons. TFAM overexpression and all ER UPR lines were driven by *D42-Gal4*. Flies were incubated at 25 °C for the duration of all assays except for eIF2α RNAi and PERK o/e which were lethal alone at 25 °C, and therefore incubated at 20 °C throughout. 'vs. control' = comparison of ER UPR line (expressed alone) with control flies. 'vs. TFAM o/e' = comparison of ER UPR line expressed with TFAM overexpression, with flies overexpressing TFAM alone. O/e = overexpression. ↓ on red background = significantly reduced. ↑ on green background = significantly increased. Yellow background = no significant difference. BM = Bloomington *Drosophila* Stock Center, V = Vienna *Drosophila* Resource Center, F = FlyORF (Zurich ORFeome Project), Δ = (Malzer, Daly et al. 2010), ψ = (Coelho, Cairrão et al. 2013).

4.3 Summary

In the previous chapter, I outlined alterations to ER biology that occur in *Drosophila* neurons with mitochondrial dysfunction. These changes suggest that the ER may be subject to stress under conditions of mitochondrial dysfunction, and I therefore hypothesised that 1) the ER UPR stress signalling pathway may be activated by mitochondrial dysfunction in *Drosophila* neurons, and 2) that this activation would have functional consequences for the affected neurons. In this chapter, I tested these hypotheses by a series of immunofluorescence and functional assays.

The ER UPR kinase PERK phosphorylates the translation factor eIF2α when activated by ER stress. Immunofluorescence staining revealed that levels of P-eIF2α were increased in both tested models of mitochondrial dysfunction – overexpression of TFAM, and knock-down of the complex I subunit ND-75. Canonically, phosphorylation of eIF2α causes a reduction in global translation, and I therefore hypothesised that translation may be decreased in our models of mitochondrial dysfunction. Immunostaining for the peptide chain terminator puromycin gave preliminary indications that this conjecture is false; there was no significant difference in puromycin incorporation between control brains, and those with pan-neuronal overexpression of TFAM.

Whilst phosphorylation of eIF2α normally reduces cap-dependent translation, it specifically upregulates translation of the ER UPR transcription factor ATF4. Consistent with the finding that mitochondrial dysfunction caused an increase in P-eIF2α, levels of ATF4 were also upregulated in motor neurons with TFAM overexpression and ND-75 knock-down.

In a second branch of the ER UPR, the transmembrane protein IRE1 becomes a ribonuclease upon activation, and splices mRNA of the transcription factor XBP1 to encode an active form of the protein. Use of an XBP1-EGFP fusion construct demonstrated that splicing of XBP1 to its active form also occurs in *Drosophila* motor neurons with TFAM overexpression and ND-75 knock-down.

Having determined that components that can comprise the PERK and IRE1 branches of the ER UPR are activated in *Drosophila* neurons with mitochondrial dysfunction, I examined the functional consequences of this activation via climbing and

wing inflation assays. Whilst there was some variation in the results produced by the replicate RNAi lines, some reliable observations were made; knockdown of PERK resulted in an exacerbation of the climbing and wing inflation impairments caused by TFAM overexpression whilst, conversely, knockdown of the transcription factors at the end of each UPR branch – ATF4, XBP1 and ATF6 – generally resulted in the suppression of the TFAM-overexpression phenotypes.

In this chapter, I have established that components of the ER UPR are activated in *Drosophila* neurons with mitochondrial dysfunction, and that this activation has functional consequences for the affected neurons.

5. Investigating the role of the ER UPR as a mitochondrial retrograde signalling pathway in *Drosophila* neurons.

5.1 Introduction

In Chapter 4, it was demonstrated that components of the IRE1 and PERK branches of the ER UPR are activated by mitochondrial dysfunction in *Drosophila* neurons. Genetic manipulation of the UPR modified the function of neurons with mitochondrial dysfunction in climbing and wing inflation assays. In particular, knock down of the transcription factors at the terminus of each branch partially suppressed the neuronal functional deficits caused by TFAM overexpression, suggesting that these proteins may be key therapeutic targets in neurodegenerative diseases associated with mitochondrial dysfunction.

I have hypothesised that the ER UPR is a mitochondrial retrograde signalling pathway in *Drosophila* neurons. For my conjecture to be correct, at least one of the UPR transcription factors must regulate nuclear gene transcription under conditions of mitochondrial dysfunction. The basic leucine zipper transcription factor ATF4 is the final element of the PERK branch of the ER UPR. Analysis of microarray data from human neuronal precursor cells treated with the mitochondrial complex I inhibitor MPP^+, identified ATF4 as the master regulator of transcriptional changes induced by the toxicant (Krug, Gutbier et al. 2014). ATF4 itself was transcriptionally upregulated in a mouse neocortical culture treated with another Complex I inhibitor, rotenone (Yap, Chen et al. 2013), and N2a neuroblastoma cells treated with MPP^+ (Mazzio and Soliman 2012). In addition, CHOP, a transcriptional target of mammalian ATF4, was highly upregulated in the cortex of mice with knockout of the mitochondrial serine protease HtrA2 (Moisoi, Klupsch et al. 2008). In *Drosophila*, ATF4 was discovered to be a regulator of the transcriptional response to mutations in the mitochondrial quality control factors *pink1* and *parkin* in whole fly heads (Celardo, Lehmann et al. 2017). Whilst these studies were mostly *in vitro*, or not specific to neuronal cells, they suggest that ATF4 is a strong candidate to regulate transcription in our *in vivo* models of mitochondrial dysfunction in *Drosophila* neurons. In this chapter, I will test the hypothesis that ATF4 is a

transcriptional regulator in our TFAM-overexpression model of mitochondrial dysfunction using RNA-Seq analysis.

Control of ATF4 expression is canonically at the level of translation, and is mediated by phosphorylation of the translational initiation factor eIF2α (see main Introduction). In mammalian cells, eIF2α can be phosphorylated by four kinases – including the ER UPR kinase PERK – that collectively form the integrated stress response (ISR). A multi-omics study of four disparate mitochondrial dysfunction models in HeLa cells identified the ISR as the key co-ordinator of the stress response (Quiros, Prado et al. 2017). Two of the four ISR kinases (PERK and GCN2) are conserved in *Drosophila* (Malzer, Szajewska-Skuta et al. 2013), and I will therefore also examine the extent to which upregulation of ATF4 is controlled by PERK and GCN2 in the TFAM-overexpression model of neuronal mitochondrial dysfunction.

5.1.1 Aims

In this chapter, I test the hypothesis that the ER UPR is a mitochondrial retrograde signalling pathway in *Drosophila* neurons by:

1) Determining whether ATF4 expression is controlled by the kinases PERK and GCN2 under conditions of mitochondrial dysfunction.
2) Investigating the putative role of ATF4 as a regulator of the transcriptional response to mitochondrial dysfunction by RNA-Seq analysis.
3) Validating my RNA-Seq experiment using an independent method.

5.2 Results

5.2.1 Determining whether ATF4 expression is controlled by the kinases PERK and GCN2 under conditions mitochondrial dysfunction.

I have shown in Chapter 4 that ATF4 is upregulated in *Drosophila* motor neurons under conditions of mitochondrial dysfunction, and hypothesised that this activation is mediated by the ER UPR. However, in mammalian cells, eIF2α is also the target of three other kinases that, together with PERK, comprise the ISR. Of the ISR kinases, only GCN2 is conserved alongside PERK in *Drosophila*. To establish the extent to which ATF4 expression in *Drosophila* neurons is co-ordinated by PERK and GCN2 under conditions of mitochondrial dysfunction, I performed a series of knock-down experiments.

Overexpression of TFAM, alongside knock-down of either PERK or GCN2, was driven in motor neurons by the glutamatergic driver *OK371-Gal4*. Affected cells were marked by co-expression of membrane-localised GFP (*UAS-CD8-GFP*). I used immunofluorescence in wandering third instar larvae to assess levels of ATF4 expression, employing an antibody to the protein, production and validation of which is described in the previous chapter.

Knock-down of PERK by RNAi line 16427 did not change levels of ATF4 in the nucleus of affected cells compared to control larvae (Fig. 5.1 A-B', E). However, knock-down of PERK in conjunction with TFAM overexpression resulted in a significant decrease in ATF4 expression when compared to TFAM overexpression alone ($p < 0.05$, Fig. 5.1 C-D', E), suggesting that ATF4 is regulated by PERK under conditions of mitochondrial dysfunction. This result was recapitulated by a second RNAi line against PERK; knock-down of PERK by RNAi line 42499 in concert with TFAM overexpression produced a significant reduction in ATF4 levels ($p < 0.001$, Fig. 5.1 H-J), but did not alter basal levels when expressed alone (Fig. 5.1 F-G', J). By contrast, expression of RNAi line 35355 against GCN2 did not alter levels of ATF4 in either control or mitochondrial dysfunction conditions (Fig. 5.2 A-E). Knock-down of GCN2 by an alternative RNAi line, 103976, resulted in a trend towards decreased ATF4 levels when TFAM was overexpressed (Fig. 5.2 F-J), but this was not significant. Taken together, these results suggest that in *Drosophila* motor neurons with TFAM overexpression, ATF4 is regulated by the ER UPR but not the remainder of the ISR.

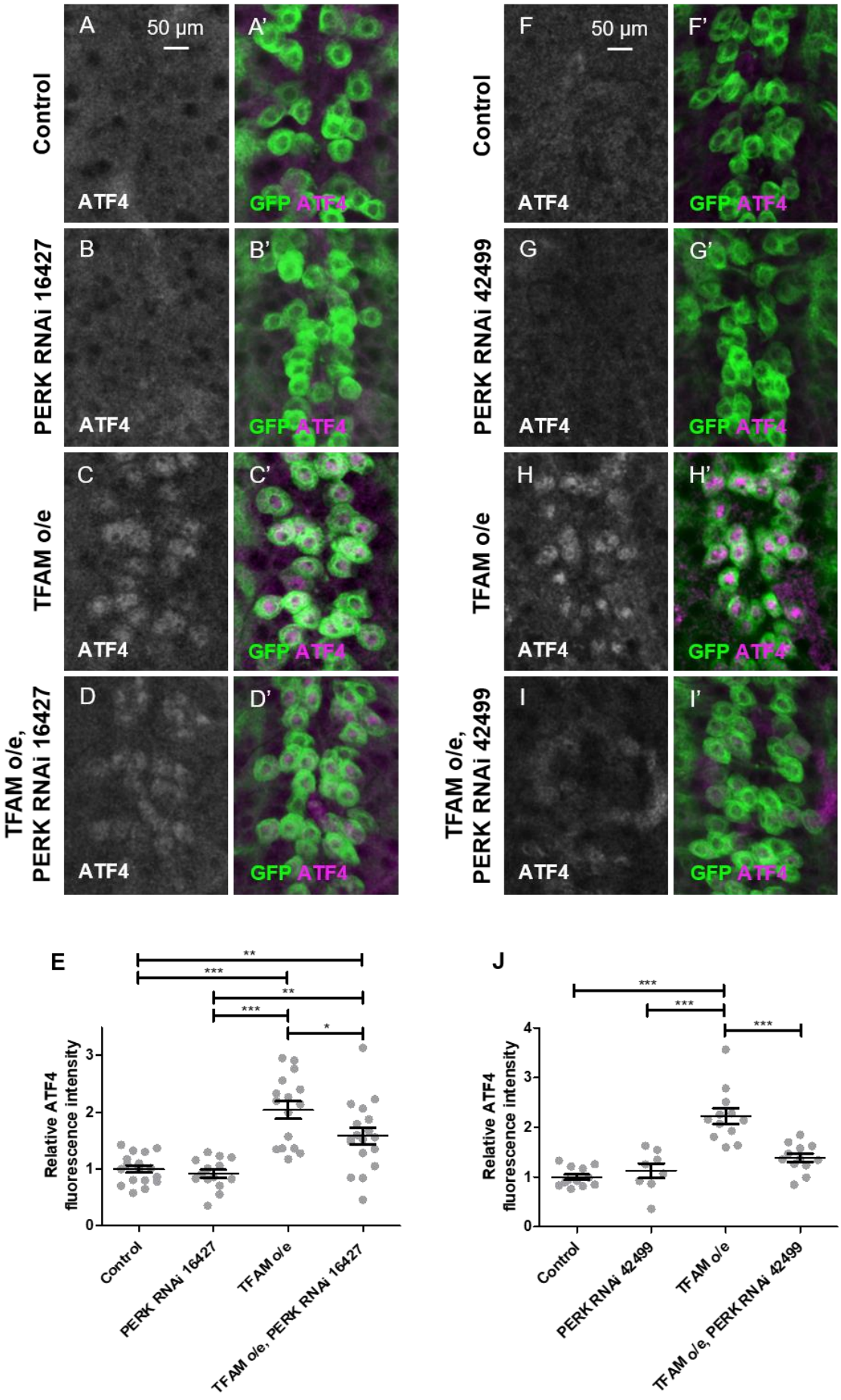
A
50 µm
A'
Control
ATF4
GFP ATF4
B
B'
PERK RNAi 16427
C
C'
TFAM o/e
D
D'
TFAM o/e, PERK RNAi 16427
F
F'
Control
G
G'
PERK RNAi 42499
H
H'
TFAM o/e
I
I'
TFAM o/e, PERK RNAi 42499
E
Relative ATF4 fluorescence intensity
Control
PERK RNAi 16427
TFAM o/e
TFAM o/e, PERK RNAi 16427
J
Relative ATF4 fluorescence intensity
Control
PERK RNAi 42499
TFAM o/e
TFAM o/e, PERK RNAi 42499

Figure 5.1 ATF4 is regulated by PERK under conditions of TFAM overexpression in Drosophila motor neurons. Membrane-targeted GFP (CD8-GFP), PERK RNAi and TFAM overexpression (o/e) driven in motor neurons of the VNC by *OK371-Gal4*. (A-A', F-F') control larvae, (C-C' and H-H') TFAM overexpression, (B-B') PERK RNAi line 16427, (D-D') TFAM overexpression and PERK RNAi 16427 combined, (G-G') PERK RNAi line 42499 and (I-I') TFAM overexpression and PERK RNAi 42499 combined. (A,B,C,D and F,G,H,I) Immunofluorescence staining with ATF4 antibody (white). (A',B',C',D' and F',G',H',I') Merged images of GFP (green) and ATF4 fluorescence (magenta). ATF4 staining for PERK RNAi 16427 quantified in (E), n = 17 (control larvae), 14 (PERK RNAi 16427), 16 (TFAM o/e) and 18 (TFAM o/e, PERK RNAi 16427). ATF4 staining for PERK RNAi 42499 quantified in (J), n = 12 (control larvae), 8 (PERK RNAi 42499), 12 (TFAM o/e) and 12 (TFAM o/e, PERK RNAi 42499). Bars = mean ± SEM. Means compared by one-way parametric ANOVA with Tukey's post-hoc test. *$p < 0.05$, **$p < 0.01$, ***$p < 0.001$.

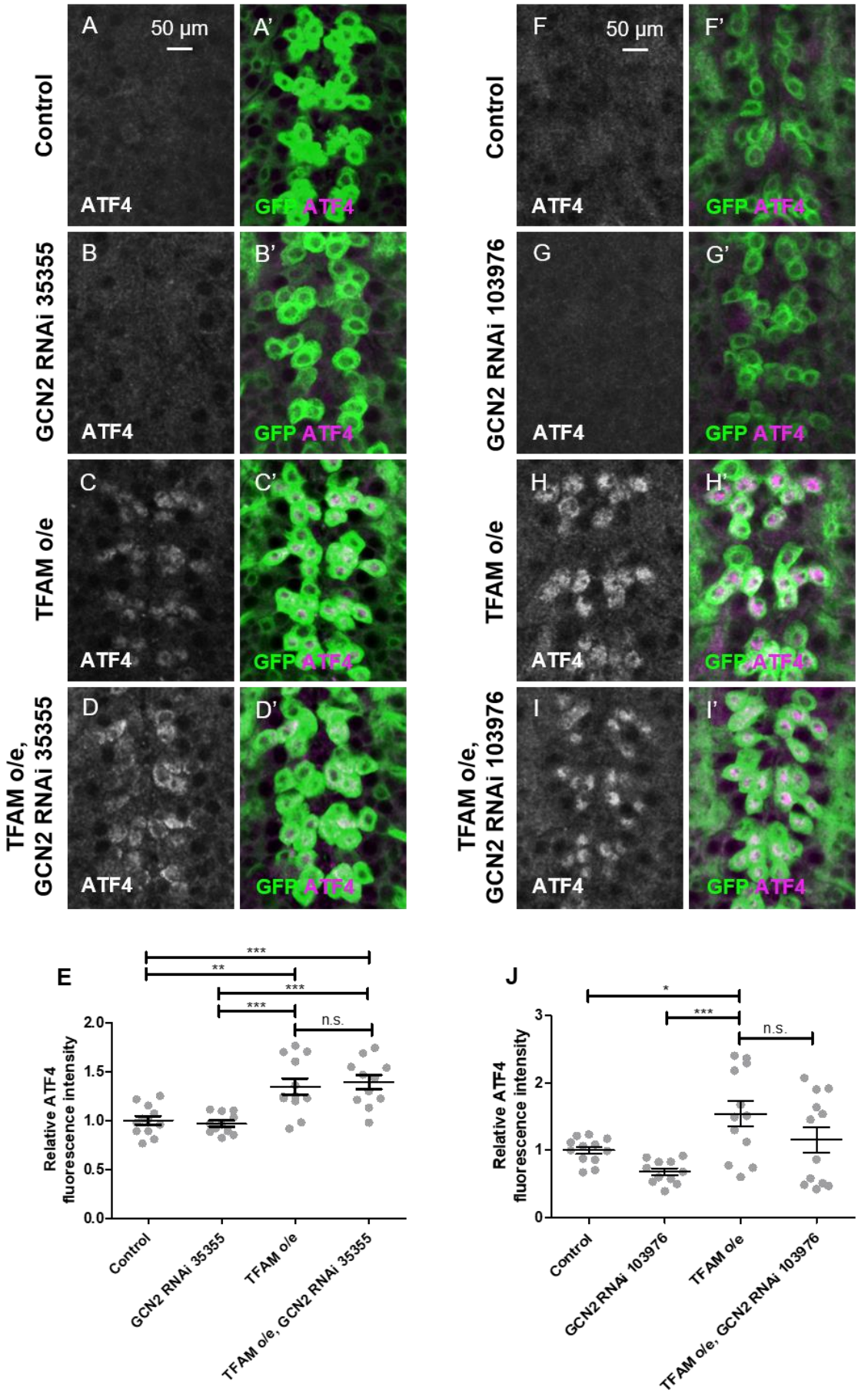
A
50 µm
A'
Control
ATF4
GFP ATF4
B
B'
GCN2 RNAi 35355
C
C'
TFAM o/e
D
D'
TFAM o/e, GCN2 RNAi 35355
F
F'
G
G'
GCN2 RNAi 103976
H
H'
I
I'
TFAM o/e, GCN2 RNAi 103976
E
Relative ATF4 fluorescence intensity
2.0
1.5
1.0
0.5
0.0
***
**
n.s.
Control
GCN2 RNAi 35355
TFAM o/e
TFAM o/e, GCN2 RNAi 35355
J
3
2
1
0
*
GCN2 RNAi 103976

Figure 5.2 ATF4 is not regulated by GCN2 under conditions of TFAM overexpression in Drosophila motor neurons. Membrane-targeted GFP (CD8-GFP), GCN2 RNAi and TFAM overexpression (o/e) driven in motor neurons of the VNC by *OK371-Gal4*. (A-A', F-F') control larvae, (C-C' and H-H') TFAM overexpression, (B-B') GCN2 RNAi line 35355, (D-D') TFAM overexpression and GCN2 RNAi 35355 combined, (G-G') GCN2 RNAi line 103976 and (I-I') TFAM overexpression and GCN2 RNAi 103976 combined. (A,B,C,D and F,G,H,I) Immunofluorescence staining with ATF4 antibody (white). (A',B',C',D' and F',G',H',I') Merged images of GFP (green) and ATF4 (magenta) fluorescence. ATF4 staining for GCN2 RNAi 35355 quantified in (E), n = 12 (control larvae), 11 (GCN2 RNAi 35355), 12 (TFAM o/e) and 11 (TFAM o/e, GCN2 RNAi 35355). ATF4 staining for GCN2 RNAi 103976 quantified in (J), n = 12 (control larvae), 11 (GCN2 RNAi 103976), 12 (TFAM o/e) and 12 (TFAM o/e, GCN2 RNAi 103976). Bars = mean ± SEM. Means compared by one-way parametric ANOVA with Tukey's post-hoc test. *$p < 0.05$, **$p < 0.01$, ***$p < 0.001$, n.s. = not significant.

5.2.2 Investigating the putative role of ATF4 as a regulator of the transcriptional response to mitochondrial dysfunction.

I have proposed that ATF4 is a key regulator of the transcriptional retrograde response to mitochondrial dysfunction in *Drosophila* neurons. To test this hypothesis, RNA sequencing (RNA-Seq) was performed on CNS tissue from wandering third instar larvae. Overexpression of TFAM, overexpression of ATF4, and overexpression of TFAM combined with ATF4 RNAi, were driven by the pan-neuronal driver *nSyb-Gal4*. Control larvae were the progeny of *nSyb-Gal4* flies crossed to w^{1118}. Since we do not detect the ATF4 protein in control larvae, *ATF4 RNAi* was omitted as a condition. Before proceeding to the RNA-Seq experiment, I performed qRT-PCR to confirm that expression of the ATF4 RNAi line (25985) reduced ATF4 mRNA abundance; ATF4 mRNA was reduced by ~90% in whole larvae with ATF4 RNAi line 25985 driven ubiquitously (Fig. 5.3).

To control for differing transcript lengths – a long transcript will produce more sequencing fragments than a shorter one – and variation in sequencing depth between runs, gene abundance in RNA-Seq analysis is presented as the normalised quantity 'fragments per kilobase of transcript per million reads' (FPKM). In all the following analyses, genes were considered meaningfully expressed if the average FPKM across the quadruplicate samples was ≥ 1 for at least one condition. This threshold was applied alongside minimum fold change cut-offs of 1.5 for upregulated genes, 0.67 (equivalent to a -1.5 fold change) for downregulated genes, and an adjusted p value cut-off of 0.05.

With the above thresholds applied, the expression of 63-169 genes were significantly changed between each pair of conditions (Fig. 5.4 and Table 4). The transcriptional retrograde response to the TFAM-overexpression model of mitochondrial dysfunction can be seen by considering the 'TFAM overexpression vs Control' pairing; 36 genes were significantly upregulated, and 63 significantly downregulated. Heatmaps showing expression of the genes up- and downregulated by TFAM overexpression can be seen in Figures 5.5 and 5.6 respectively.

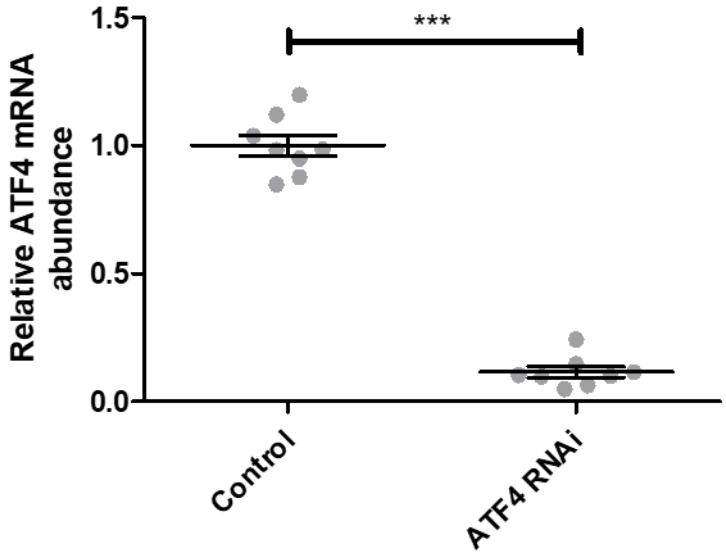

Figure 5.3 Expression of ATF4 RNAi line (25985) reduces ATF4 mRNA abundance. ATF4 RNAi line 25985 was driven ubiquitously by Da-Gal4, and qRT-PCR was performed on cDNA synthesised from RNA extracted from wandering third instar larvae. Abundance was normalised to the housekeeping gene Rpl4. Means compared by two-tailed unpaired t-test. ***$p < 0.001$.

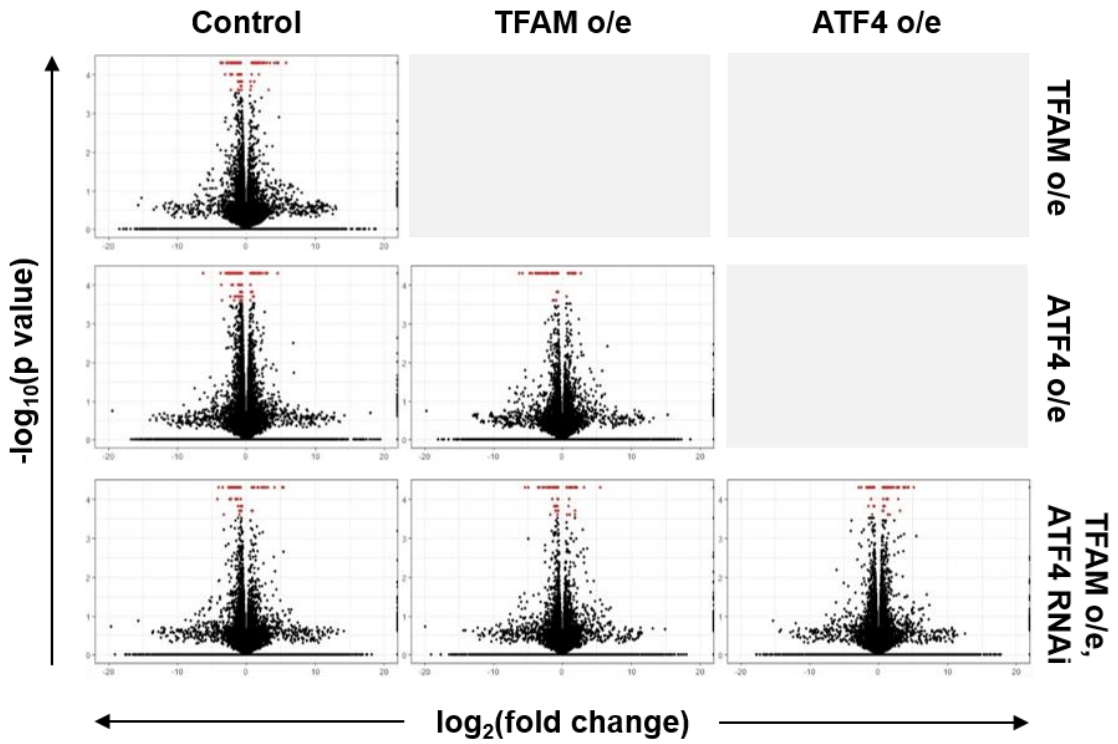

Figure 5.4 Volcano plots of pairwise gene expression changes as determined by RNA-Seq analysis. Expression changes are Y versus X, for example, the top left panel is TFAM overexpression versus Control. Significantly changed genes (p-adj <0.05) are displayed in red.

Control		TFAM o/e		ATF4 o/e		
99	36 genes ↑ (36%) 63 genes ↓ (64%)					**TFAM o/e**
169	35 genes ↑ (21%) 134 genes ↓ (79%)	68	13 genes ↑ (19%) 55 genes ↓ (81%)			**ATF4 o/e**
71	20 genes ↑ (28%) 51 genes ↓ (72%)	63	20 genes ↑ (32%) 43 genes ↓ (68%)	88	53 genes ↑ (60%) 35 genes ↓ (40%)	**TFAM o/e, ATF4 RNAi**

Table 4. Number of genes significantly regulated in each pairwise condition, as determined by RNA-Seq analysis. Comparisons are Y versus X, for example, the 36 upregulated genes in the top left are increased in the TFAM overexpression condition compared to Control. Thresholds were ≥ ±1.5 fold change in expression, mean FPKM ≥1 for at least one condition, and adjusted $p < 0.05$. ↑ = upregulated, ↓ = downregulated.

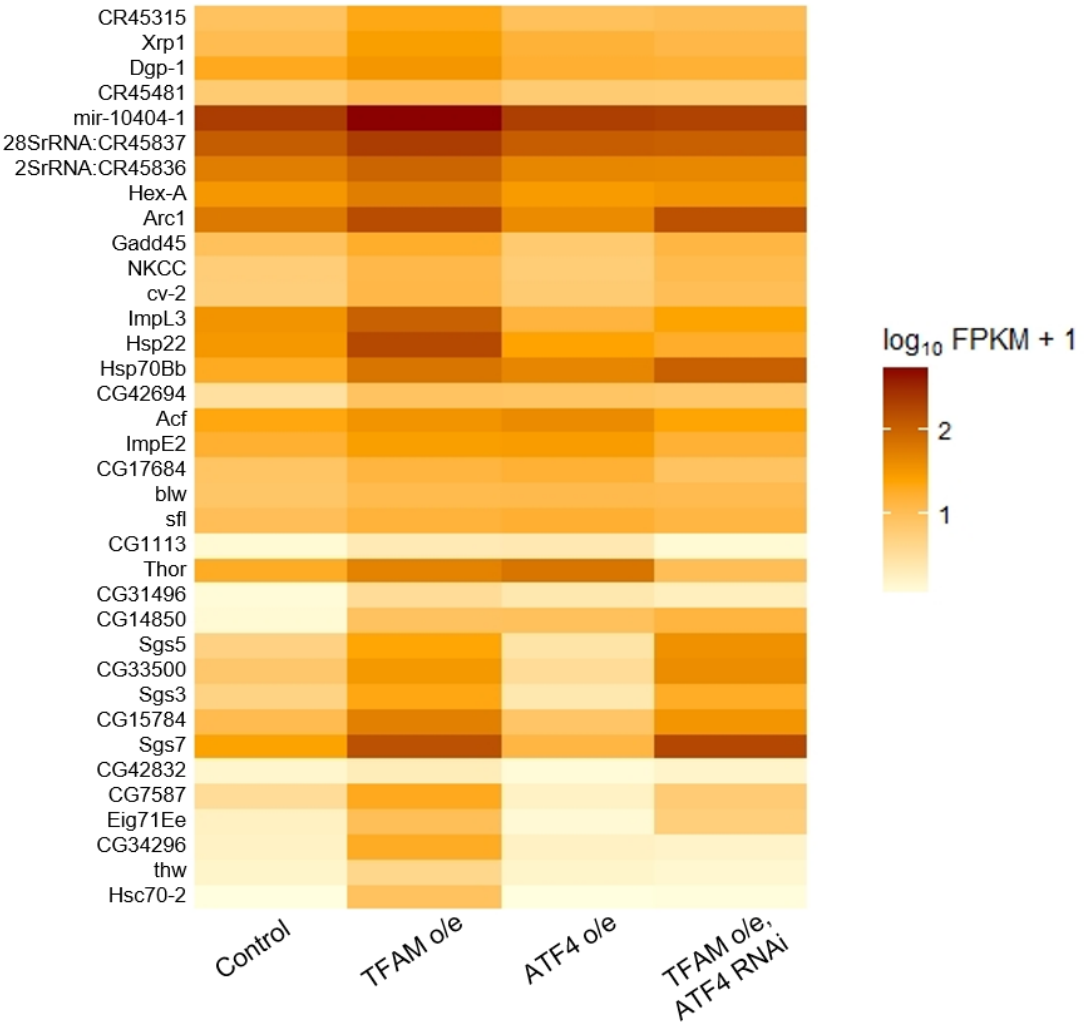

Figure 5.5 Heatmap of genes upregulated by TFAM overexpression. 36 genes upregulated by TFAM overexpression, compared to Control, as determined by RNA-Seq analysis using Cuffdiff software. As per the scale bar, expression (colour) is shown proportional to fragment counts normalised to transcript length and number of mapped reads (FPKM).

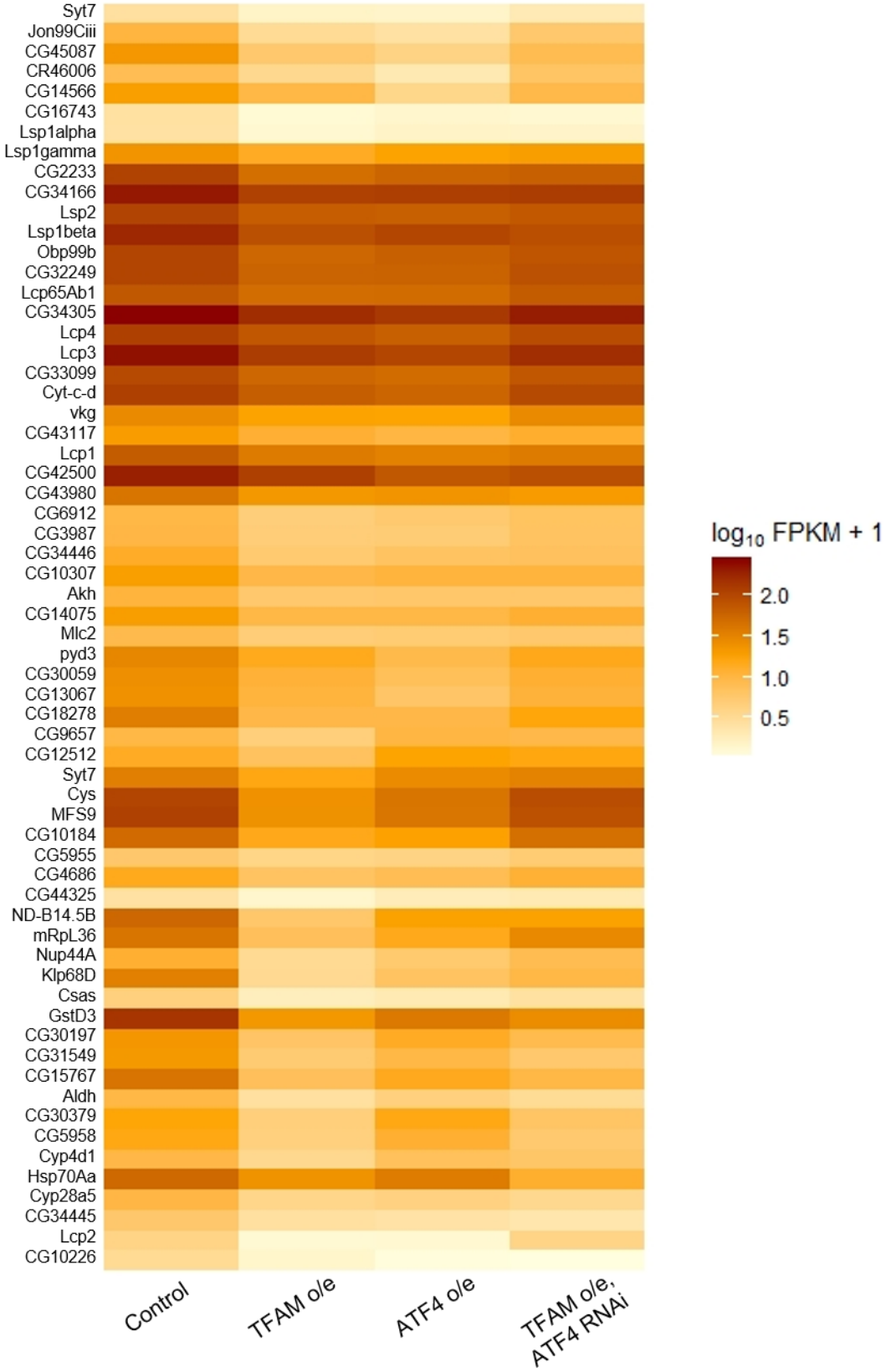

Figure 5.6 Heatmap of genes downregulated by TFAM overexpression. 63 genes downregulated by TFAM overexpression, compared to Control, as determined by RNA-Seq analysis using Cuffdiff software. As per the scale bar, expression (colour) is shown proportional to fragment counts normalised to transcript length and number of mapped reads (FPKM).

If ATF4 is to be considered an important regulator of the retrograde response to mitochondrial dysfunction in *Drosophila* neurons, then (1) ATF4 overexpression would be expected to replicate some of the transcriptional changes caused by TFAM overexpression, and (2) knock-down of ATF4 in conjunction with TFAM overexpression would be expected to reverse some of the transcriptional changes caused by TFAM overexpression.

Comparison of genes differentially expressed in the TFAM overexpression and ATF4 overexpression conditions (both relative to control) revealed striking similarities (Fig. 5.7 A); 10/36 (28%) genes upregulated by TFAM overexpression were also upregulated by ATF4 overexpression (see Appendix 8.3.1 for list), whilst 47/63 (77%) of genes downregulated by TFAM overexpression were also downregulated by ATF4 overexpression (Appendix 8.3.2). The direction of regulation was reversed for only two genes (ImpL3 and Arc1), whose expression was increased by TFAM overexpression, but decreased by ATF4 overexpression (Appendix 8.3.1). Genes that were differentially expressed in both TFAM and ATF4 overexpression conditions were significantly correlated when analysed by linear regression ($Y = 0.80X \pm 0.06$, $R^2 = 0.72$, $p < 0.0001$) (Fig. 5.7 B).

Qualitative inspection of the heatmaps in Figures 5.5 and 5.6 indicates that knock-down of ATF4 reverses many of the transcriptional changes induced by TFAM overexpression. To quantitatively characterise these transcriptional alterations, I identified the significantly regulated genes in the pairwise comparison 'TFAM overexpression, ATF4 RNAi vs TFAM overexpression' and compared them to the transcriptional changes in 'TFAM overexpression vs Control' (Fig. 5.7 C); 17/36 (47%) genes upregulated by TFAM overexpression (vs Control) were downregulated by co-expression of ATF4 RNAi (vs TFAM overexpression alone) (Appendix 8.3.3), the expression of 13/63 (21%) genes downregulated by TFAM overexpression was also reversed by ATF4 RNAi (Appendix 8.3.4). The TFAM transcriptional phenotype was exacerbated by ATF4 knock-down for only two genes – one gene upregulated by TFAM overexpression was further upregulated by simultaneous ATF4 knock-down (Hsp70Bb) (Appendix 8.3.4), and one gene downregulated by TFAM overexpression was further downregulated by ATF4 knock-down (CG14566) (Appendix 8.3.3). There was a significant negative correlation between the expression of genes regulated in both pairwise comparisons ($Y = -0.82X \pm 0.05$, $R^2 = 0.91$, $p < 0.0001$) (Fig. 5.7 D).

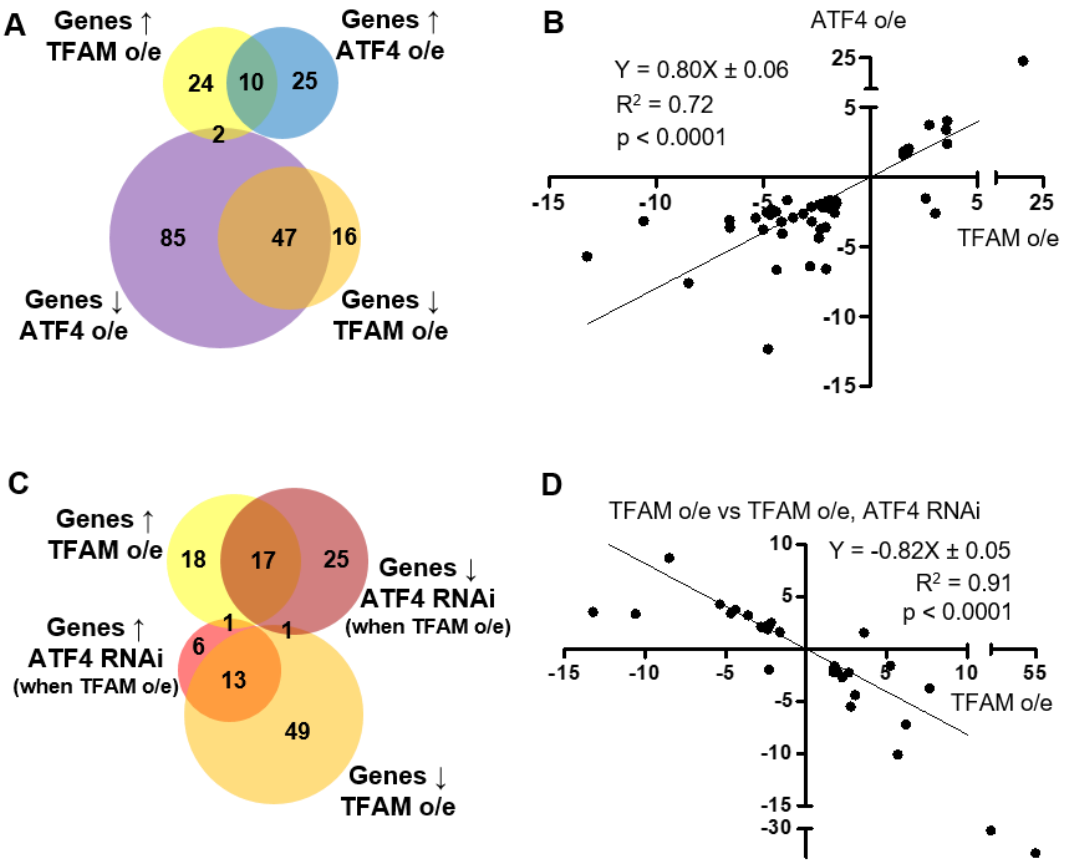

Figure 5.7 Quantitative analysis of transcriptional regulation by ATF4 in the TFAM-overexpression model of mitochondrial dysfunction. Area-proportional Venn diagrams showing (A) the number of commonly regulated genes in the TFAM overexpression (vs Control) and ATF4 overexpression (vs Control) conditions as determined by RNA-Seq, and (C) the number of commonly regulated genes in the TFAM overexpression, ATF4 RNAi (vs TFAM overexpression alone) conditions as determined by RNA-Seq. ↑ = upregulated, ↓ = downregulated. Only significantly expressed genes (≥ ±1.5 fold change in expression, mean FPKM ≥1 for at least one condition, and adjusted $p < 0.05$) were included. In (B) and (D), graphs show gene expression correlations between the same pairings of conditions. All genes plotted were significantly regulated in their respective conditions. Axis labels indicate the genotype that was compared to the control condition, apart from where otherwise stated (D, Y-axis). Lines of best-fit were determined by least squares linear regression analysis and their equations displayed on the graphs. R^2 = squared Pearson correlation coefficient.

Of the 57 genes commonly regulated by TFAM overexpression and ATF4 overexpression (i.e. up- or downregulated in both conditions), the expression of 13 was also reversed by ATF4 knock-down (vs TFAM overexpression) (Appendix 8.3.5, grey shading).

To gain insight into the function of the genes regulated by ATF4 in *Drosophila* neurons with mitochondrial dysfunction, I performed functional annotation clustering via the gene ontology software DAVID. Functional terms for each significantly regulated gene can be found in Appendix 8.3.5. To enable the software to discover clusters of relevance to the nervous system, 19 genes with solely structural roles elsewhere in the larvae – and whose presence in the list of significantly regulated genes very likely represents tissue contamination in a sample - were removed from the analysis (Appendix 8.3.6). Only one significantly enriched cluster, centred around ATP- and nucleotide binding, was identified for the genes signficantly regulated by TFAM overexpression vs control ($p = 0.038$, Fig. 5.8 B). The output from DAVID contains all identified clusters regardless of the significance of enrichment, and the same cluster also appeared in the output for ATF4 overexpression vs control, and TFAM overexpression, ATF4 RNAi vs TFAM overexpression alone, although neither was significantly enriched ($p = 0.067$ and 0.66 respectively, Fig. 5.8 B). One further cluster, which centred around oxidoreductase activity and heme/iron binding, was both common to all three conditions and significantly enriched in at least one condition (ATF4 overexpression vs control, $p = 0.002$, Fig. 5.8 A). Three highly enriched clusters, focused upon neurohormone signalling ($p = 0.0006$, Fig. 5.9 A), oxidative phosphorylation ($p = 0.028$, Fig. 5.9 B) and glutathione metabolism ($p = 0.08$, Fig. 5.9 C), were uniquely identified for the ATF4 overexpression vs control condition. One cluster containing Hsp20 chaperones was significantly enriched solely in the TFAM overexpression, ATF4 RNAi vs TFAM overexpression alone condition (Fig. 5.9 D). There were no significantly enriched clusters common to two (but not all three) conditions.

My results indicate that ATF4 has fulfilled the criteria to be considered a regulator of mitochondrial retrograde signalling in the *Drosophila* nervous system: (1) ATF4 overexpression replicated some (58%) of the transcriptional changes caused by TFAM overexpression, and (2) knock-down of ATF4 in conjunction with TFAM overexpression reversed some (30%) of the transcriptional changes caused by TFAM overexpression.

This strongly suggests that ATF4 is a key regulator of the transcriptional response to mitochondrial dysfunction in *Drosophila* neurons.

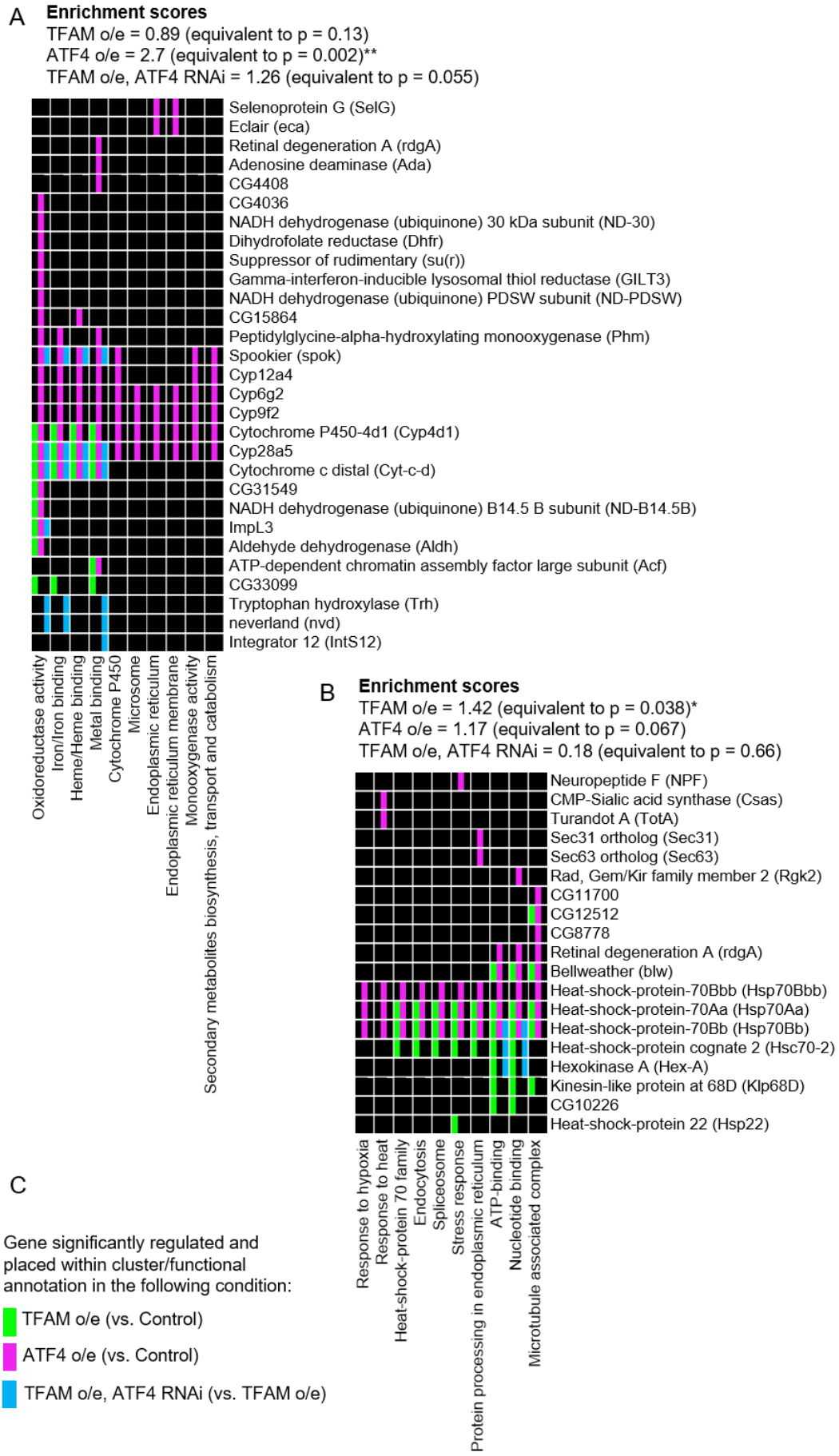
A
Enrichment scores
TFAM o/e = 0.89 (equivalent to p = 0.13)
ATF4 o/e = 2.7 (equivalent to p = 0.002)**
TFAM o/e, ATF4 RNAi = 1.26 (equivalent to p = 0.055)
Selenoprotein G (SelG)
Eclair (eca)
Retinal degeneration A (rdgA)
Adenosine deaminase (Ada)
CG4408
CG4036
NADH dehydrogenase (ubiquinone) 30 kDa subunit (ND-30)
Dihydrofolate reductase (Dhfr)
Suppressor of rudimentary (su(r))
Gamma-interferon-inducible lysosomal thiol reductase (GILT3)
NADH dehydrogenase (ubiquinone) PDSW subunit (ND-PDSW)
CG15864
Peptidylglycine-alpha-hydroxylating monooxygenase (Phm)
Spookier (spok)
Cyp12a4
Cyp6g2
Cyp9f2
Cytochrome P450-4d1 (Cyp4d1)
Cyp28a5
Cytochrome c distal (Cyt-c-d)
CG31549
NADH dehydrogenase (ubiquinone) B14.5 B subunit (ND-B14.5B)
ImpL3
Aldehyde dehydrogenase (Aldh)
ATP-dependent chromatin assembly factor large subunit (Acf)
CG33099
Tryptophan hydroxylase (Trh)
neverland (nvd)
Integrator 12 (IntS12)
Oxidoreductase activity
Iron/Iron binding
Heme/Heme binding
Metal binding
Cytochrome P450
Microsome
Endoplasmic reticulum
Endoplasmic reticulum membrane
Monooxygenase activity
Secondary metabolites biosynthesis, transport and catabolism
B
Enrichment scores
TFAM o/e = 1.42 (equivalent to p = 0.038)*
ATF4 o/e = 1.17 (equivalent to p = 0.067)
TFAM o/e, ATF4 RNAi = 0.18 (equivalent to p = 0.66)
Neuropeptide F (NPF)
CMP-Sialic acid synthase (Csas)
Turandot A (TotA)
Sec31 ortholog (Sec31)
Sec63 ortholog (Sec63)
Rad, Gem/Kir family member 2 (Rgk2)
CG11700
CG12512
CG8778
Retinal degeneration A (rdgA)
Bellweather (blw)
Heat-shock-protein-70Bbb (Hsp70Bbb)
Heat-shock-protein-70Aa (Hsp70Aa)
Heat-shock-protein-70Bb (Hsp70Bb)
Heat-shock-protein cognate 2 (Hsc70-2)
Hexokinase A (Hex-A)
Kinesin-like protein at 68D (Klp68D)
CG10226
Heat-shock-protein 22 (Hsp22)
Response to hypoxia
Response to heat
Heat-shock-protein 70 family
Endocytosis
Spliceosome
Stress response
Protein processing in endoplasmic reticulum
ATP-binding
Nucleotide binding
Microtubule associated complex
C
Gene significantly regulated and placed within cluster/functional annotation in the following condition:
TFAM o/e (vs. Control)
ATF4 o/e (vs. Control)
TFAM o/e, ATF4 RNAi (vs. TFAM o/e)

Figure 5.8 Functional annotation clusters common to the TFAM o/e, ATF4 o/e (both versus control) and TFAM o/e, ATF4 RNAi compound (versus TFAM o/e alone) conditions as determined by DAVID gene ontology software. (A) Cluster centred around oxidoreductase activity and heme/iron binding. (B) Cluster centred around ATP- and nucleotide binding. (A, B) The clustering for each condition was processed independently, and then combined into the grids (i.e. the list of genes significantly regulated by ATF4 o/e was not input into the software at the same time at the list of genes significantly regulated by TFAM o/e). DAVID outputs all detected clusters regardless of the calculated level of significance of the enrichments. Clusters displayed here are those which were identified for all three conditions, and where the terms within the cluster were significantly enriched in at least one of the conditions. Enrichment score is the negative logarithm of the geometric mean of the p values of each term within the cluster (so overall $p = 10^{-\text{enrichment score}}$). *$p < 0.05$, **$p < 0.01$.
(C) Key for clusters in (A) and (B). Green = gene significantly regulated and placed within cluster in TFAM o/e versus control, pink = gene significantly regulated and placed within cluster in ATF4 o/e versus control, blue = gene significantly regulated and placed within cluster in TFAM o/e, ATF4 RNAi versus TFAM o/e alone.

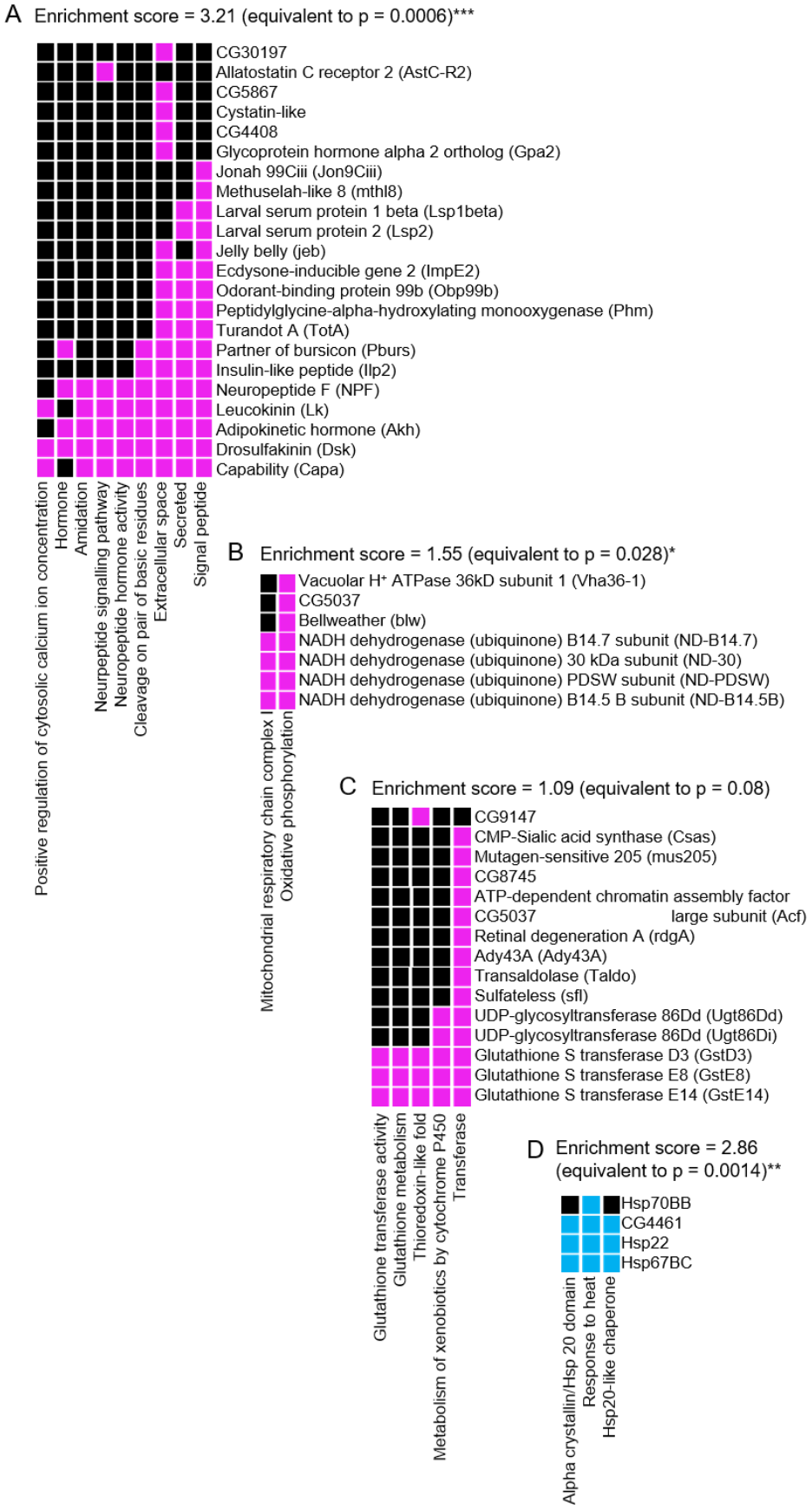
A Enrichment score = 3.21 (equivalent to p = 0.0006)***
CG30197
Allatostatin C receptor 2 (AstC-R2)
CG5867
Cystatin-like
CG4408
Glycoprotein hormone alpha 2 ortholog (Gpa2)
Jonah 99Ciii (Jon9Ciii)
Methuselah-like 8 (mthl8)
Larval serum protein 1 beta (Lsp1beta)
Larval serum protein 2 (Lsp2)
Jelly belly (jeb)
Ecdysone-inducible gene 2 (ImpE2)
Odorant-binding protein 99b (Obp99b)
Peptidylglycine-alpha-hydroxylating monooxygenase (Phm)
Turandot A (TotA)
Partner of bursicon (Pburs)
Insulin-like peptide (Ilp2)
Neuropeptide F (NPF)
Leucokinin (Lk)
Adipokinetic hormone (Akh)
Drosulfakinin (Dsk)
Capability (Capa)
Positive regulation of cytosolic calcium ion concentration
Hormone
Amidation
Neurpeptide signalling pathway
Neuropeptide hormone activity
Cleavage on pair of basic residues
Extracellular space
Secreted
Signal peptide
B Enrichment score = 1.55 (equivalent to p = 0.028)*
Vacuolar H+ ATPase 36kD subunit 1 (Vha36-1)
CG5037
Bellweather (blw)
NADH dehydrogenase (ubiquinone) B14.7 subunit (ND-B14.7)
NADH dehydrogenase (ubiquinone) 30 kDa subunit (ND-30)
NADH dehydrogenase (ubiquinone) PDSW subunit (ND-PDSW)
NADH dehydrogenase (ubiquinone) B14.5 B subunit (ND-B14.5B)
Mitochondrial respiratory chain complex I
Oxidative phosphorylation
C Enrichment score = 1.09 (equivalent to p = 0.08)
CG9147
CMP-Sialic acid synthase (Csas)
Mutagen-sensitive 205 (mus205)
CG8745
ATP-dependent chromatin assembly factor
CG5037 large subunit (Acf)
Retinal degeneration A (rdgA)
Ady43A (Ady43A)
Transaldolase (Taldo)
Sulfateless (sfl)
UDP-glycosyltransferase 86Dd (Ugt86Dd)
UDP-glycosyltransferase 86Dd (Ugt86Di)
Glutathione S transferase D3 (GstD3)
Glutathione S transferase E8 (GstE8)
Glutathione S transferase E14 (GstE14)
Glutathione transferase activity
Glutathione metabolism
Thioredoxin-like fold
Metabolism of xenobiotics by cytochrome P450
Transferase
D Enrichment score = 2.86
(equivalent to p = 0.0014)**
Hsp70BB
CG4461
Hsp22
Hsp67BC
Alpha crystallin/Hsp 20 domain
Response to heat
Hsp20-like chaperone

Figure 5.9 Functional annotation clusters unique to ATF4 overexpression (versus control) or TFAM overexpression, ATF4 RNAi (versus TFAM overexpression alone) as determined by DAVID gene ontology software. (A) Cluster centred around neurohormone signalling. (B) Oxidative phosphorylation cluster. (C) Cluster centred around glutathione metabolism. (D) Heat shock cluster. (A-C) Clusters unique to ATF4 o/e vs control. (D) Cluster unique to TFAM o/e, ATF4 RNAi vs TFAM o/e. (A-D) Enrichment score is the negative logarithm of the geometric mean of the p values of each term within the cluster (so overall $p = 10^{-\text{enrichment score}}$). *$p < 0.05$, **$p < 0.01$, ***$p < 0.001$.

5.2.3 Validation of RNA-Seq analysis using an independent method.

One of the genes whose expression was significantly upregulated by TFAM overexpression and reversed by ATF4 knock-down in my RNA-Seq analysis was *Thor*, which encodes the *Drosophila* homologue of the cap-dependent translation repressor 4E-BP1. I used immunofluorescence to explore the transcriptional regulation of *Thor* by an independent method. An *OK371-Gal4, UAS-CD8-GFP* driver line that also possesses a *Thor* transcriptional reporter (a *lacz* insertion downstream of the *Thor* promoter) was used to drive ATF4 RNAi (Fig. 5.10) alongside TFAM overexpression in motor neurons. Levels of *Thor* transcription were assessed by quantification of β-Gal immunofluorescence staining in the cell bodies of targeted neurons, as demarcated by GFP expression. Transcription of *Thor* was significantly increased by TFAM overexpression (Fig. 5.10 C-C'', E, $p < 0.001$), slightly decreased by ATF4 RNAi alone (Fig. 5.10 B-B'', E, $p < 0.01$), and also decreased to that same level when ATF4 was knocked down in conjunction with TFAM overexpression (Fig. 5.10 D-D'', E, $p < 0.001$). This result confirms that ATF4 regulates *Thor* transcription in *Drosophila* motor neurons under conditions of TFAM overexpression, and validates my RNA-Seq analysis for this gene.

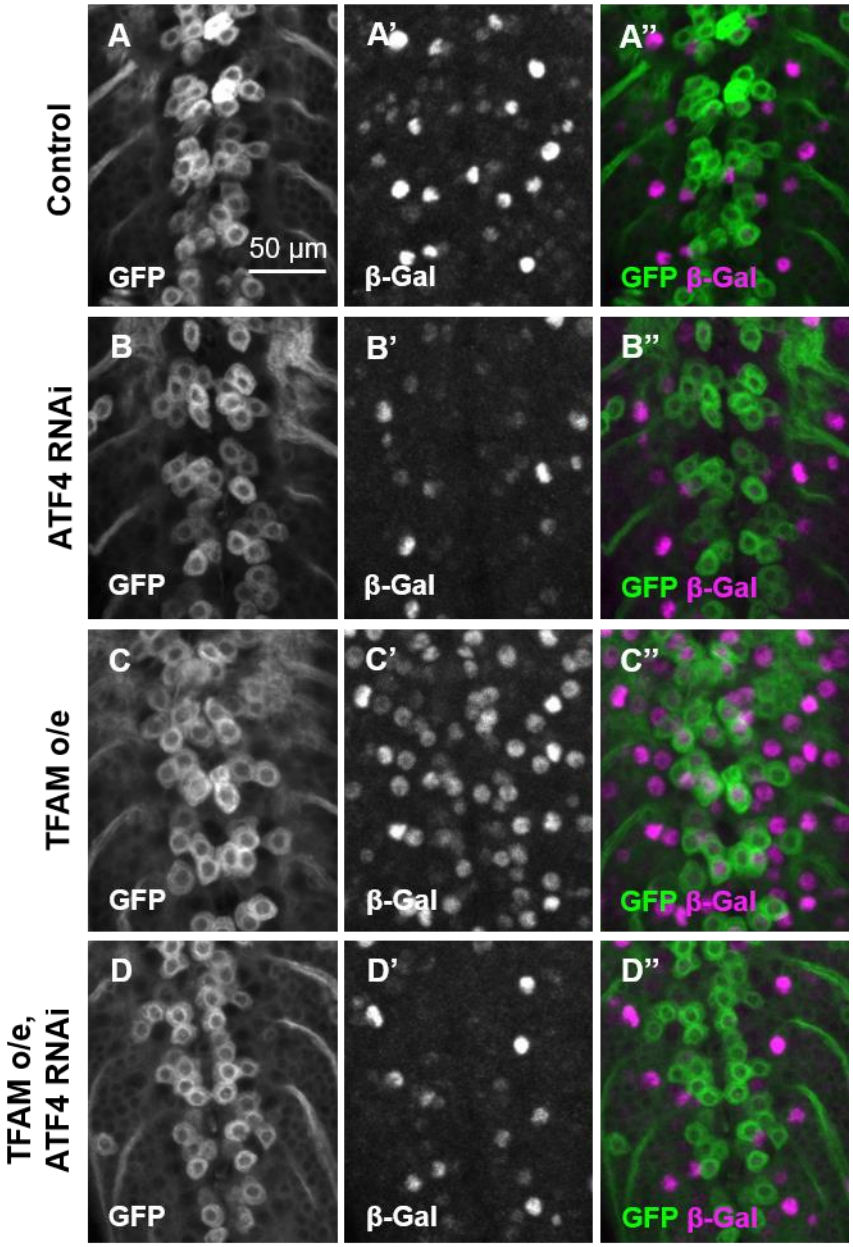
Control
ATF4 RNAi
TFAM o/e
TFAM o/e, ATF4 RNAi
A
A'
A''
B
B'
B''
C
C'
C''
D
D'
D''
50 µm
GFP
β-Gal
GFP β-Gal

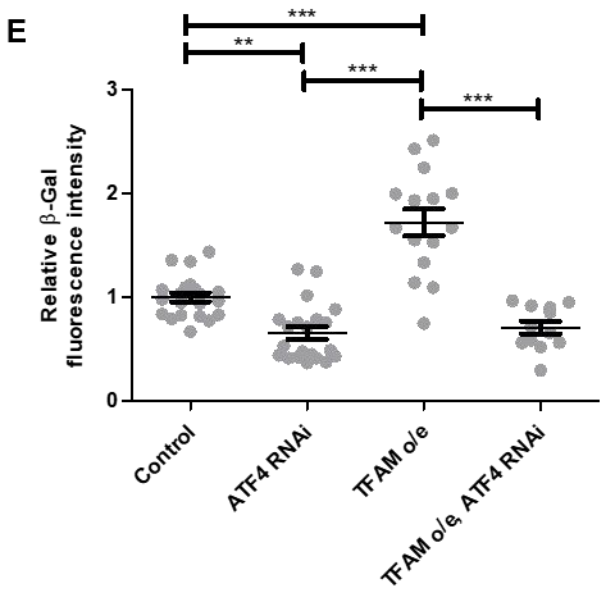
E
Relative β-Gal fluorescence intensity
0
1
2
3
***
**
***
***
Control
ATF4 RNAi
TFAM o/e
TFAM o/e, ATF4 RNAi

Figure 5.10 ATF4 regulates transcription of Thor under conditions of TFAM overexpression in Drosophila motor neurons. Membrane-targeted GFP (*CD8-GFP*), ATF4 RNAi (in B-B''), TFAM overexpression (o/e) (in C-C'') and TFAM overexpression, ATF4 RNAi combined (D-D'') driven in motor neurons of the VNC by *OK371-Gal4*. (A,B,C,D) GFP fluorescence (white). (A',B',C',D') Immunofluorescence staining with for β-Gal (white). (A'',B'',C'',D'') Merged images (GFP green, β-Gal magenta). β-Gal staining quantified in (E), n = 21 (control larvae), 21 (ATF4 RNAi), 15 (TFAM o/e) and 12 (TFAM o/e, ATF4 RNAi). Bars = mean ± SEM. Means compared by one-way parametric ANOVA with Tukey's post-hoc test. **$p < 0.01$, ***$p < 0.001$.

5.3 Summary

In this chapter I aimed to establish whether the ER UPR is a mitochondrial retrograde signalling pathway in *Drosophila* neurons.

In Chapter 4, I demonstrated that components of the PERK branch of the ER UPR are activated in our models of mitochondrial dysfunction. In particular, I showed that phosphorylation of the translational regulator eIF2α is increased by TFAM overexpression, and that levels of the ATF4 protein also increase. In this chapter, to investigate whether the PERK branch of the ER UPR is indeed the pathway responsible for the upregulation of ATF4, I performed immunofluorescence knock-down experiments. Two RNAi lines demonstrated that PERK regulates the expression of ATF4 under conditions of TFAM overexpression; PERK knock-down in conjunction with TFAM overexpression significantly reduced ATF4 levels compared to overexpression of TFAM alone. Conversely, knock-down of the ISR kinase GCN2 - which can also phosphorylate eIF2α - by two independent RNAi lines did not significantly alter ATF4 levels in either control or mitochondrial dysfunction conditions. Taken together, these results strongly suggest that the ER UPR, with limited or no contribution from GCN2, regulates ATF4 expression in *Drosophila* motor neurons in the TFAM-overexpression model of mitochondrial dysfunction.

To be a mitochondrial retrograde signalling pathway, the ER UPR must alter nuclear gene transcription in response to mitochondrial dysfunction. Having confirmed that ATF4 is regulated by the ER UPR when TFAM is overexpressed in motor neurons, I performed RNA-Seq analysis on larval CNS tissue with pan-neuronal TFAM overexpression to investigate the putative role of the protein in transcriptional regulation.

The expression of 99 genes was significantly altered by overexpression of TFAM compared to control samples. This retrograde transcriptional signature was substantially replicated by overexpression of ATF4; 57/99 (58%) genes that underwent transcriptional changes in the TFAM overexpression condition were similarly regulated by ATF4 overexpression. Only 2/99 (2%) genes displayed inverted regulation – they were increased by TFAM overexpression but decreased by ATF4 overexpression.

Knock down of ATF4 in conjunction with TFAM overexpression reversed the transcriptional changes induced by TFAM overexpression for 30/99 (30%) genes. ATF4 RNAi enhanced the effects of TFAM overexpression - further increased or decreased expression - for just 2/99 (2%) genes. Enriched functional clusters for the genes significantly regulated by TFAM and/or ATF4 included ATP- and nucleotide binding, oxidoreductase activity, neurohormone signalling, oxidative phosphorylation and molecular chaperones.

The *Drosophila 4E-BP1* homologue, *Thor*, was amongst the genes regulated by ATF4 in my RNA-Seq analysis; expression of *Thor* was upregulated by TFAM overexpression and suppressed by co-expression of ATF4 RNAi. This pattern was replicated in immunofluorescence experiments which utilised a *lacz* reporter downstream of the *Thor* promoter, thus confirming that ATF4 can control nuclear gene transcription under conditions of neuronal mitochondrial dysfunction, and suggesting that the ER UPR is a mitochondrial retrograde signalling pathway in *Drosophila* neurons.

6. Discussion

6.1 Alterations to mitochondrial and ER biology in *Drosophila* neurons with mitochondrial dysfunction

6.1.1 Alterations to Ca^{2+} handling

I detected dramatically elevated mitochondrial Ca^{2+} levels in the cell bodies of TFAM overexpressing motor neurons. This is in line with some other models of mitochondrial dysfunction, including instances of oxidative stress (Hawkins, Irrinki et al. 2010), Complex II inhibition (Nasr, Gursahani et al. 2003, Mbaya, Oulès et al. 2010), and *PINK1* mutation in *Drosophila* (Lee, Huh et al. 2018). Retention of the facility to import significant Ca^{2+} suggests that any putative reduction in membrane potential caused by TFAM overexpression, may be overcome by the high Ca^{2+} microdomains at expanded ER-mitochondrial contacts.

The mitochondrial enzymes pyruvate dehydrogenase, isocitrate dehydrogenase and α-ketoglutarate dehydrogenase are known to be activated by Ca^{2+} ions (Denton and McCormack 1980), and therefore raised mitochondrial Ca^{2+} could facilitate an increase in the conversion of pyruvate to acetyl-CoA, and its subsequent oxidation in the Krebs cycle. However, RNA-Seq analysis indicated that lactate dehydrogenase (ImpL3) was upregulated ~3-fold by TFAM overexpression, and it is therefore likely that the excess pyruvate consumed for conversion to lactate (with concomitant oxidation of NADH), would prevent any meaningful increase in acetyl-CoA supply to the Krebs cycle.

Ca^{2+} overload can also activate pathological pathways within the mitochondria. Mitochondrial permeability transition (MPT) is the sudden increase in IMM permeability that permits the efflux of molecules ≤ 1.5 kDa into the intermembrane space (Haworth and Hunter 1979), usually followed by mitochondrial swelling and sometimes by OMM rupture and the release of apoptotic factors such as cytochrome c. Raised mitochondrial Ca^{2+} can trigger MPT (Chalmers and Nicholls 2003), but TFAM overexpression in *Drosophila* motor neurons does not cause cell loss in third instar larvae (Cagin, Duncan et al. 2015), so it is unlikely that MPT is occuring in this model. This could be due to a

lack of other pro-MPT/apoptotic signals such as ceramide (Szalai, Krishnamurthy et al. 1999).

Cytosolic GCaMP and CaMPARI reporters indicated that TFAM overexpression does not change the level of cytosolic Ca^{2+} in *Drosophila* motor neurons. Larvae expressing CaMPARI were exposed to UV whilst crawling, implying that their motor neurons were activated when Ca^{2+} levels were being recorded by photoconversion of the CaMPARI reporter. Repeated neuronal stimulation via the heat-activated TrpA1 channel did however lead to increased Ca^{2+} levels in TFAM overexpressing neurons, suggesting subtle elevations in cytosolic Ca^{2+} caused by TFAM overexpression that could only be detected by hyper-stimulation.

An increase in cytosolic Ca^{2+} could lead to the activation of myriad pathways, many of which could only be discovered by analysis of post-translational modifications, and would not be obviously detectable by RNA-Seq analysis of the transcriptional changes caused by TFAM overexpression. The kinase ERK is activated by TFAM overexpression in *Drosophila* motor neurons, and knock-down of components of the Ras-ERK-ETS pathway suppressed the climbing and wing inflation impairments of TFAM overexpressing flies (Duncan, Granat et al. 2018). Phosphorylation (activation) of ERK is Ca^{2+}-dependent and can be regulated by both CaMKs (Enslen, Tokumitsu et al. 1996, Schmitt, Wayman et al. 2004) and calcineurin (Dougherty, Ritt et al. 2009), suggesting that elevated cytosolic Ca^{2+} could be the activator of the counterproductive ERK-mediated retrograde signalling in *Drosophila* motor neurons with mitochondrial dysfunction.

6.1.2 Alterations to mitochondrial morphology

I did not assess any direct parameters of mitochondrial function in this thesis, but did investigate the morphology of mitochondria in *Drosophila* neurons with TFAM overexpression. The morphology of purified mitochondria from whole young (15 day old) flies is remarkably homogeneous; a subset of only 10% of isolated mitochondria displayed greater elongation or widened cristae. By contrast, the morphology of mitochondria extracted from aged (70 day old) flies was diverse and included abnormally

thin and branched mitochondria, suggesting that the mitochondrial uniformity seen in the young adults was not an artefact of the isolation procedure, and that mitochondrial structure may be similar across diverse tissues in the young fly (Brandt, Mourier et al. 2017). In support of this, *in vivo* imaging of the *Drosophila* embryo revealed a reticular network highly similar in appearance to that which I imaged in *Drosophila* motor neurons (Macchi, El Fissi et al. 2013). Overexpression of TFAM in *Drosophila* motor neurons caused significant changes to the morphology of the mitochondrial network in the cell bodies. Whilst the total area of mitochondria remained unchanged, the number of mitochondria increased and the average size decreased, suggesting increased fragmentation and a tip of the fission/fusion balance towards fission.

In rat liver cells, mitochondrial fragmentation was found to be dependent on mitochondrial Ca^{2+} influx and components of the OMM scission machinery, Drp1 and Fis1. The fragmentation could be reversed if the elevated level of mitochondrial Ca^{2+} was transient, but became permanent if mitochondrial Ca^{2+} levels were persistently raised (Hom, Gewandter et al. 2007). Recently, two independent groups have found that Drp1-independent constrictions of the IMM occur during mitochondrial fission (Cho, Cho et al. 2017, Chakrabarti, Ji et al. 2018). These constrictions are dependent on enhanced mitochondrial Ca^{2+} uptake which, when examined, was mediated by increased ER-mitochondrial contacts (Chakrabarti, Ji et al. 2018). Knockdown of the VDAC-to-IP_3 receptor linker GRP75 in an oxidative stress model reduced mitochondral fragmentation, lending weight to the idea that excess Ca^{2+} transfer from the ER to the mitochondria could underly at least some fragmentation (Honrath, Metz et al. 2017).

Whilst Ca^{2+}-induced pathological fragmentation is probably occuring in *Drosophila* neurons with TFAM overexpression, a proportion of the smaller mitochondrial units could also be mitochondria-derived vesicles (MDVs). MDVs transport damaged mitochondrial components for degradation, and are proposed to limit the need for mitophagy in tissues with a high energy demand, such as cardiac muscle and the nervous system (Roberts, Tang et al. 2016). MDV formation is regulated, with specific cargo and structure, and increased by oxidative stress or ETC inhibition (Soubannier, McLelland et al. 2012). Single-membrane MDVs canonically contain the OMM proteins TOM20 and VDAC, and lack IMM and matrix components. Double-membrane MDVs

have been found to contain pyruvate dehydrogenase and a subunit of Complex III, but not VDAC or TOM20 (Soubannier, McLelland et al. 2012, Soubannier, Rippstein et al. 2012). Double-membrane MDVs are targeted to the lysosome (McLelland, Soubannier et al. 2014). Single-membrane MDVs are also targeted to the lysosome unless they are of a subset that is enriched for the OMM SUMO E3 ligase mitochondrial-anchored protein ligase (MAPL) and lack TOM20, in which case the peroxisome is the destination (Neuspiel, Schauss et al. 2008).

Formation of the double-membrane MDVs which traffick damaged IMM and matrix proteins for degradation, requires wild-type PINK1 and parkin in mammalian cell culture (McLelland, Soubannier et al. 2014). In *Drosophila* heads, a proportion of the PINK1/parkin-dependent turnover of ETC components is independent of mitophagy, but a role for MDVs was not explored (Vincow, Merrihew et al. 2013). In PINK1 and parkin loss-of-function or knock-down models, reports of mitochondrial morphology conflict. Both mitochondrial fragmentation (Yang, Gehrke et al. 2006, Lutz, Exner et al. 2009) and enlargement (Poole, Thomas et al. 2008, Lee, Huh et al. 2018) or branching (Mortiboys, Thomas et al. 2008) have been observed. It is clear that the morphological outcome is context specific, and it may be that in cases where elevated mitochondrial Ca^{2+} is not sufficient to cause fragmentation by excess fission or MPT-induced rupture – perhaps due to the absence of a co-factor - that swelling or branching is seen due to impaired MDV formation.

6.1.3 Alterations to ER morphology

As with mitochondria, the morphology of the ER is dynamic (Lee and Chen 1988). I used three fluorescent fusion constructs to record snapshots of ER morphology under control and mitochondrial dysfunction conditions. The luminal diameter of *Drosophila* ER sheets is approximately 30 nm (Shibata, Shemesh et al. 2010), well below the resolution limits of green ($\lambda \approx 500$ nm, NA = 1.3, therefore $d \approx 190$ nm as per (Abbe 1873)) and red ($\lambda \approx 600$ nm, $d \approx 230$ nm) light in standard confocal microscopy, so the fluorescent constructs report only an approximation of ER morphology, but are nevertheless useful tools for preliminary investigations. The putative reduction in ER reticulation suggested by two of the reporters merits follow-up with higher resolution techniques such as electron

microscopy, and the perinuclear localisation of the most pronounced changes may guide these investigations and others that utilise antibodies against subcellular compartments.

Each of the three fluorescent reporters had different targeting and retention sequences, and therefore the potential to mark distinct regions of the ER. Whilst animal cells make almost exclusive use of the KDEL retention motif, *Drosophila* proteins utilise HDEL and KDEL in roughly equal proportion (Abrams, Cheng et al. 2013). The identity of the retention signal has been shown to impact the intra-ER localisation of proteins in plant and animal cells (Napier, Fowke et al. 1992, Gilham, Alam et al. 2005), although not in a predictable manner; in both cases the KDEL motif correlated with restricted distribution of its allied proteins, but one was to perinuclear ER and the other sub-cortical. In addition, structures and/or sequences outside of the known targeting and retention motifs seem to play a role in trafficking to ER subdomains in a cell-type specific manner. Remarkably, a DsRed-KDEL fusion marked solely ER-derived vesicles in hippocampal neurons, whilst a second construct (GFP-KDEL), that differed only in the identity of the fluorophore, displayed reticular patterning. In COS-7 cells, both reporters were reticular (Bannai, Inoue et al. 2004). Sec61β is a subunit of the complex that transports nascent polypeptides into the ER lumen (Gorlich and Rapoport 1993), and therefore the tdTomato-Sec61β construct should demarcate the rough ER membrane, however fluorescent fusions with human Sec61β were seen throughout the ER (Shibata, Voss et al. 2008) and did not integrate into translocon complexes (Snapp, Hegde et al. 2003), again suggesting that subdomain targeting is a function of the complete protein. Given these findings, further investigation would be required to establish the intra-ER localisation of the three fusion constructs I used to examine ER morphology. However, since the BiP-sfGFP-HDEL and tdTomato-Sec61β reporters both indicated extremely similar changes to ER morphology, it is likely there is substantial overlap in their localisation. The lyso-RFP-KDEL reporter also exhibited reticular patterning, but did not recapitulate the results seen with the other constructs, suggesting that it localised to a different, although potentially overlapping, subset of ER domains. Taken together the results indicate that morphological changes of neuronal ER caused by mitochondrial dysfunction may be more acute in some ER domains, and that alterations are not restricted to the external structure of the organelle, but may also include a functional reassignment of internal ER regions. A caveat to these observations is that overexpression of ER-targeted fluorescent chimeras has been reported to alter ER morphology (Snapp,

Hegde et al. 2003), however any such changes should have occurred in both the control and mitochondrial dysfunction conditions, and therefore does not invalidate the preliminary conclusion that mitochondrial dysfunction alters ER morphology in the cell bodies of *Drosophila* neurons.

A reduction in the reticular nature of the ER in response to mitochondrial dysfunction may correspond to an increase in sheet content, classically associated with the rough ER and protein synthesis. Recently, a paradigm-shifting examination of ER morphology using high resolution microscopy techniques has proposed that regions of the ER previously classified as sheets are in fact dense matrices of tubules, the voids in which could not be distinguished by lower resolution imaging (Nixon-Abell, Obara et al. 2016). If corroborated, this finding will have wide-ranging implications in the field of ER dynamics, but may not revolutionise the concept that 'sheets' are the site of protein synthesis, given that ribosomes have been extensively imaged on these regions and the proposed tubular densities would also present regions of reduced curvature that can accommodate the ribosome.

Removal of the 40S subunit from actively synthesising ribosomes on the ER caused the immediate loss of interphase ER sheets in CHO-K1 cells (Puhka, Vihinen et al. 2007). The authors speculated that Ca^{2+} leakage from the remaining 60S-translocon complex may signal the rearrangement of ER structure via the highly conserved EF-hand protein, p22. Regulation of ER morphology during the cell cycle seems not to be conserved between mammals and flies (Bobinnec, Marcaillou et al. 2003) and, although possible, increased ribosome occupancy of the ER is an unlikely response to neuronal mitochondrial dysfunction given the phosphorylation of eIF2α that canonically reduces global translation. Therefore, it seems improbable that the hypothetical ER sheet expansion seen in the TFAM overexpression condition is due to stabilisation by ribosomes.

Increased cytosolic Ca^{2+} concentration has been shown to increase the number of ER-plasma membrane contacts (Chang, Hsieh et al. 2013, Giordano, Saheki et al. 2013) and induce dramatic fragmentation of the ER (Subramanian and Meyer 1997, Ribeiro,

McKay et al. 2000). In addition, Ca^{2+} activation of p22 increases ER network formation (Andrade, Zhao et al. 2004), indicating that it is also unlikely that a reduction in ER reticulation would be mediated by the increased levels of cytosolic Ca^{2+} seen in stimulated *Drosophila* neurons with mitochondrial dysfunction.

Expansion of ER sheets in yeast has been observed in response to treatment with the reducing agent DTT and glycolsylation inhibitor tunicamycin, and attributed to activation of lipid biosynthesis by the ER UPR protein IRE1 (Schuck, Prinz et al. 2009). Cell survival was increased by ER sheet expansion, independently of chaperone activation. IRE1 is also required for the increase in ER sheets in the developing photoreceptor cells of *Drosophila* (Xu, Chikka et al. 2016). It has been demonstrated that increased lipid packing density activates the ER UPR in yeast and mammals (Volmer, van der Ploeg et al. 2013, Halbleib, Pesek et al. 2017). The mechanism determined in yeast was a mechano-sensitive amphipathic helix in the IRE1 transmembrane domain that is conserved in fellow ER UPR sensor PERK, and across species (Halbleib, Pesek et al. 2017). Coupled with my results, these findings suggest a mechanism for ER sheet expansion whereby mitochondrial dysfunction disturbs lipid homeostasis causing aberrant ER membrane composition that activates the UPR, which then augments the initial changes to ER morphology.

6.1.4 Alterations to ER-mitochondrial contacts

At the NMJ, TFAM overexpression decreased the number of candidate ER-mitochondrial contact sites. TFAM overexpression results in a significant loss of mitochondria from the NMJ, and the alteration to candidate ER-mitochondria contact sites may therefore simply be a reflection of this reduction – particularly given that I did not detect changes to ER morphology at the NMJ. In the motor neuron cell bodies, my results indicate that TFAM overexpression increased the number of candidate ER-mitochondrial contact sites, and this may reflect changes in the morphology of both organelles. In recent years, altered ER-mitochondrial contacts have been found to be a common characteristic of many diverse diseases. The changes to MAMs have not been consistent, either in their extent, topology or functional consequences.

Recently it was demonstrated in neurons from *Drosophila parkin* mutants that increased ER-mitochondrial contacts diminish ER phosphatidylserine (PS) content by augmented transfer of PS from the ER to mitochondria, where it is converted to phosphatidylethanolamine and the drive to continued PS transfer maintained (Valadas, Esposito et al. 2018). Similar lipid dysregulation in the motor neuron cell bodies of TFAM overexpressing flies, could explain the activation of the ER UPR and suggests that perturbed lipid homeostasis may constitute part of the MAM-to-ER leg of the retrograde signal from the mitochondria to the nucleus. PS supplemented food rescued the sleep abnormalities of *parkin* mutant flies indicating that PS could represent a viable oral therapy for neurological diseases associated with increased ER-mitochondrial contacts.

Dysregulated Ca^{2+} signalling may also contribute to the MAM-to-ER signalling of mitochondrial dysfunction in *Drosophila* neurons. An amyotrophic lateral sclerosis (ALS)-associated mutation in the mitochondrial tethering protein VAPB, results in extended MAM formation and increased Ca^{2+} transfer from the ER to the mitochondria in cell lines and rat cortical neurons (De Vos, Mórotz et al. 2012). Similarly, in *Drosophila*, mutation of the PD-associated *PINK1* increases ER-mitochondria contacts in dopaminergic neurons leading to elevated mitochondrial Ca^{2+} and cell death (Lee, Huh et al. 2018). Both studies indicate that enhanced ER-mitochondrial Ca^{2+} transfer is detrimental to neuronal health. This idea is supported by the finding that knock-down of the VDAC-IP_3 receptor linker, GRP75, protects hippocampal HT22 cells from oxidative stress, putatively by reducing mitochondrial Ca^{2+} overload (Honrath, Metz et al. 2017). In addition, GRP75 overexpression exacerbated the deleterious affects of rotenone treatment in rat mesencephalic cells (Jin, Hulette et al. 2006). However, mutations in the sigma-1 receptor, which has roles in both ER-mitochondrial lipid and Ca^{2+} transfer, underly some cases of ALS. Knockout of the sigma-1 receptor disturbed ER-mitochondrial contacts, exacerbated locomotor phenotypes (Bernard-Marissal, Medard et al. 2015) and hastened death in a mouse model of motor neuron disease (Mavlyutov, Epstein et al. 2013), whilst sigma-1 receptor activation has been shown to be beneficial in both *in vivo* and *in vitro* ALS models (Mancuso, Oliván et al. 2012, Ono, Tanaka et al. 2014). This is contradictory to the idea that reducing Ca^{2+} and lipid transfer in neuronal disease is beneficial, and indicates that much work remains to uncover the context-specific factors that determine whether increased ER-mitochondria contacts have ameliorative or pathological consequences.

6.2 Communicating mitochondrial dysfunction from the ER to the nucleus in *Drosophila* neurons.

6.2.1 Communication via the ER lumen

I have shown that the ER UPR is activated in response to mitochondrial dysfunction in *Drosophila* motor neurons, and conveys a retrograde signal to the nucleus via the cytoplasm. However, the ER is continuous with the outer nuclear membrane, and hence the ER lumen is continuous with the intermembrane space of the nuclear envelope. Therefore, it is conceivable that mitochondrial dysfunction could also send signals that are carried internally via the ER lumen to the nucleus.

The nucleoplasmic reticulum (NR) is the name given to invaginations of the nuclear envelope that protrude into the nucleoplasm, and has been widely observed in a variety of species. Two types of NR invaginations have been described; those that involve only the inner nuclear membrane are classified as type I, whilst those that comprise both the inner and outer nuclear membranes and hence create cul-de-sacs of cytosol wending into the nucleus – or sometimes tunnels completely traversing the nucleus (Fricker, Hollinshead et al. 1997) - are designated type II (Malhas, Goulbourne et al. 2011).

Type II invaginations retain some of the molecular features of the ER, including the presence of protein disulfide isomerase, glucose-6-phosphatase (Fricker, Hollinshead et al. 1997) and calreticulin (Goulbourne, Malhas et al. 2011). Therefore the changes to perinuclear ER morphology suggested by two of the fluorescent reporters, may extend to altered NR morphology. As already discussed, the putative expansion of ER sheets and increase in ER-mitochondrial contacts suggest altered lipid synthesis in *Drosophila* neurons with mitochondrial dysfunction. Activity of CTP:phosphocholine cytidyltransferase (CCT), the rate-limiting enzyme in the synthesis of phosphatidylcholine (PC), is regulated by its localisation. The soluble cytosolic/nucleoplasmic CCT fraction is inactive. A reduction in membrane PC content prompts the insertion of CCT into the membrane, and its activation via the necessary conformational change. Overexpression of the nuclear-targeted isoform CCTα, caused proliferation of type II NR in CHO cells, an effect that was separately mediated by both

membrane insertion and PC synthesis (Lagace and Ridgway 2005). Thus disturbed PC levels in *Drosophila* neurons with mitochondrial dysfunction could cause changes to NR morphology.

In HeLa cells, mitochondria have been shown to cluster around the cytoplasmic entrance to the type II invaginations, and remarkably, to shuttle in and out of the channels, buffering Ca^{2+} whilst inside (Lui, Chan et al. 2003). Further, the sigma-1 receptor, a component of MAMs, was found to localise to the NR in a murine motor neuron-like cell line (Mavlyutov, Yang et al. 2017), raising the possibility that ER-mitochondrial contacts continue into the nuclear domain, creating a very direct communication of the mitochondria with the nucleus. Alongside the increase in ER-mitochondrial contacts in *Drosophila* neurons detected by both fluorescent reporters in response to TFAM overexpression, the tdTomato-Sec61β reporter indicated a relocation of these contacts away from the perinuclear region. Whilst this finding was not recapitulated by the lyso-RFP-KDEL reporter, it does suggest that at least in some ER domains, mitochondrial dysfunction may alter the relationship between mitochondria and the NR, possibly leading to increased Ca^{2+} levels in the NR invaginations.

NR Ca^{2+} concentration is extremely relevant in a signalling context. Both a Na^{+}/Ca^{2+} exchanger for the extrusion of Ca^{2+} from the nucleoplasm (Galva, Artigas et al. 2012), and the IP_3 and RyR (Marius, Guerra et al. 2006) receptors for the influx of Ca^{2+}, have been found in the NR, suggesting fully functional Ca^{2+} regulation in the nucleus. In mouse cardiomycocytes, Ca^{2+} release into the nucleoplasm by agonist activation of the IP_3 receptor altered the transcription of cardio-related genes (Garcia, Shah et al. 2004). Several transcription factors are known to be regulated by nuclear (rather than cytosolic) Ca^{2+}, including CREB (Chawla, Hardingham et al. 1998) and Elk-1 (Pusl, Wu et al. 2002). In hippocampal neurons, a signalling programme involving transcriptional changes to >150 genes is regulated by nuclear Ca^{2+} changes in response to synaptic activity (Zhang, Zou et al. 2009). Also in hippocampal neurons, ATF3 is upregulated by CREB in a nuclear Ca^{2+}-dependent manner, and mediates a neuroprotective response to excitotoxicity (Ahlgren, Bas-Orth et al. 2014).

The ends of type II NR invaginations are substantially associated with nucleoli (Bourgeois, Hemon et al. 1979, Fricker, Hollinshead et al. 1997) – the sites of ribosome and signal recognition particle (SRP) biogenesis - suggesting a direct way in which global and ER-targeted translation could be modulated to maintain ER proteostasis, either through Ca^{2+} release into the nucleoli microdomain, or perhaps the interaction of NR transmembrane proteins or lamins with components of the nucleoli.

Lamins are members of the intermediate filament family which form a meshwork under the inner nuclear membrane. The structure of chromatin within the nucleus has been shown to regulate the formation of the NR, with both condensation (Bozler, Nguyen et al. 2015), dispersal (Dellaire, Kepkay et al. 2009) and an increase in actively transcribed chromatin (Galiova, Bartova et al. 2008) shown to cause NR expansion, hypothetically via lamin-chromatin contacts and the mechanical forces exterted by chromatin reorganisation. Sequestration by lamin at the periphery of the nucleoplasm has been shown to repress the transcription of hundreds of *Drosophila* genes, including members of the cytochrome P450 family (Pickersgill, Kalverda et al. 2006), indicating that the extent and morphology of the NR could play an active role in gene expression in a number of physiological contexts, including mitochondrial dysfunction.

6.2.2 Activation of the ER UPR

6.2.2.1 Functional consequences of IRE1 and XBP1 activation

The IRE1 branch of the ER UPR was upregulated by TFAM overexpression in *Drosophila* motor neurons, as indicated by increased splicing of the XBP1 transcription factor to its active form. Knock-down of IRE1 produced varying modifications to the climbing and wing inflation ability of flies with neuronal mitochondrial dysfunction – one RNAi line exacerbated the functional impairments, whilst another suppressed them. This inconsistency was also seen in RNAi lines targeting GADD34 and could be due to off-target effects or differing levels of knock-down – a small reduction in mRNA abundance may perhaps be beneficial, whilst a substantial knockdown could be detrimental to neuronal function. The efficiency of the RNAi lines will need to be assayed before any conclusions can be drawn. XBP1 knock-down produced largely beneficial

alterations to climbing and wing inflation ability, indicating that despite the hypothesised beneficial role in enhanced lipid synthesis, activation of the IRE1 pathway in *Drosophila* neurons with mitochondrial dysfunction is, on balance, functionally damaging.

Reports of the detrimental effects of IRE1 activation are mostly restricted to the induction of apoptosis, however we do not see cell loss in the TFAM overexpression model, indicating that the suppression of the mitochondrial dysfunction phenotypes by IRE1 knock-down is not due to a reduction in cell death. In models of atherosclerosis, IRE1 upregulates the transcription of deleterious proinflammatory cytokines and chemokines (Tufanli, Telkoparan Akillilar et al. 2017). My RNA-Seq analysis of TFAM overexpressing neurons does not reveal any significant regulation of inflammatory markers or mediators. Knock-out of XBP1 beneficially upregulated autophagy in a murine ALS model (Hetz, Thielen et al. 2009), but further work will be needed to establish whether suppressed autophagy is the counterproductive element of IRE1 pathway activation in TFAM overexpressing neurons.

6.2.2.2 Activation of the PERK branch

I identified increased levels of phosphorylated eIF2α (P-eIF2α) in the cytoplasm of motor neurons with both TFAM overexpression and ND-75 knock-down, which according to canonical UPR signalling would suggest downstream activation of ATF4. However, in human patients with nonalcoholic fatty liver or steatohepatitis, liver histology revealed increased phosphorylation of eIF2α, but unchanged ATF4 protein and mRNA levels (Puri, Mirshahi et al. 2008). A rat model of brain-wide ischaemia-reperfusion injury also detected increased P-eIF2α without upregulation of the ATF4 protein (Kumar, Krause et al. 2003). In both reports, the authors attributed hepatocyte and neuron death in part to failure to activate the protective elements of the downstream ER UPR. Having observed elevated levels of P-eIF2α in our models of mitochondrial dysfunction, dysregulation of the downstream components of the ER UPR would be a feasible mechanism to explain the association of mitochondrial dysfunction with neurodegenerative disease and premature organismal death, however I detected robust upregulation of ATF4 protein levels, indicating that the canonical P-eIF2α-ATF4 axis is operating in *Drosophila* motor neurons with mitochondrial dysfunction.

In mammals, eIF2α can be phosphorylated by four kinases that constitute upstream arms of the integrated stress response. Of those four kinases, only GCN2 and PERK are conserved in *Drosophila*. GCN2 is typically considered to mediate the response to amino acid starvation, but has been shown to be the kinase responsible for eIF2α phosphorylation in oligomycin-induced mitochondrial dysfunction in gastric (Wang, Chen et al. 2016) and colon (Martínez-Reyes, Sánchez-Aragó et al. 2012) cancer cells, and two *in vivo* genetic models of mitochondrial dysfunction in *C. elegans* (Baker, Nargund et al. 2012). An extensive multiomics study of four drug-induced models of mitochondrial dysfunction in HeLa cells concluded that all four ISR kinases could redundantly phosphorylate eIF2α in response to treatment with the ionophore carbonyl cyanide-4-(trifluoromethoxy)phenylhydrazone (FCCP), since individual knock-down of the kinases had no effect on ATF4 induction. However, the authors examined only ATF4 mRNA – and not protein – levels, and their reasoning is therefore incomplete (Quirós, Prado et al. 2017). In our TFAM overexpression model of mitochondrial dysfunction, levels of ATF4 were significantly reduced by knock-down of PERK, but unaltered by GCN2 knock-down, indicating that it is solely the ER UPR arm of the ISR that is regulating ATF4 in *Drosophila* motor neurons with mitochondrial dysfunction. In the oligomycin-treated gastric cancer cells, and both the *C. elegans* models, addition of an antioxidant reduced the GCN2-mediated phosphorylation of eIF2α, implying that reactive oxygen species (ROS) were activating this arm of the ISR, and suggesting therefore that ROS do not play a role in mitochondrial retrograde signalling via ATF4 in *Drosophila* neurons.

6.2.2.2.1 Other pathways to ATF4 activation

Knock-down of PERK in *Drosophila* neurons with mitochondrial dysfunction did not return ATF4 to control levels, and whilst this could simply be because the knock-down was inefficient or only low levels of PERK are required for meaningful phosphorylation of eIF2α, it raises the possibility that ATF4 is also controlled by pathways unrelated to eIF2α. Canonically, ATF4 is regulated at the level of translation, but instances of transcriptional control that can bypass or enhance the effects of P-eIF2α have been noted: UV radiation increased phosphorylation of eIF2α in mouse embryonic fibroblasts (MEFs), but also reduced ATF4 mRNA levels and thus negated activation of

the protein via the usual translational mechanism. In the same cells, the sarco/endoplasmic reticulum Ca^{2+} ATPase (SERCA) inhibitor thapsigargin increased both ATF4 mRNA and P-eIF2α levels (Dey, Baird et al. 2010). I did not detect significant up- or downregulation of ATF4 mRNA levels by TFAM overexpression in my RNA-Seq analysis. This is consistent with previous observations that ATF4 was not significantly altered in microarrays of *Drosophila* CNS tissue with pan-neuronal overexpression of TFAM or knock-down of ATP synthase subunit F6 (Cagin, Duncan et al. 2015), which strongly indicates that ATF4 is not regulated by transcriptional mechanisms in *Drosophila* neurons with mitochondrial dysfunction.

In many cases, eIF2α-independent regulation of ATF4 has been documented, but the underlying mechanism not elucidated. ATF4 protein expression was uncoupled from both P-eIF2α and ATF4 transcript levels in mouse sarcomas (Lehman, Ryeom et al. 2015) and lymphoma cell lines (Ishizawa, Kojima et al. 2016). The authors of the former study excluded variations in copy number and mutations that would have changed ATF4 expression, and speculated that altered regulation of ATF4 degradation (β-TrCP and PHD3) and/or stabilisation (p300) factors may be responsible. I did not detect changes in the transcript abundance of the fly homologues of these proteins (slmb, Hph & nej) in my RNA-Seq experiment, but it is possible that they undergo post-transcriptional regulation and the dynamics of ATF4 degradation may be changed in *Drosophila* neurons with mitochondrial dysfunction. In the lymphoma cell study, the mechanism of ATF4 activation was suggested to be post-transcriptional and similar to the uORF system, but was examined by a GFP reporter construct in MEFs, without the authors confirming that the fibroblasts regulated ATF4 in the same eIF2α-independent way as the lymphoma cells.

Of particular interest to ATF4 in the nervous system, application of brain-derived neurotrophic factor (BDNF) to cultures of rat cortical and hippocampal neurons produced an elevation in both ATF4 mRNA and protein that was entirely independent of eIF2α, and instead mediated via tropomyosin receptor kinase B (TrkB) signalling and as yet undiscovered factors (Liu, Amar et al. 2018). Once again, I did not detect transcriptional alterations to the *Drosophila* BDNF or TrkB homologues, the NT1 and Kek genes.

Whilst I have not detected gene changes corresponding to the above studies, a gene that was not only significantly upregulated by TFAM overexpression, but also upregulated by ATF4 overexpression and reversed by ATF4 RNAi was the cap-dependent translation repressor *Thor* (*4E-BP* in mammals). Phosphorylation of 4E-BP1 by the nutrient sensor mTOR prevents the binding of 4E-BP1 to the translation initiation factor eIF4E, and permits cap-dependent translation to proceed. Inhibition of mTOR activity was recently shown to reduce ATF4 translation in a 4E-BP-dependent manner (Park, Reyna-Neyra et al. 2017). Increased levels of active (unphosphorylated) 4E-BP and the resultant reduction in cap-dependent translation were hypothesized to lead to an increase in the availability of ternary complexes (eIF2-GTP-tRNA$_i$Met) that allowed the ribosome to initiate at the 5'UTR decoy uORFs, rather than the start codon, of ATF4. The transcriptional upregulation of *4E-BP1* by ATF4 in *Drosophila* neurons with mitochondrial dysfunction could therefore represent a novel negative feedback loop within the ER UPR pathway.

It is known that the *Drosophila* homologue of hypoxia-inducible factor 1α (HIF-1α) is a key player in the regulation of mitochondrial retrograde signalling in the nervous system (Cagin, Duncan et al. 2015). Excitingly, a recent discovery could explain the eIF2α-independent regulation of ATF4 in many of the above studies, and tantalisingly suggests how the ISR, response to hypoxia and nutrient sensing could all simultaneously converge upon ATF4 in response to mitochondrial dysfunction. Translation of ATF4 mRNA in response to amino acid starvation was shown to be controlled by methylation of adenosine (m^6A) in the uORF proximal to the translational start site (uORF2) (Zhou, Wan et al. 2018). The presence of methylation impeded ribosome scanning and caused translation to initiate at uORF2 in preference to the overlapping ATF4 coding sequence. Knock-down of the m^6A methyltransferase complex components METTL3 and METTL14 led to a substantial increase in ATF4 protein levels above those already induced by P-eIF2α, whilst knock-down of the m^6A demethylases ALKBH5 and FTO largely abrogated the upregulation of ATF4 by eIF2α phosphorylation. ALKBH5 is induced by hypoxia in multiple cancer cell lines, in a HIF-1α-dependent manner (Thalhammer, Bencokova et al. 2011, Zhang, Samanta et al. 2016), suggesting that regulation of transcription by stabilised HIF-1α could impinge upon ATF4 translation. METTL3, METTL14 and the YTH domain family of m^6A reading proteins are conserved in *Drosophila*, but neither homologues of ALKBH5 and FTO, nor alternative m^6A

demethylases have been identified in the fly genome (Lence, Soller et al. 2017), indicating that much works remains to determine whether ATF4 mRNA marks the intersection of the ISR and the epigenetic response to mitochondrial dysfunction in *Drosophila* neurons.

6.2.3 Functional consequences of ER UPR activation

6.2.3.1 Functional consequences of PERK activation

Knock-down of PERK exacerbated the neuronal functional deficits of TFAM overexpressing flies. It has recently been demonstrated that PERK acts to protect mitochondrial integrity in response to ER stress. Knock-out or inhibition of PERK increased mitochondrial fragmentation in MEFs treated with the ER stressors tunicamycin or thapsigargin, and this fragmentation was accompanied by decreased respiratory capacity. The protection by PERK was unaffected by knockout of ATF4, or inhibition of the IRE1 and ATF6 pathways, but did require the phosphorylation of eIF2α (Lebeau, Saunders et al. 2018). Also in MEFs, PERK has been detected within MAMs. PERK knockout reduced the number of ER-mitochondria contacts and the induction of apoptosis in response to ER stress mediated by (ER localised) ROS, suggesting that PERK and ER-mitochondrial tethering were required to communicate stress from the ER to the mitochondria (Verfaillie, Rubio et al. 2012). Similarly in rat cardiomyocytes, PERK – but not IRE1 or ATF6 – was discovered in MAMs and knock-down of the protein again protected against ROS-induced apoptosis, however ER-mitochondria contacts were not quantified (Liu, Zhu et al. 2013). These results raise the possiblity that the increased numbers of ER-mitochondrial contacts seen in the TFAM overexpression condition may be dependent on PERK.

Fascinatingly, in mammalian cells, elevated cytosolic Ca^{2+} has been found to cause the expansion of ER-plasma membrane contacts via PERK-regulated changes to the actin cytoskeleton. These changes required the interaction of PERK with the actin

crosslinker Filamin A, but not PERK kinase activity. The increased ER-plasma membrane contacts served as expanded platforms for oligomerised STIM to trigger store-operated Ca^{2+} entry and hypothetically replenish the intraluminal Ca^{2+} concentration of the ER (van Vliet, Giordano et al. 2017). Remarkably, IRE1 has also been shown to interact with Filamin A in diverse models including *Drosophila* hemocytes, functioning as a scaffold that governed cell motility (Urra, Henriquez et al. 2018).

6.2.3.2 Functional consequences of ATF4 activation

Although downstream of PERK, in *Drosophila* neurons with mitochondrial dysfunction, knock-down of ATF4 was able to suppress the neuronal functional deficits displayed in climbing and wing inflation assays. This suggests both that mitochondrial retrograde signalling is responsible for some neuronal functional pathology in addition to the original mitochondrial insult, and more specifically that activation of ATF4 is detrimental in neurons with mitochondrial dysfunction. The pathological element of retrograde signalling is in agreement with the previous finding that knock-down of HIF-1α also suppressed the mitochondrial dysfunction phenotype in *Drosophila* neurons (Cagin, Duncan et al. 2015), but the consequences of ATF4 activation as a stress responder in the nervous system have been an enigma.

The normal physiological role of ATF4 in unstressed neurons appears to be the facilitation of synaptic plasticity and memory (Liu, Pasini et al. 2014, Hu, Levine et al. 2015, Pasini, Corona et al. 2015). It should be noted that - in keeping with the divisive nature of ATF4 - conflicting reports have suggested that it inhibits plasticity (Chen, Muzzio et al. 2003, Costa-Mattioli, Gobert et al. 2007, Kandel 2012, Trinh, Kaphzan et al. 2012), however these studies drew conclusions solely from phosphorylation of eIF2α, or relied upon broad-spectrum inhibitors of the entire CREB family, and are therefore considered less reliable than the investigations that utilised direct manipulation of ATF4 and described a positive role in plasticity. In the CNS of control *Drosophila*, I detected ATF4 protein solely in three bilaterally paired loci of the VNC, which I speculate may represent leg precursor regions. However, knock-down of ATF4 resulted in a slight decrease of β-Gal expression driven by the *Thor* promoter, suggesting that there may be

levels of ATF4 in the *Drosophila* CNS that were below the detection window of the ATF4 antibody, and indicating that the protein may also have functional roles in the unstressed fly CNS.

Several studies have identified ATF4 as a protective factor in response to mitochondrial dysfunction. Activating mutations in ATF4 increased resistance to oxidative stress in hippocampal HT22 and pheochromocytoma PC12 cell lines (Lewerenz, Sato et al. 2012). Dissipation of mitochondrial membrane potential by the protonophore carbonyl cyanide *m*-chlorophenyl hydrazine (CCCP) resulted in ER stress in HEK293T and SH-SY5Y neuroblastoma cells (Bouman, Schlierf et al. 2011). In these models, the parkin was a direct transcriptional target of ATF4, and its upregulation mediated cell survival in response to the CCCP treatment. Parkin was also the effector of ATF4-mediated protection of PC12 cells following application of MPP^+ or 6-OHDA (Sun, Liu et al. 2013), and SH-SY5Y cells after rotenone treatment (Wu, Luo et al. 2014). Interestingly, whilst parkin is convincingly the agent of cellular preservation in these proliferating cell line models, it was not upregulated in my RNA-Seq experiments with TFAM overexpression, either of two *Drosophila ex vivo* microarrays - also with pan-neuronal TFAM expression - (Cagin, Duncan et al. 2015, Duncan, Granat et al. 2018), nor in the cortex of mice with knockout of the mitochondrial serine protease HtrA2 (Moisoi, Klupsch et al. 2008). These observations, combined with my finding that ATF4 knock-down can partially suppress the neuronal deficits of TFAM-overexpressing flies, suggest that parkin does not play the same protective role in non-proliferating cells, and indicates contrasting roles for ATF4 in proliferating cells and terminally differentiated neurons. Consistent with this idea, a number of investigations in primary neurons have reported a detrimental role for ATF4 in response to stress. $ATF4^{-/-}$ murine primary cortical neurons were more resistant to oxidative stress induced by the glutamate analogue homocysteate (HCA) (Lange, Chavez et al. 2008), and apoptosis induced by the ER stressors tunicamycin and thapsigargin (Galehdar, Swan et al. 2010), with the latter protection stemming from reduced induction of PUMA via an ATF4-CHOP axis. Further, intra-axonal translation of ATF4 spread Alzheimer's-associated $A\beta_{1\text{-}42}$ pathology in murine brains, causing neuron loss that was abolished by siRNA targeting ATF4 or its downstream effector CHOP (Baleriola, Walker et al. 2014). To date, the only primary neuronal model of mitochondrial or mitochondria-related dysfunction to demonstrate protection by parkin was 6-OHDA treatment of ventral midbrain neurons (Sun, Aime et

al. 2018). The role of ATF4 in the regulation of parkin, and *in vivo* protection mediated by guanabenz, a small-molecule inhibitor of GADD34, was inferred from studies in proliferating cells. The authors also reported that ATF4 knockout substantially reduced the neuroprotective effect of guanabenz in primary cortical neuron cultures treated with the DNA-damage inducing agent camptothecin. This is in partial agreement with a previous study that showed ATF4 overexpression protected murine cortical neurons against camptothecin, but also demonstrated unchanged levels of the ATF4 protein in response to treatment with the toxin (Galehdar, Swan et al. 2010). Frustratingly, the authors of the guanabenz study were unclear as to the species of their primary cells, preventing direct comparison between the camptothecin results. *Drosophila* do not have a homologue of CHOP. Therefore, if my conjecture that absence of proliferation is the switch that changes the role of ATF4 from good to bad in neuronal mitochondrial dysfunction models is correct, it will not simply be the case that upregulation of parkin (good) in proliferating cells switches to upregulation of CHOP (bad) in terminally differentiated neurons, and may instead be a complex remodelling of the cells' metabolic needs.

6.2.4 ATF4 as a regulator of mitochondrial retrograde signalling

There was substantial overlap in the genes regulated by TFAM overexpression and ATF4 overexpression in *Drosophila* neurons. In addition, knock-down of ATF4 in conjunction with TFAM overexpression reversed many of the transcriptional changes caused by overexpression of TFAM. Whilst my RNA-Seq analysis requires further validation by qRT-PCR, taken together these findings indicate that ATF4 is a regulator of mitochondrial retrograde signalling in the *Drosophila* nervous system.

Interestingly, whilst ATF4 is well characterised in the UPR pathway downstream of ER stress, overexpression of ATF4 in *Drosophila* neurons resulted in the downregulation of a number of ETC Complex I subunits. Transcriptional regulation of the ETC enzymes was less pronounced by TFAM overexpression, and unaffected by knock-down of ATF4 alongside TFAM overexpression, suggesting that ATF4 may have the facility to regulate mitochondrial function in the *Drosophila* nervous system, but does not predominantly do so in the context of mitochondrial dysfunction. Instead, gene expression changes regulated by ATF4 are largely targeted to pathways that alter the

molecular or functional outcome of mitochondrial dysfunction, rather than to 'fixing' the mitochondrial defect.

6.2.4.1 Glycolysis

ATF4 is known to upregulate glycolytic genes in *Drosophila* S2 cells in response to ER stress induced by the reducing agent dithiothreitol (DTT) (Lee, Oney et al. 2015). However, it has not been demonstrated before that ATF4 can regulate glycolysis in the neurons of any organism. My results show that overexpression of ATF4 in *Drosophila* neurons downregulated expression of lactate dehydrogenase (ImpL3) and transaldolase (Taldo), the linker enzyme between the pentose-phosphate and glycolytic pathways, suggesting a concerted effort to maintain the supply of pyruvate to the Krebs cycle. TFAM overexpression caused the significant upregulation of Hexokinase A and ImpL3, whilst knock-down of ATF4 in conjunction with TFAM overexpression downregulated these genes, the trehalose transporter (Tret1-1), and the mitochondrial isoform of phosphoenolpyruvate carboxykinase 2 (Pepck2/CG10924). Trehalose, a disaccharide of glucose, is the predominant sugar in insects (Wyatt and Kale 1957), and Tret1-1 mediates its uptake into cells (Kanamori, Saito et al. 2010) prior to its hydrolysis into two glucose molecules by trehalase (Yoshida, Matsuda et al. 2016). Pepck2 catalyses the conversion of oxaloacetate to phosphoenolpyruvate via the elimination of CO_2, an irreversible step in gluconeogenesis (Ashmore, Wagle et al. 1964). These changes indicate that ATF4 upregulates gluconeogenesis and glycolysis in response to neuronal mitochondrial dysfunction caused by TFAM overexpression, hypothetically as a protective measure to counter reduced ATP production by the compromised ETC/Complex V. Upregulation of ImpL3 suggests that an increased proportion of the NADH produced by glycolysis is re-oxidised in the cytosol, rather than transferred to the mitochondria for oxidation by the ETC.

6.2.4.2 Oxidative stress and apoptosis

Several cytochrome p450 proteins were downregulated by ATF4 overexpression. Two of those proteins were also downregulated by TFAM overexpression, and the expression of one was reversed by ATF4 knock-down, suggesting that ATF4 mediates a downregulation of members of the cytochrome P450 family in response to neuronal mitochondrial dysfunction. Cytochrome P450s are oxidases that function to metabolise

endogenous substances and xenobiotics, but are also constitutive producers of ROS even in the absence of substrates (reviewed in (Zangar, Davydov et al. 2004)). Coupled with the downregulation of Complex I subunits (mostly in the absence of mitochondrial dysfunction) by ATF4, this suggests a protective transcriptional programme to reduce oxidative stress, and possibly the consequent apoptosis. This idea is supported by the ATF4-mediated downregulation of cytochrome c distal (cyt-c-d) in response to TFAM overexpression. *Drosophila* possess two cytochrome c proteins, cyt-c-d and cytochrome c proximal (cyt-c-p). cyt-c-p is highly expressed in somatic cells of the fly throughout development and adulthood, whilst cyt-c-d transcripts are low (Arama, Bader et al. 2006). However, whilst cyt-c-p functions predominantly in the ETC, cyt-c-d promotes apoptosis in both the testes (where it is abundant) (Arama, Bader et al. 2006) and the developing retina (Mendes, Arama et al. 2006). In the retina, cyt-c-p is unable to fulfill the pro-apoptotic role in the absence of cyt-c-d. This suggests that downregulation of cyt-c-d by ATF4 protects *Drosophila* neurons from apoptosis in response to TFAM overexpression. Paradoxically, ATF4 also appeared to downregulate a number of glutathione S-transferase (GST) enzymes in *Drosophila* neurons, both with and without TFAM overexpression. These proteins can function as anti-oxidants (Yang, Cheng et al. 2001, Singhal, Singh et al. 2015), and have not been reported to generate ROS, so it is unclear why reducing their expression would be beneficial, and it may be that downregulation of the GST proteins is one of the functionally detrimental affects of ATF4 that is alleviated by its knock-down.

6.2.4.3 Molecular chaperones

A canonical aspect of the ER UPR is the upregulation of molecular chaperones to alleviate protein stress within the ER. Indeed, transcriptional upregulation of BiP (*Drosophila* Hsc70-3) is frequently used as a marker of ER UPR activation. Surprisingly BiP was not significantly regulated by either TFAM overexpression or ATF4 overexpression, nor were any other ER-resident chaperones. Instead, the expression of Hsp22, which is known to be a mitochondrial chaperone (Morrow, Inaguma et al. 2000), and Hsc70-2, which is predicted to be a mitochondrial protein from sequence analysis (Sardiello, Licciulli et al. 2003), were upregulated by TFAM overexpression in a manner that appeared to be dependent on ATF4 (was reversed by ATF4 RNAi). This suggests that in *Drosophila* neurons with mitochondrial dysfunction, ATF4 ameliorates unfolded

protein stress by regulating the mtUPR, rather than the ER UPR. Given that TFAM overexpression would be expected to cause an unfolded protein burden in the mitochondria, caused by both mis-assembled ETC complexes and the stress of its own folding on the mitochondrial machinery, this suggests the existence of an unknown trigger that is able to switch ATF4 chaperone regulation in response to the main location of the unfolded protein overload.

The regulation of cytosolic chaperones is more complicated. Hsp67Bc, which is known to promote autophagy in *Drosophila* (Carra, Boncoraglio et al. 2010), was downregulated by ATF4 knock-down in the TFAM overexpression condition, suggesting that it is upregulated by ATF4 in response to TFAM overexpression, and that ATF4 may promote autophagy in *Drosophila* neurons with mitochondrial dysfunction.

Three members of the cytosolic *Drosophila Hsp70* family were also significantly regulated in my RNA-Seq analysis, however these genes inhabit a fascinating niche in the evolutionary landscape. Six *Hsp70* genes exist in two clusters on chromosome 3. The *Hsp70A* genes (*Hsp70Aa* and *Hsp70Ab*) comprise one cluster, and the *Hsp70B* genes (*Hsp70Ba*, *Hsp70Bb, Hsp70Bbb* and *Hsp70Bc*) the other (Gong and Golic 2006). Remarkably, there are no fixed nucleotide differences between the members of each cluster, and therefore within each cluster all the members have identical amino acid sequences. Additionally, despite the duplication event that created the *Hsp70B* cluster from the *Hsp70A* loci occurring 12-15 million years ago (Bettencourt and Feder 2002), the chaperones of the two clusters differ by only six amino acids. Unsurprisingly, the six *Hsp70* genes appear to be functionally equivalent. (Gong and Golic 2006). Whilst all the genes have near identical 5'UTRs and coding sequences, the clusters can be distinguished by the different sequences in their 3'UTRs, and in-situ hybridisation has suggested that the clusters can be separately regulated in response to heat shock (Lakhotia and Prasanth 2002). The output from my RNA-Seq analysis reports that Hsp70Aa and Hsp70Bbb were downregulated, and Hsp70Bb upregulated by TFAM overexpression and/or ATF4 overexpression, however it is extremely unlikely that the reads from the *Hsp70* family could be definitively aligned to the gene from which they originated. 'Multi-read correct' was enabled in the transcript assembly software Cufflinks and therefore, at least theoretically, ambiguous Hsp70 reads could have been distributed according to a weighting of the reads from the 3'UTRs. However, it is likely that Cufflinks was

hamstrung by the upstream software Bowtie2, which performs the initial alignment procedure within the mapping software TopHat, and randomly assigns multi-mapped reads to one of the matching locations in the genome. Therefore, it is likely that on average the Hsp70 chaperones were not significantly regulated by either TFAM overexpression or ATF4 overexpression.

6.2.4.4 Anabolic pathways

Upregulation of one-carbon metabolism and the related nucleotide salvage pathway have previously been shown to occur in *Drosophila pink1* and *parkin* mutants, and to protect these flies against dopaminergic neuron loss (Tufi, Gandhi et al. 2014, Celardo, Lehmann et al. 2017). Upregulation of the one-carbon metabolism genes, SHMT2 and MTHFD2, that are required for the synthesis of formylmethionine for mitochondrial proteins, was shown to be dependent on ATF4 (Celardo, Lehmann et al. 2017). In my RNA-Seq analysis, ATF4 overexpression suppressed the transcription of dihydrofolate reductase (Dhfr), an upstream enzyme in tetrahydrofolate synthesis, but otherwise one-carbon metabolism and nucleotide salvage genes were not significantly regulated. This may be because in TFAM overexpressing neurons, functional pink1 and parkin would permit the recycling of dysfunctional mitochondria via MDV formation and mitophagy, hypothetically leading to the continual supply of formylmethionine and other anabolic components without the need for nucleotide salvage or the upregulation of one-carbon metabolism.

6.2.4.5 Sialylation

Csas, encoding CMP-sialic acid synthetase, was downregulated by both TFAM overexpression and ATF4 overexpression. Co-expression of ATF4 RNAi increased *Csas* expression an average 1.4 fold versus TFAM overexpression alone, but this change was not significant ($p = 0.00395$, adjusted $p = 0.335$). CMP-sialic acid is the activated substrate of the transferases which sialylate the terminal glycans of both proteins and lipids. *Drosophila Csas* mutants display locomotor defects and are paralysed at elevated temperatures. These phenotypes can be explained by a dose-dependent reduction in

evoked excitatory junction potentials (EJPs) – null mutants had a stronger impairment than hypomorphs – that was caused by decreased neuronal excitability rather than defects in synaptic transmission (Islam, Nakamura et al. 2013). Downregulation of *Csas* by TFAM or ATF4 overexpression is therefore likely to be functionally adverse, but is probably explained by the drive to produce and conserve ATP; synthesis of sialic acid consumes pyruvate (Roseman 1962) – reducing its availability for conversion to lactate by ImpL3, with the concomitant reoxidation of NADH to be used in the glycolytic pathway - and it's conjugation to CMP consumes a molecule of CTP.

The function of sialylation in the nervous system is complex, but it appears to mask healthy neurites from microglial surveillance, whilst desialylated processes undergo phagocytosis (Linnartz, Kopatz et al. 2012, Linnartz-Gerlach, Schuy et al. 2016). A loss of neurites may explain the reduced neuronal excitability seen in *Csas* mutant flies, and some of the impairments to neuronal function in TFAM overexpressing flies. Sialylation is central to the processing of the Alzheimer's-associated protein amyloid-β, with both positive and negative affects on neurotoxicity reported (Nakagawa, Kitazume et al. 2006, Patel, Henry et al. 2007, Nolan, McHale-Owen et al. 2017).

Whilst my results show that knock-down of PERK is detrimental in *Drosophila* neurons with mitochondrial dysfunction, important work from the Mallucci lab has determined that the ER UPR is activated in mouse models of prion disease, and inhibition of PERK or the downstream effects of eIF2α phosphorylation reduces prion-mediated neurodegeneration (Moreno, Radford et al. 2012, Moreno, Halliday et al. 2013, Halliday, Radford et al. 2015). Interestingly, loss of sialylation from the pathogenic configuration of the prion protein, PrP^{Sc}, promotes enhanced amplification of PrP^{Sc}, removal of the cross-species barrier to infection, and increased neuroinflammation (Katorcha, Makarava et al. 2014, Katorcha, Makarava et al. 2015, Srivastava, Katorcha et al. 2018). Knockout of neuronal sialidases (neuramidases) did not affect the sialylation status of PrP^{Sc} (Katorcha, Klimova et al. 2015), indicating that it is the rate of sialyl transfer that controls sialylation levels of PrP^{Sc}. If ATF4 also downregulates the transcription of *Csas* in the mammalian nervous system, and thus hypothetically reduces levels of sialylation, this may explain why inhibition of PERK or P-eIF2α, with consequent reduction in ATF4, was therapeutic in murine prion disease models. In our *Drosophila* model of

mitochondrial dysfunction, it is likely that the benefits of increased sialylation from knock-down of PERK would be outweighed by the putative increase in mitochondrial fragmentation and reduced ER Ca^{2+}.

6.3 Conclusions and Future Directions

I hypothesised that mitochondrial dysfunction in *Drosophila* neurons would cause alterations to ER biology, activate ER stress signalling, and that this signalling would regulate nuclear gene transcription. In addition, I began my investigation by assessing mitochondrial morphology, and my work has therefore spanned from the source of the mitochondrial dysfunction, across contacts with, and changes to, the intervening ER, to the nucleus. My results show that ER stress signalling was activated in *Drosophila* neurons by mitochondrial dysfunction, and the breadth of my investigation has allowed me to place the activation of ER UPR components in a wider context.

Whilst knock-down of many UPR proteins was functionally beneficial, knock-down of PERK exacerbated the climbing and wing inflation deficits of TFAM overexpressing flies. My characterisation of fragmented mitochondria, increased numbers of candidate ER-mitochondria contacts and altered cytosolic Ca^{2+} allow me to speculate that PERK is a key player in the response to neuronal mitochondrial dysfunction, and that the seemingly beneficial presence of PERK is independent of its role within canonical UPR signalling. PERK has been shown to protect mitochondrial respiration and morphology in response to ER stress – suggesting a possible loop whereby mitochondrial dysfunction causes ER stress which then activates mitochondrial defense mechanisms – to be enriched at MAMs, and to modulate ER-plasma membrane contacts in response to elevated cytosolic Ca^{2+}, putatively to restore luminal ER Ca^{2+} via store-operated Ca^{2+} entry.

When characterising the role of PERK in response to neuronal mitochondrial dysfunction, it will first be necessary to confirm the changes to mitochondrial

morphology and increase in ER-mitochondria contacts via higher-resolution techniques such as electron microscopy, then whether PERK is also present at *Drosophila* neuronal MAMs and if PERK knock-down reduces these contacts. Verfaillie, Rubio et al. 2012 established that expression of a kinase-dead PERK in PERK$^{-/-}$ MEFs was sufficient to maintain ER-mitochondrial contacts, whilst a cytoplasmic deletion mutant of PERK was not. Creation of similar *Drosophila* tools would allow us to dissect the contribution of PERK to ER-mitochondrial contacts away from its role in ER UPR signalling – which requires the kinase activity of PERK to phosphorylate eIF2α.

To examine the putatively beneficial regulation of ER-plasma membrane contacts by PERK, further work first needs to be done to fully characterise the Ca^{2+} dynamics in *Drosophila* neurons with mitochondrial dysfunction. In particular, we need to know whether ER Ca^{2+} is depleted in the TFAM overexpression model in both resting and stimulated neurons, as theoretically PERK activity raises the intra-luminal ER Ca^{2+} concentration, and therefore may be detrimental if ER Ca^{2+} is abnormally high. Development of *in vivo* ER Ca^{2+} sensors derived from mammalian ER-GCaMPs (de Juan-Sanz, Holt et al. 2017) or Calcium-measuring organelle-entrapped protein indicators (CEPIAs) (Suzuki, Kanemaru et al. 2014) will require the optimisation of K_ds and dynamic ranges suitable for *Drosophila* neurons, but would be extremely useful in this characterisation. Live imaging of cytosolic Ca^{2+} levels in neurons stimulated by the heat-activated TrpA1 channel required immobilisation of the CNS in agarose to reduce movement caused by heating of the surrounding media. Live imaging of Ca^{2+} in the reticular mitochondrial network could not be achieved via this method as the residual movement of the CNS was too great to keep single mitochondria in the focal plane. New techniques, probably utilising electrophysiology, will therefore have to be developed to image Ca^{2+} fluctuations in the ER and mitochondria of stimulated *Drosophila* neurons.

Whilst PERK knock-down was detrimental, ATF4 knock-down suppressed the functional deficits of TFAM overexpressing neurons. This presents a therapeutic conflict between the head and tail of the PERK ER UPR branch that is unlikely to be solved by strategies targeting the intermediary eIF2α; the repression of global translation that is usually mediated by phosphorylation of eIF2α may meaningfully reduce the energetic burden on neurons with compromised ATP supply. The effect of eIF2α phosphorylation

on translation in neurons with mitochondrial dysfunction may be assessed without glial contamination by used of a tagged ribosomal subunit expressed via the *Gal4-UAS* system (Thomas, Lee et al. 2012). Tagged ribosomes can be pulled down, and the associated mRNA content assessed by sequencing. Inhibition of ATF4 itself would be a blunt therapeutic approach to neurological diseases associated with mitochondrial dysfunction, that risked reducing the hypothetically neuroprotective upregulation of glycolysis and decrease in ROS production that I have identified. Interventions directed at selected transcriptional targets of ATF4 that have been identified to be pathological may therefore represent better therapies.

Transcription of CMP-Sialic acid synthetase (*Csas*) was downregulated by both TFAM overexpression and ATF4 overexpression in *Drosophila* neurons, with putatively damaging effects. I have discussed how the hypothetical modulation of sialylation by PERK may reconcile my observation that PERK knock-down exacerbates the TFAM overexpression phenotype, with the suppression of prion disease in murine models by PERK inhibition. With the caveat that further investigation of PERK be undertaken, the breadth of my work, which spans both the proximal and distal effects of PERK activation, enables me to suggest a two-pronged therapeutic strategy for diseases with mitochondrial dysfunction whereby PERK is activated to boost its hypothetically protective effects on mitochondrial morphology and Ca^{2+} homeostasis, but the transcriptional regulation of selected downstream targets by ATF4 is reversed. In particular, methods to block the downregulation of *Csas* or increase the activity of its encoded protein may protect otherwise healthy neurites from phagocytosis and enhance neural transmission. In the short-term, it should be established whether overexpression of Csas can suppress the functional deficits of TFAM overexpressing neurons, and if so, further experiments should then be undertaken to determine the role of sialylation in neuronal mitochondrial dysfunction, including examination of the number and morphology of neurites, and neuronal excitability in flies with genetic manipulations of Csas and TFAM.

Alongside the activation of ER stress signalling, I also detected the hypothesised changes to ER biology in *Drosophila* neurons with mitochondrial dysfunction. In particular, two fluorescent ER markers suggested a reduction in the reticulation of the ER that was most profound in the perinuclear region. It has been established that knockout of

mitofusin (de Brito and Scorrano 2009), and mutation of the OMM fusion regulator SLC25A46 (Janer, Prudent et al. 2016), lead to altered ER morphology, however mitofusin and SLC25A46 are MAM components, and it is therefore not surprising that their absence affects ER morphology. My results are the first preliminary confirmation that dysfunctional mitochondria – as opposed to dysfunctional regulators of mitochondria such as mitofusin – can alter the shape of the ER, and the first demonstration that specific subdomains of the ER may be more acutely altered. It is likely that ER morphology has been underinvestigated *in vivo* due to an absence of suitable tools, and indeed electron microscopy or higher resolution fluorescence microscopy will be needed to verify the alterations to ER morphology suggested by the fluorescent BiP-sfGFP-HDEL and tdTomato-Sec61β reporters. The IRE1 and ATF6 branches (Maiuolo, Bulotta et al. 2011) of the ER UPR have been shown to regulate the lipid synthesis that drives the ER sheet expansion that could explain the hypothetical loss of reticulation in TFAM overexpressing flies.

In addition to creating changes to ER lipid composition, the ER UPR can also be activated by altered ER lipid density. Increased ER-mitochondrial contacts in *Drosophila parkin* mutants detrimentally enhance the transfer of phosphatidylserine (PS) to the mitochondria, resulting in depletion of PS from the ER. PS has been widely and successfully trialled as an orally administered agent for improving the cognitive function in older adults with subjective memory complaints (Kato-Kataoka, Sakai et al. 2010, Richter, Herzog et al. 2010, Vakhapova, Cohen et al. 2010, Richter, Herzog et al. 2013, Moré, Freitas et al. 2014, Vakhapova, Cohen et al. 2014). PS supplementation also improved the memory performance of patients with the more severe classification 'age-associated memory impairment' in two studies (Crook, Tinklenberg et al. 1991, Schreiber, Kampf-Sherf et al. 2000), but not in a third (Jorissen, Brouns et al. 2001) and has been shown to significantly improve the vocabulary and picture recall of Alzheimer's patients, albeit very mildly (Zhang, Yang et al. 2015). In addition, PS has improved cognitive performance in an extensive range of animal models (reviewed in (Reddan, White et al. 2018)). These studies demonstrate that enhanced consumption of PS can positively impact the function of the nervous system, but the benefits have been largely linked to protection from oxidative stress or inflammation. If PS supplementation is shown to improve the climbing and/or wing inflation impairment of TFAM overexpressing flies, it will be important to determine whether the benefits were mediated

by changes in ER lipid composition and consequently reduced activation of the ER UPR. Regardless, if ROS are increased in the cell bodies of *Drosophila* motor neurons by TFAM overexpression, PS therapy could represent an effective neuroprotective strategy for reduction of oxidative damage.

Whilst abnormal lipid handling is merely a candidate for transferring the retrograde signal from ER-mitochondrial contacts to the ER in response to mitochondrial dysfunction in *Drosophila* neurons, it is clear that the ER UPR represents at least part of the signal over the next leg from the ER to the nucleus. I characterised the transcriptional changes regulated by ATF4 in response to TFAM overexpression in *Drosophila* neurons, however knock-down of the the other UPR transcription factors ATF6 and XBP1 was also functionally beneficial in climbing and wing inflation assays. XBP1 has been shown to form heterodimers with ATF6 and ATF4 in response to ER stress (Yamamoto, Sato et al. 2007, Cho, Lee et al. 2008) to mediate combined regulation of target genes. It will be important to analyse the transcriptional regulation mediated by ATF6 and XBP1 in TFAM overexpressing neurons, as genes commonly regulated by all three ER UPR transcription factors would be prime candidates to underly the adverse effects of ER UPR activation, and represent novel therapeutic targets.

The ER is continuous with the outer nuclear membrane, and it is therefore conceivable that ER stress signals could also be communicated internally through the ER lumen to the nucleoplasmic reticulum (NR), and thence into the nucleoplasm. Intra-ER-to-nucleus signalling is a fascinating and underexplored topic. In order to determine the role, if any, of the NR in mitochondrial retrograde signalling in *Drosophila* neurons, it will first be required to establish whether invaginations of the nuclear envelope occur in either control or TFAM overexpressing neurons, and their relative frequency and extent. Given that mitochondria can be found within the type II NR channels, an initial experiment would be to examine the overlap of mitoGFP expression with that of a nuclear marker such as nuclear-targeted β-Gal. However, this would be merely a proxy for NR formation, and establishing a staining protocol for the ER/NR marker concanavalin A in *Drosophila* neurons would facilitate examination of the NR directly, and assessment of any localisation with the nucleoli by simultaneous use of DAPI staining. It will be important to include the nucleus in electron micrograph analysis of TFAM

overexpressing neurons, to determine at higher resolution whether there are alterations to NR morphology or the invasion of mitochondria into the channels formed by type II invaginations. Investigation of a functional role for NR Ca^{2+} handling in mitochondrial retrograde signalling could be undertaken by genetic manipulation of the Ca^{2+}-dependent transcriptional regulator CaMKIV, which is only active within the nucleus (Lemrow, Anderson et al. 2004). Further analysis of NR function in response to mitochondrial dysfunction would likely require knowledge of the protein components that constitute the hypothetical NR-mitochondrial contacts, or are enriched in the NR. Theoretically this could be achieved by isolating the nuclear fraction of the cells, pulling down proteins associated with e.g. VDAC, and then performing mass spectrometry. However, it may be difficult to demonstrate that mitochondrial components pulled down from the nuclear fraction were not simply contaminants.

In this thesis, I have demonstrated that mitochondrial dysfunction in *Drosophila* neurons alters mitochondrial morphology, ER morphology, ER-mitochondrial contacts and cellular Ca^{2+} handling, and that the ER stress signalling UPR is activated and regulates nuclear gene transcription. I have speculated that the retrograde signal from the mitochondria to the nucleus is conveyed from ER-mitochondria contacts to the ER by dysregulated lipid synthesis and/or Ca^{2+} handling, and from the ER to the nucleus by the ER UPR or, as yet undiscovered, intra-luminal pathways. How the initial signal from the mitochondria results in increased ER-mitochondrial contacts remains a very open question. In other models, PERK plays a pivotal role in the maintenance of mitochondrial morphology and ER-mitochondrial contacts independently of its function within the ER UPR, and therefore is a candidate for translating mitochondrial dysfunction into an augmented ER-mitochondrial interface – by an unknown mechanism. Elevated Ca^{2+} within one or more cellular compartments may also underly the increase in ER-mitochondrial contacts, but again the mechanism is presently unclear. My work has been conducted *in vivo* in the nervous system, and its breadth has permitted me to suggest further investigation of therapeutic strategies for diseases associated with neuronal mitochondrial dysfunction that span the length of the retrograde signal from the mitochondria to the nucleus.

7. References

Abbe, E. (1873). "Beiträge zur Theorie des Mikroskops und der mikroskopischen Wahrnehmung." Archiv für mikroskopische Anatomie **9**(1): 413-418.

Abrahams, J. P., et al. (1994). "Structure at 2.8 A resolution of F1-ATPase from bovine heart mitochondria." Nature **370**(6491): 621-628.

Abrams, E. W., et al. (2013). "Drosophila KDEL receptor function in the embryonic salivary gland and epidermis." PLoS ONE **8**(10): e77618.

Adams, M. D., et al. (2000). "The genome sequence of Drosophila melanogaster." Science **287**(5461): 2185-2195.

Aebi, M. (2013). "N-linked protein glycosylation in the ER." Biochimica et Biophysica Acta (BBA) - Molecular Cell Research **1833**(11): 2430-2437.

Ahlgren, H., et al. (2014). "The Nuclear Calcium Signaling Target, Activating Transcription Factor 3 (ATF3), Protects against Dendrotoxicity and Facilitates the Recovery of Synaptic Transmission after an Excitotoxic Insult." J Biol Chem **289**(14): 9970-9982.

AhYoung, A. P., et al. (2015). "Conserved SMP domains of the ERMES complex bind phospholipids and mediate tether assembly." Proc Natl Acad Sci U S A **112**(25): E3179-3188.

Aldridge, J. E., et al. (2007). "Discovery of Genes Activated by the Mitochondrial Unfolded Protein Response (mtUPR) and Cognate Promoter Elements." PLoS ONE **2**(9): e874.

Ali, M. M. U., et al. (2011). "Structure of the Ire1 autophosphorylation complex and implications for the unfolded protein response." The EMBO Journal **30**(5): 894-905.

Allen, D. and J. Seo (2018). "ER Stress Activates the TOR Pathway through Atf6." Journal of Molecular Signaling **13**: 1.

Aloni, Y. and G. Attardi (1971). "Expression of the mitochondrial genome in HeLa cells. II. Evidence for complete transcription of mitochondrial DNA." J Mol Biol **55**(2): 251-267.

Amuthan, G., et al. (2002). "Mitochondrial stress-induced calcium signaling, phenotypic changes and invasive behavior in human lung carcinoma A549 cells." Oncogene **21**(51): 7839-7849.

Amuthan, G., et al. (2001). "Mitochondria-to-nucleus stress signaling induces phenotypic changes, tumor progression and cell invasion." The EMBO Journal **20**(8): 1910-1920.

Anderson, S., et al. (1981). "Sequence and organization of the human mitochondrial genome." Nature **290**(5806): 457-465.

Andrade, J., et al. (2004). "The EF-Hand Ca(2+)-binding Protein p22 Plays a Role in Microtubule and Endoplasmic Reticulum Organization and Dynamics with Distinct Ca(2+)-binding Requirements." Molecular Biology of the Cell **15**(2): 481-496.

Annunziata, I., et al. (2018). "Mitochondria-associated ER membranes (MAMs) and lysosomal storage diseases." Cell Death & Disease **9**(3): 328.

Anwar, K., et al. (2012). "The dynamin-like GTPase Sey1p mediates homotypic ER fusion in S. cerevisiae." J Cell Biol **197**(2): 209-217.

Apostolova, N., et al. (2013). "ER stress in human hepatic cells treated with Efavirenz: Mitochondria again." Journal of Hepatology **59**(4): 780-789.

Arama, E., et al. (2006). "The two Drosophila cytochrome C proteins can function in both respiration and caspase activation." The EMBO Journal **25**(1): 232-243.

Arnould, T., et al. (2002). "CREB activation induced by mitochondrial dysfunction is a new signaling pathway that impairs cell proliferation." The EMBO Journal **21**(1-2): 53-63.

Ashmore, J., et al. (1964). "Studies on gluconeogenesis." Advances in Enzyme Regulation **2**: 101-114.

Baker, B. M., et al. (2012). "Protective coupling of mitochondrial function and protein synthesis via the eIF2α kinase GCN-2." PLoS Genetics **8**(6).

Baleriola, J., et al. (2014). "Axonally synthesized ATF4 transmits a neurodegenerative signal across brain regions." Cell **158**(5): 1159-1172.

Bannai, H., et al. (2004). "Kinesin dependent, rapid, bi-directional transport of ER sub-compartment in dendrites of hippocampal neurons." J Cell Sci **117**(Pt 2): 163-175.

Baqri, R. M., et al. (2014). "Mitochondrial chaperone TRAP1 activates the mitochondrial UPR and extends healthspan in Drosophila." Mech Ageing Dev **141-142**: 35-45.

Baughman, J. M., et al. (2011). "Integrative genomics identifies MCU as an essential component of the mitochondrial calcium uniporter." Nature **476**(7360): 341-345.

Baum, D. A. and B. Baum (2014). "An inside-out origin for the eukaryotic cell." BMC Biology **12**: 76.

Beckervordersandforth, R., et al. (2017). "Role of Mitochondrial Metabolism in the Control of Early Lineage Progression and Aging Phenotypes in Adult Hippocampal Neurogenesis." Neuron **93**(3): 560-573.e566.

Benson, K. R. (2001). "T. H. Morgan's resistance to the chromosome theory." Nature Reviews Genetics **2**: 469.

Bernard-Marissal, N., et al. (2015). "Dysfunction in endoplasmic reticulum-mitochondria crosstalk underlies SIGMAR1 loss of function mediated motor neuron degeneration." Brain **138**(Pt 4): 875-890.

Bertolotti, A., et al. (2000). "Dynamic interaction of BiP and ER stress transducers in the unfolded-protein response." Nat Cell Biol **2**(6): 326-332.

Bettencourt, B. R. and M. E. Feder (2002). "Rapid concerted evolution via gene conversion at the Drosophila hsp70 genes." J Mol Evol **54**(5): 569-586.

Bian, X., et al. (2011). "Structures of the atlastin GTPase provide insight into homotypic fusion of endoplasmic reticulum membranes." Proc Natl Acad Sci U S A **108**(10): 3976-3981.

Biczo, G., et al. (2018). "Mitochondrial Dysfunction, Through Impaired Autophagy, Leads to Endoplasmic Reticulum Stress, Deregulated Lipid Metabolism, and Pancreatitis in Animal Models." Gastroenterology **154**(3): 689-703.

Bier, E. (2005). "Drosophila, the golden bug, emerges as a tool for human genetics." Nat Rev Genet **6**(1): 9-23.

Bischof, J., et al. (2013). "A versatile platform for creating a comprehensive UAS-ORFeome library in Drosophila." Development **140**(11): 2434-2442.

Bobinnec, Y., et al. (2003). "Dynamics of the endoplasmic reticulum during early development of Drosophila melanogaster." Cell Motil Cytoskeleton **54**(3): 217-225.

Bonifati, V., et al. (2003). "Mutations in the DJ-1 gene associated with autosomal recessive early-onset parkinsonism." Science **299**(5604): 256-259.

Borkenhagen, L. F., et al. (1961). J. Biol. Chem. **236**.

Bottinger, L., et al. (2016). "How lipids modulate mitochondrial protein import." J Bioenerg Biomembr **48**(2): 125-135.

Bottinger, L., et al. (2012). "Phosphatidylethanolamine and cardiolipin differentially affect the stability of mitochondrial respiratory chain supercomplexes." J Mol Biol **423**(5): 677-686.

Bouman, L., et al. (2011). "Parkin is transcriptionally regulated by ATF4: Evidence for an interconnection between mitochondrial stress and ER stress." Cell Death Differ **18**(5): 769-782.

Bourgeois, C. A., et al. (1979). "Structural relationship between the nucleolus and the nuclear envelope." J Ultrastruct Res **68**(3): 328-340.

Bozler, J., et al. (2015). "Condensins Exert Force on Chromatin-Nuclear Envelope Tethers to Mediate Nucleoplasmic Reticulum Formation in Drosophila melanogaster." G3: Genes|Genomes|Genetics **5**(3): 341-352.

Brand, A. H. and N. Perrimon (1993). "Targeted gene expression as a means of altering cell fates and generating dominant phenotypes." Development **118**(2): 401-415.

Brandt, T., et al. (2017). "Changes of mitochondrial ultrastructure and function during ageing in mice and Drosophila." Elife **6**.

Bravo, R., et al. (2011). "Increased ER–mitochondrial coupling promotes mitochondrial respiration and bioenergetics during early phases of ER stress." Journal of Cell Science **124**(13): 2143-2152.

Breckenridge, D. G., et al. (2003). "Caspase cleavage product of BAP31 induces mitochondrial fission through endoplasmic reticulum calcium signals, enhancing cytochrome c release to the cytosol." J Cell Biol **160**(7): 1115-1127.

Broadwell, R. D. and A. M. Cataldo (1983). "The neuronal endoplasmic reticulum: its cytochemistry and contribution to the endomembrane system. I. Cell bodies and dendrites." J Histochem Cytochem **31**(9): 1077-1088.

Broadwell, R. D. and A. M. Cataldo (1984). "The neuronal endoplasmic reticulum: its cytochemistry and contribution to the endomembrane system. II. Axons and terminals." J Comp Neurol **230**(2): 231-248.

Budnik, V., et al. (1990). "Morphological plasticity of motor axons in Drosophila mutants with altered excitability." J Neurosci **10**(11): 3754-3768.

Burgermeister, M., et al. (2004). "Contribution of different pathways to the supply of phosphatidylethanolamine and phosphatidylcholine to mitochondrial membranes of the yeast Saccharomyces cerevisiae." Biochim Biophys Acta **1686**(1-2): 161-168.

Butow, R. A. and N. G. Avadhani (2004). "Mitochondrial Signaling: The Retrograde Response." Mol Cell **14**(1): 1-15.

Byrnes, L. J., et al. (2013). "Structural basis for conformational switching and GTP loading of the large G protein atlastin." Embo j **32**(3): 369-384.

Byrnes, L. J. and H. Sondermann (2011). "Structural basis for the nucleotide-dependent dimerization of the large G protein atlastin-1/SPG3A." Proc Natl Acad Sci U S A **108**(6): 2216-2221.

Cadenas, E., et al. (1977). "Production of superoxide radicals and hydrogen peroxide by NADH-ubiquinone reductase and ubiquinol-cytochrome c reductase from beef-heart mitochondria." Arch Biochem Biophys **180**(2): 248-257.

Cagin, U., et al. (2015). "Mitochondrial retrograde signaling regulates neuronal function." Proceedings of the National Academy of Sciences of the United States of America **112**(44): E6000-E6009.

Calvo, S. E., et al. (2016). "MitoCarta2.0: an updated inventory of mammalian mitochondrial proteins." Nucleic Acids Res **44**(D1): D1251-1257.

Carpenter, F. W. (1905). "The Reactions of the Pomace Fly (Drosophila ampelophila Loew) to Light, Gravity, and Mechanical Stimulation." The American Naturalist **39**(459): 157-171.

Carra, S., et al. (2010). "Identification of the Drosophila Ortholog of HSPB8: IMPLICATION OF HSPB8 LOSS OF FUNCTION IN PROTEIN FOLDING DISEASES." J Biol Chem **285**(48): 37811-37822.

Carreras-Sureda, A., et al. (2018). "Calcium signaling at the endoplasmic reticulum: fine-tuning stress responses." Cell Calcium **70**: 24-31.

Celardo, I., et al. (2017). "DATF4 regulation of mitochondrial folate-mediated one-carbon metabolism is neuroprotective." Cell Death Differ **24**(4): 638-648.

Chakrabarti, R., et al. (2018). "INF2-mediated actin polymerization at the ER stimulates mitochondrial calcium uptake, inner membrane constriction, and division." J Cell Biol **217**(1): 251-268.

Chalmers, S. and D. G. Nicholls (2003). "The relationship between free and total calcium concentrations in the matrix of liver and brain mitochondria." J Biol Chem **278**(21): 19062-19070.

Chandel, N. S., et al. (1998). "Mitochondrial reactive oxygen species trigger hypoxia-induced transcription." Proceedings of the National Academy of Sciences of the United States of America **95**(20): 11715-11720.

Chang, C. L., et al. (2013). "Feedback regulation of receptor-induced Ca2+ signaling mediated by E-Syt1 and Nir2 at endoplasmic reticulum-plasma membrane junctions." Cell Rep **5**(3): 813-825.

Chang, S. C., et al. (1998). "The PEL1 gene (renamed PGS1) encodes the phosphatidylglycero-phosphate synthase of Saccharomyces cerevisiae." J Biol Chem **273**(16): 9829-9836.

Chang, S. C., et al. (1998). "Isolation and characterization of the gene (CLS1) encoding cardiolipin synthase in Saccharomyces cerevisiae." J Biol Chem **273**(24): 14933-14941.

Chawla, S., et al. (1998). "CBP: a signal-regulated transcriptional coactivator controlled by nuclear calcium and CaM kinase IV." Science **281**(5382): 1505-1509.

Chelstowska, A. and R. A. Butow (1995). "RTG genes in yeast that function in communication between mitochondria and the nucleus are also required for expression of genes encoding peroxisomal proteins." J Biol Chem **270**(30): 18141-18146.

Chen, A., et al. (2003). "Inducible enhancement of memory storage and synaptic plasticity in transgenic mice expressing an inhibitor of ATF4 (CREB-2) and C/EBP proteins." Neuron **39**(4): 655-669.

Chen, E. J. and C. A. Kaiser (2003). "LST8 negatively regulates amino acid biosynthesis as a component of the TOR pathway." J Cell Biol **161**(2): 333-347.

Chen, J., et al. (2011). "Arabidopsis RHD3 mediates the generation of the tubular ER network and is required for Golgi distribution and motility in plant cells." J Cell Sci **124**(Pt 13): 2241-2252.

Chen, J. J., et al. (1991). "Cloning of the cDNA of the heme-regulated eukaryotic initiation factor 2 alpha (eIF-2 alpha) kinase of rabbit reticulocytes: homology to yeast GCN2 protein kinase and human double-stranded-RNA-dependent eIF-2 alpha kinase." Proc Natl Acad Sci U S A **88**(17): 7729-7733.

Chen, T.-W., et al. (2013). "Ultra-sensitive fluorescent proteins for imaging neuronal activity." Nature **499**(7458): 295-300.

Chen, X., et al. (2002). "The luminal domain of ATF6 senses endoplasmic reticulum (ER) stress and causes translocation of ATF6 from the ER to the Golgi." J Biol Chem **277**(15): 13045-13052.

Chen, Y. G., et al. (2016). "Identification and characterization of a mitochondrial unfolded protein response transcription factor ATFS-1 in Litopenaeus vannamei." Fish Shellfish Immunol **54**: 144-152.

Chérasse, Y., et al. (2007). "The p300/CBP-associated factor (PCAF) is a cofactor of ATF4 for amino acid-regulated transcription of CHOP." Nucleic Acids Research **35**(17): 5954-5965.

Cho, B., et al. (2017). "Constriction of the mitochondrial inner compartment is a priming event for mitochondrial division." Nat Commun **8**: 15754.

Cho, W. S., et al. (2008). "Visualization of protein-protein interactions between bZIP transcription factors in the unfolded protein response using BiFC analysis." Genes and Genomics **30**(5): 477-485.

Choi, S., et al. (2017). "Mitochondrial calcium uniporter in Drosophila transfers calcium between the endoplasmic reticulum and mitochondria in oxidative stress-induced cell death." Journal of Biological Chemistry **292**(35): 14473-14485.

Chowdhary, S., et al. (2017). "Analysis of mitochondrial organization and function in the Drosophila blastoderm embryo." Scientific Reports **7**(1).

Cipolat, S., et al. (2004). "OPA1 requires mitofusin 1 to promote mitochondrial fusion." Proc Natl Acad Sci U S A **101**(45): 15927-15932.

Clark, I. E., et al. (2006). "Drosophila pink1 is required for mitochondrial function and interacts genetically with parkin." Nature **441**(7097): 1162-1166.

Coelho, D. S., et al. (2013). "Xbp1-Independent Ire1 Signaling Is Required for Photoreceptor Differentiation and Rhabdomere Morphogenesis in Drosophila." Cell Reports **5**(3): 791-801.

Colla, E., et al. (2012). "Endoplasmic reticulum stress is important for the manifestations of α-synucleinopathy in vivo." J Neurosci **32**(10): 3306-3320.

Colombini, M. (1979). "A candidate for the permeability pathway of the outer mitochondrial membrane." Nature **279**(5714): 643-645.

Connerth, M., et al. (2012). "Intramitochondrial transport of phosphatidic acid in yeast by a lipid transfer protein." Science **338**(6108): 815-818.

Cosson, P., et al. (2012). "Mitofusin-2 independent juxtaposition of endoplasmic reticulum and mitochondria: an ultrastructural study." PLoS ONE **7**(9): e46293.

Costa-Mattioli, M., et al. (2007). "eIF2alpha phosphorylation bidirectionally regulates the switch from short- to long-term synaptic plasticity and memory." Cell **129**(1): 195-206.

Cox, J. S. and P. Walter (1996). "A novel mechanism for regulating activity of a transcription factor that controls the unfolded protein response." Cell **87**(3): 391-404.

Crompton, M., et al. (1977). "The calcium-induced and sodium-induced effluxes of calcium from heart mitochondria. Evidence for a sodium-calcium carrier." Eur J Biochem **79**(2): 549-558.

Crompton, M., et al. (1978). "The interrelations between the transport of sodium and calcium in mitochondria of various mammalian tissues." Eur J Biochem **82**(1): 25-31.

Crook, T. H., et al. (1991). "Effects of phosphatidylserine in age-associated memory impairment." Neurology **41**(5): 644-649.

Csordás, G., et al. (2006). "Structural and functional features and significance of the physical linkage between ER and mitochondria." Journal of Cell Biology **174**(7): 915-921.

Csordás, G., et al. (2018). "Endoplasmic Reticulum–Mitochondrial Contactology: Structure and Signaling Functions." Trends in Cell Biology **28**(7): 523-540.

Dagda, R. K., et al. (2009). "Loss of PINK1 Function Promotes Mitophagy through Effects on Oxidative Stress and Mitochondrial Fission." J Biol Chem **284**(20): 13843-13855.

Das, I., et al. (2015). "Preventing proteostasis diseases by selective inhibition of a phosphatase regulatory subunit." Science **348**(6231): 239-242.

Davies, R. E. and A. G. Ogston (1950). "On the mechanism of secretion of ions by gastric mucosa and by other tissues." Biochemical Journal **46**(3): 324.

de Brito, O. M. and L. Scorrano (2009). "Mitofusin-2 regulates mitochondrial and endoplasmic reticulum morphology and tethering: the role of Ras." Mitochondrion **9**(3): 222-226.

de Juan-Sanz, J., et al. (2017). "Axonal endoplasmic reticulum Ca(2+) content controls release probability in CNS nerve terminals." Neuron **93**(4): 867-881.e866.

De Stefani, D., et al. (2012). "VDAC1 selectively transfers apoptotic Ca(2+) signals to mitochondria." Cell Death Differ **19**(2): 267-273.

De Stefani, D., et al. (2011). "A forty-kilodalton protein of the inner membrane is the mitochondrial calcium uniporter." Nature **476**(7360): 336-340.

De Vos, K. J., et al. (2012). "VAPB interacts with the mitochondrial protein PTPIP51 to regulate calcium homeostasis." Human Molecular Genetics **21**(6): 1299-1311.

Dellaire, G., et al. (2009). "High resolution imaging of changes in the structure and spatial organization of chromatin, gamma-H2A.X and the MRN complex within etoposide-induced DNA repair foci." Cell Cycle **8**(22): 3750-3769.

Deluca, H. F. and G. W. Engstrom (1961). "Calcium uptake by rat kidney mitochondria." Proc Natl Acad Sci U S A **47**: 1744-1750.

Dennis, E. A. and E. P. Kennedy (1972). "Intracellular sites of lipid synthesis and the biogenesis of mitochondria." J Lipid Res **13**(2): 263-267.

Denton, R. M. and J. G. McCormack (1980). "On the role of the calcium transport cycle in heart and other mammalian mitochondria." FEBS Lett **119**(1): 1-8.

Devaud, J. M., et al. (2001). "Odor exposure causes central adaptation and morphological changes in selected olfactory glomeruli in Drosophila." J Neurosci **21**(16): 6274-6282.

Dever, T. E., et al. (1992). "Phosphorylation of initiation factor 2 alpha by protein kinase GCN2 mediates gene-specific translational control of GCN4 in yeast." Cell **68**(3): 585-596.

Dey, S., et al. (2010). "Both transcriptional regulation and translational control of ATF4 are central to the integrated stress response." Journal of Biological Chemistry **285**(43): 33165-33174.

Dietzl, G., et al. (2007). "A genome-wide transgenic RNAi library for conditional gene inactivation in Drosophila." Nature **448**(7150): 151-156.

Dougherty, M. K., et al. (2009). "KSR2 is a Calcineurin Substrate that Promotes ERK Cascade Activation in Response to Calcium Signals." Mol Cell **34**(6): 652-662.

Drago, I. and R. L. Davis (2016). "Inhibiting the Mitochondrial Calcium Uniporter during Development Impairs Memory in Adult Drosophila." Cell Reports **16**(10): 2763-2776.

Dudai, Y., et al. (1976). "dunce, a mutant of Drosophila deficient in learning." Proc Natl Acad Sci U S A **73**(5): 1684-1688.

Duncan, O. F., et al. (2018). "Ras-ERK-ETS inhibition alleviates neuronal mitochondrial dysfunction by reprogramming mitochondrial retrograde signaling." PLoS Genet **14**(7): e1007567.

Enslen, H., et al. (1996). "Regulation of mitogen-activated protein kinases by a calcium/calmodulin-dependent protein kinase cascade." Proceedings of the National Academy of Sciences of the United States of America **93**(20): 10803-10808.

Epstein, C. B., et al. (2001). "Genome-wide Responses to Mitochondrial Dysfunction." Molecular Biology of the Cell **12**(2): 297-308.

Erbay, E., et al. (2009). "Reducing endoplasmic reticulum stress through a macrophage lipid chaperone alleviates atherosclerosis." Nat Med **15**(12): 1383-1391.

Ernster, L. and G. Schatz (1981). "Mitochondria: a historical review." J Cell Biol **91**(3 Pt 2): 227s-255s.

Fang, D., et al. (2016). "Development and Dynamic Regulation of Mitochondrial Network in Human Midbrain Dopaminergic Neurons Differentiated from iPSCs." Stem Cell Reports **7**(4): 678-692.

Farrell, P. J., et al. (1977). "Phosphorylation of initiation factor elF-2 and the control of reticulocyte protein synthesis." Cell **11**(1): 187-200.

Fearnley, I. M. and J. E. Walker (1992). "Conservation of sequences of subunits of mitochondrial complex I and their relationships with other proteins." BBA - Bioenergetics **1140**(2): 105-134.

Feng, Y., et al. (2004). "A modified minimal hemolymph-like solution, HL3.1, for physiological recordings at the neuromuscular junctions of normal and mutant Drosophila larvae." Journal of Neurogenetics **18**(2): 377-402.

Feske, S., et al. (2006). "A mutation in Orai1 causes immune deficiency by abrogating CRAC channel function." Nature **441**(7090): 179-185.

Filadi, R., et al. (2015). "Mitofusin 2 ablation increases endoplasmic reticulum-mitochondria coupling." Proc Natl Acad Sci U S A **112**(17): E2174-2181.

Filadi, R., et al. (2017). "On the role of Mitofusin 2 in endoplasmic reticulum-mitochondria tethering." Proc Natl Acad Sci U S A **114**(12): E2266-e2267.

Fiorese, C. J., et al. (2016). "The Transcription Factor ATF5 Mediates a Mammalian Mitochondrial UPR." Curr Biol **26**(15): 2037-2043.

Fire, A., et al. (1998). "Potent and specific genetic interference by double-stranded RNA in Caenorhabditis elegans." Nature **391**: 806.

Fisher, R. P. and D. A. Clayton (1988). "Purification and characterization of human mitochondrial transcription factor 1." Mol Cell Biol **8**(8): 3496-3509.

Fisher, R. P., et al. (1992). "DNA wrapping and bending by a mitochondrial high mobility group-like transcriptional activator protein." J Biol Chem **267**(5): 3358-3367.

Flis, V. V. and G. Daum (2013). "Lipid Transport between the Endoplasmic Reticulum and Mitochondria." Cold Spring Harbor Perspectives in Biology **5**(6): a013235.

Formentini, L., et al. (2012). "The mitochondrial ATPase inhibitory factor 1 triggers a ROS-mediated retrograde prosurvival and proliferative response." Mol Cell **45**(6): 731-742.

Fortini, M. E., et al. (2000). "A Survey of Human Disease Gene Counterparts in the Drosophila Genome." J Cell Biol **150**(2): 23-30.

Fosque, B. F., et al. (2015). "Labeling of active neural circuits in vivo with designed calcium integrators." Science **347**(6223): 755-760.

Frank, S., et al. (2001). "The role of dynamin-related protein 1, a mediator of mitochondrial fission, in apoptosis." Dev Cell **1**(4): 515-525.

Freeman, M. R. (2015). "Drosophila Central Nervous System Glia." Cold Spring Harbor Perspectives in Biology **7**(11): a020552.

Fricker, M., et al. (1997). "Interphase Nuclei of Many Mammalian Cell Types Contain Deep, Dynamic, Tubular Membrane-bound Invaginations of the Nuclear Envelope." J Cell Biol **136**(3): 531-544.

Friedman, J. R., et al. (2011). "ER Tubules Mark Sites of Mitochondrial Division." Science **334**(6054): 358-362.

Galabru, J. and A. G. Hovanessian (1985). "Two interferon-induced proteins are involved in the protein kinase complex dependent on double-stranded RNA." Cell **43**(3 Pt 2): 685-694.

Galehdar, Z., et al. (2010). "Neuronal apoptosis induced by endoplasmic reticulum stress is regulated by ATF4-CHOP-mediated induction of the Bcl-2 homology 3-only member PUMA." J Neurosci **30**(50): 16938-16948.

Galiova, G., et al. (2008). "Chromatin changes induced by lamin A/C deficiency and the histone deacetylase inhibitor trichostatin A." Eur J Cell Biol **87**(5): 291-303.

Galva, C., et al. (2012). "Nuclear Na⁺/K⁺-ATPase plays an active role in nucleoplasmic Ca²⁺ homeostasis." Journal of Cell Science **125**(24): 6137.

Garcia, K. D., et al. (2004). "Immunolocalization of type 2 inositol 1,4,5-trisphosphate receptors in cardiac myocytes from newborn mice." Am J Physiol Cell Physiol **287**(4): C1048-1057.

Garrido, N., et al. (2003). "Composition and dynamics of human mitochondrial nucleoids." Molecular Biology of the Cell **14**(4): 1583-1596.

Gasser, S. M., et al. (1982). "Import of proteins into mitochondria. Energy-dependent uptake of precursors by isolated mitochondria." Journal of Biological Chemistry **257**(21): 13034-13041.

Gauthier, S. A. and R. S. Hewes (2006). "Transcriptional regulation of neuropeptide and peptide hormone expression by the Drosophila dimmed and cryptocephal genes." J Exp Biol **209**(Pt 10): 1803-1815.

Gauthier, S. A., et al. (2012). "Cryptocephal, the Drosophila melanogaster ATF4, is a specific coactivator for ecdysone receptor isoform B2." PLoS Genet **8**(8): e1002883.

Gerencser, A. A., et al. (2012). "Quantitative measurement of mitochondrial membrane potential in cultured cells: calcium-induced de- and hyperpolarization of neuronal mitochondria." J Physiol **590**(12): 2845-2871.

Getz, G. S., et al. (1968). "The phospholipids of various sheep organs, rat liver and of their subcellular fractions." Biochimica et Biophysica Acta (BBA)/Lipids and Lipid Metabolism **152**(2): 325-339.

Ghisla, S. (2004). "Beta-oxidation of fatty acids. A century of discovery." Eur J Biochem **271**(3): 459-461.

Gilham, D., et al. (2005). "Triacylglycerol Hydrolase Is Localized to the Endoplasmic Reticulum by an Unusual Retrieval Sequence where It Participates in VLDL Assembly without Utilizing VLDL Lipids as Substrates." Molecular Biology of the Cell **16**(2): 984-996.

Giordano, F., et al. (2013). "PI(4,5)P(2) DEPENDENT AND Ca(2+)-REGULATED ER-PLASMA MEMBRANE INTERACTIONS MEDIATED BY THE EXTENDED-SYNAPTOTAGMINS." Cell **153**(7): 1494-1509.

Godin, J. D., et al. (2016). "Emerging Roles for the Unfolded Protein Response in the Developing Nervous System." Trends Neurosci **39**(6): 394-404.

Gohil, V. M., et al. (2005). "Synthetic lethal interaction of the mitochondrial phosphatidylethanolamine and cardiolipin biosynthetic pathways in Saccharomyces cerevisiae." J Biol Chem **280**(42): 35410-35416.

Goldstein, L. S. B. and S. Gunawardena (2000). "Flying through the Drosophila Cytoskeletal Genome." J Cell Biol **150**(2): F63.

Gomez-Suaga, P., et al. (2017). "The ER-Mitochondria Tethering Complex VAPB-PTPIP51 Regulates Autophagy." Curr Biol **27**(3): 371-385.

Gong, W. J. and K. G. Golic (2006). "Loss of Hsp70 in Drosophila Is Pleiotropic, With Effects on Thermotolerance, Recovery From Heat Shock and Neurodegeneration." Genetics **172**(1): 275-286.

Gonzalez, T. N., et al. (1999). "Mechanism of non-spliceosomal mRNA splicing in the unfolded protein response pathway." The EMBO Journal **18**(11): 3119-3132.

Gorlich, D. and T. A. Rapoport (1993). "Protein translocation into proteoliposomes reconstituted from purified components of the endoplasmic reticulum membrane." Cell **75**(4): 615-630.

Gorman, G. S., et al. (2015). "Prevalence of nuclear and mitochondrial DNA mutations related to adult mitochondrial disease." Annals of neurology **77**(5): 753-759.

Goulbourne, C. N., et al. (2011). "The induction of a nucleoplasmic reticulum by prelamin A accumulation requires CTP:phosphocholine cytidylyltransferase-α." Journal of Cell Science **124**(24): 4253-4266.

Greene, J. C., et al. (2003). "Mitochondrial pathology and apoptotic muscle degeneration in Drosophila parkin mutants." Proceedings of the National Academy of Sciences of the United States of America **100**(7): 4078-4083.

Greenleaf, A. L., et al. (1986). "Yeast RPO41 gene product is required for transcription and maintenance of the mitochondrial genome." Proc Natl Acad Sci U S A **83**(10): 3391-3394.

Greenspan, R. J. (2008). "The origins of behavioral genetics." Current Biology **18**(5): R192-R198.

Guha, M., et al. (2009). "Heterogeneous Nuclear Ribonucleoprotein A2 Is a Common Transcriptional Coactivator in the Nuclear Transcription Response to Mitochondrial Respiratory Stress." Molecular Biology of the Cell **20**(18): 4107-4119.

Guha, M., et al. (2007). "Activation of a novel calcineurin-mediated insulin-like growth factor-1 receptor pathway, altered metabolism, and tumor cell invasion in cells subjected to mitochondrial respiratory stress." J Biol Chem **282**(19): 14536-14546.

Guha, M., et al. (2010). "Role of calcineurin, hnRNPA2 and Akt in mitochondrial respiratory stress-mediated transcription activation of nuclear gene targets." Biochim Biophys Acta **1797**(6-7): 1055-1065.

Gunter, K. K. and T. E. Gunter (1994). "Transport of calcium by mitochondria." Journal of Bioenergetics and Biomembranes **26**(5): 471-485.

Gunter, T. E. and D. R. Pfeiffer (1990). "Mechanisms by which mitochondria transport calcium." Am J Physiol **258**(5 Pt 1): C755-786.

Guo, J., et al. (2011). "Frequent truncating mutation of TFAM induces mitochondrial DNA depletion and apoptotic resistance in microsatellite-unstable colorectal cancer." Cancer Res **71**(8): 2978-2987.

Hai, T. and M. G. Hartman (2001). "The molecular biology and nomenclature of the activating transcription factor/cAMP responsive element binding family of transcription factors: activating transcription factor proteins and homeostasis." Gene **273**(1): 1-11.

Hai, T. W., et al. (1989). "Transcription factor ATF cDNA clones: an extensive family of leucine zipper proteins able to selectively form DNA-binding heterodimers." Genes Dev **3**(12b): 2083-2090.

Haines, T. H. and N. A. Dencher (2002). "Cardiolipin: a proton trap for oxidative phosphorylation." FEBS Lett **528**(1-3): 35-39.

Hajnóczky, G. and G. Csordás (2010). "Calcium Signalling: Fishing Out Molecules of Mitochondrial Calcium Transport." Curr Biol **20**(20): R888-R891.

Halbleib, K., et al. (2017). "Activation of the Unfolded Protein Response by Lipid Bilayer Stress." Mol Cell **67**(4): 673-684.e678.

Halliday, M., et al. (2015). "Partial restoration of protein synthesis rates by the small molecule ISRIB prevents neurodegeneration without pancreatic toxicity." Cell Death & Disease **6**(3): e1672.

Hamada, F. N., et al. (2008). "An internal thermal sensor controlling temperature preference in Drosophila." Nature **454**(7201): 217-220.

Hampl, V., et al. (2008). "Genetic evidence for a mitochondriate ancestry in the 'amitochondriate' flagellate Trimastix pyriformis." PLoS ONE **3**(1): e1383.

Harding, H. P., et al. (2000). "Perk is essential for translational regulation and cell survival during the unfolded protein response." Mol Cell **5**(5): 897-904.

Harding, H. P., et al. (1999). "Protein translation and folding are coupled by an endoplasmic-reticulum-resident kinase." Nature **397**(6716): 271-274.

Hawkins, B. J., et al. (2010). "S-glutathionylation activates STIM1 and alters mitochondrial homeostasis." J Cell Biol **190**(3): 391-405.

Haworth, R. A. and D. R. Hunter (1979). "The Ca2+-induced membrane transition in mitochondria. II. Nature of the Ca2+ trigger site." Arch Biochem Biophys **195**(2): 460-467.

Haynes, C. M., et al. (2013). "Evaluating and responding to mitochondrial dysfunction: The UPR(mt) and beyond." Trends in Cell Biology **23**(7): 311-318.

Haynes, C. M., et al. (2007). "ClpP mediates activation of a mitochondrial unfolded protein response in C. elegans." Dev Cell **13**(4): 467-480.

Haynes, C. M., et al. (2010). "The matrix peptide exporter HAF-1 signals a mitochondrial UPR by activating the transcription factor ZC376.7 in C. elegans." Mol Cell **37**(4): 529-540.

Haze, K., et al. (1999). "Mammalian transcription factor ATF6 is synthesized as a transmembrane protein and activated by proteolysis in response to endoplasmic reticulum stress." Mol Biol Cell **10**(11): 3787-3799.

He, C. H., et al. (2001). "Identification of activating transcription factor 4 (ATF4) as an Nrf2-interacting protein. Implication for heme oxygenase-1 gene regulation." J Biol Chem **276**(24): 20858-20865.

Hegde, V. R., et al. (2014). "Glia are critical for the neuropathology of complex I deficiency in Drosophila." Human Molecular Genetics **23**(17): 4686-4692.

Heigwer, F., et al. (2018). "RNA Interference (RNAi) Screening in <em>Drosophila</em&gt." Genetics **208**(3): 853.

Hetz, C., et al. (2009). "XBP-1 deficiency in the nervous system protects against amyotrophic lateral sclerosis by increasing autophagy." Genes Dev **23**(19): 2294-2306.

Hewes, R. S., et al. (2000). "The cryptocephal gene (ATF4) encodes multiple basic-leucine zipper proteins controlling molting and metamorphosis in Drosophila." Genetics **155**(4): 1711-1723.

Hinkle, P. C., et al. (1967). "Partial resolution of the enzymes catalyzing oxidative phosphorylation. XV. Reverse electron transfer in the flavin-cytochrome beta region of the respiratory chain of beef heart submitochondrial particles." J Biol Chem **242**(22): 5169-5173.

Hirabayashi, Y., et al. (2017). "ER-mitochondria tethering by PDZD8 regulates Ca(2+) dynamics in mammalian neurons." Science **358**(6363): 623-630.

Hollien, J., et al. (2009). "Regulated Ire1-dependent decay of messenger RNAs in mammalian cells." J Cell Biol **186**(3): 323-331.

Hollien, J. and J. S. Weissman (2006). "Decay of Endoplasmic Reticulum-Localized mRNAs During the Unfolded Protein Response." Science **313**(5783): 104.

Holt, I. J. and A. Reyes (2012). "Human Mitochondrial DNA Replication." Cold Spring Harbor Perspectives in Biology **4**(12): a012971.

Holtz, W. A. and K. L. O'Malley (2003). "Parkinsonian mimetics induce aspects of unfolded protein response in death of dopaminergic neurons." J Biol Chem **278**(21): 19367-19377.

Hom, J. R., et al. (2007). "Thapsigargin induces biphasic fragmentation of mitochondria through calcium-mediated mitochondrial fission and apoptosis." J Cell Physiol **212**(2): 498-508.

Honrath, B., et al. (2017). "Glucose-regulated protein 75 determines ER–mitochondrial coupling and sensitivity to oxidative stress in neuronal cells." Cell Death Discovery **3**: 17076.

Horibe, T. and N. J. Hoogenraad (2007). "The Chop Gene Contains an Element for the Positive Regulation of the Mitochondrial Unfolded Protein Response." PLoS ONE **2**(9): e835.

Hu, J.-Y., et al. (2015). "cJun and CREB2 in the Postsynaptic Neuron Contribute to Persistent Long-Term Facilitation at a Behaviorally Relevant Synapse." The Journal of Neuroscience **35**(1): 386-395.

Hu, J., et al. (2009). "A class of dynamin-like GTPases involved in the generation of the tubular ER network." Cell **138**(3): 549-561.

Huang da, W., et al. (2009). "Systematic and integrative analysis of large gene lists using DAVID bioinformatics resources." Nat Protoc **4**(1): 44-57.

Humphrey, D. M., et al. (2012). "Alternative oxidase rescues mitochondria-mediated dopaminergic cell loss in Drosophila." Hum Mol Genet **21**(12): 2698-2712.

Hunt, R. J. and J. M. Bateman (2018). "Mitochondrial retrograde signaling in the nervous system." FEBS Lett **592**(5): 663-678.

Iborra, F. J., et al. (2004). "The functional organization of mitochondrial genomes in human cells." BMC Biol **2**: 9.

Ishizawa, J., et al. (2016). "ATF4 induction through an atypical integrated stress response to ONC201 triggers p53-independent apoptosis in hematological malignancies." Science Signaling **9**(415).

Islam, R., et al. (2013). "The Role of Drosophila Cytidine Monophosphate-Sialic Acid Synthetase in the Nervous System." The Journal of Neuroscience **33**(30): 12306-12315.

Istiaq Alam, T., et al. (2003). "Human mitochondrial DNA is packaged with TFAM." Nucleic Acids Research **31**(6): 1640-1645.

Iwata, S., et al. (1995). "Structure at 2.8 A resolution of cytochrome c oxidase from Paracoccus denitrificans." Nature **376**(6542): 660-669.

Jakob, R., et al. (2014). "Molecular and functional identification of a mitochondrial ryanodine receptor in neurons." Neuroscience Letters **575**: 7-12.

Janer, A., et al. (2016). "SLC25A46 is required for mitochondrial lipid homeostasis and cristae maintenance and is responsible for Leigh syndrome." EMBO Molecular Medicine **8**(9): 1019-1038.

Javaux, E. J., et al. (2001). "Morphological and ecological complexity in early eukaryotic ecosystems." Nature **412**(6842): 66-69.

Jiang, D., et al. (2009). "Genome-wide RNAi screen identifies Letm1 as a mitochondrial Ca2+/H+ antiporter." Science **326**(5949): 144-147.

Jin, J., et al. (2006). "Proteomic identification of a stress protein, mortalin/mthsp70/GRP75: relevance to Parkinson disease." Mol Cell Proteomics **5**(7): 1193-1204.

Jorissen, B. L., et al. (2001). "The influence of soy-derived phosphatidylserine on cognition in age-associated memory impairment." Nutr Neurosci **4**(2): 121-134.

Kanamori, Y., et al. (2010). "The trehalose transporter 1 gene sequence is conserved in insects and encodes proteins with different kinetic properties involved in trehalose import into peripheral tissues." Insect Biochem Mol Biol **40**(1): 30-37.

Kandel, E. R. (2012). "The molecular biology of memory: cAMP, PKA, CRE, CREB-1, CREB-2, and CPEB." Mol Brain **5**: 14.

Kang, K., et al. (2015). "A Drosophila Reporter for the Translational Activation of ATF4 Marks Stressed Cells during Development." PLoS ONE **10**(5): e0126795.

Karpinski, B. A., et al. (1992). "Molecular cloning of human CREB-2: an ATF/CREB transcription factor that can negatively regulate transcription from the cAMP response element." Proceedings of the National Academy of Sciences of the United States of America **89**(11): 4820-4824.

Karren, M. A., et al. (2005). "The role of Fis1p–Mdv1p interactions in mitochondrial fission complex assembly." J Cell Biol **171**(2): 291-301.

Kato-Kataoka, A., et al. (2010). "Soybean-derived phosphatidylserine improves memory function of the elderly Japanese subjects with memory complaints." J Clin Biochem Nutr **47**(3): 246-255.

Katorcha, E., et al. (2015). "Loss of Cellular Sialidases Does Not Affect the Sialylation Status of the Prion Protein but Increases the Amounts of Its Proteolytic Fragment C1." PLoS ONE **10**(11): e0143218.

Katorcha, E., et al. (2015). "Sialylation of the prion protein glycans controls prion replication rate and glycoform ratio." Scientific Reports **5**: 16912.

Katorcha, E., et al. (2014). "Sialylation of Prion Protein Controls the Rate of Prion Amplification, the Cross-Species Barrier, the Ratio of PrP(Sc) Glycoform and Prion Infectivity." PLoS Pathogens **10**(9): e1004366.

Kaufman, B. A., et al. (2007). "The mitochondrial transcription factor TFAM coordinates the assembly of multiple DNA molecules into nucleoid-like structures." Molecular Biology of the Cell **18**(9): 3225-3236.

Kaufman, T. C. (2017). "A Short History and Description of Drosophila melanogaster Classical Genetics: Chromosome Aberrations, Forward Genetic Screens, and the Nature of Mutations." Genetics **206**(2): 665-689.

Kelly, S., et al. (2011). "Archaeal phylogenomics provides evidence in support of a methanogenic origin of the Archaea and a thaumarchaeal origin for the eukaryotes." Proceedings of the Royal Society B: Biological Sciences **278**(1708): 1009-1018.

Kennedy, E. P. and A. L. Lehninger (1949). "Oxidation of fatty acids and tricarboxylic acid cycle intermediates by isolated rat liver mitochondria." J Biol Chem **179**(2): 957-972.

Kim, H., et al. (2016). "Tumor Necrosis Factor Receptor-associated Protein 1 (TRAP1) Mutation and TRAP1 Inhibitor Gamitrinib-triphenylphosphonium (G-TPP) Induce a Forkhead Box O (FOXO)-dependent Cell Protective Signal from Mitochondria." J Biol Chem **291**(4): 1841-1853.

Kim, Y., et al. (2008). "PINK1 controls mitochondrial localization of Parkin through direct phosphorylation." Biochem Biophys Res Commun **377**(3): 975-980.

Kimata, Y., et al. (2007). "Two regulatory steps of ER-stress sensor Ire1 involving its cluster formation and interaction with unfolded proteins." J Cell Biol **179**(1): 75-86.

Kirichok, Y., et al. (2004). "The mitochondrial calcium uniporter is a highly selective ion channel." Nature **427**(6972): 360-364.

Kitada, T., et al. (1998). "Mutations in the parkin gene cause autosomal recessive juvenile parkinsonism." Nature **392**(6676): 605-608.

Klingenberg, M. and E. Pfaff (1966). "Structural and functional compartmentation in mitochondria." Regulation of Metabolic Processes in Mitochondria **7**: 180-201.

Konopka, R. J. and S. Benzer (1971). "Clock mutants of Drosophila melanogaster." Proc Natl Acad Sci U S A **68**(9): 2112-2116.

Korennykh, A. V., et al. (2009). "The unfolded protein response signals through high-order assembly of Ire1." Nature **457**(7230): 687-693.

Kornmann, B., et al. (2009). "An ER-Mitochondria Tethering Complex Revealed by a Synthetic Biology Screen." Science **325**(5939): 477-481.

Koshiba, T., et al. (2004). "Structural basis of mitochondrial tethering by mitofusin complexes." Science **305**(5685): 858-862.

Kozutsumi, Y., et al. (1988). "The presence of malfolded proteins in the endoplasmic reticulum signals the induction of glucose-regulated proteins." Nature **332**(6163): 462-464.

Krebs, H. A. (1937). "THE INTERMEDIATE METABOLISM OF CARBOHYDRATES." The Lancet **230**(5952): 736-738.

Krebs, H. A. and W. A. Johnson (1937). "The role of citric acid in intermediate metabolism in animal tissues." Enzymologia **4**: 148-156.

Krebs, H. A., et al. (1938). "The formation of citric and α-ketoglutaric acids in the mammalian body." Biochemical Journal **32**(1): 113-117.

Krug, A. K., et al. (2014). "Transcriptional and metabolic adaptation of human neurons to the mitochondrial toxicant MPP +." Cell Death and Disease **5**(5).

Kukat, C., et al. (2015). "Cross-strand binding of TFAM to a single mtDNA molecule forms the mitochondrial nucleoid." Proceedings of the National Academy of Sciences of the United States of America **112**(36): 11288-11293.

Kumar, R., et al. (2003). "Dysfunction of the unfolded protein response during global brain ischemia and reperfusion." Journal of Cerebral Blood Flow and Metabolism **23**(4): 462-471.

Lagace, T. A. and N. D. Ridgway (2005). "The Rate-limiting Enzyme in Phosphatidylcholine Synthesis Regulates Proliferation of the Nucleoplasmic Reticulum." Molecular Biology of the Cell **16**(3): 1120-1130.

Lahiri, S., et al. (2014). "A Conserved Endoplasmic Reticulum Membrane Protein Complex (EMC) Facilitates Phospholipid Transfer from the ER to Mitochondria." PLoS Biology **12**(10): e1001969.

Lake, N. J., et al. (2015). "Leigh syndrome: neuropathology and pathogenesis." J Neuropathol Exp Neurol **74**(6): 482-492.

Lakhotia, S. C. and K. V. Prasanth (2002). "Tissue- and development-specific induction and turnover of hsp70 transcripts from loci 87A and 87C after heat shock and during recovery in Drosophila melanogaster." J Exp Biol **205**(Pt 3): 345-358.

Lange, P. S., et al. (2008). "ATF4 is an oxidative stress–inducible, prodeath transcription factor in neurons in vitro and in vivo." The Journal of Experimental Medicine **205**(5): 1227-1242.

Langston, J. W., et al. (1983). "Chronic Parkinsonism in humans due to a product of meperidine-analog synthesis." Science **219**(4587): 979-980.

Lassot, I., et al. (2001). "ATF4 Degradation Relies on a Phosphorylation-Dependent Interaction with the SCF(βTrCP) Ubiquitin Ligase." Mol Cell Biol **21**(6): 2192-2202.

Leal, N. S., et al. (2016). "Mitofusin-2 knockdown increases ER-mitochondria contact and decreases amyloid beta-peptide production." J Cell Mol Med **20**(9): 1686-1695.

Lebeau, J., et al. (2018). "The PERK Arm of the Unfolded Protein Response Regulates Mitochondrial Morphology during Acute Endoplasmic Reticulum Stress." Cell Reports **22**(11): 2827-2836.

Lee, A. S. (1987). "Coordinated regulation of a set of genes by glucose and calcium ionophores in mammalian cells." Trends in Biochemical Sciences **12**(C): 20-23.

Lee, C. and L. B. Chen (1988). "Dynamic behavior of endoplasmic reticulum in living cells." Cell **54**(1): 37-46.

Lee, J. E., et al. (2015). "Drosophila melanogaster activating transcription factor 4 regulates glycolysis during endoplasmic reticulum stress." G3: Genes, Genomes, Genetics **5**(4): 667-675.

Lee, K. S., et al. (2018). "Altered ER-mitochondria contact impacts mitochondria calcium homeostasis and contributes to neurodegeneration in vivo in disease models." Proc Natl Acad Sci U S A **115**(38): E8844-e8853.

Lee, Y.-Y., et al. (2009). "An Upstream Open Reading Frame Regulates Translation of GADD34 during Cellular Stresses That Induce eIF2α Phosphorylation." J Biol Chem **284**(11): 6661-6673.

Legros, F., et al. (2004). "Organization and dynamics of human mitochondrial DNA." J Cell Sci **117**(Pt 13): 2653-2662.

Lehman, S. L., et al. (2015). "Signaling through alternative Integrated Stress Response pathways compensates for GCN2 loss in a mouse model of soft tissue sarcoma." Scientific Reports **5**.

Lemrow, S. M., et al. (2004). "Catalytic activity is required for calcium/calmodulin-dependent protein kinase IV to enter the nucleus." J Biol Chem **279**(12): 11664-11671.

Lence, T., et al. (2017). "A fly view on the roles and mechanisms of the m(6)A mRNA modification and its players." RNA Biology **14**(9): 1232-1240.

Levin, D., et al. (1976). "Regulation of protein synthesis in reticulocyte lysates: phosphorylation of methionyl-tRNAf binding factor by protein kinase activity of translational inhibitor isolated from hemedeficient lysates." Proceedings of the National Academy of Sciences of the United States of America **73**(9): 3112-3116.

Lewerenz, J., et al. (2012). "Mutation of ATF4 mediates resistance of neuronal cell lines against oxidative stress by inducing xCT expression." Cell Death Differ **19**(5): 847-858.

Lewis, D. L., et al. (1995). "Drosophila melanogaster mitochondrial DNA: completion of the nucleotide sequence and evolutionary comparisons." Insect Mol Biol **4**(4): 263-278.

Li, S., et al. (2017). "Oxidative stress drives CD8(+) T-cell skin trafficking in patients with vitiligo through CXCL16 upregulation by activating the unfolded protein response in keratinocytes." J Allergy Clin Immunol **140**(1): 177-189.e179.

Liao, X. and R. A. Butow (1993). "RTG1 and RTG2: two yeast genes required for a novel path of communication from mitochondria to the nucleus." Cell **72**(1): 61-71.

Liao, X. S., et al. (1991). "Intramitochondrial functions regulate nonmitochondrial citrate synthase (CIT2) expression in Saccharomyces cerevisiae." Mol Cell Biol **11**(1): 38-46.

Lightowlers, R. N., et al. (2015). "Mutations causing mitochondrial disease: What is new and what challenges remain?" Science **349**(6255): 1494-1499.

Lim, J. H., et al. (2009). "Coupling mitochondrial dysfunction to endoplasmic reticulum stress response: A molecular mechanism leading to hepatic insulin resistance." Cellular Signalling **21**(1): 169-177.

Lin, Y. J., et al. (1998). "Extended life-span and stress resistance in the Drosophila mutant methuselah." Science **282**(5390): 943-946.

Linnartz-Gerlach, B., et al. (2016). "Sialylation of neurites inhibits complement-mediated macrophage removal in a human macrophage-neuron Co-Culture System." Glia **64**(1): 35-47.

Linnartz, B., et al. (2012). "Sialic acid on the neuronal glycocalyx prevents complement C1 binding and complement receptor-3-mediated removal by microglia." J Neurosci **32**(3): 946-952.

Liou, J., et al. (2005). "STIM is a Ca2+sensor essential for Ca2+-store- depletion-triggered Ca2+influx." Current Biology **15**(13): 1235-1241.

Litonin, D., et al. (2010). "Human mitochondrial transcription revisited: Only TFAM and TFB2M are required for transcription of the mitochondrial genes in vitro." Journal of Biological Chemistry **285**(24): 18129-18133.

Liu, J., et al. (2018). "Brain-Derived Neurotrophic Factor Elevates Activating Transcription Factor 4 (ATF4) in Neurons and Promotes ATF4-Dependent Induction of Sesn2." Front Mol Neurosci **11**(62).

Liu, J., et al. (2014). "Activating transcription factor 4 (ATF4) modulates post-synaptic development and dendritic spine morphology." Front Cell Neurosci **8**: 177.

Liu, Z.-W., et al. (2013). "Protein kinase RNA- like endoplasmic reticulum kinase (PERK) signaling pathway plays a major role in reactive oxygen species (ROS)-mediated endoplasmic reticulum stress- induced apoptosis in diabetic cardiomyopathy." Cardiovascular Diabetology **12**(1): 158.

Liu, Z., et al. (2003). "Retrograde signaling is regulated by the dynamic interaction between Rtg2p and Mks1p." Mol Cell **12**(2): 401-411.

López-Crisosto, C., et al. (2015). "ER-to-mitochondria miscommunication and metabolic diseases." Biochimica et Biophysica Acta (BBA) - Molecular Basis of Disease **1852**(10, Part A): 2096-2105.

Loschen, G., et al. (1974). "Superoxide radicals as precursors of mitochondrial hydrogen peroxide." FEBS Lett **42**(1): 68-72.

Lowe, N., et al. (2014). "Analysis of the expression patterns, Subcellular localisations and interaction partners of drosophila proteins using a pigp protein trap library." Development (Cambridge) **141**(20): 3994-4005.

Luan, H., et al. (2006). "Functional dissection of a neuronal network required for cuticle tanning and wing expansion in Drosophila." Journal of Neuroscience **26**(2): 573-584.

Lui, P. P. Y., et al. (2003). "The nucleus of HeLa cells contains tubular structures for Ca2+ signaling with the involvement of mitochondria." Biochem Biophys Res Commun **308**(4): 826-833.

Lutz, A. K., et al. (2009). "Loss of Parkin or PINK1 Function Increases Drp1-dependent Mitochondrial Fragmentation." J Biol Chem **284**(34): 22938-22951.

Lynes, E. M. and T. Simmen (2011). "Urban planning of the endoplasmic reticulum (ER): How diverse mechanisms segregate the many functions of the ER." Biochimica et Biophysica Acta (BBA) - Molecular Cell Research **1813**(10): 1893-1905.

Ma, K., et al. (2002). "Dimerization and release of molecular chaperone inhibition facilitate activation of eukaryotic initiation factor-2 kinase in response to endoplasmic reticulum stress." J Biol Chem **277**(21): 18728-18735.

Macchi, M., et al. (2013). "The Drosophila inner-membrane protein PMI controls crista biogenesis and mitochondrial diameter." J Cell Sci **126**(Pt 3): 814-824.

Mahr, A. and H. Aberle (2006). "The expression pattern of the Drosophila vesicular glutamate transporter: A marker protein for motoneurons and glutamatergic centers in the brain." Gene Expression Patterns **6**(3): 299-309.

Mailloux, R. J. (2015). "Teaching the fundamentals of electron transfer reactions in mitochondria and the production and detection of reactive oxygen species." Redox Biol **4**: 381-398.

Maiuolo, J., et al. (2011). "Selective activation of the transcription factor ATF6 mediates endoplasmic reticulum proliferation triggered by a membrane protein." Proc Natl Acad Sci U S A **108**(19): 7832-7837.

Malhas, A., et al. (2011). "The nucleoplasmic reticulum: form and function." Trends Cell Biol **21**(6): 362-373.

Malzer, E., et al. (2010). "Impaired tissue growth is mediated by checkpoint kinase 1 (CHK1) in the integrated stress response." Journal of Cell Science **123**(17): 2892-2900.

Malzer, E., et al. (2013). "Coordinate regulation of eIF2α phosphorylation by PPP1R15 and GCN2 is required during Drosophila development." Journal of Cell Science **126**(6): 1406-1415.

Mancuso, R., et al. (2012). "Sigma-1R Agonist Improves Motor Function and Motoneuron Survival in ALS Mice." Neurotherapeutics **9**(4): 814-826.

Manczak, M., et al. (2004). "Differential expression of oxidative phosphorylation genes in patients with Alzheimer's disease: implications for early mitochondrial dysfunction and oxidative damage." Neuromolecular Med **5**(2): 147-162.

Manoharan, S., et al. (2016). "The Role of Reactive Oxygen Species in the Pathogenesis of Alzheimer's Disease, Parkinson's Disease, and Huntington's Disease: A Mini Review." Oxidative Medicine and Cellular Longevity **2016**: 8590578.

Marciniak, S. J., et al. (2004). "CHOP induces death by promoting protein synthesis and oxidation in the stressed endoplasmic reticulum." Genes Dev **18**(24): 3066-3077.

Marinetti, G. V., et al. (1958). "Phosphatides of pig heart cell fractions." J Biol Chem **233**(3): 562-565.

Marius, P., et al. (2006). "Calcium release from ryanodine receptors in the nucleoplasmic reticulum." Cell Calcium **39**(1): 65-73.

Martin, C. A. and D. E. Krantz (2014). "Drosophila melanogaster as a genetic model system to study neurotransmitter transporters." Neurochemistry International **73**: 71-88.

Martínez-Reyes, I., et al. (2012). "AMPK and GCN2-ATF4 signal the repression of mitochondria in colon cancer cells." Biochemical Journal **444**(2): 249-259.

Martinus, R. D., et al. (1996). "Selective induction of mitochondrial chaperones in response to loss of the mitochondrial genome." Eur J Biochem **240**(1): 98-103.

Martoglio, B. and B. Dobberstein (1998). "Signal sequences: more than just greasy peptides." Trends Cell Biol **8**(10): 410-415.

Mattiazzi Ušaj, M., et al. (2015). "Genome-Wide Localization Study of Yeast Pex11 Identifies Peroxisome–Mitochondria Interactions through the ERMES Complex." Journal of Molecular Biology **427**(11): 2072-2087.

Maurer, I., et al. (2000). "A selective defect of cytochrome c oxidase is present in brain of Alzheimer disease patients." Neurobiol Aging **21**(3): 455-462.

Mavlyutov, T. A., et al. (2013). "Lack of sigma-1 receptor exacerbates ALS progression in mice." Neuroscience **240**: 129-134.

Mavlyutov, T. A., et al. (2017). "APEX2-enhanced electron microscopy distinguishes sigma-1 receptor localization in the nucleoplasmic reticulum." Oncotarget **8**(31): 51317-51330.

Mazzio, E. and K. F. A. Soliman (2012). "Whole genome expression profile in neuroblastoma cells exposed to 1-methyl-4-phenylpyridine." Neurotoxicology **33**(5): 1156-1169.

Mbaya, E., et al. (2010). "Calcium signalling-dependent mitochondrial dysfunction and bioenergetics regulation in respiratory chain Complex II deficiency." Cell Death Differ **17**: 1855.

McLelland, G. L., et al. (2014). "Parkin and PINK1 function in a vesicular trafficking pathway regulating mitochondrial quality control." Embo j **33**(4): 282-295.

Meeusen, S., et al. (2004). "Mitochondrial fusion intermediates revealed in vitro." Science **305**(5691): 1747-1752.

Mendes, C. S., et al. (2006). "Cytochrome c-d regulates developmental apoptosis in the Drosophila retina." EMBO Rep **7**(9): 933-939.

Meurers, B. H., et al. (2009). "Low dose rotenone treatment causes selective transcriptional activation of cell death related pathways in dopaminergic neurons in vivo." Neurobiology of disease **33**(2): 182-192.

Meusser, B., et al. (2005). "ERAD: the long road to destruction." Nature Cell Biology **7**: 766.

Miceli, M. V., et al. (2011). "Loss of Mitochondrial Membrane Potential Triggers the Retrograde Response Extending Yeast Replicative Lifespan." Frontiers in Genetics **2**: 102.

Miller, R. M., et al. (2004). "Dysregulation of gene expression in the 1-methyl-4-phenyl-1,2,3,6-tetrahydropyridine-lesioned mouse substantia nigra." J Neurosci **24**(34): 7445-7454.

Mitchell, P. (1961). "Coupling of phosphorylation to electron and hydrogen transfer by a chemi-osmotic type of mechanism." Nature **191**: 144-148.

Mitchell, P. (1976). "Possible molecular mechanisms of the protonmotive function of cytochrome systems." J Theor Biol **62**(2): 327-367.

Miyata, N., et al. (2016). "Phosphatidylserine transport by Ups2–Mdm35 in respiration-active mitochondria." J Cell Biol **214**(1): 77.

Moisoi, N., et al. (2008). "Mitochondrial dysfunction triggered by loss of HtrA2 results in the activation of a brain-specific transcriptional stress response." Cell Death Differ **16**: 449.

Monaghan, R. M., et al. (2015). "A nuclear role for the respiratory enzyme CLK-1/COQ7 in regulating mitochondrial stress responses and longevity." Nature Cell Biology **17**(6): 782-792.

Montoya, J., et al. (1982). "Identification of initiation sites for heavy-strand and light-strand transcription in human mitochondrial DNA." Proc Natl Acad Sci U S A **79**(23): 7195-7199.

Moore, K. and J. Hollien (2015). "Ire1-mediated decay in mammalian cells relies on mRNA sequence, structure, and translational status." Molecular Biology of the Cell **26**(16): 2873-2884.

Moré, M. I., et al. (2014). "Positive Effects of Soy Lecithin-Derived Phosphatidylserine plus Phosphatidic Acid on Memory, Cognition, Daily Functioning, and Mood in Elderly Patients with Alzheimer's Disease and Dementia." Advances in Therapy **31**: 1247-1262.

Moreno, J. A., et al. (2013). "Oral treatment targeting the unfolded protein response prevents neurodegeneration and clinical disease in prion-infected mice." Sci Transl Med **5**(206): 206ra138.

Moreno, J. A., et al. (2012). "Sustained translational repression by eIF2alpha-P mediates prion neurodegeneration." Nature **485**(7399): 507-511.

Morgan, T. H., et al. (1915). The Mechanism of Mendelian Heredity. New York, Henry Holt & Co.

Mori, K. (2009). "Signalling pathways in the unfolded protein response: development from yeast to mammals." J Biochem **146**(6): 743-750.

Moro, L., et al. (2009). "Mitochondrial DNA depletion in prostate epithelial cells promotes anoikis resistance and invasion through activation of PI3K/Akt2." Cell Death Differ **16**(4): 571-583.

Morrow, G., et al. (2000). "The small heat shock protein Hsp22 of Drosophila melanogaster is a mitochondrial protein displaying oligomeric organization." J Biol Chem **275**(40): 31204-31210.

Mortiboys, H., et al. (2008). "Mitochondrial function and morphology are impaired in parkin mutant fibroblasts." Annals of neurology **64**(5): 555-565.

Muller, H. J. (1918). "Genetic Variability, Twin Hybrids and Constant Hybrids, in a Case of Balanced Lethal Factors." Genetics **3**(5): 422-499.

Mummery-Widmer, J. L., et al. (2009). "Genome-wide analysis of Notch signalling in Drosophila by transgenic RNAi." Nature **458**(7241): 987-992.

Munch, C. and J. W. Harper (2016). "Mitochondrial unfolded protein response controls matrix pre-RNA processing and translation." Nature **534**(7609): 710-713.

Munro, S. and H. R. Pelham (1986). "An Hsp70-like protein in the ER: identity with the 78 kd glucose-regulated protein and immunoglobulin heavy chain binding protein." Cell **46**(2): 291-300.

Murphy, Michael P. (2009). "How mitochondria produce reactive oxygen species." Biochemical Journal **417**(Pt 1): 1-13.

Nakagawa, K., et al. (2006). "Sialylation enhances the secretion of neurotoxic amyloid-beta peptides." J Neurochem **96**(4): 924-933.

Nakai, J., et al. (2001). "A high signal-to-noise Ca(2+) probe composed of a single green fluorescent protein." Nat Biotechnol **19**(2): 137-141.

Naon, D., et al. (2016). "Critical reappraisal confirms that Mitofusin 2 is an endoplasmic reticulum-mitochondria tether." Proc Natl Acad Sci U S A **113**(40): 11249-11254.

Naon, D., et al. (2017). "Reply to Filadi et al.: Does Mitofusin 2 tether or separate endoplasmic reticulum and mitochondria?" Proc Natl Acad Sci U S A **114**(12): E2268-e2269.

Napier, R. M., et al. (1992). "Immunological evidence that plants use both HDEL and KDEL for targeting proteins to the endoplasmic reticulum." J Cell Sci **102 (Pt 2)**: 261-271.

Narendra, D., et al. (2008). "Parkin is recruited selectively to impaired mitochondria and promotes their autophagy." J Cell Biol **183**(5): 795-803.

Nargund, A. M., et al. (2012). "Mitochondrial import efficiency of ATFS-1 regulates mitochondrial UPR activation." Science **337**(6094): 587-590.

Nasr, P., et al. (2003). "Influence of cytosolic and mitochondrial Ca2+, ATP, mitochondrial membrane potential, and calpain activity on the mechanism of neuron death induced by 3-nitropropionic acid." Neurochem Int **43**(2): 89-99.

Nass, M. M. (1966). "The circularity of mitochondrial DNA." Proceedings of the National Academy of Sciences of the United States of America **56**(4): 1215-1222.

Nass, M. M. (1969). "Mitochondrial DNA. I. Intramitochondrial distribution and structural relations of single- and double-length circular DNA." J Mol Biol **42**(3): 521-528.

Nass, S. and M. M. K. Nass (1963). "INTRAMITOCHONDRIAL FIBERS WITH DNA CHARACTERISTICS : II. Enzymatic and Other Hydrolytic Treatments." J Cell Biol **19**(3): 613-629.

Nathans, D. (1964). "PUROMYCIN INHIBITION OF PROTEIN SYNTHESIS: INCORPORATION OF PUROMYCIN INTO PEPTIDE CHAINS." Proceedings of the National Academy of Sciences of the United States of America **51**(4): 585-592.

Neuspiel, M., et al. (2008). "Cargo-selected transport from the mitochondria to peroxisomes is mediated by vesicular carriers." Curr Biol **18**(2): 102-108.

Ngo, H. B., et al. (2011). "The mitochondrial transcription and packaging factor Tfam imposes a U-turn on mitochondrial DNA." Nature Structural &Amp; Molecular Biology **18**: 1290.

Nicklas, W. J., et al. (1985). "Inhibition of NADH-linked oxidation in brain mitochondria by 1-methyl-4-phenyl-pyridine, a metabolite of the neurotoxin, 1-methyl-4-phenyl-1,2,5,6-tetrahydropyridine." Life Sci **36**(26): 2503-2508.

Nixon-Abell, J., et al. (2016). "Increased spatiotemporal resolution reveals highly dynamic dense tubular matrices in the peripheral ER." Science **354**(6311).

Nolan, W., et al. (2017). "Sialylated glycosylphosphatidylinositols suppress the production of toxic amyloid-beta oligomers." Biochem J **474**(17): 3045-3058.

Novoa, I., et al. (2001). "Feedback Inhibition of the Unfolded Protein Response by GADD34-Mediated Dephosphorylation of eIF2α." J Cell Biol **153**(5): 1011-1022.

Nüsslein-Volhard, C. and E. Wieschaus (1980). "Mutations affecting segment number and polarity in Drosophila." Nature **287**: 795.

Nüsslein-Volhard, C., et al. (1984). "Mutations affecting the pattern of the larval cuticle inDrosophila melanogaster." Wilhelm Roux's archives of developmental biology **193**(5): 267-282.

Nyathi, Y., et al. (2013). "Co-translational targeting and translocation of proteins to the endoplasmic reticulum." Biochim Biophys Acta **1833**(11): 2392-2402.

O'Brien, T. W. (1971). "The general occurrence of 55 S ribosomes in mammalian liver mitochondria." J Biol Chem **246**(10): 3409-3417.

O'Sullivan, N. C., et al. (2012). "Reticulon-like-1, the drosophila orthologue of the hereditary spastic paraplegia gene reticulon 2, is required for organization of endoplasmic reticulum and of distal motor axons." Human Molecular Genetics **21**(15): 3356-3365.

Ojala, D., et al. (1981). "tRNA punctuation model of RNA processing in human mitochondria." Nature **290**(5806): 470-474.

Ono, Y., et al. (2014). "SA4503, a sigma-1 receptor agonist, suppresses motor neuron damage in in vitro and in vivo amyotrophic lateral sclerosis models." Neurosci Lett **559**: 174-178.

Orso, G., et al. (2009). "Homotypic fusion of ER membranes requires the dynamin-like GTPase atlastin." Nature **460**(7258): 978-983.

Osman, C., et al. (2010). "A mitochondrial phosphatase required for cardiolipin biosynthesis: the PGP phosphatase Gep4." Embo j **29**(12): 1976-1987.

Owusu-Ansah, E., et al. (2013). "Muscle mitohormesis promotes longevity via systemic repression of insulin signaling." Cell **155**(3): 699-712.

Paillusson, S., et al. (2016). "There's Something Wrong with my MAM; the ER-Mitochondria Axis and Neurodegenerative Diseases." Trends Neurosci **39**(3): 146-157.

Palade, G. E. (1953). "An electron microscope study of the mitochondrial structure." J Histochem Cytochem **1**(4): 188-211.

Palade, G. E. (1955). "STUDIES ON THE ENDOPLASMIC RETICULUM : II. SIMPLE DISPOSITIONS IN CELLS IN SITU." The Journal of Biophysical and Biochemical Cytology **1**(6): 567-582.

Palty, R., et al. (2010). "NCLX is an essential component of mitochondrial Na+/Ca2+ exchange." Proc Natl Acad Sci U S A **107**(1): 436-441.

Papa, L. and D. Germain (2011). "Estrogen receptor mediates a distinct mitochondrial unfolded protein response." Journal of Cell Science **124**(9): 1396-1402.

Parikh, V. S., et al. (1987). "The mitochondrial genotype can influence nuclear gene expression in yeast." Science **235**(4788): 576-580.

Parisi, M. A., et al. (1993). "A human mitochondrial transcriptional activator can functionally replace a yeast mitochondrial HMG-box protein both in vivo and in vitro." Mol Cell Biol **13**(3): 1951-1961.

Park, J., et al. (2006). "Mitochondrial dysfunction in Drosophila PINK1 mutants is complemented by parkin." Nature **441**(7097): 1157-1161.

Park, Y., et al. (2017). "mTORC1 Balances Cellular Amino Acid Supply with Demand for Protein Synthesis through Post-transcriptional Control of ATF4." Cell Rep **19**(6): 1083-1090.

Parsons, D. F., et al. (1966). "Characteristics of isolated and purified preparations of the outer and inner membranes of mitochondria." Ann N Y Acad Sci **137**(2): 643-666.

Pasini, S., et al. (2015). "Specific downregulation of hippocampal ATF4 reveals a necessary role in synaptic plasticity and memory." Cell Rep **11**(2): 183-191.

Patel, D. A., et al. (2007). "Attenuation of β-amyloid induced toxicity by sialic acid-conjugated dendrimers: role of sialic acid attachment." Brain Research **1161**: 95-105.

Pebay-Peyroula, E., et al. (2003). "Structure of mitochondrial ADP/ATP carrier in complex with carboxyatractyloside." Nature **426**: 39.

Pelham, H. R. (1989). "Control of protein exit from the endoplasmic reticulum." Annu Rev Cell Biol **5**: 1-23.

Percy, A. K., et al. (1983). "Characterization of brain phosphatidylserine decarboxylase: Localization in the mitochondrial inner membrane." Archives of Biochemistry and Biophysics **223**(2): 484-494.

Pesah, Y., et al. (2004). "Drosophila parkin mutants have decreased mass and cell size and increased sensitivity to oxygen radical stress." Development **131**(9): 2183-2194.

Pfeiffer, K., et al. (2003). "Cardiolipin stabilizes respiratory chain supercomplexes." J Biol Chem **278**(52): 52873-52880.

Pichler, H., et al. (2001). "A subfraction of the yeast endoplasmic reticulum associates with the plasma membrane and has a high capacity to synthesize lipids." Eur J Biochem **268**(8): 2351-2361.

Pickersgill, H., et al. (2006). "Characterization of the Drosophila melanogaster genome at the nuclear lamina." Nat Genet **38**(9): 1005-1014.

Pilling, A. D., et al. (2006). "Kinesin-1 and dynein are the primary motors for fast transport of mitochondria in Drosophila motor axons." Molecular Biology of the Cell **17**(4): 2057-2068.

Pimenta de Castro, I., et al. (2012). "Genetic analysis of mitochondrial protein misfolding in Drosophila melanogaster." Cell Death Differ **19**(8): 1308-1316.

Pincus, D., et al. (2010). "BiP Binding to the ER-Stress Sensor Ire1 Tunes the Homeostatic Behavior of the Unfolded Protein Response." PLoS Biology **8**(7): e1000415.

Poole, A. C., et al. (2008). "The PINK1/Parkin pathway regulates mitochondrial morphology." Proceedings of the National Academy of Sciences **105**(5): 1638.

Porter, K. R., et al. (1945). "A STUDY OF TISSUE CULTURE CELLS BY ELECTRON MICROSCOPY : METHODS AND PRELIMINARY OBSERVATIONS." The Journal of Experimental Medicine **81**(3): 233-246.

Porter, K. R. and F. L. Kallman (1952). "SIGNIFICANCE OF CELL PARTICULATES AS SEEN BY ELECTRON MICROSCOPY." Annals of the New York Academy of Sciences **54**(6): 882-891.

Power, M. E. (1943). "The brain of Drosophila melanogaster." Journal of Morphology **72**(3): 517-559.

Pray-Grant, M. G., et al. (2002). "The novel SLIK histone acetyltransferase complex functions in the yeast retrograde response pathway." Mol Cell Biol **22**(24): 8774-8786.

Puhka, M., et al. (2007). "Endoplasmic reticulum remains continuous and undergoes sheet-to-tubule transformation during cell division in mammalian cells." J Cell Biol **179**(5): 895-909.

Puigserver, P., et al. (1998). "A cold-inducible coactivator of nuclear receptors linked to adaptive thermogenesis." Cell **92**(6): 829-839.

Puri, P., et al. (2008). "Activation and Dysregulation of the Unfolded Protein Response in Nonalcoholic Fatty Liver Disease." Gastroenterology **134**(2): 568-576.

Pusl, T., et al. (2002). "Epidermal growth factor-mediated activation of the ETS domain transcription factor Elk-1 requires nuclear calcium." J Biol Chem **277**(30): 27517-27527.

Putney, J. W. and T. Tomita (2012). "Phospholipase C Signaling and Calcium Influx." Advances in biological regulation **52**(1): 152-164.

Qiu, Q., et al. (2013). "Toll-like receptor-mediated IRE1α activation as a therapeutic target for inflammatory arthritis." The EMBO Journal **32**(18): 2477-2490.

Quinlan, C. L., et al. (2012). "Mitochondrial complex II can generate reactive oxygen species at high rates in both the forward and reverse reactions." J Biol Chem **287**(32): 27255-27264.

Quiros, P. M., et al. (2017). "Multi-omics analysis identifies ATF4 as a key regulator of the mitochondrial stress response in mammals." J Cell Biol **216**(7): 2027-2045.

Quirós, P. M., et al. (2017). "Multi-omics analysis identifies ATF4 as a key regulator of the mitochondrial stress response in mammals." Journal of Cell Biology **216**(7): 2027-2045.

Raimundo, N., et al. (2011). "Revisiting the TCA cycle: signaling to tumor formation." Trends in molecular medicine **17**(11): 641-649.

Raimundo, N., et al. (2012). "Mitochondrial stress engages E2F1 apoptotic signaling to cause deafness." Cell **148**(4): 716-726.

Rainbolt, T. K., et al. (2013). "Stress-Regulated Translational Attenuation Adapts Mitochondrial Protein Import Through Tim17A Degradation." Cell metabolism **18**(6): 908-919.

Ramachandran, A., et al. (2017). "Human mitochondrial transcription factors TFAM and TFB2M work synergistically in promoter melting during transcription initiation." Nucleic Acids Research **45**(2): 861-874.

Rampelt, H., et al. (2017). "Role of the mitochondrial contact site and cristae organizing system in membrane architecture and dynamics." Biochimica et Biophysica Acta (BBA) - Molecular Cell Research **1864**(4): 737-746.

Ranu, R. S. and I. M. London (1976). "Regulation of protein synthesis in rabbit reticulocyte lysates: purification and initial characterization of the cyclic 3':5'-AMP independent protein kinase of the heme-regulated translational inhibitor." Proceedings of the National Academy of Sciences of the United States of America **73**(12): 4349-4353.

Rath, E., et al. (2012). "Induction of dsRNA-activated protein kinase links mitochondrial unfolded protein response to the pathogenesis of intestinal inflammation." Gut **61**(9): 1269-1278.

Reddan, J. M., et al. (2018). "Glycerophospholipid Supplementation as a Potential Intervention for Supporting Cerebral Structure in Older Adults." Frontiers in Aging Neuroscience **10**(49).

Redman, C. M. (1969). "Biosynthesis of serum proteins and ferritin by free and attached ribosomes of rat liver." J Biol Chem **244**(16): 4308-4315.

Ribeiro, C. M. P., et al. (2000). "Effects of elevated cytoplasmic calcium and protein kinase C on endoplasmic reticulum structure and function in HEK293 cells." Cell Calcium **27**(3): 175-185.

Richter, Y., et al. (2010). "The effect of phosphatidylserine-containing omega-3 fatty acids on memory abilities in subjects with subjective memory complaints: a pilot study." Clin Interv Aging **5**: 313-316.

Richter, Y., et al. (2013). "The effect of soybean-derived phosphatidylserine on cognitive performance in elderly with subjective memory complaints: a pilot study." Clin Interv Aging **8**: 557-563.

Rizzuto, R., et al. (1993). "Microdomains with high Ca2+ close to IP3-sensitive channels that are sensed by neighboring mitochondria." Science **262**(5134): 744-747.

Rizzuto, R., et al. (1998). "Close contacts with the endoplasmic reticulum as determinants of mitochondrial Ca2+ responses." Science **280**(5370): 1763-1766.

Roberts, A., et al. (2011). "Improving RNA-Seq expression estimates by correcting for fragment bias." Genome Biology **12**(3).

Roberts, R. F., et al. (2016). "Defending the mitochondria: The pathways of mitophagy and mitochondrial-derived vesicles." The International Journal of Biochemistry & Cell Biology **79**: 427-436.

Robertson, J. D. (1960). "The molecular structure and contact relationships of cell membranes." Prog Biophys Mol Biol **10**: 343-418.

Robinson, N. C., et al. (1990). "Cardiolipin-depleted bovine heart cytochrome c oxidase: binding stoichiometry and affinity for cardiolipin derivatives." Biochemistry **29**(38): 8962-8969.

Roos, J., et al. (2005). "STIM1, an essential and conserved component of store-operated Ca 2+ channel function." Journal of Cell Biology **169**(3): 435-445.

Roseman, S. (1962). "ENZYMATIC SYNTHESIS OF CYTIDINE 5′-MONOPHOSPHO-SIALIC ACIDS." Proceedings of the National Academy of Sciences of the United States of America **48**(3): 437-441.

Rowlands, A. G., et al. (1988). "The catalytic mechanism of guanine nucleotide exchange factor action and competitive inhibition by phosphorylated eukaryotic initiation factor 2." J Biol Chem **263**(12): 5526-5533.

Ryoo, H. D., et al. (2007). "Unfolded protein response in a Drosophila model for retinal degeneration." EMBO Journal **26**(1): 242-252.

Ryu, E. J., et al. (2005). "Analysis of gene expression changes in a cellular model of Parkinson disease." Neurobiol Dis **18**(1): 54-74.

Sancak, Y., et al. (2013). "EMRE is an essential component of the mitochondrial calcium uniporter complex." Science **342**(6164): 1379-1382.

Saneto, R. P., et al. (2013). "Alpers-Huttenlocher syndrome: A review." Pediatric neurology **48**(3): 167-178.

Sanyal, S. (2009). "Genomic mapping and expression patterns of C380, OK6 and D42 enhancer trap lines in the larval nervous system of Drosophila." Gene Expression Patterns **9**(5): 371-380.

Sardiello, M., et al. (2003). "MitoDrome: a database of Drosophila melanogaster nuclear genes encoding proteins targeted to the mitochondrion." Nucleic Acids Research **31**(1): 322-324.

Schapira, A. H., et al. (1989). "Mitochondrial complex I deficiency in Parkinson's disease." Lancet **1**(8649): 1269.

Schmitt, J. M., et al. (2004). "Calcium activation of ERK mediated by calmodulin kinase I." J Biol Chem **279**(23): 24064-24072.

Schreiber, S., et al. (2000). "An open trial of plant-source derived phosphatydilserine for treatment of age-related cognitive decline." Isr J Psychiatry Relat Sci **37**(4): 302-307.

Schroeder, E. A., et al. (2013). "Epigenetic silencing mediates mitochondria stress-induced longevity." Cell Metab **17**(6): 954-964.

Schuck, S., et al. (2009). "Membrane expansion alleviates endoplasmic reticulum stress independently of the unfolded protein response." J Cell Biol **187**(4): 525-536.

Sekito, T., et al. (2000). "Mitochondria-to-nuclear signaling is regulated by the subcellular localization of the transcription factors Rtg1p and Rtg3p." Mol Biol Cell **11**(6): 2103-2115.

Sha, D., et al. (2010). "Phosphorylation of parkin by Parkinson disease-linked kinase PINK1 activates parkin E3 ligase function and NF-kappaB signaling." Hum Mol Genet **19**(2): 352-363.

Shao, L. W., et al. (2016). "Neuropeptide signals cell non-autonomous mitochondrial unfolded protein response." Cell Res **26**(11): 1182-1196.

Shen, J., et al. (2002). "ER stress regulation of ATF6 localization by dissociation of BiP/GRP78 binding and unmasking of Golgi localization signals." Dev Cell **3**(1): 99-111.

Shibata, Y., et al. (2010). "Mechanisms determining the morphology of the peripheral ER." Cell **143**(5): 774-788.

Shibata, Y., et al. (2008). "The Reticulon and Dp1/Yop1p Proteins Form Immobile Oligomers in the Tubular Endoplasmic Reticulum." J Biol Chem **283**(27): 18892-18904.

Sidrauski, C. and P. Walter (1997). "The transmembrane kinase Ire1p is a site-specific endonuclease that initiates mRNA splicing in the unfolded protein response." Cell **90**(6): 1031-1039.

Singhal, S. S., et al. (2015). "Antioxidant role of glutathione S-transferases: 4-Hydroxynonenal, a key molecule in stress-mediated signaling." Toxicol Appl Pharmacol **289**(3): 361-370.

Skladal, D., et al. (2003). "Minimum birth prevalence of mitochondrial respiratory chain disorders in children." Brain **126**(Pt 8): 1905-1912.

Slater, E. C. (1983). "The Q cycle, an ubiquitous mechanism of electron transfer." Trends in Biochemical Sciences **8**(7): 239-242.

Smith Eble, K., et al. (1990). "Tightly associated cardiolipin in the bovine heart mitochondrial ATP synthase as analyzed by31P nuclear magnetic resonance spectroscopy." Journal of Biological Chemistry **265**(32): 19434-19440.

Snapp, E. L., et al. (2003). "Formation of stacked ER cisternae by low affinity protein interactions." J Cell Biol **163**(2): 257-269.

So, J., et al. (2007). "Impaired endoplasmic reticulum stress response in B-lymphoblasts from patients with bipolar-I disorder." Biol Psychiatry **62**(2): 141-147.

Sokka, A. L., et al. (2007). "Endoplasmic reticulum stress inhibition protects against excitotoxic neuronal injury in the rat brain." J Neurosci **27**(4): 901-908.

Sommerweiss, D., et al. (2013). "Oleate rescues INS-1E beta-cells from palmitate-induced apoptosis by preventing activation of the unfolded protein response." Biochem Biophys Res Commun **441**(4): 770-776.

Sood, R., et al. (2000). "A mammalian homologue of GCN2 protein kinase important for translational control by phosphorylation of eukaryotic initiation factor-2alpha." Genetics **154**(2): 787-801.

Soubannier, V., et al. (2012). "A vesicular transport pathway shuttles cargo from mitochondria to lysosomes." Curr Biol **22**(2): 135-141.

Soubannier, V., et al. (2012). "Reconstitution of mitochondria derived vesicle formation demonstrates selective enrichment of oxidized cargo." PLoS ONE **7**(12): e52830.

Srivastava, S., et al. (2018). "Inflammatory response of microglia to prions is controlled by sialylation of PrPSc." Scientific Reports **8**(1): 11326.

Su, Q., et al. (2008). "Modulation of the eukaryotic initiation factor 2 alpha-subunit kinase PERK by tyrosine phosphorylation." J Biol Chem **283**(1): 469-475.

Subramanian, K. and T. Meyer (1997). "Calcium-induced restructuring of nuclear envelope and endoplasmic reticulum calcium stores." Cell **89**(6): 963-971.

Sullivan, K. M. C., et al. (2000). "The ryanodine receptor is essential for larval development in Drosophila melanogaster." Proceedings of the National Academy of Sciences of the United States of America **97**(11): 5942-5947.

Summerville, J. B., et al. (2016). "The effects of ER morphology on synaptic structure and function in Drosophila melanogaster." Journal of Cell Science **129**(8): 1635-1648.

Sun, X., et al. (2018). "Guanabenz promotes neuronal survival via enhancement of ATF4 and parkin expression in models of Parkinson disease." Exp Neurol **303**: 95-107.

Sun, X., et al. (2013). "ATF4 protects against neuronal death in cellular Parkinson's disease models by maintaining levels of parkin." J Neurosci **33**(6): 2398-2407.

Suzuki, J., et al. (2014). "Imaging intraorganellar Ca2+ at subcellular resolution using CEPIA." Nature Communications **5**: 4153.

Swerdlow, R. H., et al. (2014). "The Alzheimer's Disease Mitochondrial Cascade Hypothesis: Progress and Perspectives." Biochim Biophys Acta **1842**(8): 1219-1231.

Szabadkai, G., et al. (2006). "Chaperone-mediated coupling of endoplasmic reticulum and mitochondrial Ca2+ channels." Journal of Cell Biology **175**(6): 901-911.

Szalai, G., et al. (1999). "Apoptosis driven by IP(3)-linked mitochondrial calcium signals." The EMBO Journal **18**(22): 6349-6361.

Tain, L. S., et al. (2009). "Rapamycin activation of 4E-BP prevents parkinsonian dopaminergic neuron loss." Nat Neurosci **12**(9): 1129-1135.

Takeshima, H., et al. (1994). "Isolation and characterization of a gene for a ryanodine receptor/calcium release channel in Drosophila melanogaster." FEBS Letters **337**(1): 81-87.

Tanouye, M. A., et al. (1981). "Abnormal action potentials associated with the Shaker complex locus of <em>Drosophila</em&gt." Proceedings of the National Academy of Sciences **78**(10): 6548.

Tasseva, G., et al. (2013). "Phosphatidylethanolamine deficiency in Mammalian mitochondria impairs oxidative phosphorylation and alters mitochondrial morphology." J Biol Chem **288**(6): 4158-4173.

Teske, B. F., et al. (2011). "The eIF2 kinase PERK and the integrated stress response facilitate activation of ATF6 during endoplasmic reticulum stress." Molecular Biology of the Cell **22**(22): 4390-4405.

Thalhammer, A., et al. (2011). "Human AlkB homologue 5 is a nuclear 2-oxoglutarate dependent oxygenase and a direct target of hypoxia-inducible factor 1alpha (HIF-1alpha)." PLoS ONE **6**(1): e16210.

Thomas, A., et al. (2012). "A versatile method for cell-specific profiling of translated mRNAs in Drosophila." PLoS ONE **7**(7): e40276.

Tian, H. F., et al. (2012). "The evolution of cardiolipin biosynthesis and maturation pathways and its implications for the evolution of eukaryotes." BMC Evol Biol **12**: 32.

Tiranti, V., et al. (1997). "Identification of the gene encoding the human mitochondrial RNA polymerase (h-mtRPOL) by cyberscreening of the Expressed Sequence Tags database." Hum Mol Genet **6**(4): 615-625.

Trapnell, C., et al. (2012). "Differential gene and transcript expression analysis of RNA-seq experiments with TopHat and Cufflinks." Nature Protocols **7**: 562.

Traven, A., et al. (2001). "Interorganellar communication. Altered nuclear gene expression profiles in a yeast mitochondrial dna mutant." J Biol Chem **276**(6): 4020-4027.

Trinh, M. A., et al. (2012). "Brain-specific disruption of the eIF2alpha kinase PERK decreases ATF4 expression and impairs behavioral flexibility." Cell Rep **1**(6): 676-688.

Tsukihara, T., et al. (1995). "Structures of metal sites of oxidized bovine heart cytochrome c oxidase at 2.8 A." Science **269**(5227): 1069-1074.

Tsuru, A., et al. (2016). "Novel mechanism of enhancing IRE1α-XBP1 signalling via the PERK-ATF4 pathway." Scientific Reports **6**: 24217.

Tsuyama, T., et al. (2017). "Mitochondrial dysfunction induces dendritic loss via eIF2α phosphorylation." J Cell Biol.

Tufanli, O., et al. (2017). "Targeting IRE1 with small molecules counteracts progression of atherosclerosis." Proc Natl Acad Sci U S A **114**(8): E1395-e1404.

Tufi, R., et al. (2014). "Enhancing nucleotide metabolism protects against mitochondrial dysfunction and neurodegeneration in a PINK1 model of Parkinson's disease." Nat Cell Biol **16**(2): 157-166.

Tuller, G., et al. (1999). "Lipid composition of subcellular membranes of an FY1679-derived haploid yeast wild-type strain grown on different carbon sources." Yeast **15**(14): 1555-1564.

Urra, H., et al. (2018). "IRE1α governs cytoskeleton remodelling and cell migration through a direct interaction with filamin A." Nature Cell Biology **20**(8): 942-953.

Vakhapova, V., et al. (2014). "Phosphatidylserine containing omega-3 Fatty acids may improve memory abilities in nondemented elderly individuals with memory complaints: results from an open-label extension study." Dement Geriatr Cogn Disord **38**(1-2): 39-45.

Vakhapova, V., et al. (2010). "Phosphatidylserine containing omega-3 fatty acids may improve memory abilities in non-demented elderly with memory complaints: a double-blind placebo-controlled trial." Dement Geriatr Cogn Disord **29**(5): 467-474.

Valadas, J. S., et al. (2018). "ER Lipid Defects in Neuropeptidergic Neurons Impair Sleep Patterns in Parkinson's Disease." Neuron **98**(6): 1155-1169.e1156.

Valdés, P., et al. (2014). "Control of dopaminergic neuron survival by the unfolded protein response transcription factor XBP1." Proceedings of the National Academy of Sciences of the United States of America **111**(18): 6804-6809.

Valente, E. M., et al. (2004). "Hereditary early-onset Parkinson's disease caused by mutations in PINK1." Science **304**(5674): 1158-1160.

Van Bruggen, E. F. J., et al. (1966). "Circular mitochondrial DNA." BBA Section Nucleic Acids And Protein Synthesis **119**(2): 437-439.

van Vliet, A. R., et al. (2017). "The ER Stress Sensor PERK Coordinates ER-Plasma Membrane Contact Site Formation through Interaction with Filamin-A and F-Actin Remodeling." Mol Cell **65**(5): 885-899.e886.

Vance, J. E. (1990). "Phospholipid synthesis in a membrane fraction associated with mitochondria." J Biol Chem **265**(13): 7248-7256.

Vance, J. E. (2015). "Phospholipid synthesis and transport in mammalian cells." Traffic **16**(1): 1-18.

Vanden Broeck, L., et al. (2013). "TDP-43 Loss-of-Function Causes Neuronal Loss Due to Defective Steroid Receptor-Mediated Gene Program Switching In Drosophila." Cell Reports **3**(1): 160-172.

Vannuvel, K., et al. (2013). "Functional and morphological impact of ER stress on mitochondria." Journal of Cellular Physiology **228**(9): 1802-1818.

Vattem, K. M. and R. C. Wek (2004). "Reinitiation involving upstream ORFs regulates ATF4 mRNA translation in mammalian cells." Proc Natl Acad Sci U S A **101**(31): 11269-11274.

Veltri, K. L., et al. (1990). "Distinct genomic copy number in mitochondria of different mammalian organs." J Cell Physiol **143**(1): 160-164.

Verfaillie, T., et al. (2012). "PERK is required at the ER-mitochondrial contact sites to convey apoptosis after ROS-based ER stress." Cell Death Differ **19**(11): 1880-1891.

Vig, M., et al. (2006). "CRACM1 is a plasma membrane protein essential for store-operated Ca 2+ entry." Science **312**(5777): 1220-1223.

Vincow, E. S., et al. (2013). "The PINK1–Parkin pathway promotes both mitophagy and selective respiratory chain turnover in vivo." Proceedings of the National Academy of Sciences of the United States of America **110**(16): 6400-6405.

Virbasius, J. V. and R. C. Scarpulla (1994). "Activation of the human mitochondrial transcription factor A gene by nuclear respiratory factors: a potential regulatory link between nuclear and mitochondrial gene expression in organelle biogenesis." Proceedings of the National Academy of Sciences of the United States of America **91**(4): 1309-1313.

Vissers, J. H. A., et al. (2016). "A Drosophila RNAi library modulates Hippo pathway-dependent tissue growth." Nature Communications **7**: 10368.

Voeltz, G. K., et al. (2006). "A class of membrane proteins shaping the tubular endoplasmic reticulum." Cell **124**(3): 573-586.

Volmer, R., et al. (2013). "Membrane lipid saturation activates endoplasmic reticulum unfolded protein response transducers through their transmembrane domains." Proc Natl Acad Sci U S A **110**(12): 4628-4633.

Walter, P., et al. (1984). "Protein translocation across the endoplasmic reticulum." Cell **38**(1): 5-8.

Wang, P. T., et al. (2015). "Distinct mechanisms controlling rough and smooth endoplasmic reticulum contacts with mitochondria." J Cell Sci **128**(15): 2759-2765.

Wang, S. F., et al. (2016). "Mitochondrial dysfunction enhances cisplatin resistance in human gastric cancer cells via the ROS-activated GCN2-eIF2α- ATF4-xCT pathway." Oncotarget **7**(45): 74132-74151.

Wang, X. and X. J. Chen (2015). "A cytosolic network suppressing mitochondria-mediated proteostatic stress and cell death." Nature **524**(7566): 481-484.

Watanabe, Y., et al. (2015). "Structural and mechanistic insights into phospholipid transfer by Ups1-Mdm35 in mitochondria." Nat Commun **6**: 7922.

Watson, M. L. (1955). "The nuclear envelope; its structure and relation to cytoplasmic membranes." J Biophys Biochem Cytol **1**(3): 257-270.

Weidner, U., et al. (1993). "The Gene Locus of the Proton-translocating NADH : Ubiquinone Oxidoreductase in Escherichia coli. Organization of the 14 Genes and Relationship Between the Derived Proteins and Subunits of Mitochondrial Complex I." Journal of Molecular Biology **233**(1): 109-122.

Weisiger, R. A. and I. Fridovich (1973). "Superoxide dismutase. Organelle specificity." J Biol Chem **248**(10): 3582-3592.

Westrate, L. M., et al. (2015). "Form follows function: the importance of endoplasmic reticulum shape." Annu Rev Biochem **84**: 791-811.

Whitworth, A. J., et al. (2005). "Increased glutathione S-transferase activity rescues dopaminergic neuron loss in a Drosophila model of Parkinson's disease." Proc Natl Acad Sci U S A **102**(22): 8024-8029.

Wiedemann, N. and N. Pfanner (2017). "Mitochondrial Machineries for Protein Import and Assembly." Annual Review of Biochemistry **86**(1): 685-714.

Williams, T. A. and T. M. Embley (2014). "Archaeal “Dark Matter” and the Origin of Eukaryotes." Genome Biology and Evolution **6**(3): 474-481.

Williams, T. A., et al. (2012). "A congruent phylogenomic signal places eukaryotes within the Archaea." Proc Biol Sci **279**(1749): 4870-4879.

Wirth, C., et al. (2016). "Structure and function of mitochondrial complex I." Biochim Biophys Acta **1857**(7): 902-914.

Wong, Y. C., et al. (2018). "Mitochondria–lysosome contacts regulate mitochondrial fission via RAB7 GTP hydrolysis." Nature **554**: 382.

Wrobel, L., et al. (2015). "Mistargeted mitochondrial proteins activate a proteostatic response in the cytosol." Nature **524**(7566): 485-488.

Wu, L., et al. (2014). "Salubrinal protects against rotenone-induced SH-SY5Y cell death via ATF4-parkin pathway." Brain Research **1549**: 52-62.

Wu, Y., et al. (2014). "Multilayered Genetic and Omics Dissection of Mitochondrial Activity in a Mouse Reference Population." Cell **158**(6): 1415-1430.

Wu, Z., et al. (1999). "Mechanisms controlling mitochondrial biogenesis and respiration through the thermogenic coactivator PGC-1." Cell **98**(1): 115-124.

Wyatt, G. R. and G. F. Kale (1957). "The chemistry of insect hemolymph. II. Trehalose and other carbohydrates." J Gen Physiol **40**(6): 833-847.

Xu, Z., et al. (2016). "Ire1 supports normal ER differentiation in developing Drosophila photoreceptors." J Cell Sci **129**(5): 921-929.

Yalçın, B., et al. (2017). "Modeling of axonal endoplasmic reticulum network by spastic paraplegia proteins." eLife **6**.

Yamamoto, K., et al. (2007). "Transcriptional induction of mammalian ER quality control proteins is mediated by single or combined action of ATF6alpha and XBP1." Dev Cell **13**(3): 365-376.

Yamamoto, Y., et al. (2014). "Arl6IP1 has the ability to shape the mammalian ER membrane in a reticulon-like fashion." Biochem J **458**(1): 69-79.

Yan, L., et al. (2015). "Structures of the yeast dynamin-like GTPase Sey1p provide insight into homotypic ER fusion." J Cell Biol **210**(6): 961.

Yang, D., et al. (1985). "Mitochondrial origins." Proceedings of the National Academy of Sciences of the United States of America **82**(13): 4443-4447.

Yang, Y., et al. (2001). "Role of glutathione S-transferases in protection against lipid peroxidation. Overexpression of hGSTA2-2 in K562 cells protects against hydrogen peroxide-induced apoptosis and inhibits JNK and caspase 3 activation." J Biol Chem **276**(22): 19220-19230.

Yang, Y., et al. (2006). "Mitochondrial pathology and muscle and dopaminergic neuron degeneration caused by inactivation of Drosophila Pink1 is rescued by Parkin." Proc Natl Acad Sci U S A **103**(28): 10793-10798.

Yankovskaya, V., et al. (2003). "Architecture of succinate dehydrogenase and reactive oxygen species generation." Science **299**(5607): 700-704.

Yano, M. (2017). "ABCB10 depletion reduces unfolded protein response in mitochondria." Biochem Biophys Res Commun **486**(2): 465-469.

Yap, Y. W., et al. (2013). "Gene expression profiling of rotenone-mediated cortical neuronal death: Evidence for inhibition of ubiquitin–proteasome system and autophagy-lysosomal pathway, and dysfunction of mitochondrial and calcium signaling." Neurochemistry International **62**(5): 653-663.

Ye, J., et al. (2000). "ER stress induces cleavage of membrane-bound ATF6 by the same proteases that process SREBPs." Mol Cell **6**(6): 1355-1364.

Yoshida, H., et al. (1998). "Identification of the cis-acting endoplasmic reticulum stress response element responsible for transcriptional induction of mammalian glucose-regulated proteins. Involvement of basic leucine zipper transcription factors." J Biol Chem **273**(50): 33741-33749.

Yoshida, H., et al. (2001). "XBP1 mRNA is induced by ATF6 and spliced by IRE1 in response to ER stress to produce a highly active transcription factor." Cell **107**(7): 881-891.

Yoshida, M., et al. (2016). "Molecular characterization of Tps1 and Treh genes in Drosophila and their role in body water homeostasis." Scientific Reports **6**: 30582.

Yoshikawa, S., et al. (2011). "Proton-Pumping Mechanism of Cytochrome c Oxidase." Annual Review of Biophysics **40**(1): 205-223.

Yu, C.-A. and L. Yu (1980). "Structural role of phospholipids in ubiquinol-cytochrome c reductase." Biochemistry **19**(25): 5715-5720.

Yu, M., et al. (2009). "Mitochondrial DNA depletion promotes impaired oxidative status and adaptive resistance to apoptosis in T47D breast cancer cells." Eur J Cancer Prev **18**(6): 445-457.

Zalman, L. S., et al. (1980). "Mitochondrial outer membrane contains a protein producing nonspecific diffusion channels." Journal of Biological Chemistry **255**(5): 1771-1774.

Zangar, R. C., et al. (2004). "Mechanisms that regulate production of reactive oxygen species by cytochrome P450." Toxicology and Applied Pharmacology **199**(3): 316-331.

Zhang, C., et al. (2016). "Hypoxia induces the breast cancer stem cell phenotype by HIF-dependent and ALKBH5-mediated m(6)A-demethylation of NANOG mRNA." Proc Natl Acad Sci U S A **113**(14): E2047-2056.

Zhang, H. and J. Hu (2016). "Shaping the Endoplasmic Reticulum into a Social Network." Trends Cell Biol **26**(12): 934-943.

Zhang, S.-J., et al. (2009). "Nuclear Calcium Signaling Controls Expression of a Large Gene Pool: Identification of a Gene Program for Acquired Neuroprotection Induced by Synaptic Activity." PLoS Genetics **5**(8): e1000604.

Zhang, S. L., et al. (2006). "Genome-wide RNAi screen of Ca2+influx identifies genes that regulate Ca2+release-activated Ca2+channel activity." Proceedings of the National Academy of Sciences of the United States of America **103**(24): 9357-9362.

Zhang, Y. Y., et al. (2015). "Effect of phosphatidylserine on memory in patients and rats with Alzheimer's disease." Genet Mol Res **14**(3): 9325-9333.

Zhao, Q., et al. (2002). "A mitochondrial specific stress response in mammalian cells." The EMBO Journal **21**(17): 4411-4419.

Zhou, J., et al. (2006). "The crystal structure of human IRE1 luminal domain reveals a conserved dimerization interface required for activation of the unfolded protein response." Proc Natl Acad Sci U S A **103**(39): 14343-14348.

Zhou, J., et al. (2018). "N(6)-Methyladenosine Guides mRNA Alternative Translation during Integrated Stress Response." Mol Cell **69**(4): 636-647.e637.

Zimprich, A., et al. (2004). "Mutations in LRRK2 cause autosomal-dominant parkinsonism with pleomorphic pathology." Neuron **44**(4): 601-607.

8. Apendix

8.1 Individual GCaMP6m traces

Traces of GCaMP6m fluorescence for each sample in dorsal medial motor neuron cell bodies (A), axons (B) and neuropil (C) as TrpA1 channels were activated by 20 second (s) on/off pulses of 25 °C heat, as indicated by the horizontal black lines below the graph (line = heat on, space = heat off). Control samples = black traces, TFAM overexpression samples = red traces

.

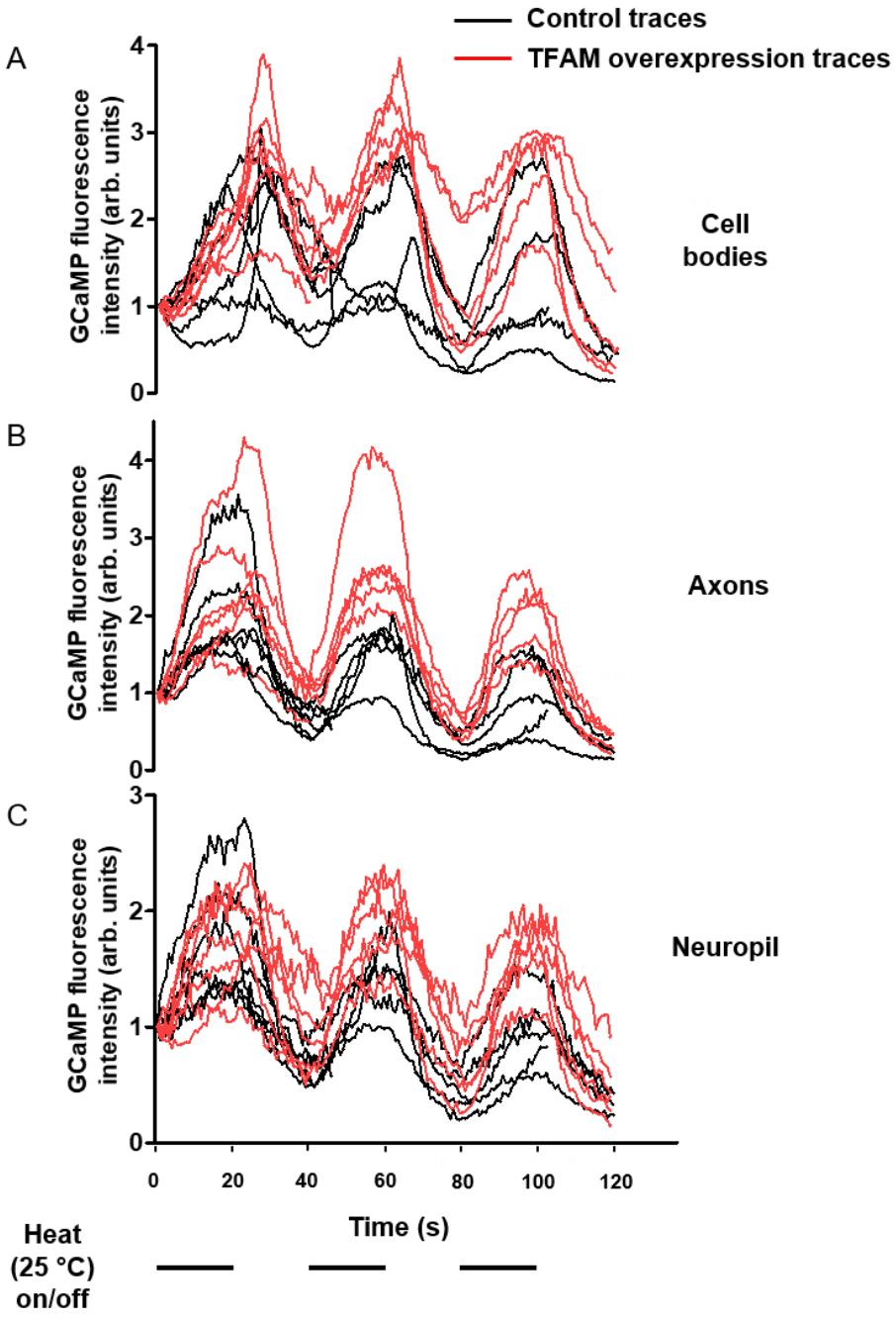

8.2 Supplementary climbing and wing inflation assays

8.2.1 Functional consequences of genetic manipulation of components of the PERK ER UPR pathway (PERK and GADD34) in Drosophila motor neurons with TFAM overexpression.

(A, B) Climbing (A) and wing inflation (B) assays with PERK knock-down (line 35162). (C, D) Climbing (C) and wing inflation (D) assays with PERK knock-down (line 42499). (E, F) Climbing (E) and wing inflation (F) assays with GADD34 knock-down (line 107545). TFAM overexpression and all ER UPR RNAi and overexpression lines were driven by *D42-Gal4*. Wing inflation assay: number of flies per genotype displayed at the base of each column. Climbing assays: n = 20. Bars = mean ± SEM. Means were compared by one-way parametric ANOVA with Tukey's post-hoc test. Wing inflation: significance was tested by Chi-squared test on the raw data. n.s. = not significant, ***p < 0.001.

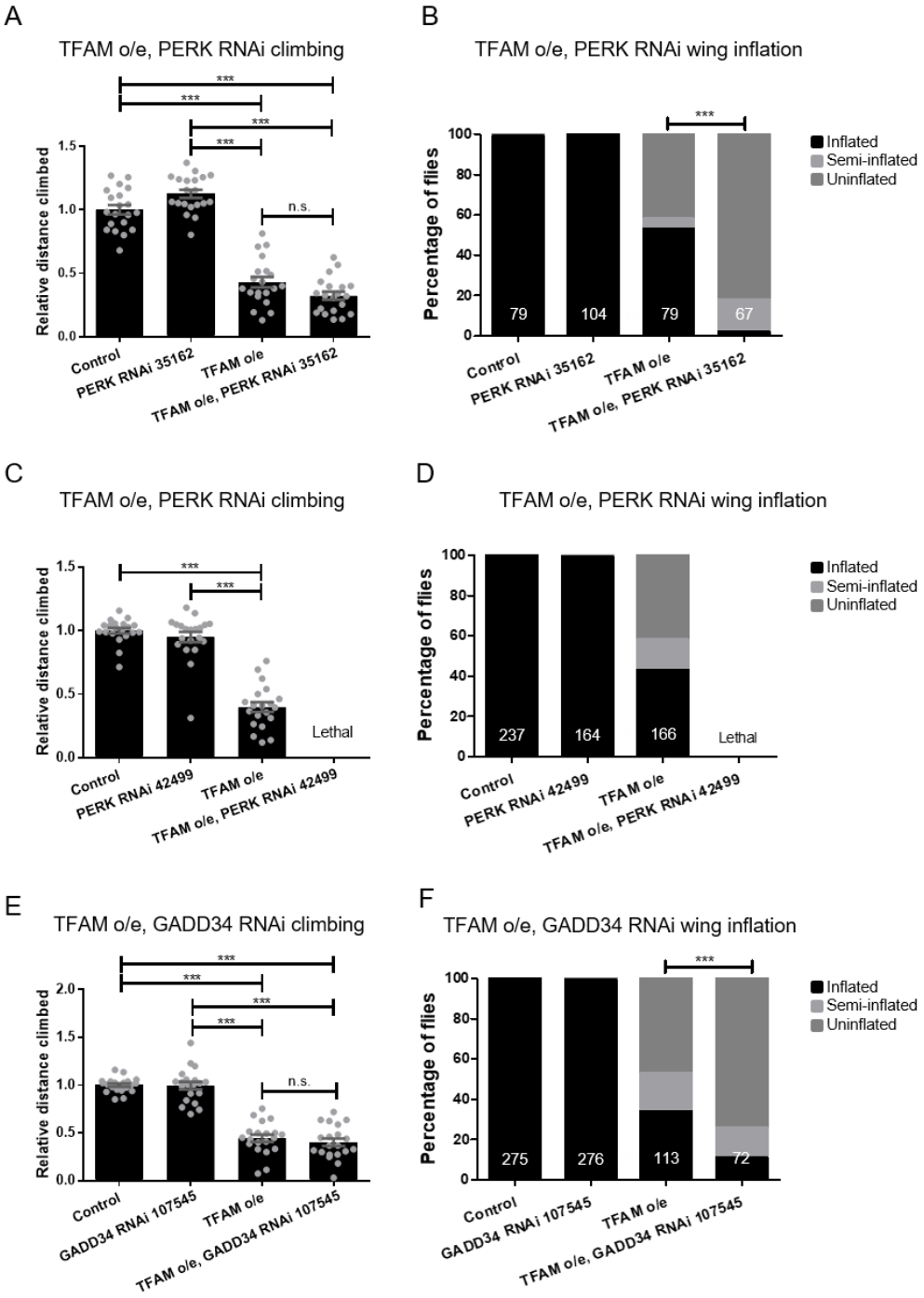

8.2.2 Functional consequences of genetic manipulation of the IRE1 ER UPR pathway in *Drosophila* motor neurons with TFAM overexpression

(A, B) Climbing (A) and wing inflation (B) assays with IRE1 knock-down (line 62156). (C, D) Climbing (C) and wing inflation (D) assays with IRE1 mutant f02170. (E, F) Climbing (E) and wing inflation (F) assays with XBP1 knock-down (line 36755). TFAM overexpression and all ER UPR RNAi and overexpression lines were driven by *D42-Gal4*. Wing inflation assay: number of flies per genotype displayed at the base of each column. Climbing assays: n = 15 for all genotypes in (A), n = 20 for all other genotypes. Bars = mean ± SEM. Means were compared by one-way parametric ANOVA with Tukey's post-hoc test. Wing inflation: significance was tested by Chi-squared test on the raw data. n.s. = not significant, *p < 0.05, ***p < 0.001.

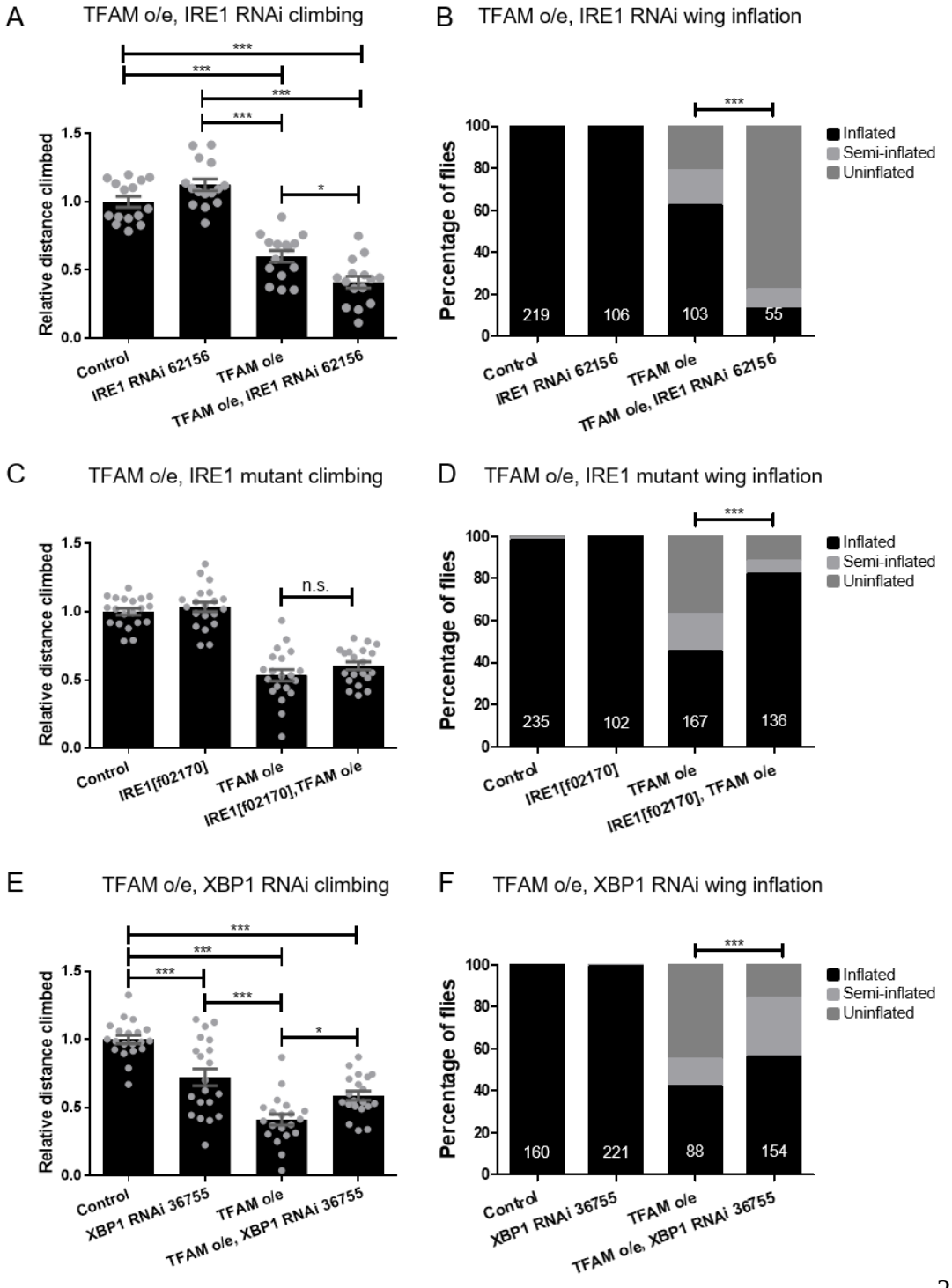

8.3 RNA-Seq appendices

8.3.1 Genes upregulated by TFAM o/e and ATF4 o/e compared to control.

Cut-offs: FPKM ≥ 1 for at least one condition, fold change ≥1.5, adjusted p value < 0.05. Grey shading = gene upregulated in both conditions. Bold outline = gene inversely regulated (upregulated by TFAM o/e, downregulated by ATF4 o/e).

Genes upregulated by TFAM o/e			Genes upregulated by ATF4 o/e		
Gene ID	**Fold change**	**Adj. p value**	**Gene ID**	**Fold change**	**Adj. p value**
CG14850	22.88	0.0119	CG14850	24.54	0.0119
CG1113	3.59	0.0217	CG1113	4.04	0.0119
Hsp70Bb	3.59	0.0119	Hsp70Bb	2.39	0.0119
CG42694	3.54	0.0119	CG42694	3.40	0.0119
Thor	2.76	0.0119	Thor	3.76	0.0119
CG17684	1.78	0.0119	CG17684	2.06	0.0119
ImpE2	1.71	0.0217	ImpE2	1.80	0.0119
Acf	1.58	0.0453	Acf	1.87	0.0119
blw	1.56	0.0303	blw	1.59	0.0119
sfl	1.55	0.0303	sfl	1.74	0.0119
Hsc70-2	54.84	0.0119	Cpr49Ae	8.17	0.0119
CG34296	25.12	0.0119	SelG	7.07	0.0119
Eig71Ee	11.24	0.0119	CG15021	4.86	0.0119
CG31496	9.33	0.0453	Rgk2	3.26	0.0119
CG7587	7.66	0.0119	Crg-1	2.61	0.0119
thw	6.18	0.0119	Cht5	2.25	0.0119
Sgs7	6.07	0.0119	CG17211	2.20	0.0119
Sgs5	5.71	0.0119	Blimp-1	2.16	0.0119
Hsp22	5.67	0.0119	CG34232	2.16	0.0380
Sgs3	5.50	0.0119	CG5830	2.12	0.0119
CG15784	5.22	0.0119	spg	2.00	0.0380
CG33500	4.85	0.0119	CG15864	1.98	0.0119
ImpL3	3.04	0.0119	Eip93F	1.89	0.0119
Xrp1	2.68	0.0119	nrm	1.82	0.0303
CR45315	2.64	0.0119	rdgA	1.81	0.0119
Arc1	2.59	0.0119	ImpE1	1.78	0.0119
cv-2	2.43	0.0119	Sec31	1.77	0.0119
mir-10404-1	2.39	0.0119	CG11700	1.71	0.0119
NKCC	2.28	0.0303	CR44027	1.66	0.0303
CG42832	2.26	0.0119	trv	1.61	0.0119
Gadd45	2.03	0.0119	Indy	1.58	0.0453
28SrRNA:CR45837	1.95	0.0119	AstC-R2	1.53	0.0119
CR45481	1.76	0.0217	jeb	1.52	0.0217
Hex-A	1.75	0.0119	CR46004	1.52	0.0119
2SrRNA:CR45836	1.72	0.0119	CG43901	1.50	0.0453
Dgp-1	1.68	0.0380			

8.3.2 Genes downregulated by TFAM o/e and ATF4 o/e compared to control

Cut-offs: FPKM ≥ 1 for at least one condition, fold change ≤0.67 (equivalent to ≤ -1.5), adjusted p value < 0.05. Grey shading = gene downregulated in both conditions. Bold outline = gene inversely regulated (downregulated by ATF4 o/e, upregulated by TFAM o/e).

Genes downregulated by TFAM o/e			Genes downregulated by ATF4 o/e		
Gene ID	**Fold change**	**Adj. p value**	**Gene ID**	**Fold change**	**Adj. p value**
Lcp65Ab1	0.08	0.0119	Lcp65Ab1	0.17	0.0119
Lcp3	0.09	0.0119	Lcp3	0.32	0.0119
Jon99Ciii	0.12	0.0217	Jon99Ciii	0.13	0.0119
CG34166	0.15	0.0119	CG34166	0.33	0.0119
Obp99b	0.15	0.0119	Obp99b	0.28	0.0119
Lcp4	0.19	0.0119	Lcp4	0.34	0.0119
Cyp4d1	0.20	0.0119	Cyp4d1	0.27	0.0217
CG2233	0.21	0.0119	CG2233	0.40	0.0119
GstE14	0.21	0.0217	GstE14	0.08	0.0217
Lcp1	0.21	0.0119	Lcp1	0.37	0.0119
Lsp2	0.22	0.0119	Lsp2	0.44	0.0380
CG42500	0.23	0.0119	CG42500	0.41	0.0119
CG34445	0.23	0.0119	CG34445	0.15	0.0119
CG32249	0.24	0.0119	CG32249	0.31	0.0119
CG34446	0.24	0.0119	CG34446	0.25	0.0119
Lsp1beta	0.26	0.0119	Lsp1beta	0.61	0.0119
CG43117	0.28	0.0119	CG43117	0.60	0.0119
CR46006	0.32	0.0119	CR46006	0.38	0.0119
Cyp28a5	0.36	0.0119	Cyp28a5	0.16	0.0119
CG18278	0.36	0.0119	CG18278	0.47	0.0119
CG45087	0.36	0.0119	CG45087	0.32	0.0119
CG10307	0.42	0.0119	CG10307	0.23	0.0119
Cyt-c-d	0.42	0.0119	Cyt-c-d	0.51	0.0119
Akh	0.43	0.0217	Akh	0.27	0.0119
CG12512	0.43	0.0119	CG12512	0.52	0.0119
Aldh	0.44	0.0119	Aldh	0.52	0.0119
CG9657	0.45	0.0119	CG9657	0.46	0.0119
pyd3	0.48	0.0119	pyd3	0.48	0.0119
CG14075	0.48	0.0119	CG14075	0.28	0.0119
Hsp70Aa	0.48	0.0217	Hsp70Aa	0.15	0.0119
CG30059	0.50	0.0303	CG30059	0.53	0.0453
CG30197	0.50	0.0119	CG30197	0.59	0.0217
Syt7	0.51	0.0119	Syt7	0.54	0.0119
Mlc2	0.51	0.0119	Mlc2	0.54	0.0303
CG15767	0.53	0.0119	CG15767	0.54	0.0119
GstD3	0.53	0.0119	GstD3	0.61	0.0119
ND-B14.5B	0.54	0.0217	ND-B14.5B	0.44	0.0119
MFS9	0.54	0.0119	MFS9	0.47	0.0119
Csas	0.57	0.0119	Csas	0.58	0.0119
CG4686	0.58	0.0303	CG4686	0.50	0.0119
CG10184	0.58	0.0380	CG10184	0.48	0.0119
CG44325	0.58	0.0119	CG44325	0.53	0.0119
Cys	0.60	0.0303	Cys	0.39	0.0119
Nup44A	0.60	0.0303	Nup44A	0.49	0.0119
CG5955	0.61	0.0453	CG5955	0.60	0.0453
CG31549	0.61	0.0217	CG31549	0.60	0.0119
mRpL36	0.63	0.0380	mRpL36	0.54	0.0119
CG34305	0.21	0.0453	CG32198	0.01	0.0119
CG5958	0.23	0.0217	GILT3	0.08	0.0119
Lcp2	0.24	0.0217	Jon99Fi	0.08	0.0453
Lsp1gamma	0.24	0.0119	GstE8	0.16	0.0119
Lsp1alpha	0.24	0.0119	CG8087	0.16	0.0119
CG33099	0.29	0.0119	CG5867	0.21	0.0119
CG16743	0.30	0.0119	phm	0.21	0.0380
CG10226	0.33	0.0119	Ugt86Dd	0.23	0.0217
CG3987	0.42	0.0119	Cyp6g2	0.24	0.0217
CG14566	0.43	0.0119	CG11300	0.27	0.0119
CG43980	0.43	0.0303	Hsp70Bbb	0.28	0.0119
CG6912	0.46	0.0453	CG14545	0.29	0.0119
CG13067	0.47	0.0453	CG17105	0.29	0.0453
CG30379	0.57	0.0380	TotA	0.33	0.0380
vkg	0.59	0.0217	spok	0.33	0.0119
Klp68D	0.66	0.0303	Pburs	0.33	0.0119
			Fit2	0.34	0.0380
			ImpL3	0.35	0.0119
			snRNA:U1:95Ca	0.36	0.0119
			rtet	0.36	0.0119
			Ugt86Di	0.38	0.0119
			CG43085	0.38	0.0119

			Sec63	0.39	0.0119
			Tsp42El	0.41	0.0119
			snoRNA:Me28S-	0.42	0.0119
			alpha-Est7	0.43	0.0217
			Elal	0.44	0.0119
			Dsk	0.45	0.0119
			su(r)	0.47	0.0119
			Ada	0.47	0.0119
			mt:ND2	0.47	0.0119
			CG14985	0.47	0.0119
			Gpa2	0.48	0.0380
			CG9147	0.48	0.0119
			NPF	0.49	0.0119
			CG14572	0.50	0.0217
			mthl8	0.50	0.0119
			CR46012	0.51	0.0119
			Ilp2	0.51	0.0119
			CG43069	0.52	0.0119
			Lk	0.52	0.0119
			CG31437	0.52	0.0119
			CG4036	0.53	0.0119
			CG4408	0.53	0.0119
			CG12926	0.54	0.0119
			Dhfr	0.54	0.0119
			Ady43A	0.56	0.0119
			Tspo	0.56	0.0119
			Cyp12a4	0.56	0.0217
			Ssb-c31a	0.57	0.0119
			CG5567	0.57	0.0119
			CR44922	0.57	0.0119
			CG17333	0.58	0.0217
			mre11	0.59	0.0119
			CG4789	0.59	0.0303
			asrij	0.59	0.0119
			Idgf6	0.59	0.0380
			Capa	0.59	0.0119
			CG8369	0.60	0.0217
			RpS15Ab	0.61	0.0303
			Tsp42Ej	0.61	0.0119
			dmGlut	0.62	0.0303
			Arp10	0.62	0.0119
			CR45044	0.62	0.0453
			mRpL46	0.62	0.0217
			CG8778	0.62	0.0380
			ND-PDSW	0.63	0.0380
			Taldo	0.63	0.0119
			veli	0.63	0.0119
			ND-B14.7	0.63	0.0303
			CG6723	0.63	0.0453
			mus205	0.63	0.0217
			CG8745	0.63	0.0303
			DNaseII	0.63	0.0217
			Dbi	0.64	0.0119
			Cyp9f2	0.64	0.0217
			CG7630	0.64	0.0303
			CG12237	0.64	0.0119
			CG31220	0.64	0.0303
			CG5037	0.65	0.0217
			spab	0.65	0.0380
			Vha36-1	0.65	0.0217
			ND-30	0.65	0.0303
			Arc1	0.66	0.0119
			CR43727	0.66	0.0380
			eca	0.66	0.0119
			CG15083	0.67	0.0453

8.3.3 Genes upregulated by TFAM o/e (compared to control) and downregulated by ATF4 RNAi (compared to TFAM o/e).

Cut-offs: FPKM ≥ 1 for at least one condition, fold change ≥ 1.5 for upregulated genes, ≤ 0.67 (equivalent to ≤ -1.5) for downregulated genes, adjusted p value < 0.05. Grey shading = gene significantly regulated in both conditions. Bold outline = gene downregulated by both TFAM o/e (vs. control) and ATF4 RNAi (vs. TFAM o/e).

Genes upregulated by TFAM o/e (compared to control)			**Genes downregulated by ATF4 RNAi (compared to TFAM o/e)**		
Gene ID	**Fold change**	**Adj. p value**	**Gene ID**	**Fold change**	**Adj. p value**
Hsc70-2	54.83975	0.011923	Hsc70-2	0.023551	0.011923
CG34296	25.11731	0.011923	CG34296	0.032484	0.011923
Hsp22	5.665409	0.011923	Hsp22	0.099148	0.011923
thw	6.176074	0.011923	Thw	0.138438	0.011923
Thor	2.760883	0.011923	Thor	0.181409	0.011923
ImpL3	3.040566	0.011923	ImpL3	0.227202	0.011923
CG7587	7.660826	0.011923	CG7587	0.266966	0.011923
mir-10404-1	2.393713	0.011923	mir-10404-1	0.366509	0.011923
CR45315	2.64112	0.011923	CR45315	0.443686	0.030286
Dgp-1	1.682773	0.038022	Dgp-1	0.451444	0.011923
2SrRNA:CR45836	1.718037	0.011923	2SrRNA:CR45836	0.460371	0.011923
28SrRNA:CR45837	1.947199	0.011923	28SrRNA:CR45837	0.461739	0.011923
ImpE2	1.709605	0.021652	ImpE2	0.560237	0.011923
CR45481	1.759764	0.021652	CR45481	0.560763	0.011923
CG17684	1.784646	0.011923	CG17684	0.571801	0.011923
Hex-A	1.746982	0.011923	Hex-A	0.603018	0.021652
CG15784	5.217541	0.011923	CG15784	0.625984	0.011923
CG14850	22.87928	0.011923	CG32198	0.086399	0.011923
Eig71Ee	11.2393	0.011923	Nvd	0.147745	0.011923
CG31496	9.333512	0.045272	CG8087	0.262768	0.011923
Sgs7	6.073213	0.011923	Spok	0.293286	0.011923
Sgs5	5.707465	0.011923	CG9304	0.42645	0.011923
Sgs3	5.503807	0.011923	Tret1-1	0.449833	0.011923
CG33500	4.847531	0.011923	CG7386	0.478006	0.011923
CG1113	3.5937	0.021652	Cpr49Ac	0.500482	0.011923
Hsp70Bb	3.592056	0.011923	CG10924	0.506765	0.038022
CG42694	3.542088	0.011923	CG14566	0.509249	0.030286
Xrp1	2.68083	0.011923	Nlaz	0.552464	0.030286
Arc1	2.592457	0.011923	AdamTS-A	0.556644	0.011923
cv-2	2.427767	0.011923	CG16700	0.55732	0.011923
NKCC	2.282666	0.030286	ImpE1	0.59857	0.011923
CG42832	2.262911	0.011923	CG4461	0.598629	0.011923
Gadd45	2.03214	0.011923	CG42240	0.613788	0.038022
Acf	1.57506	0.045272	28SrRNA:CR45844	0.626306	0.038022
blw	1.563285	0.030286	CG9416	0.631623	0.038022
sfl	1.548391	0.030286	Dtg	0.634611	0.011923
			Hsp67Bc	0.653536	0.011923
			CG3036	0.659177	0.011923
			mthl8	0.661428	0.038022
			MFS3	0.665052	0.021652
			CG43083	-∞	0.011923
			CR44803	-∞	0.011923
			CR44522	-∞	0.011923

8.3.4 Genes downregulated by TFAM o/e (compared to control) and upregulated by ATF4 RNAi (compared to TFAM o/e).

Cut-offs: FPKM ≥ 1 for at least one condition, fold change ≥ 1.5 for upregulated genes, ≤ 0.67 (equivalent to ≤ -1.5) for downregulated genes, adjusted p value < 0.05. Grey shading = gene significantly regulated in both conditions. Bold outline = gene upregulated by both TFAM o/e (vs. control) and ATF4 RNAi (vs. TFAM o/e).

Downregulated by TFAM o/e (compared to control)			**Upregulated by ATF4 RNAi (compared to TFAM o/e)**		
Gene ID	**Fold change**	**Adj. p_value**	**Gene ID**	**Fold change**	**Adj. p value**
Jon99Ciii	0.117642	0.0001	Jon99Ciii	8.719649	5.00E-05
Lcp4	0.18671	0.00005	Lcp4	4.298431	5.00E-05
CG42500	0.226998	0.00005	CG42500	3.761792	5.00E-05
Lcp65Ab1	0.083695	0.00005	Lcp65Ab1	3.53206	0.00025
Lcp1	0.214003	0.00005	Lcp1	3.409216	5.00E-05
Lcp3	0.09438	0.00005	Lcp3	3.360556	5.00E-05
CG43117	0.27702	0.00005	CG43117	3.217834	5.00E-05
CG6912	0.458022	0.00025	CG6912	2.517846	5.00E-05
CG3987	0.422537	0.00005	CG3987	2.259181	5.00E-05
CG43980	0.43324	0.00015	CG43980	2.128962	0.00025
Cyp28a5	0.35623	0.00005	Cyp28a5	2.10754	0.00025
Cyt-c-d	0.418054	0.00005	Cyt-c-d	1.870023	5.00E-05
CG5955	0.608924	0.00025	CG5955	1.639396	0.00025
CG34166	0.15204	5.00E-05	CG9377	3.575215	0.0002
Obp99b	0.152081	5.00E-05	CG9737	3.503799	5.00E-05
Cyp4d1	0.19976	5.00E-05	Trh	2.150437	5.00E-05
CG2233	0.20667	5.00E-05	GstT3	2.058338	0.0001
GstE14	0.209291	0.0001	IntS12	1.817772	5.00E-05
CG34305	0.213528	0.00025	roq	1.81435	0.00015
Lsp2	0.21608	5.00E-05	Hsp70Bb	1.556655	5.00E-05
CG5958	0.226131	0.0001			
CG34445	0.228471	5.00E-05			
CG32249	0.24074	5.00E-05			
Lcp2	0.241096	0.0001			
Lsp1gamma	0.242198	5.00E-05			
CG34446	0.24339	5.00E-05			
Lsp1alpha	0.244707	5.00E-05			
Lsp1beta	0.257381	5.00E-05			
CG33099	0.285126	5.00E-05			
CG16743	0.300197	5.00E-05			
CR46006	0.318369	5.00E-05			
CG10226	0.329315	5.00E-05			
CG18278	0.363715	5.00E-05			
CG45087	0.364874	5.00E-05			
CG10307	0.41605	5.00E-05			
Akh	0.426838	0.0001			
CG12512	0.431039	5.00E-05			
CG14566	0.432505	5.00E-05			
Aldh	0.435203	5.00E-05			
CG9657	0.452475	5.00E-05			
CG13067	0.469511	0.00025			
pyd3	0.477575	5.00E-05			
CG14075	0.481214	5.00E-05			
Hsp70Aa	0.482988	0.0001			
CG30059	0.496178	0.00015			
CG30197	0.50129	5.00E-05			
Syt7	0.508668	5.00E-05			
Mlc2	0.514539	5.00E-05			
CG15767	0.527311	5.00E-05			
GstD3	0.529395	5.00E-05			
ND-B14.5B	0.537751	0.0001			
MFS9	0.538352	5.00E-05			
Csas	0.565448	5.00E-05			
CG30379	0.574726	0.0002			
CG4686	0.575607	0.00015			
CG10184	0.57671	0.0002			
CG44325	0.577882	5.00E-05			
vkg	0.59024	0.0001			
Cys	0.600728	0.00015			
Nup44A	0.604107	0.00015			
CG31549	0.612032	0.0001			
mRpL36	0.631517	0.0002			
Klp68D	0.655904	0.00015			

8.3.5 Gene ontology terms for genes significantly regulated by TFAM o/e, ATF4 o/e (both compared to control) or 'TFAM o/e, ATF4 RNAi' (compared to TFAM o/e).

Gene ontological biological process terms for genes significantly regulated in RNA-Seq analysis for TFAM o/e, ATF4 o/e (both compared to control) and the compound condition TFAM o/e, ATF4 RNAi (compared to TFAM o/e). Terms are those found by functional annotation software DAVID under the category 'GOTERM_BP_DIRECT'. Where no gene ontological terms were found, FlyBase.org was searched for functional notes, and where found these are added in the 'Biological process gene ontology terms' column, and the gene highlighted by a bold outline.

Grey shading = genes consistently regulated in all three conditions (i.e. upregulated by TFAM o/e, upregulated by ATF4 o/e and downregulated by ATF4 RNAi or the reverse).

Orange shading = genes consistently regulated by TFAM o/e and ATF4 o/e (i.e. up- or downregulated by both conditions), but not significantly regulated by ATF4 RNAi.

Blue shading = genes consistently regulated by TFAM o/e and ATF4 RNAi (i.e. upregulated by TFAM o/e and downregulated by ATF4 RNAi or vice versa), but not significantly regulated by ATF4 o/e.

Green shading = gene consistently regulated by ATF4 o/e and ATF4 RNAi (i.e. upregulated by ATF4 o/e and downregulated by ATF4 RNAi), but not significantly regulated by TFAM o/e.

U = upregulated, D = downregulated, X = not significantly regulated.

Gene ID	Gene Name	Biological process gene ontology terms	Regulated by TFAM o/e?	Regulated by ATF4 o/e?	Regulated by ATF4 RNAi?
CG17684	CG17684	GO:0006508~proteolysis	U	U	D
ImpE2	Ecdysone-inducible gene E2	GO:0007561~imaginal disc eversion	U	U	D
Thor	Thor	GO:0001558~regulation of cell growth GO:0006641~triglyceride metabolic process GO:0006955~immune response GO:0006979~response to oxidative stress	U	U	D

		GO:0007520~myoblast fusion GO:0007525~somatic muscle development GO:0008340~determination of adult lifespan GO:0009617~response to bacterium GO:0019731~antibacterial humoral response GO:0042594~response to starvation GO:0045792~negative regulation of cell size GO:0045947~negative regulation of translational initiation GO:0070129~regulation of mitochondrial translation GO:2000331~regulation of terminal button organization			
Hsp70Bb	Heat-shock-protein-70Bb	GO:0001666~response to hypoxia GO:0006986~response to unfolded protein GO:0009408~response to heat GO:0031427~response to methotrexate GO:0035080~heat shock-mediated polytene chromosome puffing	U	U	U
Acf	ATP-dependent chromatin assembly factor large subunit	GO:0006333~chromatin assembly or disassembly GO:0006334~nucleosome assembly GO:0006355~regulation of transcription, DNA-templated GO:0007399~nervous system development GO:0007517~muscle organ development GO:0008544~epidermis development GO:0016584~nucleosome positioning GO:0019233~sensory perception of pain GO:0031445~regulation of heterochromatin assembly GO:0031497~chromatin assembly GO:0042766~nucleosome mobilization GO:0043462~regulation of ATPase activity GO:0045892~negative regulation of transcription, DNA-templated GO:0048666~neuron development GO:0048813~dendrite morphogenesis	U	U	X
blw	bellwether	GO:0006909~phagocytosis GO:0007286~spermatid development GO:0015986~ATP synthesis coupled proton transport GO:0015991~ATP hydrolysis coupled proton transport GO:0015992~proton transport GO:0019233~sensory perception of pain GO:0019915~lipid storage GO:0022900~electron transport chain GO:0040007~growth GO:1902769~regulation of choline O-acetyltransferase activity	U	U	X
CG1113	CG1113		U	U	X
CG14850	CG14850		U	U	X
CG42694	CG42694	GO:0006508~proteolysis	U	U	X
sfl	sulfateless	GO:0006024~glycosaminoglycan biosynthetic process GO:0006790~sulfur compound metabolic process	U	U	X

		GO:0007166~cell surface receptor signaling pathway GO:0007283~spermatogenesis GO:0007367~segment polarity determination GO:0007427~epithelial cell migration, open tracheal system GO:0007428~primary branching, open tracheal system GO:0007474~imaginal disc-derived wing vein specification GO:0007507~heart development GO:0007509~mesoderm migration involved in gastrulation GO:0008543~fibroblast growth factor receptor signaling pathway GO:0008587~imaginal disc-derived wing margin morphogenesis GO:0015012~heparan sulfate proteoglycan biosynthetic process GO:0015014~heparan sulfate proteoglycan biosynthetic process, polysaccharide chain biosynthetic process GO:0016055~Wnt signaling pathway GO:0030210~heparin biosynthetic process GO:0045570~regulation of imaginal disc growth GO:0048312~intracellular distribution of mitochondria GO:0048488~synaptic vesicle endocytosis GO:0060828~regulation of canonical Wnt signaling pathway GO:0090097~regulation of decapentaplegic signaling pathway			
Arc1	Activity-regulated cytoskeleton associated protein 1	GO:0003012~muscle system process GO:0042595~behavioral response to starvation	U	D	X
ImpL3	Ecdysone-inducible gene L3	GO:0005975~carbohydrate metabolic process GO:0007520~myoblast fusion GO:0007525~somatic muscle development GO:0019752~carboxylic acid metabolic process GO:0055114~oxidation-reduction process	U	D	D
CG15784	CG15784		U	X	D
CG34296	CG34296		U	X	D
CG7587	CG7587		U	X	D
Dgp-1	Dgp-1	GO:0006414~translational elongation,	U	X	D
Hex-A	Hexokinase A	GO:0001678~cellular glucose homeostasis GO:0006096~glycolytic process GO:0046835~carbohydrate phosphorylation GO:0060361~flight	U	X	D
Hsc70-2	Heat shock protein cognate 2	GO:0006457~protein folding	U	X	D
Hsp22	Heat shock protein 22	GO:0006979~response to oxidative stress GO:0008340~determination of adult lifespan GO:0009408~response to heat GO:0061077~chaperone-mediated protein folding	U	X	D

2SrRNA: CR45836	2SrRNA: CR45836		U	X	D
CR45315	CR45315		U	X	D
CR45481	CR45481		U	X	D
mir-10404-1	mir-10404-1		U	X	D
thw	thawb	Chitin binding	U	X	D
28SrRNA: CR45837	28SrRNA: CR45837		U	X	D
CG31496	CG31496	GO:0032504~multicellular organism reproduction	U	X	X
CG33500	CG33500		U	X	X
CG42832	CG42832		U	X	X
cv-2	crossveinless 2	GO:0007474~imaginal disc-derived wing vein specification GO:0007476~imaginal disc-derived wing morphogenesis GO:0030510~regulation of BMP signaling pathway	U	X	X
Eig71Ee	Ecdysone-induced gene 71Ee	GO:0007594~puparial adhesion GO:0042381~hemolymph coagulation	U	X	X
Gadd45	Gadd45	GO:0007254~JNK cascade GO:0046662~regulation of oviposition GO:0051726~regulation of cell cycle	U	X	X
Sgs3	Salivary gland secretion 3	GO:0071390~cellular response to ecdysone	U	X	X
Sgs5	Salivary gland secretion 5	Salivary glue protein	U	X	X
Sgs7	Salivary gland secretion 7	Salivary glue protein	U	X	X
Xrp1	Xrp1	GO:0007476~imaginal disc-derived wing morphogenesis GO:0008285~negative regulation of cell proliferation GO:0009987~cellular process GO:0042048~olfactory behavior GO:0051276~chromosome organization	U	X	X
NKCC	Sodium potassium chloride cotransporter	Cation-coupled chloride transporter	U	X	X
CG42500	CG42500		D	D	U
CG43117	CG43117		D	D	U
CG5955	CG5955	NAD-dependent epimerase/dehydratase	D	D	U
Cyp28a5	Cyp28a5	GO:0046680~response to DDT GO:0046701~insecticide catabolic process GO:0055114~oxidation-reduction process	D	D	U
Cyt-c-d	Cytochrome c distal	GO:0006119~oxidative phosphorylation GO:0006122~mitochondrial electron transport, ubiquinol to cytochrome c GO:0006123~mitochondrial electron transport, cytochrome c to oxygen GO:0006919~activation of cysteine-type endopeptidase activity involved in apoptotic process GO:0007291~sperm individualization GO:0046669~regulation of compound eye retinal cell programmed cell death GO:0055114~oxidation-reduction process	D	D	U
Jon99Ciii	Jonah 99Ciii	GO:0006508~proteolysis	D	D	U

Lcp1	Larval cuticle protein 1	GO:0008363~larval chitin-based cuticle development GO:0040003~chitin-based cuticle development	D	D	U
Lcp3	Larval cuticle protein 3	GO:0008363~larval chitin-based cuticle development GO:0040003~chitin-based cuticle development	D	D	U
Lcp4	Larval cuticle protein 4	GO:0040003~chitin-based cuticle development	D	D	U
Lcp65Ab1	Lcp65Ab1	GO:0008363~larval chitin-based cuticle development GO:0040003~chitin-based cuticle development	D	D	U
Akh	Adipokinetic hormone	GO:0007218~neuropeptide signaling pathway GO:0010906~regulation of glucose metabolic process GO:0033500~carbohydrate homeostasis GO:0042594~response to starvation GO:0055088~lipid homeostasis	D	D	X
Aldh	Aldehyde dehydrogenase	GO:0006090~pyruvate metabolic process GO:0006117~acetaldehyde metabolic process GO:0045471~response to ethanol GO:0055114~oxidation-reduction process GO:1901215~negative regulation of neuron death	D	D	X
CG10184	CG10184	GO:0006520~cellular amino acid metabolic process GO:0006545~glycine biosynthetic process GO:0006567~threonine catabolic process	D	D	X
CG10307	CG10307	Leucine-rich repeat	D	D	X
CG12512	CG12512	GO:0008152~metabolic process	D	D	X
CG14075	CG14075	GO:0019233~sensory perception of pain	D	D	X
CG15767	CG15767	GO:0000413~protein peptidyl-prolyl isomerization GO:0006457~protein folding	D	D	X
CG18278	CG18278	GO:0030203~glycosaminoglycan metabolic process	D	D	X
CG2233	CG2233		D	D	X
CG30059	CG30059	GO:0030203~glycosaminoglycan metabolic process	D	D	X
CG30197	CG30197	Peptidase inhibitor activity	D	D	X
CG31549	CG31549	Oxidoreductase activity	D	D	X
CG32249	CG32249		D	D	X
CG34166	CG34166		D	D	X
CG34445	CG34445	LPS-induced tumour necrosis factor alpha factor	D	D	X
CG34446	CG34446	LPS-induced tumour necrosis factor alpha factor	D	D	X
CG44325	CG44325		D	D	X
CG45087	CG45087		D	D	X
CG4686	CG4686		D	D	X
CG9657	CG9657	GO:0055085~transmembrane transport	D	D	X
Csas	CMP-sialic acid synthase	GO:0007268~chemical synaptic transmission	D	D	X

		GO:0009408~response to heat			
Cyp4d1	Cytochrome P450-4d1	GO:0055114~oxidation-reduction process	D	D	X
Cys	Cystatin-like	GO:0032504~multicellular organism reproduction	D	D	X
GstD3	Glutathione S transferase D3	GO:0006749~glutathione metabolic process	D	D	X
GstE14	Glutathione S transferase E14	GO:0006749~glutathione metabolic process GO:0009636~response to toxic substance GO:0042632~cholesterol homeostasis GO:0045456~ecdysteroid biosynthetic process	D	D	X
Hsp70Aa	Heat-shock-protein-70Aa	GO:0001666~response to hypoxia GO:0006986~response to unfolded protein GO:0009408~response to heat GO:0035080~heat shock-mediated polytene chromosome puffing	D	D	X
Lsp1beta	Larval serum protein 1 beta	GO:0046331~lateral inhibition	D	D	X
Lsp2	Larval serum protein 2	GO:0008045~motor neuron axon guidance GO:0016201~synaptic target inhibition	D	D	X
MFS9	Major Facilitator Superfamily Transporter 9	GO:0006820~anion transport GO:0055085~transmembrane transport	D	D	X
Mlc2	Myosin light chain 2	GO:0003012~muscle system process GO:0030239~myofibril assembly GO:0060361~flight	D	D	X
mRpL36	mitochondrial ribosomal protein L36	GO:0032543~mitochondrial translation GO:0042254~ribosome biogenesis	D	D	X
ND-B14.5B	NADH dehydrogenase (ubiquinone) B14.5 B subunit	GO:0006120~mitochondrial electron transport, NADH to ubiquinone	D	D	X
NU44A	Nucleoporin at 44A	GO:0007184~SMAD protein import into nucleus GO:0007293~germarium-derived egg chamber formation GO:0007346~regulation of mitotic cell cycle GO:0010507~negative regulation of autophagy GO:0032008~positive regulation of TOR signaling GO:0034198~cellular response to amino acid starvation GO:0045793~positive regulation of cell size GO:0048477~oogenesis GO:0051445~regulation of meiotic cell cycle GO:1903432~regulation of TORC1 signaling	D	D	X
Obp99b	Odorant-binding protein 99b	GO:0006810~transport GO:0007606~sensory perception of chemical stimulus GO:0007608~sensory perception of smell GO:0019236~response to pheromone GO:0035071~salivary gland cell autophagic cell death GO:0042048~olfactory behavior GO:0048102~autophagic cell death	D	D	X

pyd3	pyd3	GO:0006207~'de novo' pyrimidine nucleobase biosynthetic process GO:0006208~pyrimidine nucleobase catabolic process GO:0006807~nitrogen compound metabolic process	D	D	X
Syt7	Synaptotagmin 7	GO:0006887~exocytosis GO:0006906~vesicle fusion GO:0007269~neurotransmitter secretion GO:0016079~synaptic vesicle exocytosis GO:0016192~vesicle-mediated transport GO:0017158~regulation of calcium ion-dependent exocytosis GO:0048791~calcium ion-regulated exocytosis of neurotransmitter	D	D	X
CR46006	CR46006		D	D	X
CG3987	CG3987	GO:0007498~mesoderm development	D	X	U
CG43980	CG43980	GO:0030162~regulation of proteolysis GO:0042787~protein ubiquitination involved in ubiquitin-dependent protein catabolic process GO:0043161~proteasome-mediated ubiquitin-dependent protein catabolic process	D	X	U
CG6912	CG6912		D	X	U
CG14566	CG14566		D	X	D
CG10226	CG10226	GO:0031427~response to methotrexate GO:0055085~transmembrane transport	D	X	X
CG13067	CG13067		D	X	X
CG16743	CG16743		D	X	X
CG30379	CG30379	Bax inhibitor 1-related	D	X	X
CG33099	CG33099	GO:0055114~oxidation-reduction process	D	X	X
CG34305	CG34305		D	X	X
CG5958	CG5958	GO:0006810~transport	D	X	X
Klp68D	Kinesin-like protein at 68D	GO:0007018~microtubule-based movement GO:0007608~sensory perception of smell GO:0008089~anterograde axonal transport GO:0030951~establishment or maintenance of microtubule cytoskeleton polarity	D	X	X
Lcp2	Larval cuticle protein 2	GO:0008363~larval chitin-based cuticle development GO:0040003~chitin-based cuticle development	D	X	X
Lsp1alpha	Larval serum protein 1 alpha	Hemocyanin domains	D	X	X
Lsp1gamma	Larval serum protein 1 gamma	Hemocyanin domains	D	X	X
vkg	viking	GO:0007443~Malpighian tubule morphogenesis GO:0007519~skeletal muscle tissue development GO:0061327~anterior Malpighian tubule development	D	X	X
ImpE1	Ecdysone-inducible gene E1	GO:0007561~imaginal disc eversion	X	U	D
AstC-R2	Allatostatin C receptor 2	GO:0007186~G-protein coupled receptor signaling pathway	X	U	X

		GO:0007187~G-protein coupled receptor signaling pathway, coupled to cyclic nucleotide second messenger GO:0007218~neuropeptide signaling pathway			
Blimp-1	Blimp-1	GO:0000122~negative regulation of transcription from RNA polymerase II promoter GO:0035074~pupation GO:0035152~regulation of tube architecture, open tracheal system GO:0071390~cellular response to ecdysone	X	U	X
CG11700	CG11700	GO:0008340~determination of adult lifespan GO:0016567~protein ubiquitination GO:2000242~negative regulation of reproductive process	X	U	X
CG15021	CG15021		X	U	X
CG15864	CG15864	GO:0055114~oxidation-reduction process	X	U	X
CG17211	CG17211	GO:0060562~epithelial tube morphogenesis	X	U	X
CG34232	CG34232		X	U	X
CG43901	CG43901		X	U	X
CG5830	CG5830	GO:0006470~protein dephosphorylation	X	U	X
Cht5	Cht5	GO:0005975~carbohydrate metabolic process GO:0006032~chitin catabolic process GO:0018990~ecdysis, chitin-based cuticle GO:0040003~chitin-based cuticle development GO:0042060~wound healing	X	U	X
Cpr49Ae	Cuticular protein 49Ae	GO:0040003~chitin-based cuticle development	X	U	X
Crg-1	Circadianly Regulated Gene	GO:0006355~regulation of transcription, DNA-templated	X	U	X
Eip93F	Ecdysone-induced protein 93F	GO:0006911~phagocytosis, engulfment GO:0006914~autophagy GO:0006919~activation of cysteine-type endopeptidase activity involved in apoptotic process GO:0008628~hormone-mediated apoptotic signaling pathway GO:0035071~salivary gland cell autophagic cell death GO:0035072~ecdysone-mediated induction of salivary gland cell autophagic cell death GO:0035096~larval midgut cell programmed cell death GO:0045893~positive regulation of transcription, DNA-templated GO:0045944~positive regulation of transcription from RNA polymerase II promoter GO:0048102~autophagic cell death GO:0071390~cellular response to ecdysone GO:0071456~cellular response to hypoxia	X	U	X
Indy	I'm not dead yet	GO:0006814~sodium ion transport GO:0006848~pyruvate transport GO:0008340~determination of adult lifespan	X	U	X

		GO:0010889~regulation of sequestering of triglyceride GO:0015744~succinate transport GO:0015746~citrate transport GO:0055085~transmembrane transport			
jeb	jelly belly	GO:0007411~Axon guidance GO:0007435~salivary gland morphogenesis GO:0007509~mesoderm migration involved in gastrulation GO:0007522~visceral muscle development GO:0042051~compound eye photoreceptor development GO:0042694~muscle cell fate specification GO:0043410~positive regulation of MAPK cascade GO:0051124~synaptic growth at neuromuscular junction GO:1900074~negative regulation of neuromuscular synaptic transmission	X	U	X
nrm	neuromusculin	GO:0008039~synaptic target recognition	X	U	X
rdgA	retinal degeneration A	GO:0006654~phosphatidic acid biosynthetic process GO:0006661~phosphatidylinositol biosynthetic process GO:0007015~actin filament organization GO:0007205~protein kinase C-activating G-protein coupled receptor signaling pathway GO:0007601~visual perception GO:0007602~phototransduction GO:0007605~sensory perception of sound GO:0007608~sensory perception of smell GO:0016056~rhodopsin mediated signaling pathway GO:0016059~deactivation of rhodopsin mediated signaling GO:0016310~phosphorylation GO:0035556~intracellular signal transduction GO:0043052~thermotaxis GO:0045494~photoreceptor cell maintenance GO:0046154~rhodopsin metabolic process GO:0046834~lipid phosphorylation	X	U	X
Rgk2	Rad, Gem/Kir family member 2	GO:0007264~small GTPase mediated signal transduction GO:1901386~negative regulation of voltage-gated calcium channel activity	X	U	X
Sec31	Sec31 ortholog	GO:0045089~positive regulation of innate immune response GO:0050829~defense response to Gram-negative bacterium GO:0090114~COPII-coated vesicle budding	X	U	X
SelG	Selenoprotein G	GO:0001700~embryonic development via the syncytial blastoderm GO:0002376~immune system process GO:0006816~calcium ion transport GO:0007350~blastoderm segmentation GO:0008340~determination of adult lifespan GO:0009790~embryo development GO:0010470~regulation of gastrulation	X	U	X

		GO:0032469~endoplasmic reticulum calcium ion homeostasis GO:0045454~cell redox homeostasis			
spg	sponge	GO:0007264~small GTPase mediated signal transduction GO:0007417~central nervous system development GO:0045466~R7 cell differentiation GO:0090630~activation of GTPase activity	X	U	X
CR44027	CR44027		X	U	X
CR46004	CR46004		X	U	X
trv	trivet	RNA-binding domain superfamily	X	U	X
CG32198	CG32198		X	D	D
CG8087	CG8087		X	D	D
mthl8	methuselah-like 8	GO:0006950~response to stress GO:0007186~G-protein coupled receptor signaling pathway GO:0008340~determination of adult lifespan GO:0042594~response to starvation	X	D	D
spok	spookier	GO:0006697~ecdysone biosynthetic process GO:0007591~molting cycle, chitin-based cuticle GO:0055114~oxidation-reduction process	X	D	D
Ada	Adenosine deaminase	GO:0006154~adenosine catabolic process GO:0009117~nucleotide metabolic process GO:0046103~inosine biosynthetic process	X	D	X
Ady43A	Ady43A	Carbohydrate/purine kinase	X	D	X
alpha-Est7	alpha-Esterase-7	GO:0007158~neuron cell-cell adhesion GO:0007416~synapse assembly GO:0008340~determination of adult lifespan GO:0019915~lipid storage GO:0046683~response to organophosphorus GO:0050804~modulation of synaptic transmission	X	D	X
Arp10	Actin-related protein 10	GO:0007010~cytoskeleton organization GO:0007018~microtubule-based movement GO:0019233~sensory perception of pain	X	D	X
asrij	asrij	GO:0035162~embryonic hemopoiesis GO:0035167~larval lymph gland hemopoiesis GO:0046425~regulation of JAK-STAT cascade GO:0048542~lymph gland development	X	D	X
Capa	Capability	GO:0006812~cation transport GO:0007204~positive regulation of cytosolic calcium ion concentration GO:0007218~neuropeptide signaling pathway GO:0038060~nitric oxide-cGMP-mediated signaling pathway GO:0042045~epithelial fluid transport	X	D	X
CG11300	CG11300		X	D	X
CG12237	CG12237	GO:0008152~metabolic process	X	D	X
CG12926	CG12926	GO:0006810~transport	X	D	X
CG14545	CG14545		X	D	X

CG14572	CG14572		X	D	X
CG14985	CG14985		X	D	X
CG15083	CG15083		X	D	X
CG17105	CG17105		X	D	X
CG17333	CG17333	GO:0005975~carbohydrate metabolic process GO:0006098~pentose-phosphate shunt	X	D	X
CG31220	CG31220	GO:0006508~proteolysis	X	D	X
CG31437	CG31437	Collagen triple helix repeat	X	D	X
CG4036	CG4036	GO:0035167~larval lymph gland hemopoiesis GO:0055114~oxidation-reduction process GO:0070988~demethylation	X	D	X
CG43069	CG43069	Ubiquitin domain	X	D	X
CG43085	CG43085		X	D	X
CG4408	CG4408	GO:0006508~proteolysis	X	D	X
CG4789	CG4789	GO:0007264~small GTPase mediated signal transduction	X	D	X
CG5037	CG5037	GO:0006783~heme biosynthetic process GO:0008535~respiratory chain complex IV assembly GO:0048034~heme O biosynthetic process GO:1902600~hydrogen ion transmembrane transport	X	D	X
CG5567	CG5567	GO:0006470~protein dephosphorylation GO:0016311~dephosphorylation	X	D	X
CG5867	CG5867	GO:0007623~circadian rhythm GO:0032504~multicellular organism reproduction	X	D	X
CG6723	CG6723	GO:0055085~transmembrane transport	X	D	X
CG7630	CG7630	Deltamethrin resistance	X	D	X
CG8369	CG8369	GO:0048190~wing disc dorsal/ventral pattern formation	X	D	X
CG8745	CG8745	GO:0019544~arginine catabolic process to glutamate GO:0035094~response to nicotine	X	D	X
CG8778	CG8778	GO:0006635~fatty acid beta-oxidation GO:0008152~metabolic process GO:0009631~cold acclimation	X	D	X
CG9147	CG9147	GO:0006635~fatty acid beta-oxidation GO:0008152~metabolic process	X	D	X
Cyp12a4	Cyp12a4	GO:0017085~response to insecticide GO:0055114~oxidation-reduction process	X	D	X
Cyp6g2	Cyp6g2	GO:0017085~response to insecticide GO:0046680~response to DDT GO:0046701~insecticide catabolic process GO:0055114~oxidation-reduction process	X	D	X
Cyp9f2	Cyp9f2	GO:0035220~wing disc development GO:0055114~oxidation-reduction process	X	D	X
Dbi	Diazepam-binding inhibitor	GO:0006810~transport GO:0042049~cellular acyl-CoA homeostasis	X	D	X
Dhfr	Dihydrofolate reductase	GO:0006260~DNA replication GO:0006545~glycine biosynthetic process GO:0006730~one-carbon metabolic process GO:0009165~nucleotide biosynthetic process	X	D	X

		GO:0046654~tetrahydrofolate biosynthetic process GO:0055114~oxidation-reduction process			
dmGlut	Dietary and metabolic glutamate transporter	GO:0006541~glutamine metabolic process GO:0007005~mitochondrion organization GO:0044341~sodium-dependent phosphate transport GO:0051938~L-glutamate import GO:0055085~transmembrane transport	X	D	X
DNaseII	Deoxyribonuclease II	GO:0006259~DNA metabolic process GO:0006308~DNA catabolic process GO:0006309~apoptotic DNA fragmentation GO:0030431~sleep GO:0045476~nurse cell apoptotic process	X	D	X
Dsk	Drosulfakinin	GO:0006939~smooth muscle contraction GO:0006940~regulation of smooth muscle contraction GO:0007204~positive regulation of cytosolic calcium ion concentration GO:0007218~neuropeptide signaling pathway GO:0007528~neuromuscular junction development GO:0008343~adult feeding behavior GO:0008344~adult locomotory behavior GO:0008345~larval locomotory behavior GO:0033555~multicellular organismal response to stress	X	D	X
eca	eclair	GO:0000003~reproduction GO:0002121~inter-male aggressive behavior GO:0006888~ER to Golgi vesicle-mediated transport GO:0007030~Golgi organization GO:0009953~dorsal/ventral pattern formation GO:0034389~lipid particle organization GO:0035220~wing disc development GO:0048042~regulation of post-mating oviposition GO:0048193~Golgi vesicle transport GO:0061357~positive regulation of Wnt protein secretion GO:0070863~positive regulation of protein exit from endoplasmic reticulum GO:0090263~positive regulation of canonical Wnt signaling pathway	X	D	X
Elal	Elastin-like	GO:0035094~response to nicotine	X	D	X
Fit2	Fermitin 2	GO:0048738~cardiac muscle tissue development	X	D	X
GILT3	Gamma-interferon-inducible lysosomal thiol reductase 3	GO:0055114~oxidation-reduction process	X	D	X
Gpa2	Glycoprotein hormone alpha 2 ortholog	GO:0009755~hormone-mediated signaling pathway	X	D	X
GstE8	Glutathione S transferase E8	GO:0006749~glutathione metabolic process	X	D	X
Hsp70Bbb	Hsp70Bbb	GO:0001666~response to hypoxia GO:0009408~response to heat	X	D	X

		GO:0035080~heat shock-mediated polytene chromosome puffing			
Ilp2	Insulin-like peptide 2	GO:0007623~circadian rhythm GO:0008284~positive regulation of cell proliferation GO:0008286~insulin receptor signaling pathway GO:0008340~determination of adult lifespan GO:0008361~regulation of cell size GO:0009758~carbohydrate utilization GO:0010906~regulation of glucose metabolic process GO:0030307~positive regulation of cell growth GO:0030431~sleep,GO:0030536~larval feeding behavior GO:0040007~growth GO:0040009~regulation of growth rate GO:0040014~regulation of multicellular organism growth GO:0040018~positive regulation of multicellular organism growth GO:0045475~locomotor rhythm GO:0046620~regulation of organ growth GO:0046626~regulation of insulin receptor signaling pathway GO:0060180~female mating behavior GO:0060250~germ-line stem-cell niche homeostasis GO:0070328~triglyceride homeostasis GO:0071333~cellular response to glucose stimulus GO:2000252~negative regulation of feeding behavior	X	D	X
Jon99Fi	Jonah 99Fi	GO:0006508~proteolysis	X	D	X
Lk	Leucokinin	GO:0007204~positive regulation of cytosolic calcium ion concentration GO:0007218~neuropeptide signaling pathway GO:0007589~body fluid secretion GO:2000252~negative regulation of feeding behavior	X	D	X
mre11	meiotic recombination 11	GO:0000723~telomere maintenance GO:0006302~double-strand break repair GO:0006974~cellular response to DNA damage stimulus GO:0007095~mitotic G2 DNA damage checkpoint GO:0016233~telomere capping GO:0031573~intra-S DNA damage checkpoint GO:0051276~chromosome organization GO:0051321~meiotic cell cycle	X	D	X
mRpL46	mitochondrial ribosomal protein L46	GO:0019233~sensory perception of pain GO:0032543~mitochondrial translation	X	D	X
mus205	mutagen-sensitive 205	GO:0000724~double-strand break repair via homologous recombination GO:0006260~DNA replication GO:0019985~translesion synthesis	X	D	X

		GO:0042276~error-prone translesion synthesis			
ND-30	NADH dehydrogenase (ubiquinone) 30 kDa subunit	GO:0055114~oxidation-reduction process GO:0072593~reactive oxygen species metabolic process	X	D	X
ND-B14.7	NADH dehydrogenase (ubiquinone) B14.7 subunit	GO:0019233~sensory perception of pain	X	D	X
ND-PDSW	NADH dehydrogenase (ubiquinone) PDSW subunit	GO:0006120~mitochondrial electron transport, NADH to ubiquinone GO:0022008~neurogenesis	X	D	X
NPF	neuropeptide F	GO:0007186~G-protein coupled receptor signaling pathway GO:0007218~neuropeptide signaling pathway GO:0007586~digestion GO:0007623~circadian rhythm GO:0008049~male courtship behavior GO:0008345~larval locomotory behavior GO:0030536~larval feeding behavior GO:0032095~regulation of response to food GO:0035176~social behavior GO:0035177~larval foraging behavior GO:0045475~locomotor rhythm GO:0048512~circadian behavior	X	D	X
Pburs	Partner of Bursicon	GO:0007186~G-protein coupled receptor signaling pathway GO:0007593~chitin-based cuticle sclerotization GO:0018990~ecdysis, chitin-based cuticle GO:0090175~regulation of establishment of planar polarity	X	D	X
phm	Peptidylglycine-alpha-hydroxylating monooxygenase	GO:0006518~peptide metabolic process GO:0007613~memory GO:0009620~response to fungus GO:0032504~multicellular organism reproduction GO:0044719~regulation of imaginal disc-derived wing size	X	D	X
RpS15Ab	Ribosomal protein S15Ab	GO:0002181~cytoplasmic translation GO:0006412~translation	X	D	X
rtet	tetracycline resistance	GO:0015904~tetracycline transport GO:0048477~oogenesis GO:0055085~transmembrane transport	X	D	X
Sec63	Sec63 ortholog	Translocation, DnaJ domain	X	D	X
snRNA:U1:95Ca	small nuclear RNA U1 at 95Ca	GO:0000398~mRNA splicing, via spliceosome	X	D	X
Ssb-c31a	Single stranded-binding protein c31A	GO:0006351~transcription, DNA-templated GO:0045892~negative regulation of transcription, DNA-templated	X	D	X
su(r)	suppressor of rudimentary	GO:0006207~'de novo' pyrimidine nucleobase biosynthetic process GO:0006212~uracil catabolic process GO:0055114~oxidation-reduction process	X	D	X
Taldo	Transaldolase	GO:0005975~carbohydrate metabolic process GO:0006098~pentose-phosphate shunt	X	D	X
TotA	Turandot A	GO:0006979~response to oxidative stress	X	D	X

		GO:0009408~response to heat GO:0009409~response to cold GO:0009411~response to UV GO:0009414~response to water deprivation GO:0009612~response to mechanical stimulus GO:0009617~response to bacterium GO:0034599~cellular response to oxidative stress GO:0034605~cellular response to heat GO:0034644~cellular response to UV GO:0042742~defense response to bacterium GO:0045087~innate immune response GO:0046689~response to mercury ion GO:0051597~response to methylmercury GO:0071260~cellular response to mechanical stimulus			
Tsp42Ej	Tetraspanin 42Ej	GO:0006897~endocytosis GO:0071486~cellular response to high light intensity	X	D	X
Tsp42El	Tetraspanin 42El	GO:0007166~cell surface receptor signaling pathway GO:0030431~sleep	X	D	X
Tspo	Translocator protein	GO:0002082~regulation of oxidative phosphorylation GO:0008340~determination of adult lifespan GO:0043065~positive regulation of apoptotic process	X	D	X
Ugt86Dd	Ugt86Dd	GO:0008152~metabolic process GO:0009813~flavonoid biosynthetic process GO:0052696~flavonoid glucuronidation	X	D	X
Ugt86Di	Ugt86Di	GO:0008152~metabolic process GO:0009813~flavonoid biosynthetic process GO:0052696~flavonoid glucuronidation	X	D	X
veli	veli	GO:0006887~exocytosis GO:0007163~establishment or maintenance of cell polarity GO:0007269~neurotransmitter secretion GO:0007298~border follicle cell migration GO:0008582~regulation of synaptic growth at neuromuscular junction GO:0045199~maintenance of epithelial cell apical/basal polarity GO:1903361~protein localization to basolateral plasma membrane	X	D	X
Vha36-1	Vacuolar H[+] ATPase 36kD subunit 1	GO:0015991~ATP hydrolysis coupled proton transport GO:0015992~proton transport	X	D	X
CR43727	CR43727		X	D	X
CR44922	CR44922		X	D	X
CR45044	CR45044		X	D	X
CR46012	CR46012		X	D	X
Idgf6	Imaginal disc growth factor 6	Glycoside hydrolase family, Chitinase	X	D	X
mt:ND2	mitochondrial NADH-ubiquinone	NADH:ubiquinone oxidoreductase, chain 2	X	D	X

	oxidoreductase chain 2				
snoRNA: Me28S-C3227a	snoRNA: Me28S-C3227a		X	D	X
spab	Space blanket		X	D	X
CG9377	CG9377	GO:0006508~proteolysis	X	X	U
CG9737	CG9737	GO:0006508~proteolysis GO:0006909~phagocytosis	X	X	U
GstT3	Glutathione S transferase T3	GO:0006749~glutathione metabolic process	X	X	U
IntS12	Integrator 12	GO:0016180~snRNA processing GO:0022008~neurogenesis GO:0034472~snRNA 3'-end processing	X	X	U
roq	roquin	GO:0000209~protein polyubiquitination	X	X	U
Trh	trachealess	GO:0006351~transcription, DNA-templated GO:0006355~regulation of transcription, DNA-templated GO:0006366~transcription from RNA polymerase II promoter GO:0007424~open tracheal system development GO:0007425~epithelial cell fate determination, open tracheal system GO:0007431~salivary gland development GO:0007435~salivary gland morphogenesis GO:0007443~Malpighian tubule morphogenesis GO:0035277~spiracle morphogenesis, open tracheal system GO:0045944~positive regulation of transcription from RNA polymerase II promoter GO:0046331~lateral inhibition GO:0048813~dendrite morphogenesis GO:0060173~limb development GO:0072175~epithelial tube formation	X	X	U
AdamTS-A	ADAM metallopeptidase with thrombospondin type 1 motif A	GO:0006508~proteolysis GO:0007280~pole cell migration GO:0007427~epithelial cell migration, open tracheal system GO:0007436~larval salivary gland morphogenesis GO:0008078~mesodermal cell migration GO:0030198~extracellular matrix organization	X	X	D
CG10924	CG10924	GO:0006094~gluconeogenesis	X	X	D
CG16700	CG16700	GO:0003333~amino acid transmembrane transport GO:0022008~neurogenesis	X	X	D
CG3036	CG3036	GO:0006820~anion transport GO:0055085~transmembrane transport	X	X	D
CG42240	CG42240		X	X	D
CG43083	CG43083		X	X	D
CG4461	CG4461	GO:0009408~response to heat	X	X	D
CG7386	CG7386	GO:0006355~regulation of transcription, DNA-templated GO:0022008~neurogenesis	X	X	D
CG9304	CG9304	GO:0007186~G-protein coupled receptor signaling pathway	X	X	D

		GO:0019236~response to pheromone			
CG9416	CG9416	Peptidase	X	X	D
Cpr49Ac	Cuticular protein 49Ac	GO:0040003~chitin-based cuticle development GO:0042381~hemolymph coagulation	X	X	D
Dtg	Dpp target gene	GO:0007369~gastrulation	X	X	D
Hsp67Bc	Heat shock gene 67Bc	GO:0006497~protein lipidation GO:0009408~response to heat GO:0010506~regulation of autophagy GO:0010998~regulation of translational initiation by eIF2 alpha phosphorylation GO:0031427~response to methotrexate	X	X	D
MFS3	Major Facilitator Superfamily Transporter 3	GO:0006820~anion transport GO:0055085~transmembrane transport	X	X	D
NLaz	Neural Lazarillo	GO:0006979~response to oxidative stress GO:0008340~determination of adult lifespan GO:0032504~multicellular organism reproduction GO:0033500~carbohydrate homeostasis GO:0070328~triglyceride homeostasis	X	X	D
nvd	neverland	GO:0002168~instar larval development GO:0007552~metamorphosis GO:0035264~multicellular organism growth GO:0045456~ecdysteroid biosynthetic process GO:0055114~oxidation-reduction process	X	X	D
Tret1-1	Trehalose transporter 1-1	GO:0015771~trehalose transport GO:0035428~hexose transmembrane transport GO:0046323~glucose import GO:0055085~transmembrane transport	X	X	D
28SrRNA:CR45844	28S ribosomal RNA:CR45844		X	X	D
CR44522	CR44522		X	X	D
CR44803	CR44803		X	X	D

8.3.6 Genes significantly regulated in RNA-Seq analysis that were excluded from DAVID functional annotation clustering analysis.

The following genes with ontological and functional terms relating solely to non-CNS structural components of the larvae were excluded from functional annotation cluster analysis to permit identification of CNS-related clusters. Ontological and functional terms were searched in DAVID, Panther (PantherDB.org) and FlyBase (FlyBase.org).

Gene symbol	Gene name
Sgs3	Salivary glue protein Sgs-3
Sgs5	Salivary glue protein Sgs-5
Sgs7	Salivary glue protein Sgs-7
Lcp1	Larval cuticle protein 1
Lcp2	Larval cuticle protein 2
Lcp3	Larval cuticle protein 3
Lcp4	Larval cuticle protein 4
Lcp65Ab1	Larval cuticle protein 5
Lsp1alpha	Larval serum protein 1 alpha chain
Lsp1gamma	Larval serum protein 1 gamma chain
thw	thawb (Chitin binding)
CG33500	Assigned as Sgs8 by DAVID & Panther
CG42832	Assigned as Mucin68Ca by DAVID & Panther
Eig71Ee	Ecdysone-induced gene 71Ee (salivary glue/hemolymph clot)
Mlc2	Myosin light chain 2
Cht5	Chitinase 5
Cpr49Ae	Cuticular protein 49Ae
Idgf6	Imaginal disc growth factor 6
Cpr49Ac	Cuticular protein 49Ac